FINITE ELEMENT PARAMETRIC STUDY OF VERTICAL STRAIN INFLUENCE FACTORS AND THE PRESSUREMETER TEST TO ESTIMATE THE SETTLEMENT OF FOOTINGS IN SAND

By

JOHN PAUL HARTMAN

A DISSERTATION PRESENTED TO THE GRADUATE COUNCIL OF THE UNIVERSITY OF FLORIDA IN PARTIAL FULFILLMENT OF THE REQUIREMENTS FOR THE DEGREE OF DOCTOR OF PHILOSOPHY

UNIVERSITY OF FLORIDA

1974

ACKNOWLEDGEMENTS

It would be impossible to acknowledge the assistance of all those who have worked with me and encouraged me in my doctoral work. I am indebted to Dr. Joe Googe, whose telephone call one day from the University of Tennessee started me back on the road to the Ph.D. I am deeply indebted to all those at Florida Technological University who have also helped and encouraged: to Dean Robert Kersten for his support and encouragement in obtaining a National Science Foundation Science Faculty Fellowship while on leave-of-absence completing my coursework; to Vice-President C.B. Gambrell and Dean Leslie Ellis for their assistance in obtaining the large quantity of computer time necessary to undertake these parametric studies.

For specific assistance in the early stages of my work I am indebted to Dr. Michael Duncan of the University of California at Berkeley, who furnished me with the original listings and data to get started. Computer assistance along the way has been obtained from Don Cruse at the University of Florida and Bill Branch at Florida Technological University. Their assistance is gratefully acknowledged.

My year in Gainesville was enhanced by contacts, assistance, and encouragement from Dr. James Schaub, Chairman of the Civil Engineering Department, Dr. Martin Mifflin of the Geology Department and a member of my committee, Dr. James C. Holden, a Churchill Fellow

from Melbourne, Australia, and fellow graduate student James Laier whose assistance with the laboratory testing and hardware information has been invaluable.

I am also grateful for the continuing support of my family over these past several years.

And finally I am most appreciative of the support and guidance given me by my adviser, Dr. John H. Schmertmann, Professor of Civil Engineering. Studying under Dr. Schmertmann has been a distinct privilege, both with formal coursework, which was of the highest caliber, as well as in the informal learning situtation afforded by this dissertation.

TABLE OF CONTENTS

	Page
Acknowledgements	ii
List of Tables	vii
List of Figures	ix
List of Symbols and Abbreviations	xxiv
Abstract	xxx
1.0 Introduction	1
2.0 Background Analytical Work	6
2.1 The Pressuremeter Test	6
2.1.1 The Classic One-Dimensional Analysis	6
2.1.2 Tranter's Two-Dimensional Analysis	18
2.1.3 Pressuremeter Test Interpretation, Factors, and Uses	27
2.2 Settlement Prediction in Sands	30
2.2.1 Strain Distribution Approach	30
2.2.2 The Pressuremeter Test for Settlement Prediction in Sands	34
2.3 The Finite Element Method	38
2.3.1 General Discussion	38
2.3.2 Applications in the Field of Soil Mechanics	45
3.0 Analytical Modeling of Sand	47
3.1 Introduction	47
3.2 Nonlinear Stress-Dependent Moduli	49
3.3 Poisson's Ratio	56
3.4 Failure Conditions	63
3.5 Octahedral Stresses and Anisotropy	64
4.0 Study of Vertical Strain Distribution in Model Sand	67
4.1 Introduction	67
4.2 Strain Distribution in Linear Isotropic Materials	70
4.2.1 Normal Loads on Flexible Footings	70
4.2.2 Normal Loads on Rigid Footings	75
4.2.3 Conclusions Based on Linear Analyses	81

Page

4.3 Strain Distribution in Nonlinear Model Sand 89
4.3.1 Axisymmetric Loading 95
4.3.2 Plane Strain Loading 122
4.3.3 Comparison of Axisymmetric and Plane Strain Cases 142
4.3.4 Influence of Lateral Stresses 153
4.4 Influence of Depth to Rigid Layer 162
4.4.1 Axisymmetric Loading 164
4.4.2 Plane Strain Loading 178
4.5 Influence of Embedment 190
4.5.1 Axisymmetric Loading 192
4.5.2 Plane Strain Loading 205
4.6 Variations Near Edge of Footing 215
4.7 Conclusions 220
4.8 Example Settlement Problem 222

5.0 Pressuremeter Test Finite Element Study 229

5.1 General Discussion 229
5.2 Parametric Study Using Linear Elastic Material 238
5.2.1 Introduction 238
5.2.2 Effect of Poisson's Ratio 238
5.2.3 Effect of Differential Pressure 239
5.2.4 Effect of Unloading Borehole 242
5.2.5 Effect of Increased Lateral Stresses and Depth 245
5.2.6 Effect of Linear Cross-Anisotropy 247
5.2.7 Effect of a "Disturbed" Zone 247
5.2.8 Effect of Unloading and Reloading the Pressuremeter 252
5.2.9 Conclusions Based on Linear Elastic Analysis 252
5.3 Parametric Study Using Nonlinear Sand Model 255
5.3.1 Introduction 255
5.3.2 Effect of Differential Pressure Magnitude 266
5.3.3 Effect of Nonlinear Analysis Parameters 271
5.3.4 Effect of Increased Lateral Stresses 283
5.3.5 Effect of Depth 283
5.3.6 Effect of Borehole Disturbance 288
5.3.7 Effect of Unloading and Reloading the Pressuremeter 302
5.4 Use of Pressuremeter Moduli in Settlement Prediction 306

6.0 Comparison Between Analytical Model and Laboratory Testing 309

6.1 Introduction 309
6.2 Description of Test Chamber 309
6.3 Triaxial Tests on Edgar Sand 310
6.4 Experimental and Analytical Pressuremeter Test Results 312
6.5 Experimental and Analytical Plate Load Test Results 322
6.6 Model Footing Settlement Tests 329

	Page
7.0 Conclusions	333
8.0 Recommendations for Further Research	340
Appendix I: FORTRAN Listing for Solution of Tranter's Two-Dimensional Displacement Equation	343
Appendix II: FORTRAN Listing for Finite Element Strain Study Program (SOILSTRN)	347
Appendix III: FORTRAN Listing for Finite Element Pressuremeter Program (PRESMETR)	365
Appendix IV: Laboratory Triaxial Tests on Edgar Sand	381
Appendix V: Laboratory Plate Bearing Tests on Edgar Sand	396
Appendix VI: Laboratory Model Footing Tests	399
List of References	401
Biographical Sketch	407

LIST OF TABLES

Table		Page
1	Alpha Values for Use in Ménard's Settlement Computations	37
2	Shape Factors for Use in Ménard's Settlement Computations	37
3	Comparison of Theoretical and Measured Elastic Constants from Plane Strain and Triaxial Testing	57
4	Settlement Influence Factors (I_w) for Flexible and Rigid Footings	82
5	Comparison of Peak Strain Influence Factor (I_{zp}) for Triangular Distribution Using Classic Solution and Settlement Influence Factors (I_w) Under Axisymmetric Loading on Linear Elastic Material for Equal Settlement	84
6	Comparison of Peak Strain Influence Factor (I_{zp}) for Triangular Distribution Using Classic Solution and Settlement Influence Factors (I_w) Under Plane Strain Loading on Linear Elastic Material for Equal Settlement	87
7	Schmertmann Embedment Correction Factor Values	200
8	Settlement Example Problem Calculations	227
9	Modulus Calculations Using Slope of Pressure-Volume Curves in Figure 133 and Equation 1: E = 50 Tsf	241
10	E_{PMT} Calculations for Varying Differential Pressures: K = 60,000; ν = 0.40; Depth = 7 Ft	269
11	E_{PMT} Calculations Using Varying Nonlinear Modulus Number Conditions: ν = 0.40; Depth = 7 Ft	274
12	E_{PMT} Calculations Using Varying Poisson's Ratios: Depth = 7 Ft	277

Table		Page
13	E_{PMT} Calculations for Varying Angles of Friction in Pressuremeter Loading: K = 60,000; ν = 0.40; Depth = 7 Ft	280
14	E_{PMT} Calculations for Varying Lateral Stresses in Pressuremeter Loading: ν = 0.40; Depth = 7 Ft	285
15	E_{PMT} Calculations for Varying Depths in Pressuremeter Loading: K = 60,000; ν = 0.40	287
16	E_{PMT} Calculations for Varying Widths of Smear Zones in Pressuremeter Loading of Nonlinear Elastic Material; ν = 0.40; Depth = 7 Ft; k_o = 0.5	290
17	E_{PMT} Calculations Including Effect of Borehole Unloading: K = 60,000; ν = 0.40; Depth = 7 Ft	295
18	Nonlinear Analysis Parameters for Edgar Sand	313
19	University of Florida Testing Chamber Modulus Results	314

LIST OF FIGURES

Figure		Page
1	Schematic of Pressuremeter Loading in Borehole	7
2	Pressuremeter Test Pressure-Volume Curve	7
3	Geometry for Uniform Cylindrical Expansion in an Infinite Elastic Medium	10
4	Geometry for Average Radial Displacement and Volume Relationship for Measuring Cell	10
5	Effect of the $(u_{ave})^2$ Term on the Calculation of the Elastic Modulus	14
6	Geometry for Loading of an Infinitely Long Thick-Walled Cylinder (Lamé's Problem)	15
7	Thick-Walled Cylinder Effect on Calculation of the Elastic Modulus	17
8	Application of Cylindrical Uniform Pressure Over Finite Length	19
9	Superposition of Cylindrical Uniform Loading by Measuring and Guard Cells	19
10	Classical Tranter Displacement Solution: $c/r_i = 5.0$; $c/r_i = 15.0$	23
11	Classical Tranter Displacement Solution: $c/r_i = 2.5$; $c/r_i = 7.5$	24
12	Ratio of Volume Displacements for Finite and Infinite Cylinder Loadings	25
13	Schmertmann's Recommended Vertical Strain Influence Factor Distribution	32
14	Pressuremeter Curve Illustrating the Various Moduli as Used in Ménard's Settlement Calculations	35

Figure		Page
15	Typical Element for Plane Strain Case	40
16	Typical Element for Axisymmetric Case	40
17	Hyperbolic Stress-Strain Curve	51
18	Transformed Hyperbolic Stress-Strain Curve	51
19	Successive Iterations Nonlinear Technique	53
20	Successive Increments Nonlinear Technique	53
21	Volumetric Strain vs. Axial Strain	59
22	Radial Strain vs. Axial Strain	59
23	Transformed Hyperbolic Axial-Radial Strain Curve	61
24	Variation of Initial Tangent Poisson Ratio with Confining Pressure	61
25	Typical Finite Element Grid for Strain Distribution Studies	68
26	Comparison of Vertical Strain Influence Factor Calculations as made by Classic Solution (SEPOL) and Finite Element Method for a Linear Elastic, Homogeneous, Isotropic Material Under Axisymmetric Flexible Loading	71
27	Vertical Strain Influence Factor Using SEPOL for Square Flexible Footing on Linear Elastic, Homogeneous, Isotropic Material	72
28	Comparison of Vertical Strain Influence Factor Calculations as made by Classic Solution (SEPOL) and Finite Element Method for a Linear Elastic, Homogeneous, Isotropic Material Under Plane Strain Flexible Loading	73
29	Comparison of Vertical Strain Influence Factor Calculations as made by Classic Rigid Circular Punch and Finite Element Method with Concrete Footing, for a Linear Elastic, Homogeneous, Isotropic Material under Axisymmetric Loading	76
30	Comparison of Vertical Strain Influence Factor Calculations as made by Classic Rigid Strip Punch and Finite Element Method with Concrete Footing, for a Linear Elastic, Homogeneous, Isotropic Material under Plane Strain Loading	79

Figure		Page
31	Recommended Triangular Vertical Strain Influence Factor Distributions Based on Study of Linear Elastic Materials Under Rigid Loading	88
32	Initial In-Situ Tangent Modulus vs. Depth, K = 15,000, $\phi = 32^{o}$, n = 0.5, $R_f = 0.85$, $\gamma = 100$ pcf (Simulated Typical Loose Sand)	91
33	Initial In-Situ Tangent Modulus vs. Depth, K = 30,000, $\phi = 37^{o}$, n = 0.5, $R_f = 0.85$, $\gamma = 100$ pcf (Simulated Typical Medium Dense Sand)	92
34	Initial In-Situ Tangent Modulus vs. Depth, K = 60,000, $\phi = 42^{o}$, n = 0.5, $R_f = 0.85$, $\gamma = 100$ pcf (Simulated Typical Dense Sand)	93
35	Vertical Centerline Strain Distribution for Axisymmetric Loading of 20 Ft Diameter Concrete Footing Using Minor Principal Stresses and Bulk Failure Condition; K = 60,000, $\nu = 0.30$, and $k_o = 0.50$	96
36	Vertical Centerline Strain Distribution for Axisymmetric Loading of 20 Ft Diameter Concrete Footing Using Minor Principal Stresses and Bulk Failure Condition; K = 60,000, $\nu = 0.40$, and $k_o = 0.50$	97
37	Vertical Centerline Strain Distribution for Axisymmetric Loading of 20 Ft Diameter Concrete Footing Using Minor Principal Stresses and Bulk Failure Condition; K = 60,000, $\nu = 0.48$, and $k_o = 0.50$	98
38	Centerline Vertical Strain Influence Factor for Axisymmetric Loading of 20 Ft Diameter Concrete Footing Using Minor Principal Stresses and Bulk Failure Condition; K = 60,000, $\nu = 0.30$, and $k_o = 0.50$	99
39	Centerline Vertical Strain Influence Factor for Axisymmetric Loading of 20 Ft Diameter Concrete Footing Using Minor Principal Stresses and Bulk Failure Condition; K = 60,000, $\nu = 0.40$, and $k_o = 0.50$	100
40	Centerline Vertical Strain Influence Factor for Axisymmetric Loading of 20 Ft Diameter Concrete Footing Using Minor Principal Stresses and Bulk Failure Condition; K = 60,000, $\nu = 0.48$, and $k_o = 0.50$	101

Figure		Page
41	Peak Vertical Centerline Strain Influence Factor for Concrete Footing on Nonlinear Material under Axisymmetric Loading as a Function of Surface Loading and Poisson's Ratio: K = 60,000; k_o = 0.50	103
42	Peak Vertical Centerline Strain Influence Factor for Flexible Axisymmetric Loading on Nonlinear Material as a Function of Surface Loading and Poisson's Ratio: K = 60,000; k_o = 0.50	104
43	Centerline Vertical Strain Influence Factor for 2000 Psf Axisymmetric Loading of 20 Ft Diameter Concrete Footing Using Minor Principal Stresses and Bulk Failure Condition: K = 60,000; k_o = 0.50	105
44	Centerline Vertical Strain Influence Factor for 4000 Psf Axisymmetric Loading of 20 Ft Diameter Concrete Footing Using Minor Principal Stresses and Bulk Failure Condition: K = 60,000; k_o = 0.50	106
45	Centerline Vertical Strain Influence Factor for 4000 Psf Axisymmetric Loading of 20 Ft Diameter Concrete Footing Using Octahedral Stresses and Bulk Failure Condition: K = 60,000; k_o = 0.50	108
46	Centerline Vertical Strain Influence Factor for 2000 Psf Axisymmetric Loading of 20 Ft Diameter Concrete Footing Using Minor Principal Stresses and Bulk Failure Condition: K = 30,000, k_o = 0.50	109
47	Peak Vertical Centerline Strain Influence Factor for Concrete Footing on Nonlinear Material under Axisymmetric Loading as a Function of Surface Loading and Poisson's Ratio: K = 30,000; k_o = 0.50	110
48	Peak Vertical Centerline Strain Influence Factor for Concrete Footing on Nonlinear Material under Axisymmetric Loading as a Function of Surface Loading and Poisson's Ratio: K = 15,000, k_o = 0.50	111
49	Centerline Vertical Strain Influence Factor Curves for Axisymmetric Loading of Varying Diameter Concrete Footings and 4000 Psf Loading: K = 60,000, ν = 0.40	114
50	Load vs. Settlement Curves for 20 Ft Diameter Concrete Footing on Dense Sand: K = 60,000	118
51	Load vs. Settlement Curves for 20 Ft Diameter Concrete Footing on Medium Dense Sand: K = 30,000	119

Figure		Page
52	Load vs. Settlement Curves for 20 Ft Diameter Concrete Footing on Loose Sand: K = 15,000	120
53	Load vs. Settlement Curves for Varying Diameter Concrete Footings	121
54	Vertical Centerline Strain Distribution for Plane Strain Loading of 20 Ft Wide Concrete Footing Using Minor Principal Stresses and Bulk Failure Condition; K = 60,000, ν = 0.30, and k_o = 0.50	123
55	Vertical Centerline Strain Distribution for Plane Strain Loading of 20 Ft Wide Concrete Footing Using Minor Principal Stresses and Bulk Failure Condition; K = 60,000, ν = 0.40, and k_o = 0.50	124
56	Vertical Centerline Strain Distribution for Plane Strain Loading of 20 Ft Wide Concrete Footing Using Minor Principal Stresses and Bulk Failure Condition; K = 60,000, ν = 0.48, and k_o = 0.50	125
57	Centerline Vertical Strain Influence Factor for Plane Strain Loading of 20 Ft Wide Concrete Footing Using Minor Principal Stresses and Bulk Failure Condition; K = 60,000, ν = 0.30, and k_o = 0.50	126
58	Centerline Vertical Strain Influence Factor for Plane Strain Loading of 20 Ft Wide Concrete Footing Using Minor Principal Stresses and Bulk Failure Condition; K = 60,000, ν = 0.40, and k_o = 0.50	127
59	Centerline Vertical Strain Influence Factor for Plane Strain Loading of 20 Ft Wide Concrete Footing Using Minor Principal Stresses and Bulk Failure Condition; K = 60,000, ν = 0.48, and k_o = 0.50	128
60	Peak Vertical Centerline Strain Influence Factor for Concrete Footing on Nonlinear Material under Plane Strain Loading as a Function of Surface Loading and Poisson's Ratio; K = 60,000, k_o = 0.50	130
61	Peak Vertical Centerline Strain Influence Factor for Flexible Plane Strain Loading on Nonlinear Material as a Function of Surface Loading and Poisson's Ratio; K = 60,000, k_o = 0.50	131
62	Centerline Vertical Strain Influence Factor for 2000 Psf Plane Strain Loading of 20 Ft Wide Concrete Footing Using Minor Principal Stresses and Bulk Failure Condition; K = 60,000, k_o = 0.50	133

Figure		Page
63	Centerline Vertical Strain Influence Factor for 4000 Psf Plane Strain Loading of 20 Ft Wide Concrete Footing Using Minor Principal Stresses and Bulk Failure Condition; K = 60,000, k_o = 0.50	134
64	Centerline Vertical Strain Influence Factor for 4000 Psf Plane Strain Loading of 20 Ft Wide Concrete Footing Using Octahedral Stresses and Bulk Failure Condition; K = 60,000, k_o = 0.50	135
65	Centerline Vertical Strain Influence Factor for 2000 Psf Plane Strain Loading of 20 Ft Wide Concrete Footing Using Minor Principal Stresses and Bulk Failure Condition; K = 30,000, k_o = 0.50	136
66	Peak Vertical Centerline Strain Influence Factor for Concrete Footing on Nonlinear Material under Plane Strain Loading as a Function of Surface Loading and Poisson's Ratio; K = 30,000, k_o = 0.50	137
67	Peak Vertical Centerline Strain Influence Factor for Concrete Footing on Nonlinear Material under Plane Strain Loading as a Function of Surface Loading and Poisson's Ratio; K = 15,000, k_o = 0.50	138
68	Centerline Vertical Strain Influence Factor Curves for Plane Strain Loading of Varying Width Concrete Footings and 4000 Psf Loading: K = 60,000, ν = 0.40	140
69	Load vs. Settlement Curves for 20 Ft Wide Concrete Footing on Dense Sand: K = 60,000	143
70	Load vs. Settlement Curves for 20 Ft Wide Concrete Footing on Medium Dense Sand: K = 30,000	144
71	Load vs. Settlement Curves for 20 Ft Wide Concrete Footing on Loose Sand: K = 15,000	145
72	Load vs. Settlement Curves for Varying Width Concrete Footings	146
73	Comparison of Axisymmetric and Plane Strain Load vs. Settlement Curves on Medium Dense Sand: K = 30,000, D = 20 Ft	150
74	Comparison of Axisymmetric and Plane Strain Load vs. Settlement Curves on Dense Sand: K = 60,000, D = 20 Ft	151

Figure		Page
75	Centerline Vertical Strain Influence Factor for 4000 Psf Axisymmetric Loading of 20 Ft Diameter Concrete Footing Using Minor Principal Stresses and Bulk Failure Condition; K = 60,000, k_o = 1.00	154
76	Peak Vertical Centerline Strain Influence Factor for Concrete Footing on Nonlinear Material under Axisymmetric Loading as a Function of Surface Loading and Poisson's Ratio; K = 60,000, k_o = 1.00	156
77	Centerline Vertical Strain Influence Factor for 4000 Psf Plane Strain Loading of 20 Ft Wide Concrete Footing Using Minor Principal Stresses and Bulk Failure Condition; K = 60,000, k_o = 1.00	157
78	Peak Vertical Centerline Strain Influence Factor for Concrete Footing on Nonlinear Material under Plane Strain Loading as a Function of Surface Loading and Poisson's Ratio; K = 60,000, k_o = 1.00	159
79	Load vs. Settlement Curves for Axisymmetric and Plane Strain Loading on Dense and Medium Dense Sand: D = 20 Ft; k_o = 1.00	160
80	Comparison of Centerline Vertical Strain Influence Factor for 4000 Psf Axisymmetric Loading of 20 Ft Diameter Concrete Footing with Varying k_o Values: K = 60,000, ν = 0.40	161
81	Centerline Vertical Strain Influence Factor for Axisymmetric Loading of 20 Ft Diameter Concrete Footing on Linear Elastic Material with Rigid Layer at a Depth of 20 Ft	165
82	Centerline Vertical Strain Influence Factor for Axisymmetric Loading of 20 Ft Diameter Concrete Footing on Linear Elastic Material with Rigid Layer at a Depth of 40 Ft	165
83	Centerline Vertical Strain Influence Factor for Axisymmetric Loading of 20 Ft Diameter Concrete Footing on Linear Elastic Material with Rigid Layer at a Depth of 60 Ft	166
84	Comparison of Centerline Vertical Strain Influence Factor for Axisymmetric Loading of 20 Ft Diameter Concrete Footing on Linear Elastic Material with Rigid Layer at Varying Depths: ν = 0.40	167

Figure		Page
85	Centerline Vertical Strain Influence Factor for 4000 Psf Axisymmetric Loading of 20 Ft Diameter Concrete Footing Using Minor Principal Stresses and Bulk Failure Condition with Rigid Layer at a Depth of 20 Ft; K = 60,000	169
86	Centerline Vertical Strain Influence Factor for 4000 Psf Axisymmetric Loading of 20 Ft Diameter Concrete Footing Using Minor Principal Stresses and Bulk Failure Condition with Rigid Layer at a Depth of 40 Ft; K = 60,000	169
87	Centerline Vertical Strain Influence Factor for 4000 Psf Axisymmetric Loading of 20 Ft Diameter Concrete Footing Using Minor Principal Stresses and Bulk Failure Condition with Rigid Layer at a Depth of 60 Ft; K = 60,000	170
88	Comparison of Centerline Vertical Strain Influence Factor for 4000 Psf Axisymmetric Loading of 20 Ft Diameter Concrete Footing Using Minor Principal Stresses and Bulk Failure Condition with Rigid Layers at Varying Depths: K = 60,000; ν = 0.40	171
89	Load vs. Settlement Curves for 20 Ft Diameter Concrete Footing on Dense Sand with Rigid Layer at Varying Depths: K = 60,000, ν = 0.48, k_o = 0.5	173
90	Load vs. Settlement Curves for 10 and 50 Ft Diameter Concrete Footings on Dense Sand with Rigid Layers at Varying Depths: K = 60,000, ν = 0.48, k_o = 0.5	175
91	Centerline Vertical Strain Influence Factor for axisymmetric Loading of 20 Ft Diameter Concrete Footing with 10 Ft Thick Rigid Layer (K = 60,000) at Various Depths and 4000 Psf Loading; K = 30,000, ν = 0.40, and k_o = 0.50	176
92	Effect of Rigid Surface Layer (K = 60,000) of Varying Thickness over Loose Deposit (K = 15,000) for 20 Ft Diameter Concrete Footing Under 4000 Psf Axisymmetric Loading	177
93	Centerline Vertical Strain Influence Factor for Plane Strain Loading of 20 Ft Wide Concrete Footing on Linear Elastic Material with Rigid Layer at a Depth of 20 Ft	179

Figure		Page
94	Centerline Vertical Strain Influence Factor for Plane Strain Loading of 20 Ft Wide Concrete Footing on Linear Elastic Material with Rigid Layer at a Depth of 40 Ft	179
95	Centerline Vertical Strain Influence Factor for Plane Strain Loading of 20 Ft Wide Concrete Footing on Linear Elastic Material with Rigid Layer at a Depth of 60 Ft	180
96	Comparison of Centerline Vertical Strain Influence Factor for Plane Strain Loading of 20 Ft Wide Concrete Footing on Linear Elastic Material with Rigid Layer at Varying Depths: $\nu = 0.40$	181
97	Centerline Vertical Strain Influence Factor for 4000 Psf Plane Strain Loading of 20 Ft Wide Concrete Footing Using Minor Principal Stresses and Bulk Failure Condition with Rigid Layer at a Depth of 20 Ft; K = 60,000	183
98	Centerline Vertical Strain Influence Factor for 4000 Psf Plane Strain Loading of 20 Ft Wide Concrete Footing Using Minor Principal Stresses and Bulk Failure Condition with Rigid Layer at a Depth of 40 Ft; K = 60,000	183
99	Centerline Vertical Strain Influence Factor for 4000 Psf Plane Strain Loading of 20 Ft Wide Concrete Footing Using Minor Principal Stresses and Bulk Failure Condition with Rigid Layer at a Depth of 60 Ft; K = 60,000	184
100	Comparison of Centerline Vertical Strain Influence Factor for 4000 Psf Plane Strain Loading of 20 Ft Wide Concrete Footing Using Minor Principal Stresses and Bulk Failure Condition with Rigid Layers at Varying Depths: K = 60,000; $\nu = 0.40$	185
101	Load vs. Settlement Curves for 20 Ft Wide Concrete Footing on Dense Sand with Rigid Layer at Varying Depths: K = 60,000, $\nu = 0.48$, $k_o = 0.5$	186
102	Load vs. Settlement Curves for 10 and 50 Ft Wide Concrete Footings on Dense Sand with Rigid Layers at Varying Depths: K = 60,000, $\nu = 0.48$, $k_o = 0.5$	187

Figure		Page
103	Centerline Vertical Strain Influence Factor for Plane Strain Loading of 20 Ft Wide Concrete Footing with 10 Ft Thick Rigid Layer (K = 60,000) at Various Depths and 4000 Psf Loading; K = 30,000, ν = 0.40, and k_o = 0.50	189
104	Steps in Unloading and Reloading Foundation for Embedment Studies	191
105	Centerline Vertical Strain Influence Factor for Axisymmetric Loading of 20 Ft Diameter Concrete Footing Embedded 5 Ft into Linear Elastic Material	193
106	Centerline Vertical Strain Influence Factor for Axisymmetric Loading of 20 Ft Diameter Concrete Footing Embedded 10 Ft into Linear Elastic Material	194
107	Centerline Vertical Strain Influence Factor for Axisymmetric Loading of 20 Ft Diameter Concrete Footing Embedded 15 Ft into Linear Elastic Material	195
108	Centerline Vertical Strain Influence Factor for 4000 Psf Axisymmetric Loading of 20 Ft Diameter Concrete Footing Embedded 5 Ft into Nonlinear Elastic Material: K = 60,000	196
109	Centerline Vertical Strain Influence Factor for 4000 Psf Axisymmetric Loading of 20 Ft Diameter Concrete Footing Embedded 10 Ft into Nonlinear Elastic Material: K = 60,000	197
110	Centerline Vertical Strain Influence Factor for 4000 Psf Axisymmetric Loading of 20 Ft Diameter Concrete Footing Embedded 15 Ft into Nonlinear Elastic Material: K = 60,000	198
111	Load vs. Settlement Curves for 5 Ft Embedment of 20 Ft Diameter Concrete Footing in Dense Sand: K = 60,000, ν = 0.48, k_o = 0.5	202
112	Load vs. Settlement Curves for 10 Ft Embedment of 20 Ft Diameter Concrete Footing in Dense Sand: K = 60,000, ν = 0.48, k_o = 0.5	203
113	Load vs. Settlement Curves for 15 Ft Embedment of 20 Ft Diameter Concrete Footing in Dense Sand: K = 60,000, ν = 0.48, k_o = 0.5	204
114	Centerline Vertical Strain Influence Factor for Plane Strain Loading of 20 Ft Wide Concrete Footing Embedded 5 Ft into Linear Elastic Material	206

Figure		Page
115	Centerline Vertical Strain Influence Factor for Plane Strain Loading of 20 Ft Wide Concrete Footing Embedded 10 Ft into Linear Elastic Material	207
116	Centerline Vertical Strain Influence Factor for Plane Strain Loading of 20 Ft Wide Concrete Footing Embedded 15 Ft into Linear Elastic Material	208
117	Centerline Vertical Strain Influence Factor for 4000 Psf Plane Strain Loading of 20 Ft Wide Concrete Footing Embedded 5 Ft into Nonlinear Elastic Material: K = 60,000	209
118	Centerline Vertical Strain Influence Factor for 4000 Psf Plane Strain Loading of 20 Ft Wide Concrete Footing Embedded 10 Ft into Nonlinear Elastic Material: K = 60,000	210
119	Centerline Vertical Strain Influence Factor for 4000 Psf Plane Strain Loading of 20 Ft Wide Concrete Footing Embedded 15 Ft into Nonlinear Elastic Material: K = 60,000	211
120	Load vs. Settlement Curves for 5 Ft Embedment of 20 Ft Wide Concrete Footing in Dense Sand: K = 60,000, $\nu = 0.48$, $k_o = 0.5$	212
121	Load vs. Settlement Curves for 10 Ft Embedment of 20 Ft Wide Concrete Footing in Dense Sand: K = 60,000, $\nu = 0.48$, $k_o = 0.5$	213
122	Load vs. Settlement Curves for 15 Ft Embedment of 20 Ft Wide Concrete Footing in Dense Sand: K = 60,000, $\nu = 0.48$, $k_o = 0.5$	214
123	Comparison of Vertical Strain Influence Factor Beneath Center and Edge of Rigid Footing on Linear Elastic Material under Axisymmetric Loading: $\nu = 0.40$	216
124	Comparison of Vertical Strain Influence Factor Beneath Center and Edge of Rigid Footing on Linear Elastic Material under Plane Strain Loading: $\nu = 0.40$	217
125	Comparison of Vertical Strain Influence Factor Beneath Center and Edge of Rigid Footing on Nonlinear Elastic Material under 4000 Psf Axisymmetric Loading: K = 60,000; $\nu = 0.40$	218

Figure		Page
126	Comparison of Vertical Strain Influence Factor Beneath Center and Edge of Rigid Footing on Nonlinear Elastic Material under 4000 Psf Plane Strain Loading: $K = 60{,}000$; $\nu = 0.40$	219
127	Recommended Triangular Strain Influence Factor Distribution for Sands	223
128	Example Settlement Problem	225
129	Background Calculations for Figure 128	226
130	Typical Finite Element Grid for Pressuremeter Finite Element Study	231
131	Comparison of Finite Element and Classic Pressuremeter Displacements; $E = 50$ Tsf, $\nu = 0.30$	232
132	Comparison of Finite Element and Classic Pressuremeter Displacements; $E = 50$ Tsf, $\nu = 0.40$	233
133	Comparison of Pressuremeter Centerline Displacements for Infinite Cylinder, Finite Element, and Classic Tranter Solutions: $c/r_i = 5$	235
134	Example of Finite Element Program Unloading of Borehole	237
135	Pressuremeter Loading of Linear Elastic Material with $E = 50$ Tsf and Varying Poisson's Ratios	240
136	Pressuremeter Loading of Linear Elastic Material with $E = 50$ Tsf, $\nu = 0.30$, and Varying Differential Pressures	243
137	Pressuremeter Loading of Unloaded Linear Elastic Material with $E = 50$ Tsf, $\nu = 0.30$, $k_o = 0.50$, and Varying Depths	244
138	Pressuremeter Loading of Unloaded Linear Elastic Material with $E = 50$ Tsf, $\nu = 0.30$, and Varying Depths for Lateral Stress Coefficients (k_o) of 0.50 and 1.00	246
139	Pressuremeter Loading of Cross-Anisotropic Linear Elastic Materials with $\nu = 0.30$	248
140	Pressuremeter Loading of Linear Elastic Material with $E = 50$ Tsf, $\nu = 0.30$, and Varying Widths of a Smear Zone with $E = 25$ Tsf	250

Figure		Page
141	Modulus Calculations as a Function of Width of Smear Zone in Linear Elastic Material with $\nu = 0.30$	251
142	Effect of Unloading and Reloading Pressuremeter in Linear Elastic Material with E = 50 Tsf, $\nu = 0.30$	253
143	Comparison of Effect of Pressure Increment and Failure Modulus in Pressuremeter Loading of Nonlinear Material Using Minor Principal Stresses: K = 60,000, $\nu = 0.40$, $k_o = 0.50$, Depth = 7 Ft	257
144	Comparison of Effect of Using Minor Principal and Octahedral Stresses in Pressuremeter Loading of Nonlinear Material: K = 60,000, $\nu = 0.40$, $k_o = 0.50$, Depth = 7 Ft	260
145	Mohr's Circle Representations of Stresses in Soil at Centerline of Pressuremeter Initially and After Loading: K = 60,000; $\nu = 0.40$	262
146	Maximum Shear Stress Contours Under Measuring Cell Pressure of 3 Psi: K = 60,000; $\nu = 0.40$; Depth = 7 Ft	263
147	Maximum Shear Stress Contours Under Measuring Cell Pressure of 6 Psi: K = 60,000; $\nu = 0.40$; Depth = 7 Ft	264
148	Maximum Shear Stress Contours Under Measuring Cell Pressure of 10 Psi: K = 60,000; $\nu = 0.40$; Depth = 7 Ft	265
149	Comparison of Effect of Varying Differential Pressure Using Minor Principal Stresses and Bulk Failure Condition: K = 60,000; $\nu = 0.40$	267
150	Comparison of Effect of Varying Nonlinear Modulus Numbers in Pressuremeter Loading: $\nu = 0.40$; Depth = 7 Ft	273
151	Comparison of Effect of Varying Poisson's Ratio in Pressuremeter Loading: K = 30,000; Depth = 7 Ft	275
152	Comparison of Effect of Varying Poisson's Ratio in Pressuremeter Loading: K = 60,000; Depth = 7 Ft	276
153	Effect of Varying the Angle of Friction in Pressuremeter Loading: K = 60,000; $\nu = 0.40$; Depth = 7 Ft	279

Figure		Page
154	Comparison of Similar Pressure-Volume Curves in Pressuremeter Loading Using Different Nonlinear Analysis Parameters	282
155	Effect of Increasing Lateral Stress Coefficient in Pressuremeter Loading: $\nu = 0.40$; Depth = 7 Ft	284
156	Effect of Varying Depth in Pressuremeter Loading: K = 60,000; $\nu = 0.40$	286
157	Effect of Smear Zone Width on Pressuremeter Loading in Nonlinear Elastic Material: K = 60,000; $\nu = 0.40$; Depth = 7 Ft	289
158	Effect of Borehole Unloading on Pressuremeter Loading: K = 60,000; $\nu = 0.40$; Depth = 7 Ft	292
159	Mohr's Circle Representations of Stresses in Soil at Centerline of Pressuremeter After Borehole Unloading and Pressuremeter Loading: K = 60,000; $\nu = 0.40$	294
160	Effect of Initial Pressure Increment on Pressuremeter Loading: K = 60,000; $\nu = 0.40$; Depth = 7 Ft	297
161	Pressuremeter Loading Curves for Varying Poisson's Ratios and Depths Including Effect of Borehole Unloading, Minor Principal Stresses, and Bulk Failure Condition: K = 60,000; $k_o = 0.50$	301
162	Effect of Unloading and Reloading the Pressuremeter Test: Borehole Not Unloaded: K = 60,000; $\nu = 0.40$; Depth = 7 Ft	303
163	Effect of Unloading and Reloading the Pressuremeter Test: Borehole Unloaded: K = 60,000; $\nu = 0.40$; Depth = 7 Ft	304
164	Simplified Sketch of University of Florida Sand Testing Chamber	311
165	Finite Element Grid for Chamber Pressuremeter Study	316
166	Comparison of Finite Element and Laboratory Pressuremeter Tests in Dense Edgar Sand: K = 53,600; $\phi = 42^{o}$; $k_o = 0.444$; Depth = 7 Ft; Differential Pressure = 1 Psi	317

Figure		Page
167	Comparison of Finite Element and Laboratory Pressuremeter Tests in Medium Dense Edgar Sand: $\phi = 36^{o}$; $k_o = 0.467$; $\nu = 0.318$; Depth = 7 Ft; Differential Pressure = 1 Psi	318
168	Finite Element Grid for Analysis of Plate Load Test in Chamber	323
169	Comparison of Finite Element, Settlement, and Plate Load Test Results in Dense Sand: K = 53,600; $\nu = 0.48$	326
170	Comparison of Finite Element, Settlement, and Plate Load Test Results in Medium Dense Sand: K = 41,100; $\nu = 0.48$	327
171	Results of Laboratory Model Footing Settlement Tests on Ottawa Sand	331

LIST OF SYMBOLS AND ABBREVIATIONS

a	Radius of circular punch
a	Hyperbolic stress-strain parameter
A	Integration constant
A	$\frac{E_v}{(1+\nu_h)(1-\nu-2n\nu_v^2)}$
b	Hyperbolic stress-strain parameter
B	Integration constant
B	Bulk Modulus
c	One-half loaded length
c	Soil cohesion
C	Constant
cm	Centimeter
CPT	Cone Penetration Test
C_1	Schmertmann's Embedment Correction Factor
C_f	Constant in Peak Strain Factor Formula
C_i	Constant in Peak Strain Factor Formula
C_u	Coefficient of Uniformity
D	Footing Diameter (Axisymmetric)
D	Footing Width (Plane Strain)
D	Least footing dimension
D'	Depth of Embedment
D_{10}	Effective Diameter

E	Elastic Modulus
E_i	Initial Tangent Modulus
E_v	Vertical Elastic Modulus
E_h	Horizontal Elastic Modulus
E_m	Micro-deformation Modulus
E_a	Unloading Modulus
E^+	Reloading or Volumetric Modulus
E_p	Elastic Modulus of Footing
E_{ps}	Elastic Modulus under Plane Strain Loading
E_{tr}	Elastic Modulus under Triaxial Loading
E_{PMT}	Elastic Modulus from pressuremeter test
E_{PMTU}	Elastic Modulus from pressuremeter test including higher order displacement terms
E_{TWC}	Elastic Modulus from thick-walled cylinder analysis
E_s	Elastic Modulus of subgrade
E_t	Tangent Elastic Modulus
E_{to}	Initial Tangent Elastic Modulus
f	Hyperbolic parameter
F	Empirical parameter
Ft,ft	Feet
G	Empirical parameter
G	Shear Modulus
G_h	Horizontal Shear Modulus
G_v	Vertical Shear Modulus
h	Depth
H	Thickness of footing
I_w	Settlement Influence Factor

I_s	Surface Intercept Strain Factor
I_z	Vertical Strain Influence Factor
I_{zp}	Peak Vertical Strain Influence Factor
j	Hyperbolic parameter
Kg, kg	Kilogram
k_o	Lateral stress coefficient
K	Nonlinear Modulus Number
K_r	Rigidity Factor
Ksf, ksf	Kips per square foot
K_{ur}	Unload-Reload Modulus Number
K_o	Modified Bessel Function of Second Kind and Order 0
K_1	Modified Bessel Function of Second Kind and Order 1
[k]	Stiffness Matrix
L	Length of measuring cell
L	Length of footing
m	G_v/E_v
n	Exponent
p	Pressure
p_a	Unit pressure
p_i	Inside pressure
p_o	Outside pressure
p_o	In-situ vertical pressure
p_L	Limit pressure
Δp	Differential pressure
Δp	Foundation load - In-situ vertical pressure
PBT	Plate Bearing Test
PMT	Pressuremeter Test

Pcf,pcf	Pounds per cubic foot
Psf,psf	Pounds per square foot
Psi,psi	Pounds per square inch
PRESMETR	Finite Element Pressuremeter Computer Program
q	Pressure
r	Radius
r	Radial coordinate
r_i	Inside radius
r_o	Outside radius
{R}	Force Vector
R_f	Failure Ratio
R	Radius of footing
SEPOL	Settlement Computer Program
SOILSTRN	Finite Element Strain Study Computer Program
SPT	Standard Penetration Test
SYM	Symmetrical
Tsf,tsf	Tons per square foot
u	Radial displacement
{u}	Displacement Vector
u_{ave}	Average radial displacement
u_r	Radial displacement
V	Volume
ΔV	Volume change
V_o	Initial volume
w	Vertical displacement
w_l	Elastic settlement

w_2	Deviatoric stress tensor settlement
w_3	Consolidation settlement
z	Vertical coordinate
Δz	Layer thickness
α	Variable of integration
α	$(E_{PMT}/E_a)^{\frac{1}{2}}$
ε	Strain
ε_a	Axial Strain
ε_r	Radial Strain
ε_v	Vertical strain
ε_z	Vertical strain
γ	Unit weight of soil
η	E_h/E_v
λ_1	Shape Factor
λ_2	Shape Factor
μ	Exponent
ν	Poisson's Ratio
ν_i	Initial Poisson's Ratio
ν_h	Horizontal Poisson's Ratio
ν_v	Vertical Poisson's Ratio
ν_p	Poisson's ratio of footing
ν_s	Poisson's ratio of subgrade
ν_{ps}	Poisson's ratio for plane strain loading
ν_{tr}	Poisson's ratio for triaxial loading
π	Pi
ρ	Settlement

σ	Normal stress
σ_θ	Tangential normal stress
σ_r	Radial normal stress
σ_z	Vertical normal stress
σ_1	Major principal stress
σ_2	Intermediate principal stress
σ_3	Minor principal stress
σ_{oct}	Octahedral normal stress
$\sigma_1-\sigma_3$	Deviator stress
$(\sigma_1-\sigma_3)_{ult}$	Ultimate deviator stress
$(\sigma_1-\sigma_3)_f$	Failure deviator stress
τ	Shear stress
τ_{max}	Maximum shear stress
θ	Circumferential angle
ϕ	Angle of friction
%	Percent

Abstract of Dissertation Presented to the Graduate Council
of the University of Florida in Partial Fulfillment of
the Requirements for the Degree of Doctor of Philosophy

FINITE ELEMENT PARAMETRIC STUDY OF VERTICAL STRAIN INFLUENCE FACTORS AND THE PRESSUREMETER TEST TO ESTIMATE THE SETTLEMENT OF FOOTINGS IN SAND

By

John Paul Hartman

March, 1974

Chairman: Dr. John H. Schmertmann
Major Department: Civil Engineering

The purpose of this study is two-fold: (a) to determine analytically the factors involved in using the vertical strain distribution approach for settlement prediction in sands and how to determine the best vertical strain distribution, and (b) to determine how the pressuremeter test can be best interpreted for use in using this vertical strain distribution approach.

The strain distribution studies are based on the work of Schmertmann and provide analytical corroboration of his simplified approach. Using a nonlinear modulus analytical sand model originally developed by Duncan and Chang, this study shows the factors which affect the strain distribution. The major factors include (1) Poisson's ratio, (2) the surface loading pressure, and (3) the footing geometry and nature of the loading, whether plane strain or axisymmetric.

A recommendation is made with respect to the form of the peak

strain factor for both plane strain and axisymmetric loadings as well as the depth of influence, location of the peak strain influence factor, and surface intercept value. These recommendations are made for loose, medium dense, and dense sand conditions. Using the normalized strain distribution approach, the writer recommends that no correction be made for the effect of lateral stresses or rigid layers. Shallow embedment studies indicate that the form of the simplified strain distribution remains the same, but some correction must be made for embedment. The writer recommends that Schmertmann's suggested correction be used or that the previously recommended peak strain influence factor relations be reduced.

The pressuremeter studies show that pressuremeter loading of a nonlinear material similar to a sand cannot be meaningfully explained by a simple one-dimensional analysis. Any test results must be interpreted with respect to (a) nonlinear modulus values, (b) Poisson's ratio, (c) measuring cell and pressuremeter geometries, (d) degree of borehole disturbance determined by borehole unloading, (e) the differential pressure magnitude, (f) the in-situ lateral stresses, and (g) possible anisotropic effects. These influences can cause large variations in the modulus as obtained from field tests. In all cases, however, the analytical model used gave results consistent with the assumptions and model parameters. The low modulus initial portion of a typical field pressure-volume curve can best be explained as being due to the effects of reloading against the inside of an unloaded borehole.

Although the initial portion of an unloaded borehole pressure-volume curve is perhaps the best indication of the initial in-situ

tangent modulus, the relatively flat portion of the pressure-volume curve resulting from the loading of an unloaded borehole is more commonly encountered in field work. This flatter slope modulus is generally higher than the initial in-situ tangent modulus. The studies indicate that perhaps an unload-reload cycle within the pressuremeter test might give a more consistent modulus for possible use in settlement and other analyses.

Controlled laboratory test results for pressuremeter and plate bearing tests on a specific sand are compared with the analytical sand models and indicate reasonable similarities.

CHAPTER 1.0

INTRODUCTION

The need for economical, rapid, and meaningful in-situ field exploration techniques in the civil engineering discipline of soil mechanics and foundation engineering has become increasingly important. Theoretical work and sophisticated laboratory testing have tended more and more toward basic research and have left a wide gap in our knowledge of field conditions which are necessary for design. Although some projects have budgets which can allow for highly sophisticated analyses and tests, the majority of civil works must be constructed using field information which is often quite limited. Unfortunately, this is often the only information available for design purposes and can result in large safety factors and uneconomical design. In other cases, overconfidence in such field data can result in a foundation design which is marginal at best, and later may require remedial work.

The problems associated with obtaining meaningful design data in cohesionless soils such as sand and silt are even more complex. It is difficult to field sample such materials in any condition, much less obtain an "undisturbed" sample. Early studies in the field of soil mechanics emphasized the engineering properties of cohesive materials. As a result, much of the information engineers have concerning the behavior of cohesionless soils is either (1) empirical, based on years of field testing, or (2) experimental, based

on controlled laboratory studies of reconstructed or specially constructed cohesionless samples.

In the past few years, however, there has been an increasing interest in the performance of structures on cohesionless soils. This reinterest is for several reasons. In many areas of the world there is accelerated construction of large civil works on soils which are predominantly cohesionless. This is true of Florida and much of the Caribbean area. As foundation design engineers have worked on such structures there has been an awareness of the lack of meaningful data for such design, and especially the lack of settlement prediction data. Although settlements in cohesionless materials are usually less than in cohesive soils (or at least soft, cohesive soils), settlement does occur and the resulting differential settlements can be harmful to structures not adequately designed.

Two specific needs in the area of soil mechanics can thus be identified: (1) A need for more meaningful field data in cohesionless materials, and (2) a need for better settlement predictive techniques in cohesionless materials.

Two in-situ field exploration techniques which meet the above needs in different ways have been developed in Europe and are slowly being reintroduced into the United States (Calhoon, 1969: Schmertmann, 1967). The static cone penetration test (CPT) consists of forcing a steel rod approximately 1.4 inches in diameter into the soil. The tip resistance is then measured and on certain models the frictional resistance on a sleeve located above the tip is also measured. De Ruiter (1971) gives further information on both mechanical and electrical cone penetration equipment. The pressuremeter test (PMT)

is based on the lateral expansion of an approximately 2 foot long probe within a borehole. The pressure and volume change measurements of the probe are then used to calculate various soil parameters. This equipment will be described in greater detail in a later section. The pressuremeter test does have the advantage in that in making the hole a sample is obtained, whereas in using the cone, separate samples are required in order to visually examine the material. In addition, the pressuremeter test has been based on a simple elastic analysis, while the cone test is currently empirical.

For several decades what little sand settlement prediction has been done in the United States has been based on field results using empirical data obtained from the Standard Penetration Test (SPT). This method of prediction has been quite unsatisfactory for a variety of reasons. Fletcher (1965) and de Mello (1971) give a thorough analysis of this test including the discrepancies and weak points.

Schmertmann (1970) has given a thorough presentation of the use of cone penetration data to predict sand settlements. The supporting documentation is very thorough and gives results much more reasonable than those obtained using Standard Penetration Test data. De Mello (1971) also suggests that the cone penetration test is more satisfactory for making sand settlement predictions than the Standard Penetration Test. It appears currently (1973), however, that until a satisfactory theoretical analysis can be developed for the static cone penetration phenomenon, the use of this test for material property predictions will remain empirical.

Since there are various analytical approaches which might be used to analyze the pressuremeter test as well as the settlement of sands,

it might be possible to model the field conditions and compare the analytical results of the pressuremeter test with the settlement predictions as an aid to understanding their interrelationship. Although sand settlement and the pressuremeter test have been analyzed using one-dimensional linear elasticity, both problems are actually complex three-dimensional boundary value problems dealing with nonlinear materials. Classical mathematical solutions for such cases are extremely difficult, if not impossible.

In the late 1950s a powerful analytical approximation technique, the finite element method, was developed. The method is based on breaking the elastic continuum into a large structural grid and then using standard structural matrix techniques for solution of the equilibrium equations. The technique has been applied to a variety of problems in continuum mechanics. Its one major advantage is that it can model very complex geometries, boundary conditions, and material properties, providing, of course, that the appropriate boundary constraints and material property parameters can be developed. The technique uses very large matrices and can only be used in conjunction with a high speed, large core computer. Hand solutions for any but the most trivial cases are impossible.

This study uses the finite element method to analyze the pressuremeter test in sand, as well as the settlement of isolated footings on sand. These analyses are then used for the following major purposes: (1) To determine analytically the factors involved in using the vertical strain distribution approach for settlement prediction in sands and how to determine the best vertical strain distribution, and (2) To determine how the pressuremeter test can be best interpreted

for use in using this vertical strain distribution approach. The study will consider both the interpretation of the results of pressuremeter analytical studies on a model sand in conjunction with the results of strain distribution studies on similar model sands.

Finally, the results of laboratory plate settlement tests are compared with predictions using the methods developed. Users' manuals and computer program listings are included in the appendices.

CHAPTER 2.0

BACKGROUND ANALYTICAL WORK

2.1 The Pressuremeter Test

2.1.1 The Classic One-Dimensional Analysis

Perhaps the first description of a form of the pressuremeter was given by Kögler prior to World War II, but Ménard (1956) is credited with its development. Although there have been refinements and design changes in the past 15 years, the basic principles of the device remain the same.

Figure 1 gives a schematic representation of the pressuremeter. A probe consisting of a measuring cell and two guard cells is lowered into a pre-bored hole. The pressure is increased on an incompressible fluid (usually water) in the cells and the resulting volume change in the measuring cell is then noted for each pressure. Usually the guard cells are maintained at a slightly lower pressure than the measuring cell and their purpose is primarily to keep the hole from collapsing and to assure a uniform cylindrical expansion of the measuring cell. There has also been a pressuremeter developed which will bore its own hole as it goes in the ground. The operation of this device is similar, but it has no guard cells (Baguelin et al., 1972).

The resulting pressure-volume curve from a field test is given in Figure 2. The three regions characteristic of each curve have been

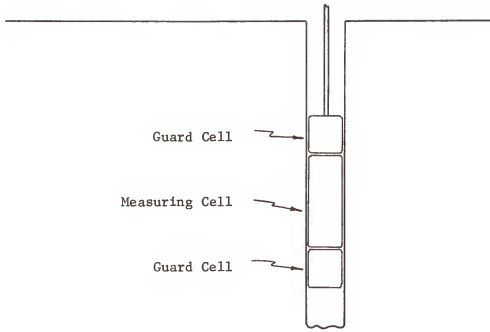


Figure 1. Schematic of Pressuremeter Loading in Borehole

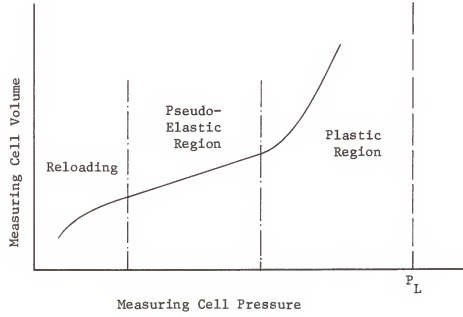


Figure 2. Pressuremeter Test Pressure-Volume Curve

identified by various engineers. In general, however, the first region is considered the reloading to the existing horizontal in-situ stress level, the second region is the elastic or pseudo-elastic expansion region, and the third region is the plastic or elastic-plastic region which ends at a limit pressure where the borehole expands indefinitely with no increase in pressure. The pressure at which this occurs is referred to as the limit pressure, P_L.

The standard equation used with this field curve to determine the elastic modulus of the soil being tested is given by:

$$E_{PMT} = 2 (1 + \nu) V_o (p_i / \Delta V) \quad (1)$$

where: E_{PMT} = Elastic Modulus determined from the pressuremeter test.

ν = Poisson's Ratio

V_o = Initial volume of the measuring cell

p_i = Pressure for a given volume change

ΔV = Volume change for a given pressure

The derivation of this relationship is based on the axially symmetric expansion of a circular opening and is thus a two-dimensional problem, although the axially symmetric assumption reduces the expansion to a one-dimensional geometric dependence upon the radial distance only. This derivation is used for either clays or sands, when assumed to be isotropic, linearly elastic, and homogeneous.

There are many ways to derive Equation 1 (Gibson and Anderson, 1961; Ménard, 1956). A method using the basic relations of the theory of elasticity follows (Boresi, 1965). Consider the uniform cylindrical expansion of a hole as illustrated in Figure 3. The

equilibrium equation for this axisymmetric condition with no body forces is

$$\frac{\delta \sigma_r}{\delta r} + \frac{\sigma_r - \sigma_\theta}{r} = 0 \qquad (2)$$

where: σ_r = radial stress

σ_θ = tangential stress

r = radial distance

The stress-displacement relations for an isotropic elastic material for the cylindrical case can be written:

$$\sigma_r = \frac{E}{(1+\nu)(1-2\nu)} \left(\nu \frac{u}{r} + (1-\nu)\frac{\delta u}{\delta r} \right) \qquad (3)$$

$$\sigma_\theta = \frac{E}{(1+\nu)(1-2\nu)} \left(\nu \frac{\delta u}{\delta r} + (1-\nu) \frac{u}{r} \right) \qquad (4)$$

where: E = Elastic Modulus

ν = Poisson's Ratio

u = radial displacement

By differentiating Equation 3 and then substituting the result as well as Equations 3 and 4 into Equation 2, the following differential equation is obtained:

$$\frac{\delta^2 u}{\delta r^2} + \frac{1}{r}\frac{\delta u}{\delta r} - \frac{u}{r^2} = 0 \qquad (5)$$

This is recognized as a linear, homogeneous, second order differential equation.

The general solution of Equation 5 is

$$u = \frac{A}{r} + Br \qquad (6)$$

where: A, B = constants to be determined from the specific boundary conditions

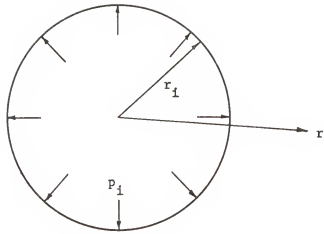


Figure 3. Geometry for Uniform Cylindrical Expansion in an Infinite Elastic Medium

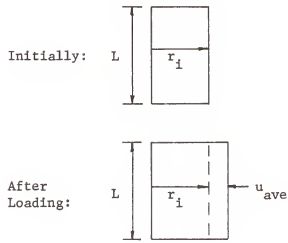


Figure 4. Geometry for Average Radial Displacement and Volume Relationship for Measuring Cell

For the case of cylindrical expansion in an infinite medium, the first boundary requirement is that as the radius increases to infinity, the displacement, u, must equal zero. Thus,

$$\underset{r \to \infty}{\text{Limit}} \left(\frac{A}{r} + Br \right) = 0 \tag{7}$$

This can only be possible if the constant B equals 0. Thus the general solution reduces to:

$$u = A/r \tag{8}$$

For the second boundary condition, it is noted that the radial stress at the inner radius, r_i, is the loading pressure, p_i. Thus,

$$\sigma_r = - p_i \qquad \text{at } r = r_i \tag{9}$$

where the negative sign is because of the compressive loading. By differentiating Equation 8, substituting in Equation 3, and applying the boundary conditions of Equation 9, the constant A is obtained:

$$A = \frac{p_i (1 + \nu) r_i^2}{E} \tag{10}$$

The general displacement as a function of radial distance is thus

$$u(r) = \frac{p_i (1 + \nu) r_i^2}{r E} \tag{11}$$

For the case of the displacement at the inner radius, r_i, Equation 11 becomes

$$u_{r=r_i} = \frac{p_i (1 + \nu) r_i}{E} \tag{12}$$

To apply Equation 12 to a cylindrical loading case where the volume of the displacement is measured, and not the radial displacement, the average radial displacement is calculated, using the geometry shown in Figure 4. Initially the volume of the cylinder is

$$V_o = \pi r_i^2 L \tag{13}$$

where: V_o = initial volume of the measuring cell

L = length of cylindrical measuring cell

After a pressure, p_i, is applied, the wall displaces. If the average wall displacement is considered, the new volume can be calculated as

$$V = \pi (r_i + u_{ave})^2 L \tag{14}$$

where: V = volume after pressure p_i is applied

u_{ave} = average radial displacement of wall surface

The change in volume can then be calculated by expanding Equation 14 and then subtracting Equation 13, which results in:

$$\Delta V = \pi L 2 r_i u_{ave} + \pi L u_{ave}^2 \tag{15}$$

where: ΔV = change in measuring cell volume

If the u_{ave}^2 term is neglected, the following very simple relationship results for the displacement as a function of the volume:

$$u_{ave} = \frac{\Delta V}{V_o} \frac{r_i}{2} \tag{16}$$

Substituting Equation 16 into Equation 12 and solving for E gives the pressuremeter modulus equation which is identical to Equation 1.

$$E_{PMT} = 2 (1 + \nu) V_o \frac{p_i}{\Delta V} \tag{1}$$

If the u_{ave}^2 is not neglected, then the average displacement is

$$u_{ave} = r_i \left(\sqrt{1 + (\Delta V/V_o)} - 1 \right) \tag{17}$$

and the modulus can be determined from:

$$E_{PMTU} = \frac{p_i (1 + \nu)}{\sqrt{1 + (\Delta V/V_o)} - 1} \tag{18}$$

where: E_{PMTU} = pressuremeter modulus including u_{ave}^2 term

The ratio of the elastic modulus calculated including the effects of the u_{ave}^2 term to that neglecting it is

$$\frac{E_{PMTU}}{E_{PMT}} = \frac{(\Delta V/V_o)}{2(\sqrt{1 + (\Delta V/V_o)} - 1)} \tag{19}$$

It is seen that any possible error in obtaining a value for the elastic modulus by neglecting the u_{ave}^2 term is a function of the ratio of the volume change to the initial volume of the probe. This relationship is plotted in Figure 5. Neglecting the u_{ave}^2 term causes a variation of less than 5 percent in calculating E_{PMT} using Equation 12 if the ratio of the volume change to the initial volume is kept below 0.20. The variation approaches 20 percent as the volume change ratio approaches 1.0. For most practical field applications therefore, neglecting the u_{ave}^2 term is reasonable.

Another way to derive the simple pressuremeter modulus relationship is to use the results of the classic expansion of a thick-walled cylinder, referred to as Lamé's problem. For the geometry illustrated in Figure 6, the equation for the displacement u as a function of the radial distance is (Venkatraman and Patel, 1970)

$$u = \frac{(1 + \nu)(r/r_i)r_i}{(r_o/r_i)^2 - 1} \left[\{(1 - 2\nu) + \frac{(r_o/r_i)^2}{(r/r_i)^2}\} \frac{p_i}{E} - \{(1 - 2\nu) + \frac{1}{(r/r_i)^2}\} (r_o/r_i)^2 \frac{p_o}{E}\right] \tag{20}$$

where: r = radius

r_i, r_o = inner and outer radius

p_i, p_o = pressure at inner and outer radius surface

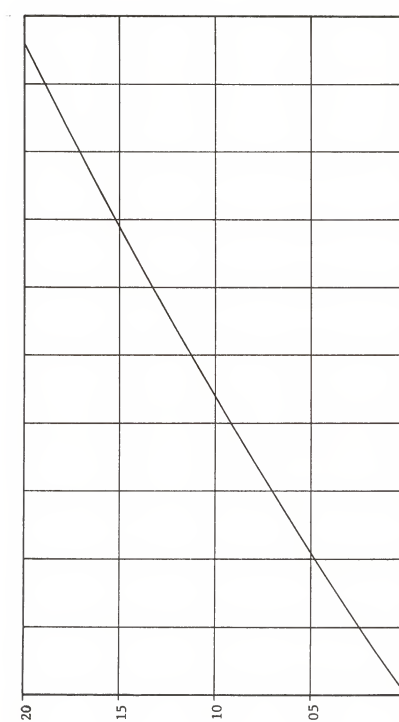


Figure 5. Effect of the $(u_{ave})^2$ Term on the Calculation of the Elastic Modulus

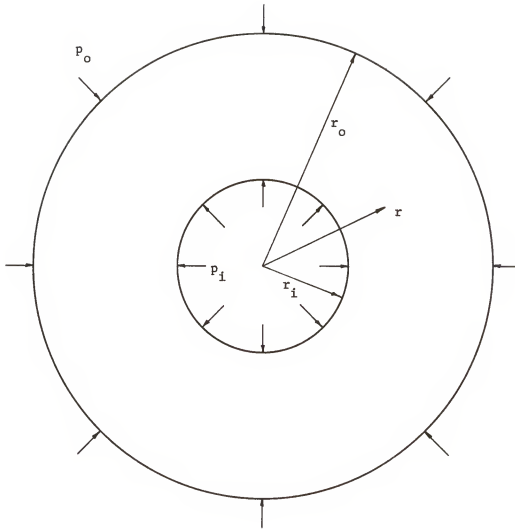


Figure 6. Geometry for Loading of an Infinitely Long Thick-Walled Cylinder (Lamé's Problem)

If the outer pressure is taken as zero and the outer radius expanded to an infinite limit, then Equation 20 takes the identical form to Equation 12 for the displacement at the inner radius, r_i. If, however, the outer pressure is taken as zero, but kept as a thick-walled cylinder, then Equation 20 can be solved for the elastic modulus to obtain

$$E_{TWC} = \frac{(1 + \nu) r_i p_i}{u} \left[\frac{(r_o/r_i)^2 - 2\nu - 1}{(r_o/r_i)^2 - 1} \right] \tag{21}$$

where: E_{TWC} = elastic modulus for a thick-walled cylinder

Using the thick-walled cylinder relationship, the elastic modulus is seen to be a function of the E for an infinite cylinder (E_{PMT}) as well as the ratio of the outer to inner radius. The ratio of the elastic modulus as determined using a thick-walled cylinder (Equation 21) to that using an infinite cylinder (Equation 12) is thus

$$\frac{E_{TWC}}{E_{PMT}} = \frac{(r_o/r_i)^2 - 2\nu - 1}{(r_o/r_i)^2 - 1} \tag{22}$$

This ratio is plotted in Figure 7. The figure shows clearly that for outer to inner radius ratios of 10 or greater, the calculation of the modulus by the infinite cylinder approach is approximately the same as for the thick-walled cylinder approach. However, for lower outer to inner radius ratios, the thick-walled cylinder approach can differ appreciably from the infinite cylinder approach. For field applications the infinite cylinder approach can be used. For laboratory testing equipment, however, the outer to inner radius should be in excess of 10 to eliminate possible thick-walled cylinder effects.

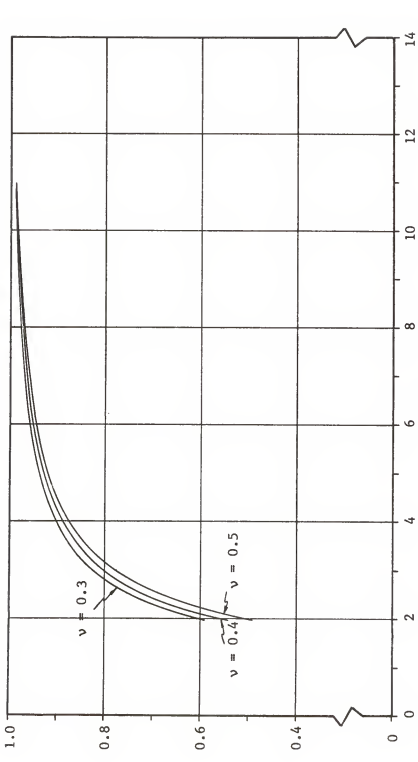


Figure 7. Thick-Walled Cylinder Effect on Calculation of the Elastic Modulus

2.1.2 Tranter's Two-Dimensional Analysis

In practice, the pressuremeter loading of the soil is not identical to a completely uniform expansion. The actual expansion is similar to that shown in Figure 8 where a uniform load is applied internally to the cylinder over a length 2c with an interior radius r_i. If the measuring cell and the guard cells have different pressures, the resulting loading of the soil is the superposition of these two loads, as illustrated in Figure 9.

Perhaps the first attempt to analyze the loading of a small segment of a cylindrical hole was done by Westergaard (1941). He used two approximation techniques to develop equations for the displacement of the cylindrical surface as a function of the inner radius, loaded length, and vertical distance. Due to the assumptions in his approximations, his results are only applicable for c/r_i ratios of 1.5 or less (depending on Poisson's ratio). For most pressuremeter applications, the ratio of the probe half-length to the radius is usually greater than 3 or 4. Thus the results of the Westergaard approximation technique cannot be meaningfully applied to theoretical pressuremeter analyses.

Tranter (1946) developed the analytical solution for the partial loading of a cylindrical hole. For the geometry illustrated in Figure 8, he derived the following relation for the radial displacement of the cylindrical wall:

$$u_{r=r_i} = \frac{4p_i r_i (1 - \nu^2)}{E \pi} \int_0^\infty \frac{K_1^2(\alpha) \text{ Sin } \{(c/r_i)\alpha\} \text{ Cos } \{(z/r_i)\alpha\} d\alpha}{\alpha \left[\{\alpha^2 + 2(1 - \nu)\} K_1^2(\alpha) - \alpha^2 K_o^2(\alpha)\right]} \quad (23)$$

where: c = one-half the loaded length

z = vertical coordinate

K_1 = Modified Bessel Function of Second Kind and Order 1

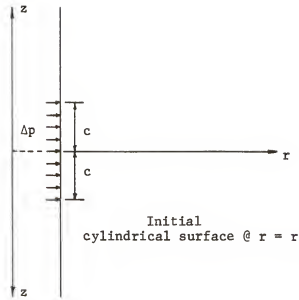


Figure 8. Application of Cylindrical Uniform Pressure Over Finite Length

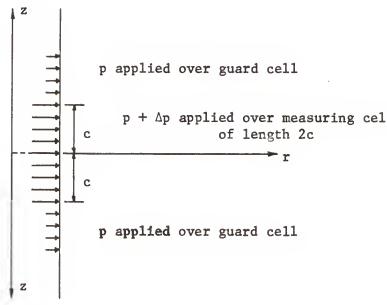


Figure 9. Superposition of Cylindrical Uniform Loading by Measuring and Guard Cells

K_o = Modified Bessel Function of Second Kind and Order 0

α = Variable of integration

Tranter went through lengthy hand calculations to show that Westergaard's approximation technique was rather crude. Tranter's analysis, unlike Westergaard's, is not restricted to low c/r_i values and thus can be studied with regard to possible applications to the pressuremeter test. It should be noted that the displacement of the inner wall surface is a function of Poisson's ratio, the elastic modulus, the internal pressure, the half-length being loaded, and the distance along the wall edge. Livneh et al. (1971) give a brief description of Tranter's work and indicate that the use of the simple radial displacement formula (Equation 12) is sufficiently accurate as long as the measuring length of the loaded probe is two-thirds or less of the full length of the loaded probe. This assumes that the pressure is the same over the full length of the probe, including both the measuring and guard cells. They made this analysis for a Poisson ratio of 0.3, and do not state what c/r_i ratio was used for the calculations.

Because Tranter's work represents the classical solution for the pressuremeter test, it is worthwhile to investigate the effects of the various parameters. The displacement equation (Equation 23) can be programmed using standard numerical integration techniques as well as standard Bessel function subroutines. Appendix I gives the sample Fortran listing for the solution of Equation 23, as well as numerical techniques for comparing this classic solution with the infinite cylinder solution. With this program it is possible to study the effects of Poisson's ratio, as well as varying the c/r_i and z/c ratios.

To set up the nonlinear finite element sand model as closely as possible to the classical results, the Tranter solution for several cases was investigated. The model pressuremeter chosen had a 12 inch measuring cell and a diameter of 2.4 inches, thus giving a c/r_i ratio for the measuring cell of 5.0. Two 12 inch guard cells were used, thus giving a c/r_i ratio of 15.0 for the entire pressuremeter.

One variable which is used in the field tests is a differential pressure which is maintained between the guard cells and the measuring cell. In order to duplicate this effect analytically, it is necessary to first consider that the measuring cell is loaded to some pressure which equals the differential pressure to be used for the test. Then additional pressure is applied over the entire pressuremeter, thus keeping the measuring cell at a differential pressure above the guard cells. This was illustrated in general in Figure 9.

Consider the case of loading the model pressuremeter with a differential pressure of 3 psi. Then the entire pressuremeter is loaded an additional 6 psi. The analytical solution for this case using the 12-12-12 pressuremeter described previously is given in Figure 10. Due to the edge effects of the loading, there will be a volume variation compared to the infinite cylinder displacement. Therefore, when the initial 3 psi differential pressure is applied, the volume measurement will differ by approximately 6.5 percent from that given by using the infinite cylinder displacement. The modulus calculation would thus vary on the high side by this same percentage since the modulus is inversely proportional to the measured volume change as shown in Equation 1.

When the entire pressuremeter is loaded, however, the volume discrepancy over the measuring cell segment reduces , as would be expected. Figure 10 shows that for a superimposed additional loading of 6 psi the volume discrepancy (and thus the modulus calculation discrepancy) will be reduced to approximately 2 percent. The analysis was for a Poisson ratio of 0.3.

A similar analytical solution was investigated for 3 psi loading of a 6 inch measuring cell with a radius of 1.2 inches ($c/r_i = 2.5$) and then superimposed loading of 6 psi over the entire pressuremeter including two 6 inch guard cells ($r/r_i = 7.5$). The results of this case are shown in Figure 11 for a Poisson ratio of 0.3. As expected, the results for the 6-6-6 pressuremeter are similar to those for the 12-12-12 pressuremeter. However, there is an initial volume variation of approximately 13 percent due to loading the central cell only, and then the volume variation is reduced to approximately 4 percent after the full-length loading is applied.

If an analysis as shown in Figures 10 and 11 is repeated for various Poisson's ratios and c/r_i ratios, the volume discrepancy for the initial loading can be obtained as a function of these parameters. Results of these calculations are shown in Figure 12. This figure shows clearly that the volume measured by a single uniformly loaded flexible cell will be within 10 percent of that for an infinite cylinder if the c/r_i ratio is 4 or greater. The volume measurement will be within 5 percent if the c/r_i ratio is 9 or greater. The volume variation is only slightly affected by the value of Poisson's ratio and is relatively insensitive to it at c/r_i ratios greater than 10.

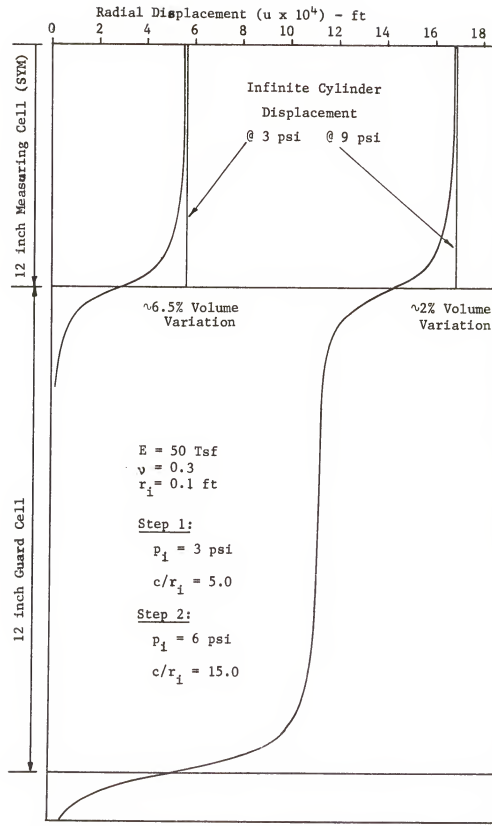


Figure 10. Classical Tranter Displacement Solution: $c/r_i = 5.0$; $c/r_i = 15.0$

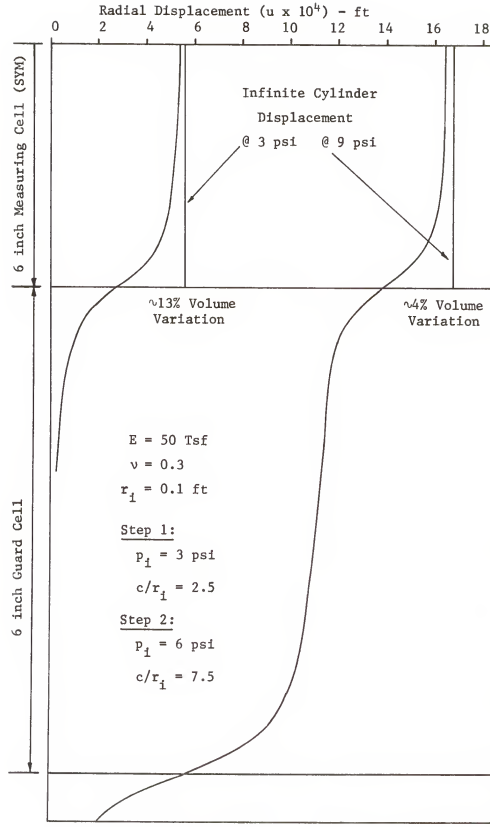


Figure 11. Classical Tranter Displacement Solution: $c/r_i = 2.5$; $c/r_i = 7.5$

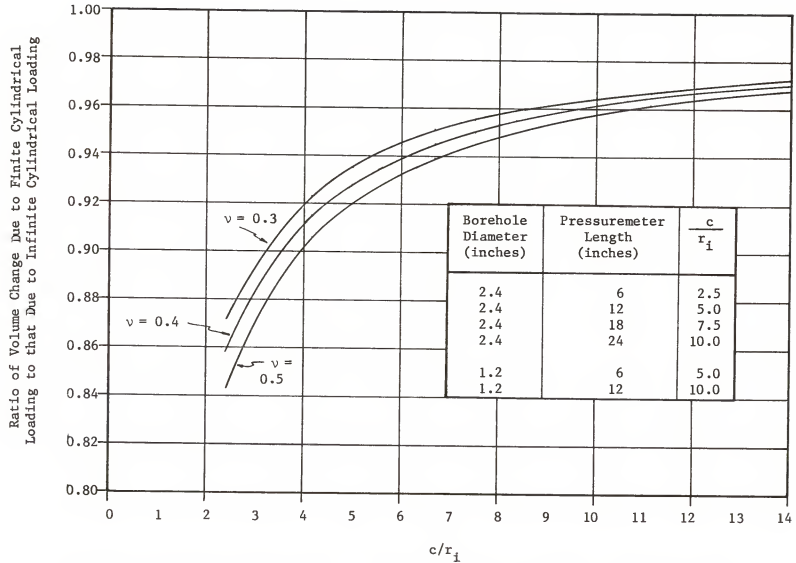


Figure 12. Ratio of Volume Displacements for Finite and Infinite Cylinder Loadings

It is emphasized that this is for single cell loading only. If an additional pressure is imposed over the full length of the pressuremeter, then the volume discrepancies will be reduced appreciably to less than 5 percent. This will be a function of the superimposed pressure, and the discrepancy will continuously reduce as the pressure increases. Additionally, if there is no differential pressure and the cells are uniformly loaded, with the measuring cell two-thirds or less of the total pressuremeter length, then the volume discrepancy will also be less than 5 percent.

As indicated by the small table included in Figure 12, most pressuremeters which are 2 and 3 feet in length meet the c/r_i requirements and the measuring cell is typically two-thirds or less of the pressuremeter length. However, there have been some pressuremeters with 6 inch measuring cells and two 2 inch guard cells. Although this design meets the two-thirds requirement, the c/r_i ratio of 4.0 for a 2.5 inch borehole is slightly low.

It can also be noted that the centerline displacement (see Figures 10 and 11) more closely approximates the infinite cylinder displacement. It thus gives a more accurate indication of an average infinite cylinder volume change, independent of edge effects, than using a flexible membrane and measuring its total volume change.

There is one additional important point to be noted. It is very important to know the actual field loading differential pressure during the initial loading if any meaningful interpretation is to be made of the initial portion of the pressure-volume curve. This point will be discussed further during the finite element analysis section of this dissertation.

2.1.3 Pressuremeter Test Interpretation, Factors, and Uses

Although the one-dimensional expansion analysis is relatively straightforward and easy to understand and work with, in practical field applications there are many testing factors which can affect the test results. Some of the major factors include:

(a) Membrane Inertia - The effect of the rigidity of the membrane in loading the soil must be accounted for. This is very critical to an understanding as to how the soil is actually being loaded, since some of the cell pressure is expanding the membrane and not actually loading the hole. This is especially critical during the early phases of the test when the applied pressures are relatively low.

(b) Soil Creep - Since soils will creep with time, it is important to establish set time intervals for readings in order to obtain uniform results.

(c) Instrumentation - All equipment must be properly calibrated and also be sufficiently accurate for the volumes and pressures being measured.

(d) Borehole Disturbance - The drilling of the borehole may cause a disturbed zone in contact with the pressuremeter probe. Loading of this disturbed zone, or seating errors, or an irregular loading surface may affect the entire pressure-volume curve. Even if the pressuremeter is forced into the soil, there is a small disturbed area around the probe.

(e) Operator Experience - Even with great care and excellent equipment, the interpretation of field results is also influenced by the experience or judgement of the engineer interpreting the data. This is especially true with regard to the interpretation of certain break points on the field curve.

Additional testing factors are extensively discussed in the field testing literature (Parsons et al., 1961; Higgins, 1969; Laier, 1973). Any use of field pressuremeter testing data must always account for the many variables involved in the test. In this study the effects of the differential pressure magnitude between the measuring and guard cells will be analyzed, as well as the effect of borehole disturbance.

In the past 15 years the literature and field information dealing

with the pressuremeter test have increased rapidly. The primary work has been done in France, where pressuremeter testing is a routine procedure. Other studies have been made on a smaller scale in other countries, primarily by individual soils engineers or agencies who are slowly incorporating pressuremeter testing into their work.

The analytical work has been somewhat limited, and has been generally restricted to one-dimensional analyses. Livneh, Gellert, and Uzan (1971) used such an analysis to indicate that the pressuremeter test measures the horizontal elastic modulus for a cross-anisotropic soil. They do not include three-dimensional effects. Ladanyi (1963a, 1963b, 1967, 1972) has published extensively and analyzed pressuremeter test interpretation in a variety of materials - from clays to granular materials. His work also does not include three-dimensional effects and the supporting data are often quite limited.

Palmer (1972) has shown a technique for determining the undrained plane strain stress-strain curve for clays using the results of pressuremeter pressure-volume curves. His technique checks that of Ladanyi (1972). Vesić (1972) presents a sophisticated analysis of cavity expansion, both spherical and cylindrical. His analysis approach is used with a pressuremeter example. However, his example assumes the validity of the pressuremeter test results and he does not question the interpretation or accuracy of the volume vs. pressure data.

Most of the previous analytical studies have emphasized the use of pressuremeter data in undrained clay materials, which are more amenable to elastic analysis. The accuracy of Equation 1 to determine the elastic modulus is usually not questioned.

Perhaps the greatest quantity of information has been developed over the past decade in the area of semi-empirical rules using pressuremeter results for the design and/or analysis of various soil properties and foundation behavior. Although some of these rules are contained in internal documents of the Louis Ménard Consulting firm, many are described in openly published literature. These techniques and rules have been applied to many engineering applications and include, but are not limited to:

(a) determination of soil cohesion (Parsons et al., 1961; Palmer, 1972).

(b) determination of the soil failure envelope (Ladanyi, 1963a; Gibson and Anderson, 1961).

(c) determination of the shear strength of cohesive soils (Higgins, 1969; Palmer, 1972; Baguelin et al., 1972).

(d) calculation of horizontal loads on sheet piles (Ménard, Bourdon, and Houy, 1964).

(e) calculation of foundation bearing capacity (Ménard, 1963).

(f) calculation of foundation settlement (Ménard and Rousseau, 1962; Dauvisis and Ménard, 1964; Ménard, 1965; Ménard, 1971).

(g) calculation of pile settlement (Gambin, 1963; Goulet, Hulo, and Jezequel, 1964; Ménard, 1971).

Although there has been increased interest in the 1970s in the pressuremeter test, its apparent current (1973) status is that of a field exploration tool which, in conjunction with semi-empirical formulas and rules, has been used for a variety of design and analysis functions in the general field of soil mechanics and foundation engineering. It has been used primarily in France and Western Europe, although there is current research and interest in many other parts of the world.

2.2 Settlement Prediction in Sands

2.2.1 Strain Distribution Approach

Perhaps the most recent and thorough discussion of techniques used to predict settlement of sands was done in 1970 by Schmertmann. As an indication of the importance of his work, he was awarded the American Society of Civil Engineers' Norman Medal for this study. Schmertmann comments on sand settlement prediction techniques as follows:

> Presently, engineers commonly use settlement estimate procedures based on two very different types of field penetrometer tests. U.S. engineers have used the Standard Penetration Test for 20 yr. The hammer blow-count, or N-value, has been empirically correlated to plate test and prototype footing settlement performance. Because of the completely empirical nature of this method the engineer sometimes finds it not very informative or satisfying to use. Some engineers believe that it often results in excessively conservative (too high) settlement predictions. Another method, based on the Static Cone Penetration Test, has a European history of over 30 yr. In this method the quasistatic bearing capacity of a steel cone provides an indicator of soil compressibility. (Schmertmann, 1970, pp. 1011-1012)

He then goes on to describe a technique he developed using the results of static cone penetration tests to predict sand settlements. Included is a very thorough study of the reasonableness of the method as substantiated by approximately 40 test cases. The major advantage of using the static cone is that it is an inexpensive in-situ test which can be used quickly over wide areas and thus indicate the major non-homogeneities in the subsurface.

Schmertmann's approach has a very general basis which could be adopted to a variety of field devices. Essentially his suggestion is that the best way to approach the prediction of sand settlements is by the integration of the strain variation with depth, as written:

$$\rho = \int_0^\infty \varepsilon_z \, dz \tag{24}$$

where: ρ = total settlement

ε_z = vertical strain

This approach is also used in calculating linear elastic settlements in the SEPOL program (Jordan and Schiffman, 1967). Since strain is the ratio of stress to elastic modulus, Schmertmann then suggests the following substitution:

$$\rho = \int_0^\infty \frac{p}{E} \, I_z \, dz \tag{25}$$

where: p = applied load, pressure units

I_z = vertical strain influence factor

Based on studies using the theory of elasticity as well as the results of field and laboratory tests, Schmertmann recommends that initially a standard triangular distribution for the vertical strain influence factor (I_z) be used. The suggested distribution is shown in Figure 13.

Since his work is directed toward the determination of the soil's elastic modulus by means of the cone penetrometer, he then shows how the variation of the elastic modulus with depth, as obtained from the cone penetrometer, can be used with the suggested strain distribution to obtain sand settlement predictions. The resulting equation for predicting sand settlements is

$$\rho = p \sum_0^{2D} \frac{I_z}{E} \, \Delta z \tag{26}$$

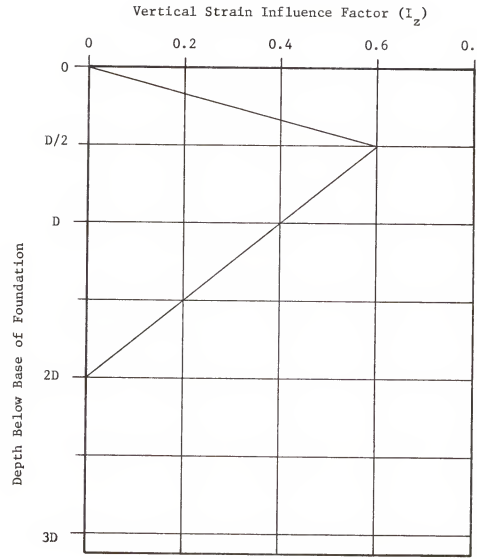


Figure 13. Schmertmann's Recommended Vertical Strain Influence Factor Distribution

where: I_z = strain influence factor value for layer

E = elastic modulus of layer

Δz = thickness of layer

Predicted settlements are then made using cone penetration data for the modulus, a standard strain influence factor diagram (Figure 13), and then numerically integrating Equation 26 (summing over each layer chosen for the analysis). Schmertmann also includes suggested corrections for embedment and creep. The technique is straightforward and easy to use and understand. Its great advantage is that it includes the results of meaningful in-situ testing and accounts for the variation of the elastic modulus with depth.

It should be noted that the strain influence factor (I_z) is given by

$$I_z = \frac{E}{p} \varepsilon_z \tag{27}$$

For a linearly elastic analysis it is easy to obtain the vertical strain influence factor by multiplying the vertical strain by the ratio E/p. However, for nonlinear analyses the interpretation is much more involved.

Since the PMT is an in-situ test, as is the CPT, it seems reasonable to pursue this settlement approach in the computer model study described in this paper. Accordingly, this study will consider both the interpretation of the results of pressuremeter analytical studies on a model sand in conjunction with the results of strain distribution studies on similar model sands.

2.2.2 The Pressuremeter Test for Settlement Prediction in Sands

Ménard and Rousseau (1962) presented the first discussion of the use of pressuremeter information for predicting settlements for a variety of soil types. However, they do not actually derive a precise formula. Their approach is somewhat theoretical and descriptive since they point out that the soil is not truly elastic, but then use the "elastic" response of a pressuremeter test in their discussion. They purposely do not include experimental results so there is no recommended design procedure included in this paper. However, in 1965 Ménard first presented the "rules" for the determination of settlement using the pressuremeter test results. Thorley et al. (1969) also discuss these rules.

According to Ménard, the settlement in general can best be expressed as the sum of three separate components which can be obtained by using the results of various loading and unloading moduli as obtained from the pressuremeter test. These moduli are illustrated in Figure 14. The total settlement is then:

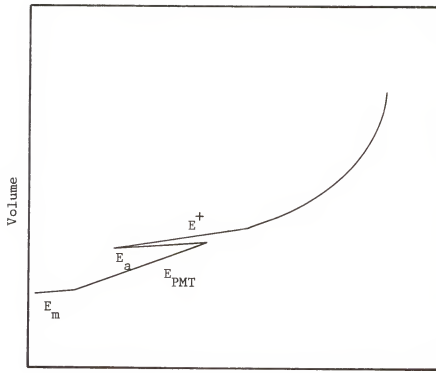
$$\rho = w_1 + w_2 + w_3 \tag{28}$$

where: w_1 = elastic settlement and is related to the micro-deformation modulus, E_m

w_2 = settlement related to the deviatoric stress tensor

w_3 = settlement due to consolidation (spherical stress tensor

Ménard then recommends that w_1 is so small that it should be neglected and that w_2 and w_3 should be given by:



E_m = micro-deformation modulus

E_{PMT} = typical pressuremeter modulus

E_a = unloading modulus

E^+ = reloading or volumetric modulus

Figure 14. Pressuremeter Curve Illustrating the Various Moduli as Used in Ménard's Settlement Calculations

$$w_2 = \frac{(1 + \nu)}{3E_{PMT}} \quad 12\ p\ (\lambda_1 \frac{D}{24})^{\alpha} \tag{29}$$

$$w_3 = \alpha \frac{p\ D}{9E_{PMT}} \quad \lambda_2 \tag{30}$$

where: D = footing "effective" diameter or width, in inches

$\alpha = (E_{PMT}/E_a)^{\frac{1}{2}}$

λ_1, λ_2 = Shape Factors (after Steinbrenner, 1934)

Based on his experience, he recommends the values for α and the shape factors λ_1 and λ_2 as given in Tables 1 and 2. It is noted from these formulas that the general approach for using the pressuremeter to estimate settlement is to use modifications of the results of various elastic analyses (Steinbrenner, 1934), but adjust them for parameters from the pressuremeter field curve. There is apparently no technique for using the variation of modulus with depth, although the pressuremeter information for various layers could be used separately.

Recently Ménard (1971) summarized the results of using pressuremeter tests to predict settlements for a variety of field conditions. He presents a general summary of several field cases with favorable comparisons. Of the 11 structure settlement examples, however, only 3 are on sandy type soils. In addition, he does not go into a detailed explanation of the calculations for each case. He also reiterates that his suggested technique is based largely on the results of experimental work.

Table 1. Alpha Values for Use in Ménard's Settlement Computations

Soil Type	α
Clay	2/3
Sand	1/3
Silt	1/2
Elastic Materials	1

Table 2. Shape Factors for Use in Ménard's Settlement Computations

Geometry	λ_1	λ_2
Round Footing	1	1
Square Footing	1.12	1.1
Rectangle (L/B = 2)	1.53	1.2
Rectangle (L/B = 10)	2.65	1.5

2.3 The Finite Element Method

2.3.1 General Discussion

Oden (1972) gives a brief historical presentation of the background of the analytical technique referred to as the finite element method. The concept of trying to represent continuous functions with piecewise approximations dates back several thousand years. The breaking up of structures into discrete systems has been used by researchers for several decades and Oden feels that Courant's work (1943) involves all the basic concepts of today's finite element method.

The birth of the modern finite element method was started by Turner et al. (1956) who used a direct stiffness structural approach and equations of elasticity to obtain properties for use in triangular elements in plane stress analysis. Clough (1960) first used the term "finite elements" in his paper describing the approach to plane strain problems. In the last decade there have been over 1000 papers on the topic as well as several books (Zienkiewicz, 1971; Oden, 1972; Desai and Abel, 1972; Martin and Carey, 1973; Ural, 1973).

The finite element method can be used to calculate solutions to non-structural problems such as heat conduction, seepage, irrotational flow, etc. since the determination of equilibrium nodal displacements as used in structural analysis is analogous to the procedure of minimizing the total potential energy of the system. The best examples of these types of problems are those dealing with solutions to Laplace's and Poisson's equations for a variety of non-classic and complex boundary conditions. The books previously cited give a thorough treatment of the many applications of the finite element method.

To analyze any elastic continuum using the finite element method, it is first necessary to divide it into a finite number of elements and nodal points, much like a large structural frame. For a plane strain or plane stress analysis, the element is essentially a two-dimensional element as illustrated in Figure 15. Figure 16 shows how an axisymmetric solid can be divided into finite elements. The solid is in the general form of a cylinder and the elements are essentially "rings" around the central axis. The plane elements and axisymmetric rings can be of any geometric cross-section, but typically the general shape is a rectangle, which is then usually subdivided for analysis purposes into 4 triangles.

The basic assumptions for these analyses, including the ones used in this study, are made in order to satisfy the necessary equations of equilibrium and continuity in an elastic medium. The two major assumptions are:

(1) In order to assure continuity between the elements of the system, linearly varying displacements are used. It would be possible to assume quadratic or other algebraic displacement relationships, but this would greatly increase the complexity and cost of the analysis without necessarily improving the results.

(2) Stresses along the boundary of each element are replaced by equivalent nodal forces. The resultant of all of the nodal forces on an element is made to equal zero in order to satisfy equilibrium.

The general procedure used to determine the nodal point displacements and then the element stresses then follows:

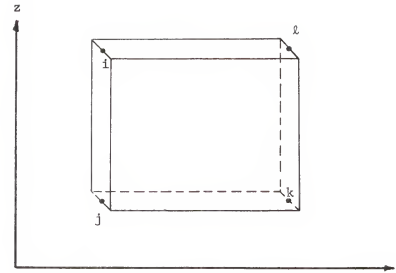


Figure 15. Typical Element for Plane Strain Case

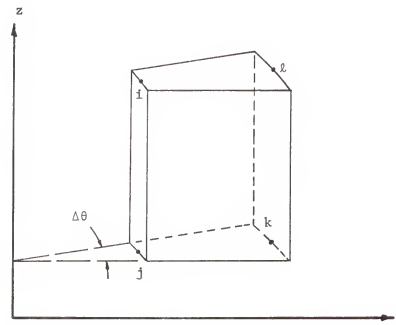


Figure 16. Typical Element for Axisymmetric Case

(1) Simulate the elastic continuum by a grid of finite elements (usually triangular or rectangular) with the subdivisions appropriate to the system chosen and the problem to be solved. This step usually requires experience, engineering judgement, and some trial-and-error runs.

(2) Evaluate the stiffness matrix for each element in the grid. This stiffness matrix is analogous to the structural stiffness matrix which relates forces and displacements at nodal points under equilibrium conditions. This matrix is dependent upon the element properties as well as the assumed displacement function as described previously.

(3) Combine the individual stiffness matrices into a single stiffness matrix for the entire continuum. This is done by standard matrix superposition techniques.

(4) Determine an entire set of equilibrium equations for each nodal point incorporating the various boundary conditions, either pressure or displacement. The general form of the equilibrium equations to be solved is

$$\{R\} = [k] \{u\} \tag{31}$$

Where: $\{R\}$ = force vector

$[k]$ = stiffness matrix

$\{u\}$ = displacement vector

The solution of these equilibrium equations by standard numerical techniques results in the nodal point displacements at equilibrium under the imposed boundary conditions.

(5) The displacements can be used to calculate strains and then the element stresses are calculated by using the stress-strain relations for the materials used in the analysis.

The plane strain and axisymmetric cases were two of the first finite element techniques to be used in engineering analysis. Clough (1960) describes the plane strain case, and Wilson (1963, 1965) describes the details of the axisymmetric case. Since these two cases are used in this study, the stress-strain matrices should be noted and discussed briefly.

For linear, homogeneous, elastic materials, the matrix representing the plane strain stress-strain relations is as follows:

$$\{\sigma\} = \frac{E}{(1+\nu)(1-2\nu)} \begin{bmatrix} 1-\nu & \nu & 0 \\ \nu & 1-\nu & 0 \\ 0 & 0 & \frac{1-2\nu}{2} \end{bmatrix} \{\varepsilon\} \qquad (32)$$

and that for the axisymmetric case:

$$\{\sigma\} = \frac{E}{(1+\nu)(1-2\nu)} \begin{bmatrix} 1-\nu & \nu & \nu & 0 \\ \nu & 1-\nu & \nu & 0 \\ \nu & \nu & 1-\nu & 0 \\ 0 & 0 & 0 & \frac{1-2\nu}{2} \end{bmatrix} \{\varepsilon\} \qquad (33)$$

It should be noted that in using this formulation, the computational precision tends to deteriorate as Poisson's ratio (ν) approaches 0.5. This is because for the normal stress components, the stress approaches infinity as ν approaches 0.5 (i.e., $(1-2\nu)$ approaches 0). The usual approach in using this technique for high Poisson's ratios is to use values close to 0.5. This does not always work, however, in spite of the use of very fine grids (Zienkiewicz, 1971). If the analysis does not work well for Poisson's ratios close to 0.5, then an entirely different approach must be used for formulating the stress-strain relationship (Herrmann, 1965).

In these studies, using a Poisson ratio of 0.48 gave reasonable results for the axisymmetric and plane strain studies (Chapter 4.0), but was slightly in error for the cylindrical axially symmetric loadings of the pressuremeter (Chapter 5.0). Accordingly, the parametric studies in that chapter primarily used Poisson's ratios of 0.3 and 0.4. The discrepancies will be discussed further in Chapter 5.0.

An attempt was made to determine some of the possible effects of cross-anisotropy, especially with respect to the elastic moduli. The matrices given in Equations 32 and 33 can be readily written in the form for cross-anisotropic cases (Zienkiewicz, 1971; Harr, 1966). For plane strain the relationship is

$$\{\sigma\} = A \begin{bmatrix} \eta(1-\eta\nu_v^2) & \eta\nu_v(1+\nu_h) & 0 \\ \eta\nu_v(1+\nu_h) & (1-\nu_h^2) & 0 \\ 0 & 0 & m(1+\nu_h)(1-\nu_h-2\eta\nu_v^2) \end{bmatrix} \{\varepsilon\} \qquad (34)$$

and for the axisymmetric case is

$$\{\sigma\} = A \begin{bmatrix} (1-\nu_h^2) & \eta\nu_v(1+\nu_h) & \eta\nu_v(1+\nu_h) & 0 \\ & \eta(1-\eta\nu_v^2) & \eta(\nu_h+\eta\nu_v^2) & 0 \\ & & \eta(1-\eta\nu_v^2) & 0 \\ \text{Symmetrical} & & & m(1+\nu_h)(1-\nu_h-2\eta\nu_v^2) \end{bmatrix} \{\varepsilon\} \qquad (35)$$

where:

$$A = \frac{E_v}{(1+\nu_h)(1-\nu_h-2\eta\nu_v^2)}$$

$$\eta = E_h/E_v$$

$$m = G_v/E_v$$

E_v = elastic modulus
G_v = shear modulus
ν_v = Poisson's ratio
— associated with behavior in direction normal to plane of strata (i.e., vertical for horizontal layering)

E_h = elastic modulus
G_h = shear modulus = $\frac{E_h}{2(1+\nu_h)}$
ν_h = Poisson's ratio
— associated with behavior in the direction in the plane of strata (i.e., horizontal)

The 5 independent parameters necessary for such an anisotropic analysis are very difficult to obtain in soils. Barden (1963) suggests that one of them can be eliminated by making the substitution:

$$G_v = \frac{E_v}{1 + \frac{E_v}{E_h} + 2\,\nu_v} \tag{36}$$

This reduces the variables to four.

For the purpose of these parametric studies, Poisson's ratio was fixed for both the horizontal and vertical cases and the primary study of cross-anisotropy was the investigation of the effects of varying the horizontal and vertical elastic moduli, E_h and E_v. The cross-anisotropic studies were certainly not exhaustive, therefore, and were included to give some introductory indication as to the possible effects of such a field condition. The study of cross-anisotropy in soils is a very promising one for both analysis and field work.

The finite element programs used were originally developed by Wilson and modified by Duncan for nonlinear soil parameters (to be discussed in Chapter 3.0). The writer has further modified these programs for cross-anisotropy and developed two programs for the

specific use of this study. One program, which is listed with a Users' Manual in Appendix II, has been modified to calculate vertical strains beneath various types of surface loadings, as well as determine the vertical strain influence factor, I_z. The other program, which is listed in Appendix III, is set up for loading and unloading conditions typical of a pressuremeter.

Since the finite element method is a generally recognized and well-documented tool in engineering analysis, the precise steps will not be explained further. The reader is referred to the texts previously cited for further information as well as extensive bibliographies.

2.3.2 Applications in the Field of Soil Mechanics

Since the latter part of the 1960s the finite element method has become a common and accepted analytical tool in the field of soil mechanics and foundation engineering. Since the first papers in the soil mechanics literature using this technique appeared in 1968, there have been over 100 papers either devoted wholly or in part to its use. The applications in soil mechanics have varied from the more classical elastic analyses to those involving potential problems and others somewhat unique to soil mechanics.

Initially there was a feeling that perhaps the finite element technique would be the answer to soils engineers' needs for any complex analysis. In discussing some of the first applications of computers to problems in soil mechanics, Little and Price (1958) made the following warning which it is important to keep in mind and which also applies to the finite element method:

> . . . . it will be necessary to guard against over-enthusiasm for complicated methods of analysis where there is danger that limitations of accuracy in measuring soil and other properties will be forgotten. (Little and Price, 1958: p. 120)

In 1970 Lambe made a similar observation at a conference on lateral earth pressures at which there was a great deal of discussion about the finite element method. Lambe said:

> The determination of the correct soil parameters, boundary conditions, and construction methods to employ in analytical techniques like BRACE (a finite element program) is a problem taxing the most able and experienced engineer. At the present time, the difficulty of making these selections correctly is so large that the Writer considers it impractical to employ these powerful tools in a routine fashion. The greatest utility of these analytical techniques at present is in parametric studies. (Lambe, 1970: p. 180)

In less than 5 years since the first uses in soil mechanics, however, the growth of the finite element technique has been so rapid and broad that the first conference devoted exclusively to its use in geotechnical engineering was held in May, 1972 (Desai, 1972).

Although this technique is now widely used, primarily for parametric studies, it is always important to keep in mind the great difficulties in obtaining meaningful soil parameters as well as the exceedingly complex nonhomogeneous, nonlinear, and nonisotropic conditions that can exist in soil deposits.

The primary use of the finite element method in this dissertation will be to make such parametric studies for some specific linear and nonlinear analytical models. The linear models, when compared to classic solutions, can be used to determine the accuracy of the method as well as determine the effects of certain easily varied and easily understood linear parameters. The nonlinear model, which is more reasonable for soils, will then extend the parametric analyses.

CHAPTER 3.0

ANALYTICAL MODELING OF SAND

3.1 Introduction

Smith and Kay (1971) have presented a summary of some of the most common techniques used in modeling the stress-strain laws for soils in finite element analyses. They point out that the most straightforward analyses are the total stress analyses which are applied to (a) undrained saturated cohesive soils which are treated as incompressible elastic solids, and (b) analyses of drained soils where the total stress equals the effective stress. They then give illustrations of various analyses using (i) linear elastic solutions, (ii) bilinear or nonlinear elastic solutions, (iii) elastic perfectly plastic solutions, and (iv) elastic work hardening plastic solutions.

In modeling sand, the total stress usually equals the effective stress under most engineering applications. This would not be true under conditions of a shock or other rapid loading, however. Although it is sometimes reasonable to work with a Poisson ratio of 0.5 for clays in developing parametric information, this assumption is not as reasonable for sands. In modeling the sand for these analyses, therefore, a model was chosen which incorporated both the nonlinear elastic and varying Poisson's ratio characteristics of the sand. Since the model was not as sensitive for varying Poisson's ratios as originally anticipated, it was also possible to run parametric studies for various

constant Poisson's ratios.

Whitman (1960) has summarized the results of many workers who have shown that the overall modulus (any tangent modulus - dilitational, Young's, or shear) of a granular medium varies as a root of the confining pressure:

$$\text{Modulus} = (\text{Confining Pressure})^{\mu} \tag{37}$$

where the power, μ, varies from 1/3 for an ideal orderly packing of single size spheres to 0.5 for compact well-graded sands and gravels to 0.6 for poorly graded sands. Chaplin (1961) presented a theoretical argument for the 0.5 power for an assembly of non-spherical particles with sharp contact edges. Chen (1948) presented the results of triaxial tests which showed that the modulus of a sand would increase with (i) the 0.5 power of the confining pressure, (ii) increased density, and (iii) increased particle roundness. These and other studies which substantiate the above conclusions indicate a general approach for a nonlinear elastic modulus of sands.

There is much less information available with regard to the determination of Poisson's ratios for sands. Most analytical studies will assume a value of from 0.2 to 0.4, and often indirect laboratory measurements will give values in this range.

Although there have been extensive studies dealing with failure conditions for sands (Lee and Seed, 1967), the most commonly used is the Mohr-Coulomb envelope. Straight-line approximations for this failure envelope are easy to work with and understand. Accordingly, this failure envelope is incorporated into the nonlinear stress-dependent modulus used in this study. For detailed analyses of the failure conditions in pressuremeter testing, a comprehensive study of failure envelopes or failure criteria would be necessary.

3.2 Nonlinear Stress-Dependent Moduli

Duncan and Chang (1970) have developed a model for soil behavior which accounts for the nonlinear stress-dependent modulus properties of a soil. This model has been chosen for use in this analysis for several reasons:

(1) The values of the required parameters may be obtained from standard triaxial test data.

(2) The model is straightforward and simple to work with in that it does not require a brand-new approach. Engineers who work with conventional simple elastic approaches and the straight-line Mohr-Coulomb failure relationships can easily understand and work with this model. It is very practical in this regard.

(3) The parameters can be determined for either total or effective stress analyses and thus the computer analyses can be run on either or both cases.

The complete development of the model including background data and test information is given in the reference, while the major features of the model will be described in this section.

Kondner and Zelasko (1963) have suggested the following hyperbolic stress-strain relationship for use with sands and clays:

$$\sigma_1 - \sigma_3 = \frac{\varepsilon_a}{a + b\varepsilon_a} \tag{38}$$

where: σ_1 = major principal stress

σ_3 = minor principal stress

ε_a = axial strain

a,b = hyperbolic parameters

This relationship is plotted in Figure 17. If the stress-strain data are replotted on a graph where the ordinate has been transformed into the ratio of axial strain to stress difference, then the two hyperbolic parameters, a and b, can be readily obtained. This is illustrated in Figure 18, which shows

$$a = \frac{1}{E_i} \tag{39}$$

$$b = \frac{1}{(\sigma_1 - \sigma_3)_{ult}} \tag{40}$$

where E_i is the initial tangent modulus and $(\sigma_1 - \sigma_3)_{ult}$ is the asymptote or ultimate stress difference. Typically the asymptotic value of $(\sigma_1 - \sigma_3)_{ult}$ is larger than the compressive strength of the soil $(\sigma_1 - \sigma_3)_f$ by a small value. This can be represented as a failure ratio (R_f) which is usually between 0.8 and 1.0 and defined as

$$R_f = \frac{(\sigma_1 - \sigma_3)_f}{(\sigma_1 - \sigma_3)_{ult}} \tag{41}$$

If Equations 39, 40, and 41 are substituted into Equation 38, the hyperbolic stress-strain expression may be rewritten

$$\sigma_1 - \sigma_3 = \frac{\varepsilon_a}{\frac{1}{E_i} + \frac{\varepsilon_a R_f}{(\sigma_1 - \sigma_3)_f}} \tag{42}$$

As pointed out in Section 3.1, the modulus of a soil is dependent upon the confining pressure, and Janbu (1963) has suggested

$$E_i = K p_a \left(\frac{\sigma_3}{p_a}\right)^n \tag{43}$$

where: K = nonlinear modulus number

p_a = unit pressure (same units as E_i)

n = exponent

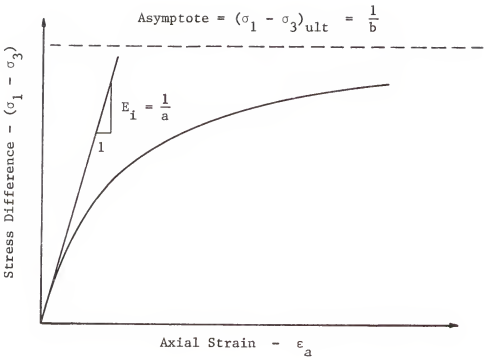


Figure 17. Hyperbolic Stress-Strain Curve

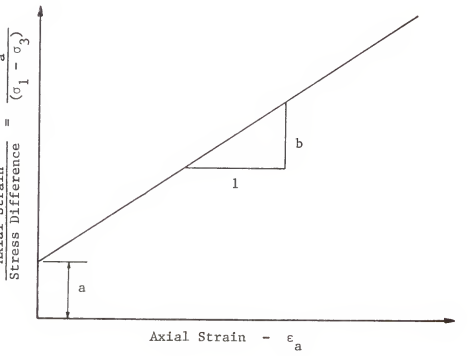


Figure 18. Transformed Hyperbolic Stress-Strain Curve

Additionally, the linear Mohr-Coulomb failure condition in terms of the stress difference at failure and the confining pressure is

$$(\sigma_1 - \sigma_3)_f = \frac{2\ (c\ \text{Cos}\ \phi + \sigma_3\ \text{Sin}\ \phi)}{1 - \text{Sin}\ \phi} \tag{44}$$

where c is the soil cohesion and ϕ is the angle of internal friction. A nonlinear failure envelope could also be used, which would add algebraic complexity, but might be more accurate. The linear failure envelope was retained in this study. Equations 42, 43, and 44 are used as the basis of the stress-dependent modulus.

Nonlinear stress-strain behavior can usually be approximated in one of two ways. The successive iterations approach (Figure 19) compares stress and strain after each analytical step with the nonlinear values. Repeated iteration is necessary for convergence. In the other approach (Figure 20), the change in loading is analyzed in a series of steps. An appropriate modulus value is selected for each increment. The nonlinear relationship is thus approximated by a series of linear steps.

Each approach has advantages and disadvantages. The iteration procedure allows for stress-strain relations after the peak, but it is difficult to work with for initial nonzero stress conditions. This is because the comparison after each step would require checking with a varying stress-dependent stress-strain curve, not a constant stress-strain curve. The successive increment procedure does not allow for stress-strain relations after the peak, but can be used when there are initial nonzero stresses as in problems in soil mechanics. This approach was used in this study.

As noted in Figure 20, the successive increment approach can be

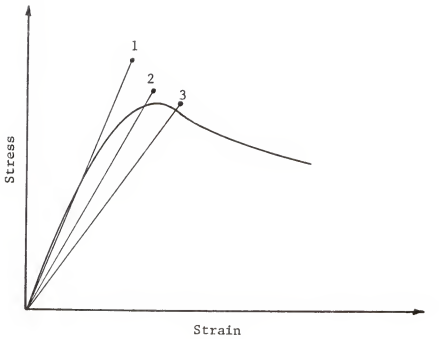


Figure 19. Successive Iterations Nonlinear Technique

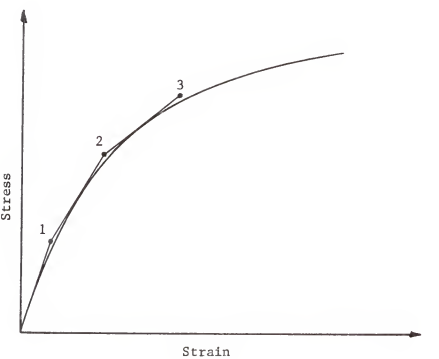


Figure 20. Successive Increments Nonlinear Technique (Used in this study)

used if repeated tangent modulus values can be obtained. The tangent modulus (E_t) may be defined using conventional triaxial stress-strain data as:

$$E_t = \frac{\delta(\sigma_1 - \sigma_3)}{\delta \varepsilon_a} \tag{45}$$

After differentiating Equation 42 and then substituting Equations 43 and 44 into the result, the nonlinear stress-dependent tangent modulus is obtained:

$$E_t = \left[1 - \frac{R_f(1 - \text{Sin } \phi)(\sigma_1 - \sigma_3)}{2c \text{ Cos } \phi + 2\sigma_3 \text{ Sin } \phi} \right]^2 Kp_a \left(\frac{\sigma_3}{p_a}\right)^n \tag{46}$$

where all terms have been defined previously. The use of Equation 46 in nonlinear analyses requires the determination of 5 parameters which are the failure ratio (R_f), the angle of internal friction (ϕ), the cohesion (c), the nonlinear modulus number (K), and the exponent relating the initial tangent modulus to the confining pressure (n).

Duncan and Chang suggested a somewhat similar approach to the case for unloading and reloading. Most triaxial tests indicate that for unloading and reloading it is reasonable to work with a linear modulus which is stress-dependent, such as:

$$E_{ur} = K_{ur} p_a \left(\frac{\sigma_3}{p_a}\right)^n \tag{47}$$

where: E_{ur} = unload-reload modulus

K_{ur} = unload-reload modulus number

This approach has also been used in this study.

Kulhawy et al. (1969) give the most thorough tabulation of possible nonlinear parameters to be used for analysis purposes. As would be expected, the precise values recommended for sands depend

on the type sand, its angularity, grain-size distribution, etc.

For the nonlinear study in this dissertation, the parameters n and R_f were taken as 0.5 and 0.85 respectively. The cohesion, c, was zero. The nonlinear modulus numbers (K) for use in the pounds-feet unit system were varied, as were the ϕ angles. The nonlinear modulus numbers (K) selected were 15,000 for $\phi = 32^o$, 30,000 for $\phi = 37^o$, and 60,000 for $\phi = 42^o$, which might be considered typical for loose, medium dense, and dense sand conditions. Study of the parametric data given by Kulhawy et al. (1969) indicates that it is reasonable to use an unload-reload modulus number approximately one-third larger than the nonlinear modulus number. This was generally done in these studies, but the unload-reload modulus number could be varied.

Lee (1970) has compared the results of plane strain and triaxial tests on sands. He points out that the angle of friction, initial tangent modulus, and Poisson's ratio are generally slightly higher for plane strain testing, compared to triaxial testing. He shows theoretically that the elastic moduli and Poisson's ratios can be compared by

$$E_{ps} = \frac{E_{tr}}{1 - \nu_{tr}^2} \tag{48}$$

and

$$\nu_{ps} = \frac{\nu_{tr}}{1 - \nu_{tr}} \tag{49}$$

where: E_{ps} = elastic modulus for plane strain loading

E_{tr} = elastic modulus for triaxial loading

ν_{ps} = Poisson's ratio for plane strain loading

ν_{tr} = Poisson's ratio for triaxial loading

Calculations based on these formulas are given in Table 3, which also includes some measured results from Lee's work. Study of these data indicate that the theoretical and measured variations in Poisson's ratio compare favorably. However, the theoretical variations in the elastic modulus are less than those measured. Whereas the theoretical variation is very slight, about 10 percent, the measured elastic modulus variations are around 40 percent.

In comparing the results of the strain studies for axisymmetric and plane strain loading, these material property variations must be considered. Further discussion on this point will be made later in section 4.3.3.

3.3 Poisson's Ratio

Kulhawy, Duncan, and Seed (1969) have developed an approach for a nonlinear stress-dependent Poisson ratio in a manner similar to that developed in Section 3.2 for the elastic modulus. Unfortunately, the technique is not as sensitive for analysis purposes as the nonlinear modulus approach. An attempt has been made to use this technique, however, and it is included as an option in the computer programs. Accordingly, the following is a brief description of its major features. An application is given in Chapter 6.0, where some of its limitations will be further discussed.

The tangent Poisson ratio, ν_t, may be defined as the rate of variation of radial strain with axial strain under conditions of axial compression without radial restraint:

$$\nu_t = \frac{\delta\varepsilon_r}{\delta\varepsilon_a} \tag{50}$$

Table 3. Comparison of Theoretical and Measured Elastic Constants from Plane Strain and Triaxial Testing (After Lee, 1970)

ν_{tr}	ν_{ps}		E_{ps}/E_{tr} **	
	Theoretical	Measured	Theoretical	Measured
0.1	0.11	0.12	1.01	1.4
0.2	0.25	0.27	1.04	1.4
0.3	0.43	0.44	1.10	1.4

** Ratio of E_i from theory and laboratory testing.

where: ν_t = tangent Poisson's ratio

ε_r = radial strain

ε_a = axial strain

Under conditions of normal triaxial testing, the axial strain and the volume strain can be measured. The average value of the radial strain may then be expressed as

$$\varepsilon_r = \frac{\varepsilon_v - \varepsilon_a}{2} \tag{51}$$

where ε_v is the volumetric strain. Typical variations of volumetric strain and radial strain as a function of axial strain are given in Figures 21 and 22. The slope of the curves in Figure 22 is the tangent Poisson ratio, and is seen to be a function of (i) confining pressure and (ii) axial strain.

Using a hyperbolic approach as described in Section 3.2, the nonlinear relationships between axial and radial strains may be written

$$\varepsilon_a = \frac{\varepsilon_r}{f + j\varepsilon_r} \tag{52}$$

where f and j are parameters to be obtained experimentally. If this relation is rewritten in the form

$$\frac{\varepsilon_r}{\varepsilon_a} = f + j\,\varepsilon_r \tag{53}$$

it can be noted that the parameter f is the value of the $\varepsilon_r/\varepsilon_a$ ratio at zero strain. The f can be redefined as the initial Poisson Ratio, ν_i. It is also noted that the parameter j is the slope of the line as represented by Equation 53. This is illustrated in Figure 23.

Kulhawy et al. give numerous examples indicating that the volume change characteristics of most soils may be represented to a reasonable

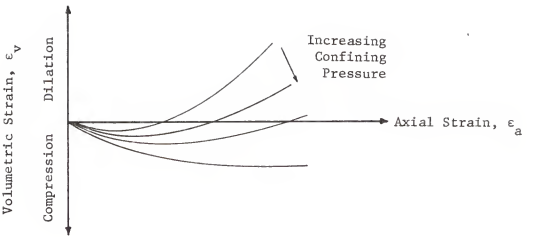


Figure 21. Volumetric Strain vs. Axial Strain

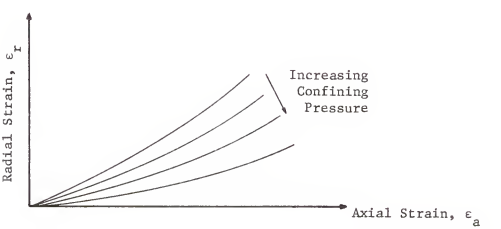


Figure 22. Radial Strain vs. Axial Strain

degree of accuracy by this hyperbolic relationship. In addition, they present the results of numerous tests to determine the effect of the initial Poisson ratio as a function of confining pressure. Figure 24 shows the typical method for presenting such results. They thus propose that the initial Poisson ratio be expressed as

$$\nu_i = G - F \log\left[\frac{\sigma_3}{p_a}\right] \tag{54}$$

where: p_a = unit pressure (same units as σ_3)

G = value of ν_i at unit pressure

F = empirical parameter representing rate of decrease of ν_i with increasing confining pressure.

Using these definitions and empirical relationships, it is then possible to express the tangent Poisson ratio for any state of stress and include both nonlinearity and stress-dependency.

Equation 50 may be rewritten

$$\frac{1}{\nu_t} = \frac{\delta\varepsilon_a}{\delta\varepsilon_r} \tag{55}$$

By differentiating Equation 52, the tangent Poisson ratio may be expressed:

$$\nu_t = \frac{f}{(1 - j\varepsilon_a)^2} \tag{56}$$

Now j is the initial Poisson ratio, which is given by Equation 54. Substituting Equation 54 into Equation 56, we obtain

$$\nu_t = \frac{G - F \log\left[\frac{\sigma_3}{p_a}\right]}{(1 - j\,\varepsilon_a)^2} \tag{57}$$

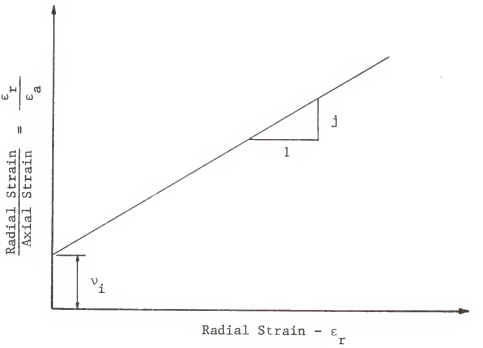


Figure 23. Transformed Hyperbolic Axial-Radial Strain Curve

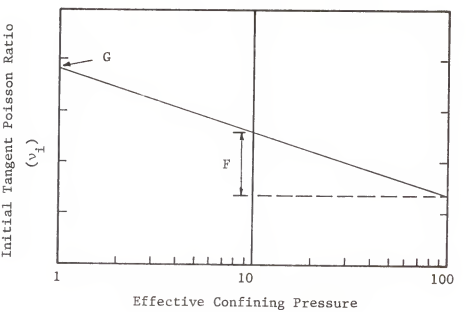


Figure 24. Variation of Initial Tangent Poisson Ratio with Confining Pressure

The axial strain may be eliminated by using the stress-strain relationships developed in Section 3.2. The resulting relationship for a nonlinear tangent Poisson ratio is

$$\nu_t = \frac{G - F \log (\sigma_3/p_a)}{\left[1 - \frac{j(\sigma_1 - \sigma_3)}{Kp_a \left\{\frac{\sigma_3}{p_a}\right\}^n \left[1 - \frac{R_f(\sigma_1 - \sigma_3)(1 - \sin\phi)}{2c\cos\phi + 2\sigma_3 \sin\phi}\right]}\right]^2} \quad (58)$$

This expression includes the five nonlinear modulus parameters previously developed in Section 3.2, as well as three additional parameters, G, F, and j.

Kulhawy et al. (1969) give some suggested values for these three parameters based on a review of triaxial test results which gave the necessary volume change measurements. Since they were primarily concerned with large embankments, their laboratory tests were at confining pressures of from 1 to 40 tsf. In using suggested values and extrapolating the results for the lower confining pressures used in these studies, the writer found that the suggested analytical model gave Poisson's ratio values greater than 0.5, and for computation purposes in the finite element program, a value of 0.48 was used.

Because it might give more meaningful parametric data if various constant Poisson's ratio values were to be used, the writer adopted this constant Poisson's ratio approach for most of the analyses. In considering some triaxial data on sand used in laboratory testing, the nonlinear approach was used and also typically resulted in a Poisson ratio of 0.48 being used in the analytical model. This will be described further in Chapter 6.0.

By running various analyses for different, but constant Poisson's ratios, it was possible to determine more effectively the importance of this parameter in addition to the nonlinear modulus number (K) and the other variables studied.

3.4 Failure Conditions

For the successive increments approach chosen for this study, it was not possible to model the stress-strain relation after the peak was reached. Since the study is primarily associated with the nonlinear elastic response of sands, however, this was not critical. However, to provide some indication of "failure" conditions in the analysis, once the Mohr-Coulomb failure criterion was developed in a given element, the modulus after failure could be treated in one of two ways.

The first way was simply to assign the modulus a very low value, but greater than 0, say 100 psf. For non-critical elements which "failed" this was often satisfactory.

Another approach, as suggested by Clough and Woodward (1967), was to rewrite the stress-strain relation from elasticity in terms of a shear and bulk modulus. For example, the stress-strain relations for plane strain conditions were given in Equation 32 as

$$\{\sigma\} = \frac{E}{(1+\nu)(1-2\nu)} \begin{bmatrix} 1-\nu & \nu & 0 \\ \nu & 1-\nu & 0 \\ 0 & 0 & \frac{1-2\nu}{2} \end{bmatrix} \{\varepsilon\} \qquad (32)$$

This could also be written as

$$\{\sigma\} = \begin{bmatrix} (B+G) & (B-G) & 0 \\ (B-G) & (B+G) & 0 \\ 0 & 0 & G \end{bmatrix} \{\varepsilon\} \qquad (59)$$

where: B = Bulk Modulus = $\frac{E}{2(1+\nu)(1-2\nu)}$

G = Shear Modulus = $\frac{E}{2(1+\nu)}$

Even after "failure" soils can carry additional normal stress. Accordingly, Clough and Woodward recommended that after the failure condition is reached in an element, the stress-strain behavior be maintained by reducing the shear modulus (G) to zero, but retaining the bulk modulus (B) to the value it had during the increment prior to the failure condition. This approach was used with reasonable results by Clough and Woodward (1967) and also by Kulhawy et al. (1969).

Both of these failure approaches were incorporated into the two computer programs used in this study. For the strain studies described in Chapter 4.0, the failure approach selected was of little consequence, since generally the loading was below failure conditions. For the pressuremeter studies described in Chapter 5.0, however, the failure approach used was more critical and the pressure-volume curve was definitely affected by the failure approach used. This effect will be discussed further in that chapter.

3.5 Octahedral Stresses and Anisotropy

The nonlinear sand model described was developed based on the results of triaxial tests. Accordingly, the model studies should use parameters which are reasonable for this model. However, a more general stress-strain approach for all materials would be to obtain

the necessary strength parameters as a function of the octahedral stress. The octahedral normal stress (σ_{oct}) is defined as

$$\sigma_{oct} = \frac{\sigma_1 + \sigma_2 + \sigma_3}{3} \tag{60}$$

where σ_2 is the intermediate principal stress. The octahedral stress approach thus includes the effects of the intermediate principal stress, which is an important factor in soil loading. In fact, the only real soil mechanics triaxial application (i.e., all around equal confining pressure) in the field, is beneath the centerline of an axisymmetric footing, with equal lateral stress in all directions. Under all other loading conditions there is an intermediate principal stress which may play a very important role in determining the stress-strain behavior of the soil.

No attempt was made to revise the nonlinear model with respect to failure conditions and other parameters. The only modification was to include σ_{oct} for σ_3 in that portion of the nonlinear model which gives the confining pressure effect. Thus the initial tangent modulus was used under the octahedral stress case as

$$E_i = K\ p_a \left[\frac{\sigma_{oct}}{p_a}\right]^n \tag{61}$$

In normal triaxial testing, σ_{oct} is continuously changing, since when $\sigma_2 = \sigma_3$,

$$\sigma_{oct} = \frac{\sigma_1 + 2\sigma_3}{3} \tag{62}$$

As σ_1 increases during normal triaxial testing, σ_{oct} also increases. It has been suggested by Newmark (1960) that the octahedral stresses be incorporated into the Mohr-Coulomb equation giving a relationship

similar to Equation 46. Although this is possible analytically, there is no testing data available in this form for use in such an analytical model. No laboratory tests were run to further study a model of this sort or to develop octahedral parameters. The approach is reasonable, however, and should be of interest for future research.

To determine any possible effects of the nonlinear modulus number (K) under anisotropic conditions, it was possible to use a different modulus number for the vertical and horizontal properties in a given stratum. It was also possible to vary all the other nonlinear parameters. Generally this was not done, however, and only the anisotropic effect of the nonlinear modulus number was considered.

This approach to anisotropy (at least for comparison with linear cross-anisotropic cases) appears reasonable. The writer knows of no nonlinear cross-anisotropic test results or studies, although this appears promising for further research. It is, of course, often difficult to get consistent isotropic nonlinear parameters for a sand, much less determine cross-anisotropic nonlinear parameters.

CHAPTER 4.0

STUDY OF VERTICAL STRAIN DISTRIBUTION IN MODEL SAND

4.1 Introduction

This study was made to obtain a better understanding of the various parameters involved in the strain distribution beneath footings on sand. The primary analytical tool employed was the finite element method. In order to determine the appropriateness of this technique for such studies, however, several classic analytical cases were investigated and compared with finite element solutions.

A sample of the typical finite element grid is shown in Figure 25. The spacing was selected in order to clearly define the peak strain locations for various types of surface loading and nonlinear model sand parameters. The large dimensions were selected in order to decrease the effects due to the bottom and side boundaries. These bottom and side boundaries were either fixed or treated as being on rollers. However, the difference in using either of these boundary constraints was generally negligible for the 100 ft by 100 ft grid.

A similar grid was used for the study of the effect of rigid layers at various depths, but it was adjusted for the bottom fixed depth position. For the close rigid layer cases, the boundary constraints were more critical.

For flexible loading, the load was applied directly to the surface.

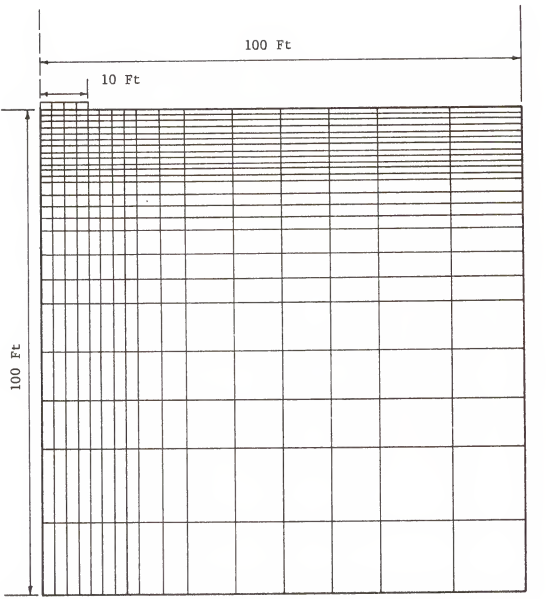


Figure 25. Typical Finite Element Grid for Strain Distribution Studies

The axisymmetric radius of loading was 10 feet (20 ft diameter) and the plane strain footing width was 20 feet, for most examples studied. For the footing loadings, a 2 ft thick concrete footing was used with the same areal dimensions.

The pressure increments could be as small as economically possible. Typically the strain study computer runs used 1000 psf increments. The difference in the resulting strain distribution curves, compared with using 500 psf increments, varied only at the peak strain locations, and the variation was generally less than 2 percent. Therefore, for computer economy, the 1000 psf increments were sufficient.

The finite element program used, which is given in Appendix II, is very similar to the one used by Duncan in his work for Schmertmann (1970). The program was modified, however, to include the plane strain case, to include cross-anisotropy, to calculate the vertical strains and strain influence factor directly, and to include the effects of octahedral confining pressures and bulk modulus failure conditions.

Several comparative runs were made to determine the effect of varying the failure condition. It was found that in general for the loadings used, the only elements which might go into "failure" were at the edge of the footing. The resulting effect on the centerline vertical strain distribution was generally negligible at pressures up to 4000 psf, but could vary up to 10 percent or more for higher pressures. For consistency in these studies, the bulk modulus failure approach was usually used.

4.2 Strain Distribution in Linear Isotropic Materials

There are many classic cases for settlement and stress distribution which have been developed (Harr, 1966). The general approach has been to develop equations, charts, and influence diagrams for obtaining the stress relationships beneath various types of surface loading on an elastic half-space. Modifications for depth to rigid layers and other boundary constraints have also been considered. Rarely is the strain distribution developed or considered.

4.2.1 Normal Loads on Flexible Footings

The classic stress and strain solutions for normal loads applied to flexible surfaces are incorporated within the ICES-SEPOL computer program as developed by M.I.T. (Jordan and Schiffman, 1967). The necessary equations for these properties can be found in Harr (1966). SEPOL was programmed for the geometries used in this study and the vertical centerline strain distribution results placed in the form of the strain influence factor, I_z, which was given by Equation 27.

The results for the 20 ft diameter flexible circular footing and the 20 ft square flexible footing are given in Figures 26 and 27. Careful study of these figures indicates that they are almost identical. The peak strain location is at a depth of from D/4 to 3D/8 and is a function of Poisson's ratio. The peak strain influence factor values vary from 0.58 for a Poisson ratio of 0.5 to a value of 0.75 for a Poisson ratio of 0.3. At a depth of 2D the value of the strain influence factor is 0.1 for all Poisson ratios.

The results for the 20 ft wide infinitely long flexible footing are somewhat different as would be expected since the loading condition is now plane strain. These results are shown in Figure 28. The peak strain

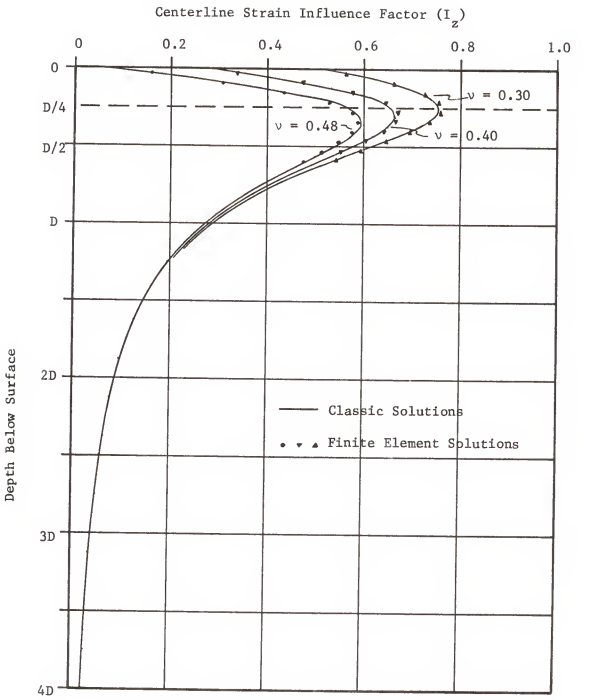


Figure 26. Comparison of Vertical Strain Influence Factor Calculations as made by Classic Solution (SEPOL) and Finite Element Method for a Linear Elastic, Homogeneous, Isotropic Material Under Axisymmetric Flexible Loading

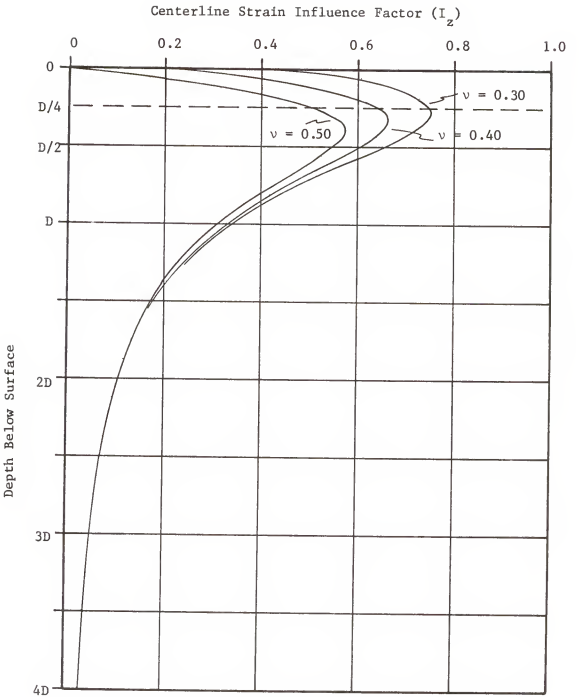


Figure 27. Vertical Strain Influence Factor Using SEPOL for Square Flexible Footing on Linear Elastic, Homogeneous, Isotropic Material

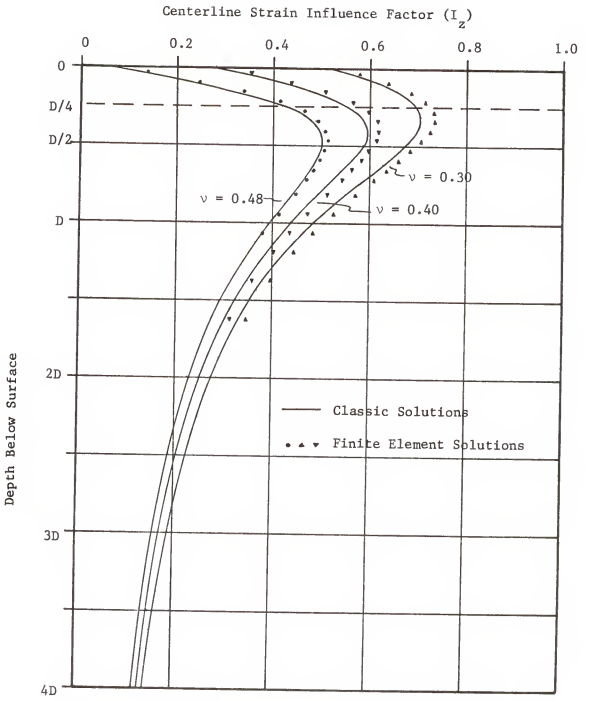


Figure 28. Comparison of Vertical Strain Influence Factor Calculations as made by Classic Solution (SEPOL) and Finite Element Method for a Linear Elastic, Homogeneous, Isotropic Material Under Plane Strain Flexible Loading

location has shifted down and varies from a depth of 5D/16 to D/2, while the peak influence factor values vary from 0.48 to 0.70 for the Poisson's ratios considered. The most noticeable difference between the circular and strip footing results, however, is in the general shape of the strain influence factor curve. At a depth of 3D the influence factor value beneath the infinite strip footing is still 0.20 and it does not fall below 0.10 until a depth of over 4D.

Both of the cases discussed above were for linear, homogeneous, isotropic materials, while the loading was completely flexible and applied directly to the surface.

For comparison purposes the circular and infinite strip cases were studied using the finite element grid shown in Figure 25. These results are superimposed on Figures 26 and 28. The axisymmetric circular case compares quite favorably. The plane strain finite element solution has the same general distribution, but gives strain influence factor values approximately 5 percent greater at the lower values of Poisson's ratio. This discrepancy is due to the confinement of the finite element grid as compared to the infinite geometry used for the classic cases.

In general, the strain influence factors from the theoretically exact solutions and from the finite element solutions for flexible surface loadings compare favorably. It would be expected, therefore, that when the nonlinear model sand is used that the results from the finite element analysis will be similarly suitable for the nonlinear material.

4.2.2 Normal Loads on Rigid Footings

Classic solutions for rigid loads on elastic half-spaces are not as common in the general literature as for the flexible case. One of the reasons why there are not as many solutions available is that the classic case using a rigid punch is more difficult to solve. There is additionally the added complexity due to the nature of the rigid punch and base interface which is usually taken as completely smooth (frictionless).

The displacement solution for the axisymmetric circular rigid punch was originally derived by Boussinesq (1885). The vertical centerline displacement for this case can also be obtained by extending the work of Harding and Sneddon (1945). In terms of the variables used in this dissertation, the resulting centerline displacement is

$$w\,(0,z) = \frac{q}{E}\, a\,(1-\nu^2)\,\mathrm{Cot}^{-1}\,\frac{z}{a} + \frac{q}{E}\,\frac{a(1+\nu)}{2}\left[\frac{z/a}{1+(z/a)^2}\right] \qquad (63)$$

where q is the average pressure on the punch of radius a, w is the vertical displacement, and z is the depth below the base of the punch. If this relationship is differentiated and placed in the form of a strain influence factor, the result is

$$I_z = \frac{(1-2\nu)(1+\nu)}{2}\left[\frac{1}{1+(z/a)^2}\right] + (1+\nu)\left[\frac{z/a}{1+(z/a)^2}\right]^2 \qquad (64)$$

Figure 29 gives the plot of this influence factor and compares it with the finite element solution using the concrete footing. The form of the influence factor relationship is similar for the two cases, but the precise peak values are different.

The major reason for the discrepancies between the finite element and the classical solutions in Figure 29 has to do with the nature of

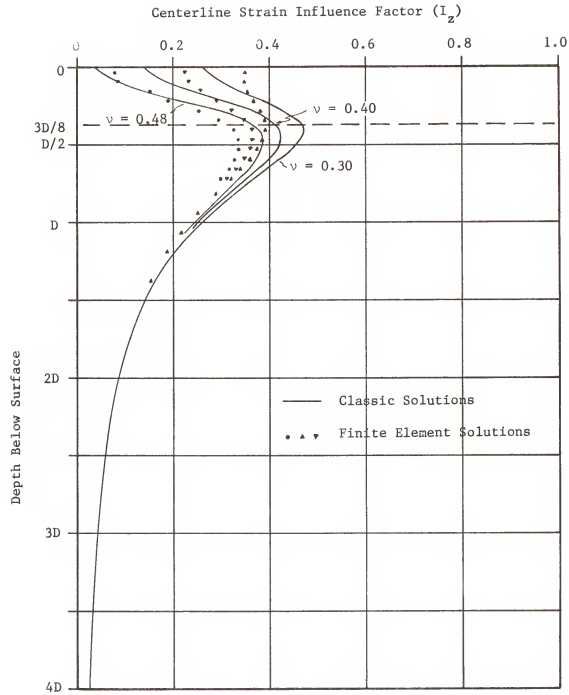


Figure 29. Comparison of Vertical Strain Influence Factor Calculations as made by Classic Rigid Circular Punch and Finite Element Method with Concrete Footing, for a Linear Elastic, Homogeneous, Isotropic Material under Axisymmetric Loading

the finite element grid used. As will be seen, the grid selected (Figure 25) gives very good results for the plane strain rigid loadings, as well as the flexible loadings previously discussed. Because of the nature of the axisymmetric loading, however, the grid at the edge of the footing should be much finer because of the high displacement gradients there when rigidly loaded.

For a classic axisymmetric study, therefore, a finer and more costly grid would be more advantageous. When using a finer grid with the nonlinear stress-dependent model, however, the smaller elements accentuated the edge failure conditions previously discussed and could cause variations in the vertical centerline strain influence factor of as much as 20 percent or more depending on the failure conditions used, the pressure applied, etc. Therefore, in order to maintain uniformity within these parametric studies, the original grid selected in Figure 25 was maintained, the bulk failure condition was used, and the loading increment was uniformly 1000 psf.

Although the rigid results do not compare as favorably as for the flexible case, they are reasonable based on the assumptions and differences involved in the two methods of solution, and including the problems associated with a general grid selection in the finite element parametric analysis.

In comparing the axisymmetric rigid case (Figure 29) with the flexible case (Figure 26), it is noted that the peak strain influence factor location has shifted to between 3D/8 and D/2 beneath the surface, while the peak influence factor variation is from 0.38 to 0.47 for the classic rigid punch, compared to 0.59 to 0.76 for the flexible loading. At a depth of 2D, the influence factor equals approximately 0.1 for

either the rigid or the flexible case and for all Poisson's ratios.

Harr (1966) has given the solution for the vertical displacement beneath a rigid infinite strip as originally presented by Egorov:

$$w(0,z) = \frac{q}{E}\frac{4a}{\pi}(1-\nu^2)\left[\text{Sinh}^{-1}\frac{z}{a} - \frac{1}{2(1-\nu)}\frac{z/a}{\{1+(z/a)^2\}^{\frac{1}{2}}}\right] + C \qquad (65)$$

where all terms have been defined and C is an arbitrary constant. If this relationship is differentiated and placed in the form of a strain influence factor, the result is

$$I_z = \frac{4}{\pi}(1-\nu^2)\left[\frac{1}{\{1+(z/a)^2\}^{\frac{1}{2}}} - \frac{1}{2(1-\nu)\{1+(z/a)^2\}^{\frac{1}{2}}} + \frac{(z/a)^2}{2(1-\nu)\{1+(z/a)^2\}^{3/2}}\right] \qquad (66)$$

This classic vertical strain influence factor has been plotted in Figure 30. These results differ from the flexible loading case (Figure 28). The peak strain is located at a depth of from D/2 to 5D/8 and the peak strain values vary from only 0.38 to 0.52 as compared to 0.48 to 0.70 for the flexible loading. As in the flexible case, the influence factor does not fall below a value of 0.1 until a depth of over 4D.

Again a comparison is made in Figure 30 with the finite element solution for a 2 ft thick concrete footing. The comparison is reasonable for all Poisson's ratios, except near the surface. As previously discussed, the major reason for the discrepancies is due to the nature of the finite element grid. Another reason is that the classic solution assumes a frictionless punch base, while the finite element footing is in continuous displacement contact with the foundation.

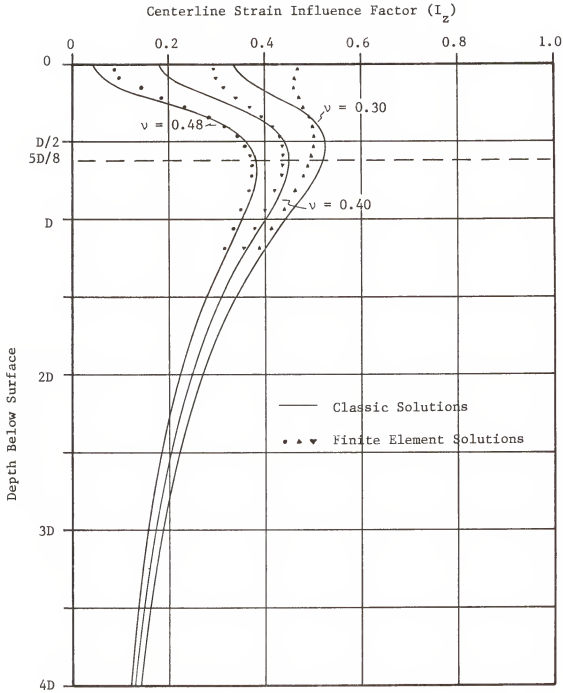


Figure 30. Comparison of Vertical Strain Influence Factor Calculations as made by Classic Rigid Strip Punch and Finite Element Method with Concrete Footing, for a Linear Elastic, Homogeneous, Isotropic Material under Plane Strain Loading

Some comments should be made with respect to the effects of rigidity. Terzaghi (1943) gives a thorough discussion of this topic and defines a rigidity factor as

$$K_r = \frac{1}{6} \frac{1-\nu_s^2}{1-\nu_p^2} \frac{E_p}{E_s} \left[\frac{H}{R}\right]^3 \tag{67}$$

where: E_p = Elastic modulus of the footing

E_s = Elastic modulus of the subgrade

ν_p = Poisson's ratio of the footing

ν_s = Poisson's ratio of the subgrade

R = radius of circular footing

H = thickness of circular footing

A K_r of zero indicates a perfectly flexible loading, while a K_r of infinity means a perfectly rigid loading. As Terzaghi shows, a rigidity factor of 1.0 or greater gives a subgrade pressure distribution very similar to that for the perfectly rigid case.

In these studies, using a 20 ft diameter, 2 ft thick concrete footing, with a Poisson ratio of 0.25 and an elastic modulus of 3,000,000 psi on a soil with a Poisson ratio of 0.4, the rigidity factor as a function of the soil modulus can be written

$$K_r = \frac{258}{E_s} \tag{68}$$

where E_s is in units of tsf. Theoretically the nonlinear soil modulus near the surface is zero because there is no confinement. However, the modulus increases rapidly with depth, and can attain values of from 100 to 300 tsf or more at depths of 5 ft depending on the sand density, lateral confinement, and other factors. Since K_r near the base is generally one or greater, the footing used in these studies is very similar to the perfectly rigid footing.

4.2.3 Conclusions Based on Linear Analyses

Study of the results of these linear elastic analyses indicates several initial conclusions.

For axisymmetric loading, it is very reasonable to assume a triangular strain influence factor distribution, as suggested by Schmertmann (1970), with a peak influence factor location between D/4 and D/2 beneath the surface and extending to a depth 2D. The value of the peak strain influence factor is a function of Poisson's ratio and varies from 0.38 to 0.47 for the rigid punch and from 0.59 to 0.76 for the flexible case.

For plane strain loading, the depth of any assumed triangular distribution should extend below 2D. Four times D, or even 6D, appear reasonable. The peak strain influence factor location varies from 3D/8 to 5D/8, with D/2 also a reasonable average location. The value of the peak strain influence factor is a function of Poisson's ratio and varies from 0.38 to 0.52 for the rigid strip and from 0.50 to 0.70 for the flexible case.

In most elastic settlement analyses in soil mechanics, it is common to use the simplified formula (Schleicher, 1926; Bowles, 1968)

$$\rho = q\ D \left[\frac{1 - \nu^2}{E}\right] I_w \tag{69}$$

where ρ is the settlement, D is the least foundation dimension, and I_w is the settlement influence factor, which differs from Schmertmann's strain influence factor (I_z). All other terms have been previously defined. The influence factors for use in this equation are given in Table 4, which is taken, in part, from Bowles (1968).

Table 4. Settlement Influence Factors (I_w) for Flexible and Rigid Footings (From Bowles, 1968)

	Flexible (Center)	Rigid
Circle	1.00	0.79
Rectangle: (L/D=10)	2.52	2.10
Rectangle: (L/D=100)	3.38	3.40

If a single triangular distribution is assumed, with a constant modulus material, then the settlement using Schmertmann's influence factor (I_z) may be written

$$\rho = \frac{q}{E} \times \frac{1}{2} \times I_{zp} \times (\text{Depth of Influence}) \tag{70}$$

where I_{zp} is the peak value assumed for the strain influence factor using the triangular distribution. If Equation 70 is equated to Equation 69, it is seen that the peak strain influence factor value can be written as

$$I_{zp} = \frac{(D)(1-\nu^2)(I_w)}{\frac{1}{2}(\text{Depth of Influence})} \tag{71}$$

Specifically, for axisymmetric loading, if the depth of influence for a triangular distribution is taken as 2D, then

$$I_{zp} = (1-\nu^2) \quad I_w \tag{72}$$

and if the depth of influence is taken as 3D, then

$$I_{zp} = \frac{2}{3} \quad (1-\nu^2) \quad I_w \tag{73}$$

If Equations 72 and 73 are solved for the peak strain influence factor (I_{zp}) as a function of the settlement influence factor (I_w) for the assumed triangular depths of influence, then the results can be compared with the classic strain influence factor peak values. These results are shown in Table 5.

Study of Table 5 indicates that using an assumed depth of 3D for the axisymmetric case gives a more favorable comparison with the classic flexible and rigid cases. However, study of Figures 26 and 29 indicates

Table 5. Comparison of Peak Strain Influence Factor (I_{zp}) for Triangular Distribution Using Classic Solution and Settlement Influence Factors (I_w) Under Axisymmetric Loading on Linear Elastic Material for Equal Settlement

Poisson's Ratio (ν)	Assumed Triangular Distribution				Actual Classic Distribution	
	Depth = 2D		Depth = 3D			
	Flexible (Center)	Rigid*	Flexible (Center)	Rigid*	Flexible (Center)	Rigid*
0.48	0.77	0.61	0.52	0.40	0.59	0.38
0.40	0.84	0.66	0.56	0.44	0.66	0.42
0.30	0.91	0.72	0.60	0.48	0.75	0.47

* Frictionless Base

that a depth of 2D is a more reasonable depth of influence for an assumed triangular distribution. Table 5 also shows that an average peak value of 0.5 to 0.7 is reasonable for either the rigid or the flexible loadings. Since most structures are not as flexible as assumed in these flexible analyses, an average peak strain influence factor value of 0.6 for all cases and all Poisson's ratios appears reasonable and is in agreement with Schmertmann's recommendations.

For plane strain loading, the depth of influence values studied were 4D, 6D, and 8D. The peak strain influence factor relations are then:

$$I_{zp} = \frac{1}{2} \quad (1-\nu^2) \quad I_w \tag{74}$$

for a depth of influence of 4D, and

$$I_{zp} = \frac{1}{3} \quad (1-\nu^2) \quad I_w \tag{75}$$

for a depth of influence of 6D, and

$$I_{zp} = \frac{1}{4} \quad (1-\nu^2) \quad I_w \tag{76}$$

for a depth of influence of 8D.

For these cases, the rectangular settlement influence factors must be used. Consider the case of a rectangular loading with L/D = 100. The settlement influence factor (I_w) from Table 4 for both flexible and rigid loading may be taken as 3.40. Table 6 gives the results of calculations using Equations 74, 75, and 76 compared to the classic results.

Study of Table 6 indicates that the most favorable comparison is made using a depth of 8D, with a peak strain influence factor value of 0.7. This is a higher peak value than is indicated by the classic plane strain studies and a depth of 8D appears unreasonable based on

an apparent extrapolation of Figures 28 and 30 for the plane strain analyses. The writer believes, therefore, that when using the strain influence factor approach under plane strain loading, a depth of 6D is reasonable. For all foundations, both flexible and rigid, and a depth of influence of 6D, a peak centerline strain influence factor value of from 0.85 to 1.00 also appears reasonable. A good average value for all Poisson's ratios might be 0.9.

The strain influence factor should have a value of zero at the surface, but only for a Poisson ratio of 0.5. It appears from a study of Figures 29 and 30, however, that it would be more reasonable to have an intercept at the surface with a value of 0.2. This would be more applicable for lower Poisson's ratios and would be reasonable for both axisymmetric and plane strain loadings.

Based on these linear studies, therefore, two simplified triangular centerline vertical strain influence factor distributions appear reasonable. The recommended axisymmetric 0.6-2D and plane strain 0.9-6D distributions, with surface intercept values of 0.2 and peak values at a depth of D/2 are shown in Figure 31.

It should be noted that the area under the plane strain distribution is approximately 4 times that under the axisymmetric distribution. According to Table 4, rectangular settlements should be from 2.5 to 4.3 times circular settlements, and are a function of the L/D ratio as well as the type of loading. Thus the distributions in Figure 31 appear reasonable based on these settlement influence factor considerations.

It should be emphasized that these studies considered the vertical centerline strain influence factor only. It is recognized

Table 6. Comparison of Peak Strain Influence Factor (I_{zp}) for Triangular Distribution Using Classic Solution and Settlement Influence Factors (I_w) Under Plane Strain Loading on Linear Elastic Material for Equal Settlement

Poisson's Ratio (ν)	Assumed Triangular Distribution			Actual Classic Distribution	
	Depth = 4D	Depth = 6D	Depth = 8D		
	Flexible and Rigid *	Flexible and Rigid *	Flexible and Rigid *	Flexible (Center)	Rigid
0.48	1.27	0.85	0.64	0.50	0.38
0.40	1.43	0.95	0.71	0.60	0.45
0.30	1.55	1.03	0.77	0.70	0.53

* L/D = 100 (From Table 3)

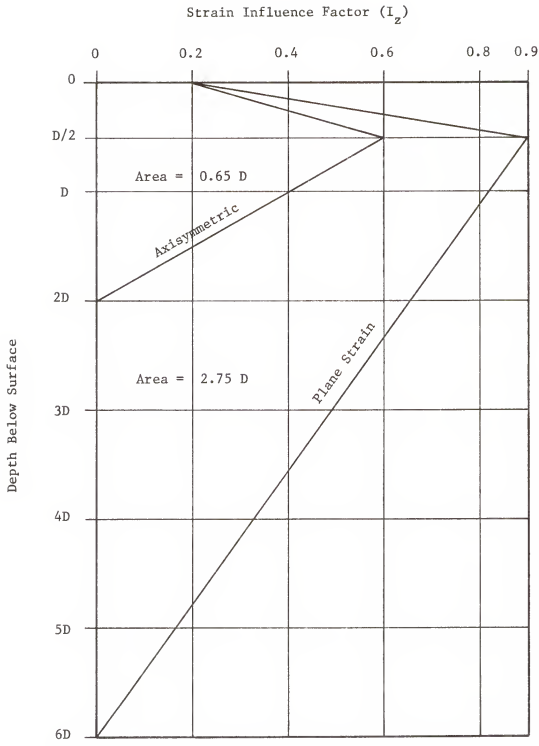


Figure 31. Recommended Triangular Vertical Strain Influence Factor Distributions Based on Study of Linear Elastic Materials Under Rigid Loading

that there is a variation in vertical strain beneath rigid footings that is different at the edge when compared to the center. Some additional comments on this will be made in Section 4.6.

4.3 Strain Distribution in Nonlinear Model Sand

Using the nonlinear sand model, a finite element study was conducted to determine the importance of various parameters in the vertical strain distribution. These parameters included the effects of the nonlinear stress-dependent modulus number (K), Poisson's ratio (ν), the influence of lateral stresses, and possible consequences due to rigid layers and foundation embedment.

Prior to loading, the soil is under geostatic gravity stresses due to the overburden. The vertical overburden pressure was herein assumed equal to the unit weight of the soil (γ) times the depth (h). The lateral stresses are obtained by multiplying the vertical stress at any depth by the lateral stress coefficient (k_o), which is also often referred to as the coefficient of lateral earth pressure.

These studies were made using a dry sand analytical model. Since the buoyancy effect due to a high ground water table decreases the effective stress, and thus the stress-dependent modulus also, this should cause an increase in the settlement. This effect was not modeled in this study, however, and could be a promising area for future research. Field exploration techniques, moreover, should measure this decreased modulus, and there might not be any major effect when using the strain factor approach to calculate settlement.

Because of this gravity stress distribution, the in-situ tangent modulus will be a function of depth. Using $\sigma_1 = \gamma h$ and $\sigma_3 = k_o \gamma h$,

the tangent modulus relationship (Equation 46) can be rewritten for the initial in-situ conditions prior to foundation loading. For a sand (c=0), and for the case of the modulus being a function of the minor principal stress, σ_3, Equation 46 then becomes:

$$E_{to}(\sigma_3) = \left[1 - R_f\left(\frac{1 - \text{Sin } \phi}{\text{Sin } \phi}\right)\left(\frac{1 - k_o}{2k_o}\right)\right]^2 Kp_a\left[\frac{\sigma_3}{p_a}\right]^n \qquad (77)$$

where $E_{to}(\sigma_3)$ is the initial in-situ tangent modulus as a function of the minor principal stress.

Using the condition of the modulus as a function of the octahedral stress, it is necessary to write the octahedral stress as a function of the in-situ stresses:

$$\sigma_{oct} = \frac{\gamma h}{3}(2k_o + 1) \qquad (78)$$

and then Equation 46 becomes:

$$E_{to}(\sigma_{oct}) = \left[1 - R_f\left(\frac{1 - \text{Sin } \phi}{\text{Sin } \phi}\right)\left(\frac{1 - k_o}{2k_o}\right)\right]^2 Kp_a\left[\frac{\gamma h}{3}\left(\frac{2k_o + 1}{p_a}\right)\right]^n \qquad (79)$$

where $E_{to}(\sigma_{oct})$ is the initial in-situ tangent modulus as a function of the octahedral stress. There is a small variation due to using octahedral stresses instead of minor principal stresses.

These initial tangent modulus variations with depth as given by Equations 77 and 79 are plotted in Figures 32 through 34 for the three typical sands selected in Section 3.2. For all cases a soil unit weight of 100 pcf was used. Using a range of densities, say 90 to 110 pcf, would cause a variation of less than 10 percent in E_{to} and even less variation in strain factor analyses.

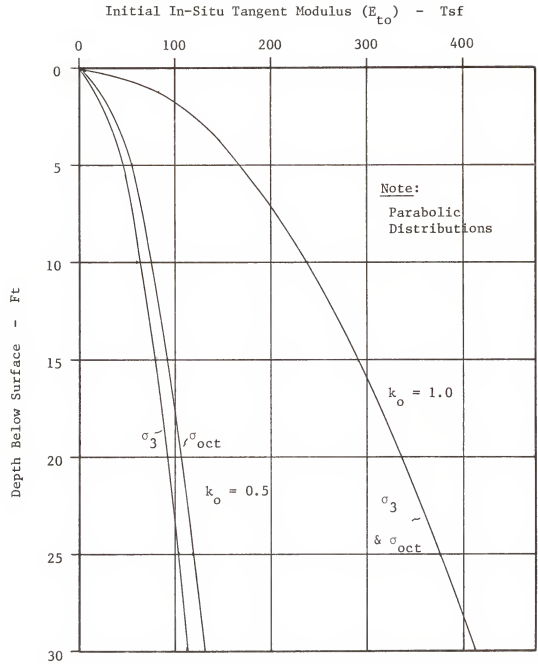


Figure 32. Initial In-Situ Tangent Modulus vs. Depth, K = 15,000, $\phi = 32^{\circ}$, n = 0.5, R_f = 0.85 γ = 100 pcf (Simulated Typical Loose Sand)

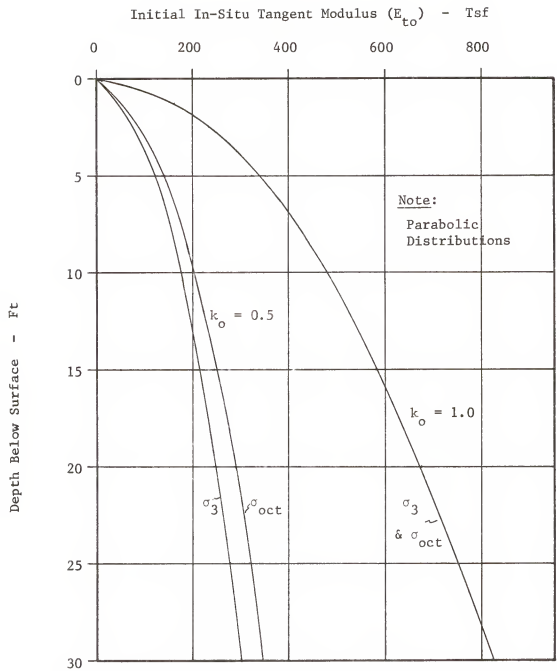


Figure 33. Initial In-Situ Tangent Modulus vs. Depth, $K = 30{,}000$, $\phi = 37^{\circ}$, $n = 0.5$, $R_f = 0.85$, $\gamma = 100$ pcf (Simulated Typical Medium Dense Sand)

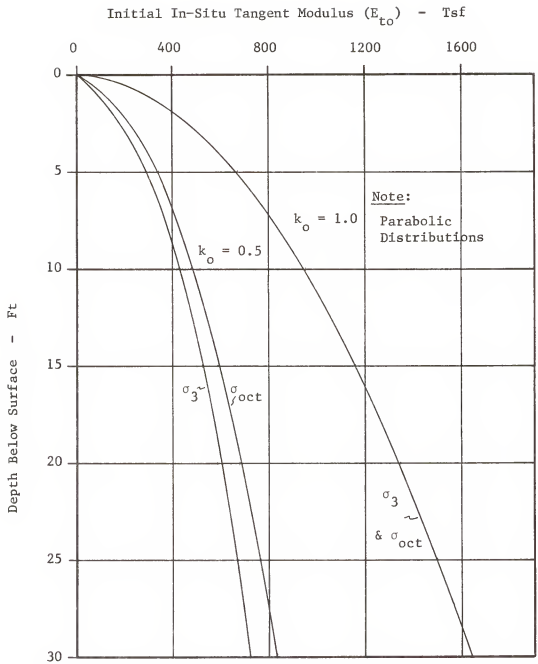


Figure 34. Initial In-Situ Tangent Modulus vs. Depth
K = 60,000, $\phi = 42^o$, n = 0.5, R_f = 0.85
γ = 100 pcf
(Simulated Typical Dense Sand)

To obtain the strain influence factors using the nonlinear model, it is necessary to normalize the strain results for each applied load and modulus used. This is a simple and straightforward procedure when analyzing linearly elastic materials, but will vary for nonlinear analyses.

The loading of a nonlinear stress-dependent modulus material is very complicated. As the load is applied the confining stresses (either minor principal or octahedral) are increased. The initial modulus therefore should increase from this effect. However, as the strain increases, the tangent modulus should decrease, and this latter effect is usually dominant. The modulus considerations are further complicated when one tries to include edge effects, local failure regions, etc.

To normalize these results from the nonlinear analyses, the applied surface load was used, as was the original in-situ initial tangent modulus (Figures 32, 33, and 34). Since theoretically this is the modulus that should be determined during any field soil exploration tests, it was selected as being the best modulus to use to obtain the dimensionless centerline vertical strain influence factor (I_z).

It is also possible to consider the use of a secant or chord type of modulus. For such a consideration, however, it is necessary to specify a certain level of stress or strain in order to determine any secant or chord modulus values. It will be seen in Chapter 5.0 that the pressuremeter analysis gives the initial in-situ tangent modulus in these analytical studies only under very precise conditions.

4.3.1 Axisymmetric Loading

The results of loading the 20 ft diameter 2 ft thick concrete footing on the nonlinear elastic sand model under axisymmetric conditions are given in this section.

Figures 35 through 37 give the centerline vertical strain distribution for K = 60,000 and Poisson's ratios of 0.3, 0.4, and 0.48 under the conditions of using the minor principal stress. The figures show that the peak strain occurs at a depth of from 3D/8 to 5D/8 and is a function of both Poisson's ratio and the surface load.

The vertical strain influence factors for nonlinear cases were obtained by dividing the vertical strain by the in-situ tangent modulus at that depth and multiplying by the applied surface load, as described previously. These centerline strain influence factors are shown in Figures 38 through 40. It is noted that the peak strain influence factor value occurs at a slightly lower depth than that for the peak vertical strain. This peak location is at a depth of from D/2 to 3D/4 and is also a function of both Poisson's ratio and the surface load. At a depth of 2D the strain influence factor value is approximately 0.1 or less.

These figures all show that a single triangular distribution extending to a depth 2D and with a peak at D/2 is very reasonable for axisymmetric loading of a nonlinear stress-dependent modulus material. The question is, however, what should be the peak strain influence factor value for such a distribution, using a depth 2D?

If the peak strain influence factor values from Figures 38 through 40 are plotted as a function of Poisson's ratio and the surface loading, the result is as shown in Figure 41. Additionally, if a similar

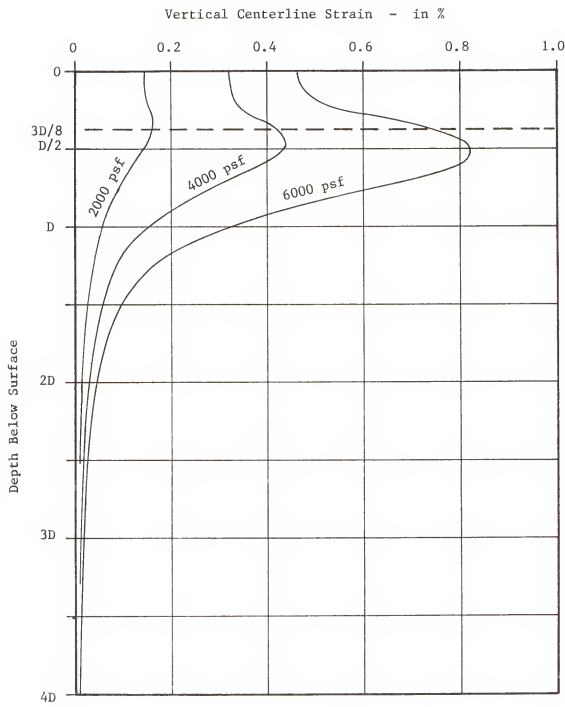


Figure 35. Vertical Centerline Strain Distribution for Axisymmetric Loading of 20 Ft Diameter Concrete Footing Using Minor Principal Stresses and Bulk Failure Condition; K = 60,000, ν = 0.30, and k_o = 0.50

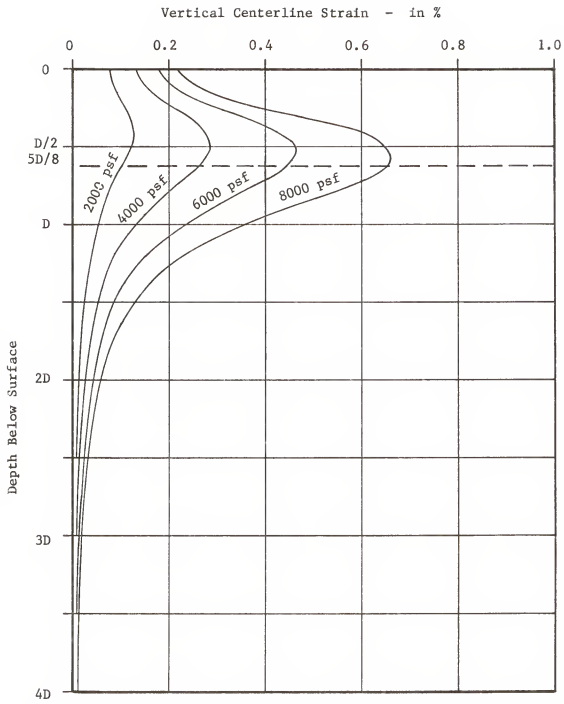


Figure 36. Vertical Centerline Strain Distribution for Axisymmetric Loading of 20 Ft Diameter Concrete Footing Using Minor Principal Stresses and Bulk Failure Condition; K = 60,000, ν = 0.40, and k_o = 0.50

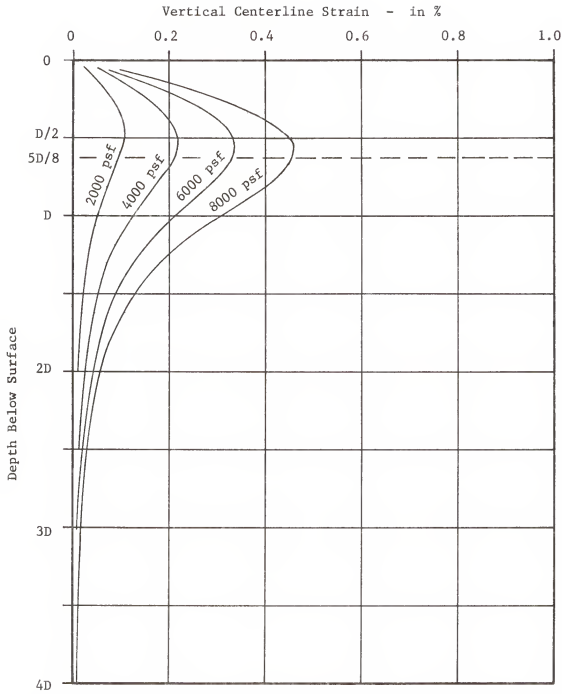


Figure 37. Vertical Centerline Strain Distribution for Axisymmetric Loading of 20 Ft Diameter Concrete Footing Using Minor Principal Stresses and Bulk Failure Condition; K = 60,000, ν = 0.48, and k_o = 0.50

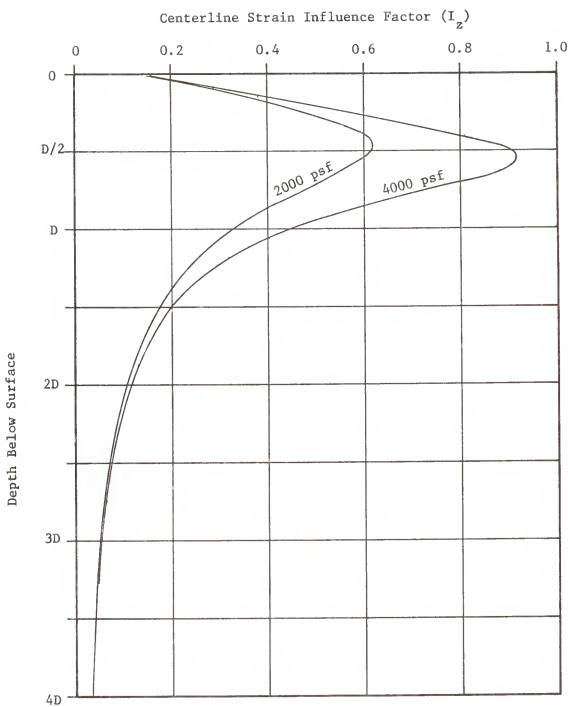


Figure 38. Centerline Vertical Strain Influence Factor for Axisymmetric Loading of 20 Ft Diameter Concrete Footing Using Minor Principal Stresses and Bulk Failure Condition; K = 60,000, ν = 0.30, and k_o = 0.50

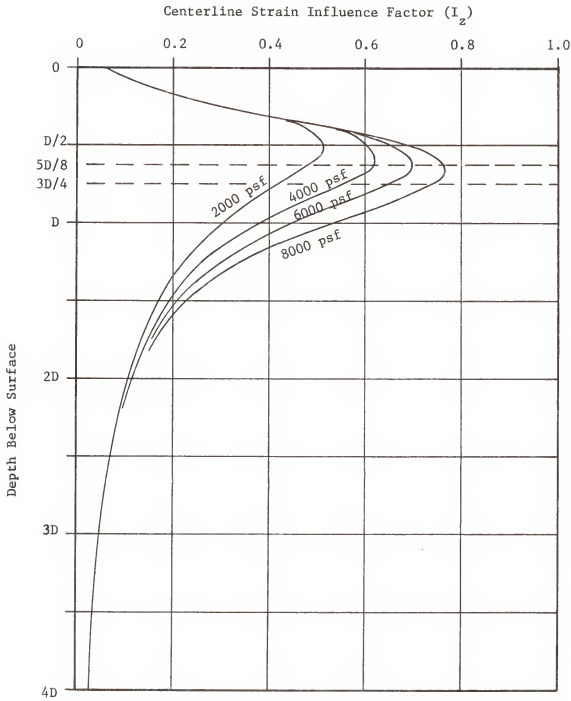


Figure 39. Centerline Vertical Strain Influence Factor for Axisymmetric Loading of 20 Ft Diameter Concrete Footing Using Minor Principal Stresses and Bulk Failure Condition; K = 60,000, ν = 0.40, and k_o = 0.50

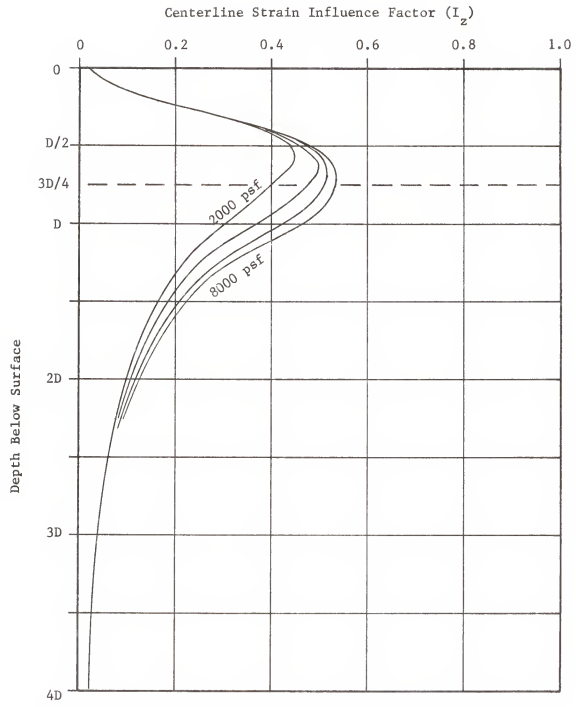


Figure 40. Centerline Vertical Strain Influence Factor for Axisymmetric Loading of 20 Ft Diameter Concrete Footing Using Minor Principal Stresses and Bulk Failure Condition; K = 60,000, ν = 0.48, and k_o = 0.50

axisymmetric analysis is made, only using flexible surface loading, and then the peak vertical centerline strain influence factors plotted, the results are as shown in Figure 42. The individual flexible loading strain distribution curves are not shown, but they are very similar in form to those in Figures 38 through 40. Also given on these figures are the equal settlement contours for the rigid footing (Figure 41) and for the center of the flexible loading (Figure 42), as well as the peak strain influence factor values from the classic axisymmetric analyses (Figures 26 and 29).

The complexity of using a single peak strain influence factor value in conjunction with an assumed triangular distribution is well illustrated in Figures 41 and 42. If it is assumed that a Poisson ratio of 0.4 is reasonable under average conditions and that loadings are typically 4000 psf, then it appears from Figure 41 that a single peak strain influence factor value of from 0.6 to 0.7 is reasonable for the concrete footing, while a value of from 0.8 to 0.9 (from Figure 42) appears more reasonable for the flexible loading case. For both these cases the settlement value is approximately 1 inch which is also reasonable.

Another way of illustrating the effect of Poisson's ratio is shown in Figures 43 and 44 where the centerline strain influence factor is plotted for three different Poisson's ratios and for specific loads of 2000 and 4000 psf. The range in peak strain influence factor values is from 0.44 to 0.92 for the loads considered. At higher surface loadings the spread would be even greater, and especially for values of Poisson's ratio less than 0.4. This large spread for higher footing loadings has already been shown in Figure 41.

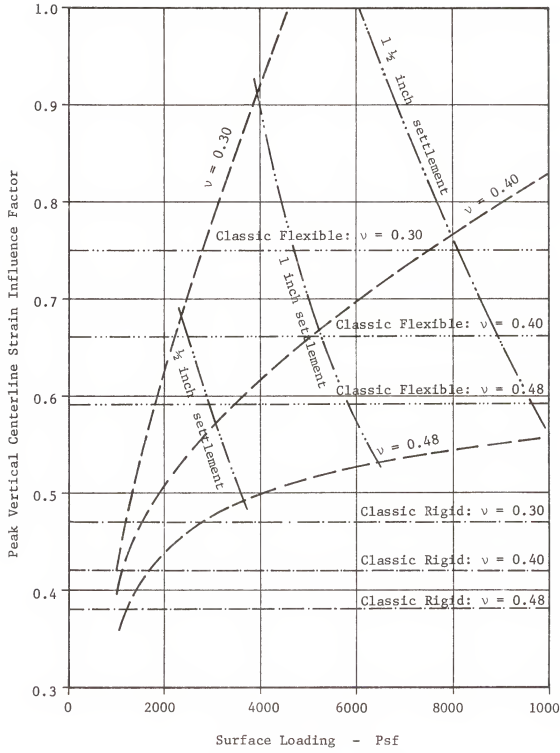


Figure 41. Peak Vertical Centerline Strain Influence Factor for Concrete Footing on Nonlinear Material under Axisymmetric Loading as a Function of Surface Loading and Poisson's Ratio; K = 60,000, k_o = 0.50

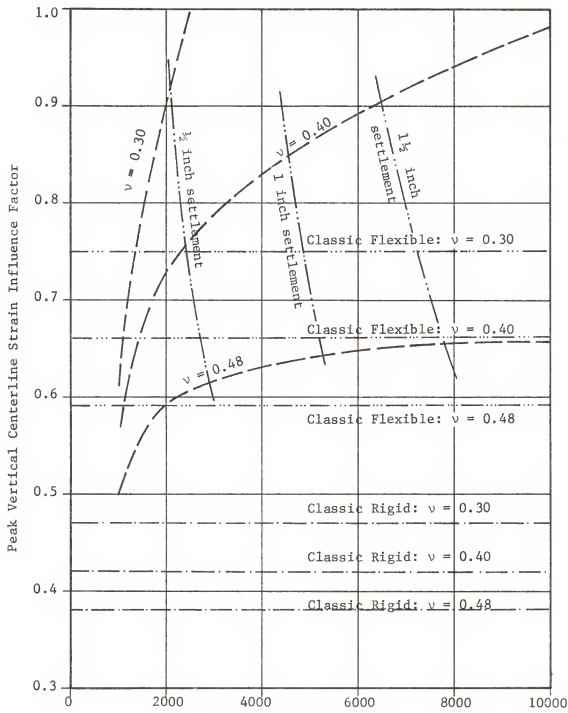


Figure 42. Peak Vertical Centerline Strain Influence Factor for Flexible Axisymmetric Loading on Nonlinear Material as a Function of Surface Loading and Poisson's Ratio; K = 60,000, k_o = 0.50

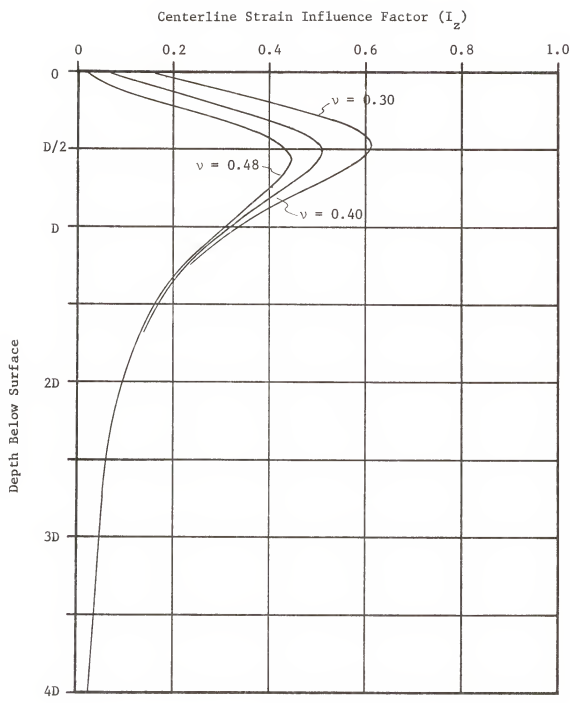


Figure 43. Centerline Vertical Strain Influence Factor for 2000 Psf Axisymmetric Loading of 20 Ft Diameter Concrete Footing Using Minor Principal Stresses and Bulk Failure Condition; K = 60,000, k_o = 0.50

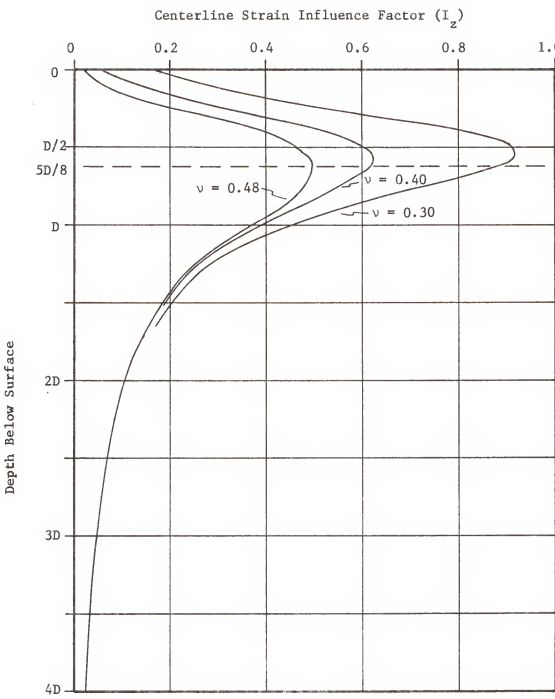


Figure 44. Centerline Vertical Strain Influence Factor for 4000 Psf Axisymmetric Loading of 20 Ft Diameter Concrete Footing Using Minor Principal Stresses and Bulk Failure Condition; K = 60,000, k_o = 0.50

Figure 45, similar to Figure 44, uses octahedral stresses instead of the minor principal stresses. Comparison of these two figures shows a discrepancy in the peak strain influence factor value of approximately 10 percent which is negligible considering the many factors involved in the nonlinear model. For other loads the discrepancy would vary from 5 to 20 percent, but would not be significant enough to affect the general results of this study.

The effect of using a lower nonlinear modulus number (K) of 30,000, typical of a medium dense sand, is shown by comparing Figures 46 and 43 for the case of a 2000 psf footing load. For the range of Poisson's ratios considered, the range of peak strain influence factors is from 0.44 to 0.62 for K = 60,000 (dense sand) and from 0.48 to 0.76 for K = 30,000 (medium dense sand). The discrepancy increases for larger loads, especially for Poisson's ratios less than 0.4. Inspection of all these figures indicates that the 2D depth of influence is reasonable for axisymmetric loading.

If the peak strain influence factor values from a series of runs using K = 30,000 (medium dense sand) and K = 15,000 (loose sand) are plotted as a function of Poisson's ratio and the surface loading, the results are as shown in Figures 47 and 48 which should be compared with Figure 41. The general result of using a lower nonlinear modulus number is to decrease the peak strain influence factor.

The results in Figures 47 and 48 are as expected. For progressively less dense soils it requires a progressively lower surface loading to get the same total settlement. Additionally, since the nonlinear modulus number is decreasing by approximately the same factor, the ratio p/E remains the same. Thus, using a simplified

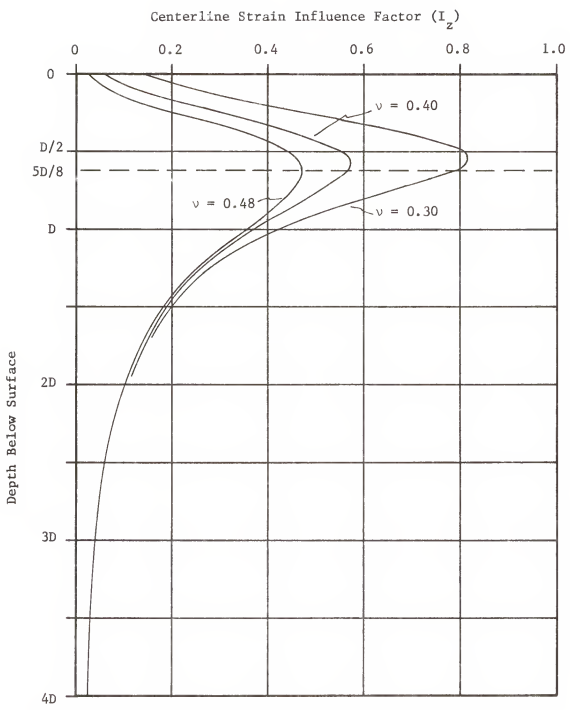


Figure 45. Centerline Vertical Strain Influence Factor for 4000 Psf Axisymmetric Loading of 20 Ft Diameter Concrete Footing Using Octahedral Stresses and Bulk Failure Condition; K = 60,000, k_o = 0.50

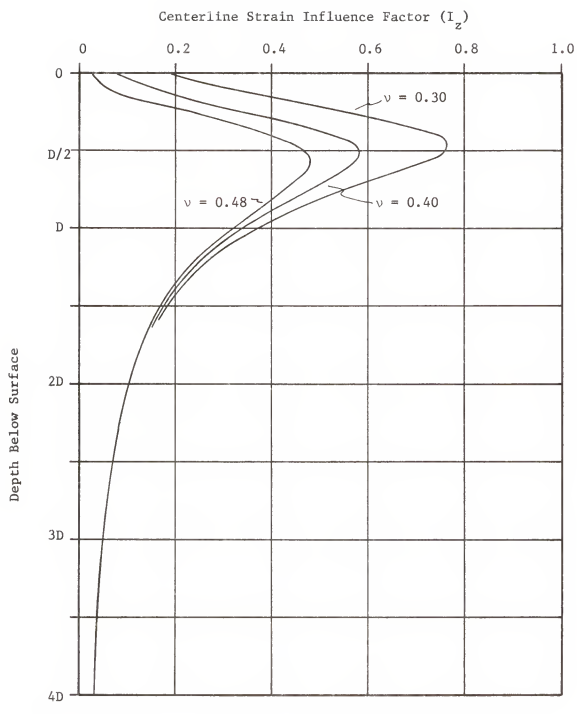


Figure 46. Centerline Vertical Strain Influence Factor for 2000 Psf Axisymmetric Loading of 20 Ft Diameter Concrete Footing Using Minor Principal Stresses and Bulk Failure Condition; K = 30,000, k_o = 0.50

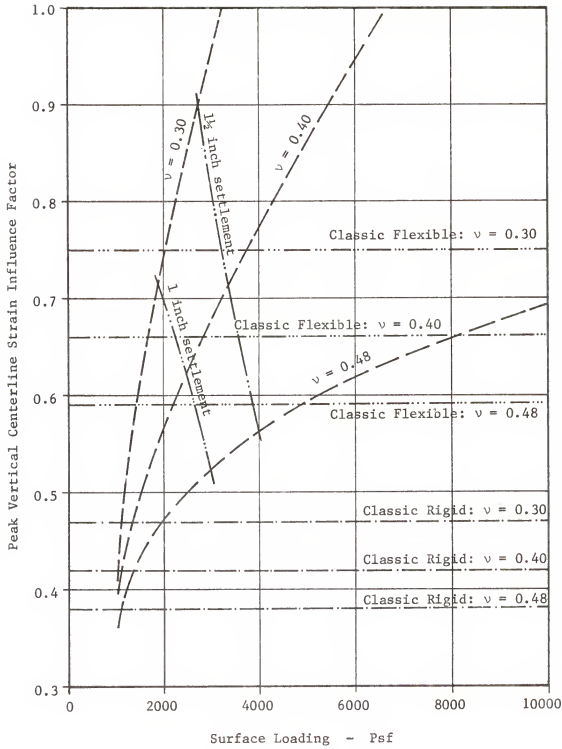


Figure 47. Peak Vertical Centerline Strain Influence Factor for Concrete Footing on Nonlinear Material under Axisymmetric Loading as a Function of Surface Loading and Poisson's Ratio; K = 30,000, k_o = 0.50

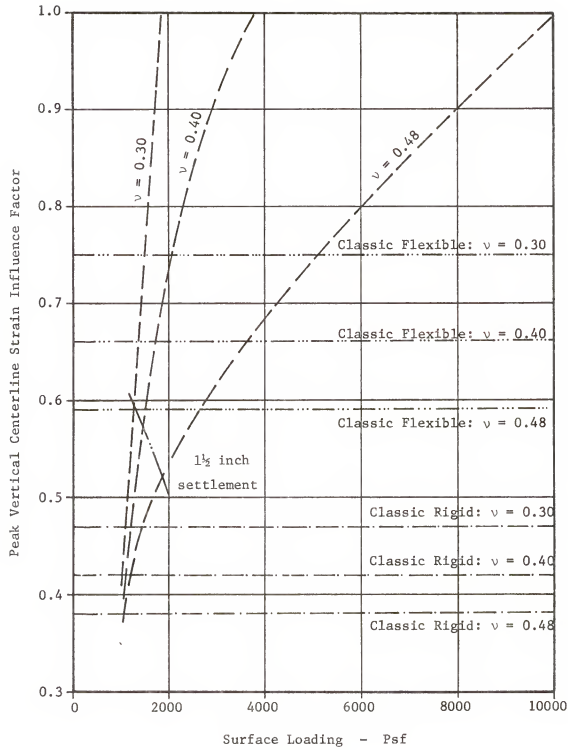


Figure 48. Peak Vertical Centerline Strain Influence Factor for Concrete Footing on Nonlinear Material under Axisymmetric Loading as a Function of Surface Loading and Poisson's Ratio; K = 15,000, k_o = 0.50

triangular distribution, the peak strain influence factor value should also be very similar, for the same total settlement. For the case of a Poisson ratio of 0.4 and 1 inch settlement, the peak vertical centerline strain influence factor from Figure 41 (dense sand) is 0.67 and the surface load 5200 psf. From Figure 47 (medium dense sand) for the same settlement and Poisson ratio, these values are 0.62 and 2500 psf, and from Figure 48 (loose sand), they are 0.46 and 1200 psf. Thus the peak centerline strain influence factors compare favorably for the dense and medium dense sands, and less favorably for the loose.

These studies have been based on the use of a 20 ft diameter rigid concrete footing. Study of Figures 32, 33, and 34 indicates, however, that the stress-dependent initial in-situ tangent modulus used in these studies varies parabolically with depth. The variation from a surface value of zero (i.e., no confinement, so modulus is zero) increases most rapidly beneath the surface. The greatest changes occur from approximately 0 to 15 feet beneath the surface and after that the modulus variation with depth is approximately linear.

It would be expected, therefore, that footings with dimensions less than 20 ft would have depths of influence which would fall almost entirely within this initial low modulus region of the soil mass, while foundations with larger dimensions should be relatively unaffected by this shallow region. When normalizing to obtain the strain influence factor in this region, the division by such low in-situ modulus values should cause an increased strain influence factor value. This would be especially true for smaller and smaller geometries.

The effect of varying the circular footing diameter is shown in

Figure 49 for K = 60,000, ν = 0.4, and 4000 psf surface loading. These curves were obtained by using finite element grids similar to the one in Figure 25, but proportionably scaled down or up from the 20 ft diameter case.

Figure 49 shows the general trend previously discussed and thus introduces an added complexity in trying to obtain a reasonable triangular strain factor distribution. It is of interest to note that for all geometries the depth of influence equal to 2D remains reasonable, as does the peak strain influence factor at a depth of D/2, but the question remains as to what would be a reasonable peak strain influence factor value for use in such a triangular distribution.

Another way to consider this problem would be to determine the settlement using an assumed triangular strain factor distribution in conjunction with the parabolic in-situ modulus distribution (Equation 77). For example, the settlement relation for the case of a triangular distribution with a depth of influence 2D, a surface intercept value of I_s, and varying peak strain influence factor values (I_{zp}) all located at a depth D/2, would be written

$$\rho = \int_0^{2D} \frac{p\, I}{E}\, dh = p \int_0^{D/2} \frac{\left(I_s + 2\{I_{zp} - I_s\}\right)\frac{h}{D}\, dh}{\left[1 - R_f\left(\frac{1-\sin\phi}{\sin\phi}\right)\left(\frac{1 - k_o}{k_o}\right)\right]^2 K(k_o \gamma h)^n}$$

$$+ p \int_{D/2}^{2D} \frac{\left[-\left(\frac{I_{zp}}{2D-D/2}\right)h + \frac{2D\, I_{zp}}{2D-D/2}\right] dh}{\left[1 - R_f\left(\frac{1-\sin\phi}{\sin\phi}\right)\left(\frac{1 - k_o}{k_o}\right)\right]^2 K(k_o \gamma\, h)^n} \qquad (80)$$

where all terms have been previously defined. This equation gives the settlement by integrating the triangular strain factor

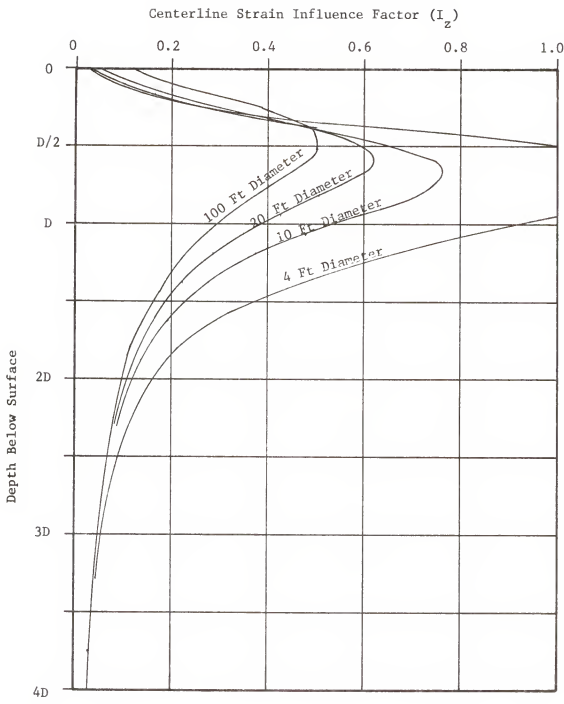


Figure 49. Centerline Vertical Strain Influence Factor Curves for Axisymmetric Loading of Varying Diameter Concrete Footings and 4000 Psf Loading: K = 60,000, ν = 0.40

distribution over a depth 2D and includes the stress-dependent initial in-situ tangent modulus.

In using this triangular strain factor distribution approach, several factors must be considered. Very dense sands more generally have an approximate Poisson ratio of 0.5, while loose sands approximate 0.3. Thus, by reference to Figures 43, 44, and 46, the surface intercept (I_s) for loose, medium dense, and dense sand conditions can be reasonably taken equal to 0.2, 0.1, and 0.0 respectively.

Additionally, these studies have indicated clearly that the peak nonlinear strain influence factor is a function of the surface pressure (see Figures 38, 39, and 40), and increases as the pressure increases. Figure 49 also indicated that the peak strain influence factor increases as the footing diameter decreases.

It would be advantageous, therefore, to include these pressure and diameter effects in using the simplified triangular strain influence factor approach. It would also be of value to attempt to model the nonlinear nature of the load vs. settlement curves. The use of a single constant value for I_{zp} will give only a linear settlement prediction, so some relation for I_{zp} must be used which will include the above effects as well as introduce reasonable nonlinearity.

Based on a study of these previous strain influence factor figures, Schmertmann suggested consideration of an equation of the form

$$I_{zp} = C_i + C_f \sqrt{p / \sigma_{D/2}} \tag{81}$$

where p is the foundation pressure, $\sigma_{D/2}$ is the in-situ vertical

stress at a depth D/2 and C_i and C_f are constants depending on the relative density of the sand. Equation 81 introduces a variable I_{zp} value which is a function of both the surface loading, p, as well as the footing diameter (as reflected in the $\sigma_{D/2}$ term). Schmertmann originally suggested a C_i value of 0.4 and C_f equal to 0.1, but left it to the writer to pursue various combinations. The relationship which is given in Equation 81 was studied in further detail and gave reasonable results.

These results, which will be described in the following pages, are essentially based on an empirical fit to the parametric data generated in the previous figures in this study. Since the results were satisfactory and also the form of the equation is simple to work with (thus meeting the requirements of a reasonable and straightforward technique for settlement analysis), other possible equations for the I_{zp} relationship were not pursued at this time. No doubt more detailed studies of the square root relationship as well as the general form of the equation itself might lead to further modifications. However, when considering the many assumptions involved in these parametric analyses, such detailed mathematical searches do not seem warranted.

If Equation 81 is included in Equation 80, and the result integrated (using n = 0.5, typical for sands), one obtains

$$\rho = \frac{p\, D^{\frac{1}{2}}}{M_o} \left\{0.943\, I_s + 1.258\left(C_i + C_f \sqrt{\frac{p}{\gamma\, D/2}}\right)\right\} \qquad (82)$$

where: M_o = Settlement Modulus

$$M_o = \left[1 - R_f \left(\frac{1 - \text{Sin } \phi}{\text{Sin } \phi}\right)\left(\frac{1 - k_o}{2\, k_o}\right)\right]^2 K\, (\gamma\, k_o)^{\frac{1}{2}} \qquad (83)$$

and p is in psf, while D and ρ are in ft. Obviously the use of these equations depends upon careful and consistent use of the units as discussed in Chapter 3.0.

The problem now is to determine the general reasonableness of the peak strain factor formula given by Equation 81, as well as the values of the constants for use in the equation. These constants could obviously be varied over a wide range to obtain better and better approximations for various cases. However, if the equation becomes too complicated, it would defeat the purpose of developing the triangular strain factor distribution as a reasonable and simple design and analysis tool.

After much trial and error, it was determined best to fix the constant C_f at a value of 0.1, independent of the density of the sand. Again, after additional trial and error, the constant C_i was taken as 0.4, 0.5, or 0.6 for the dense, medium dense, and loose sands respectively, under axisymmetric loading.

Perhaps the best settlement comparison might be made by using the pressure-settlement curves resulting from selected finite element computer runs, compared with the settlement relationships given by Equation 82, for the selected sand density cases. Such a comparison is made in Figures 50, 51, and 52 for the dense, medium dense, and loose sands, and using the 20 ft diameter footing. Selected comparisons for varying footing diameters and sand densities are illustrated in Figure 53.

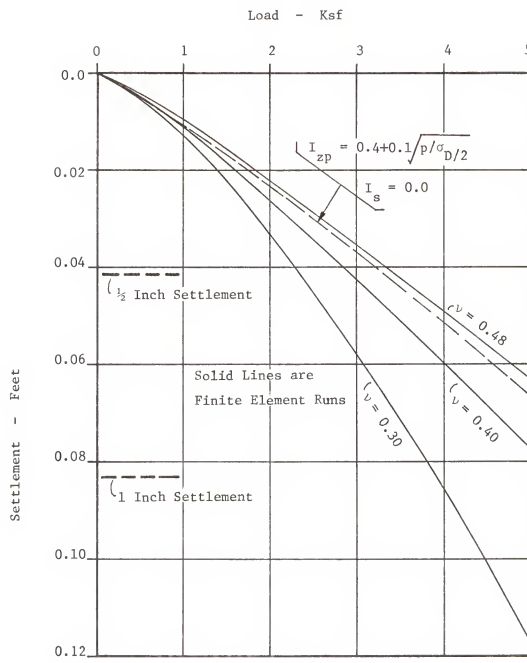


Figure 50. Load vs. Settlement Curves for 20 Ft Diameter Concrete Footing on Dense Sand: K = 60,000

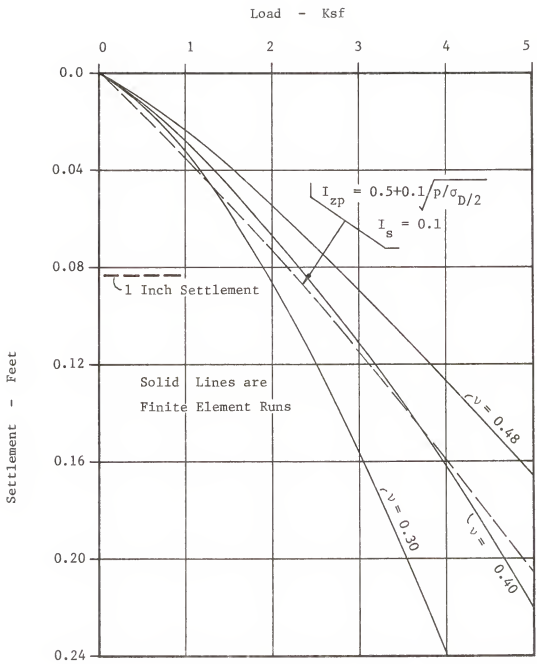


Figure 51. Load vs. Settlement Curves for 20 Ft Diameter Concrete Footing on Medium Dense Sand: K = 30,000

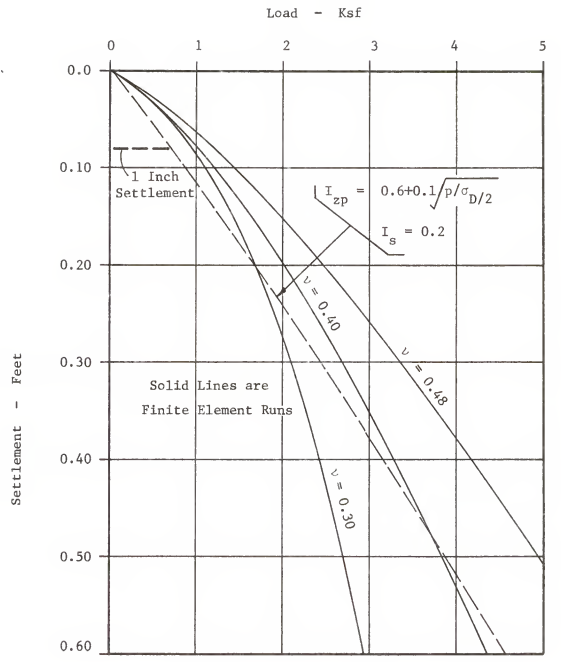


Figure 52. Load vs. Settlement Curves for 20 Ft Diameter Concrete Footing on Loose Sand: K = 15,000

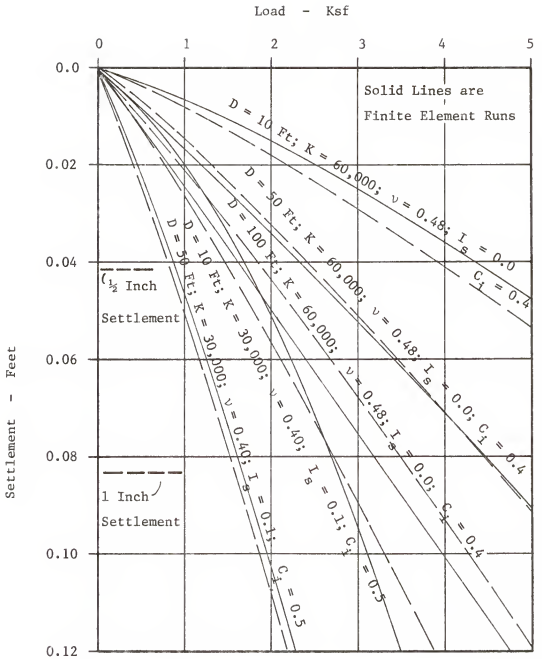


Figure 53. Load vs. Settlement Curves for Varying Diameter Concrete Footings

Study of these figures indicates that the selected constants and settlements compare very well with the finite element results for the dense and medium dense cases. There is a slightly poorer comparison for the loose case, which would be expected due to the large settlements and failure regions previously discussed.

These axisymmetric studies show that the use of a simplified triangular strain factor distribution is very reasonable, even when using a stress-dependent nonlinear modulus material. The peak strain influence factor to be used is given by Equation 81 where $C_f = 0.1$ for all sands and $C_i = 0.4$, 0.5, or 0.6 for dense, medium dense, and loose sands. The peak value should be located at a depth D/2 with a triangular depth of influence of 2D. A surface intercept value of 0.0, 0.1, or 0.2 should be used for very dense, dense, or loose sands.

4.3.2 Plane Strain Loading

The results of loading the 20 ft wide 2 ft thick concrete footing on the nonlinear elastic sand model under plane strain conditions are given in this section.

Figures 54 through 56 give the centerline vertical strain distribution for K = 60,000 and Poisson's ratios of 0.3, 0.4, and 0.48 under the conditions of using the minor principal stress. The figures show that the peak strain occurs at a depth of from D/2 to 3D/4 and is a function of both Poisson's ratio as well as the surface load.

The centerline strain influence factors are shown in Figures 57 through 59 and the location of the peak strain influence factor varies between D/2 and D. The general shape of the strain influence factor diagram differs from the axisymmetric case, and a strain

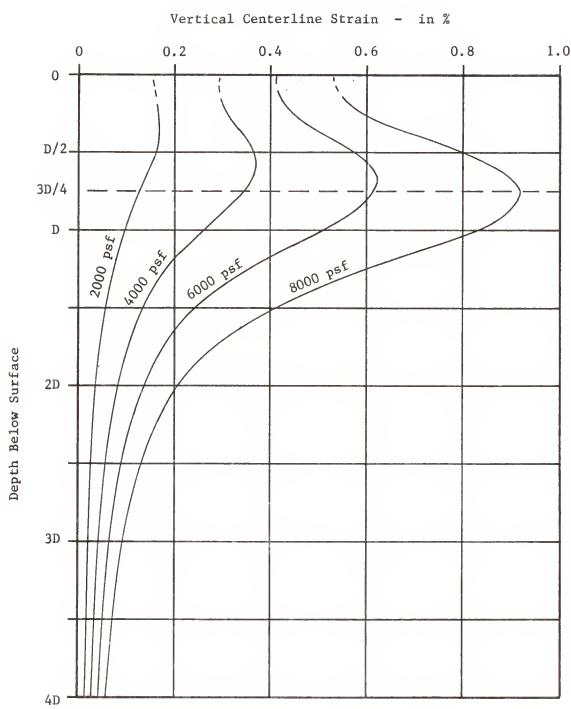


Figure 54. Vertical Centerline Strain Distribution for Plane Strain Loading of 20 Ft Wide Concrete Footing Using Minor Principal Stresses and Bulk Failure Condition; K = 60,000, ν = 0.30, and k_o = 0.50

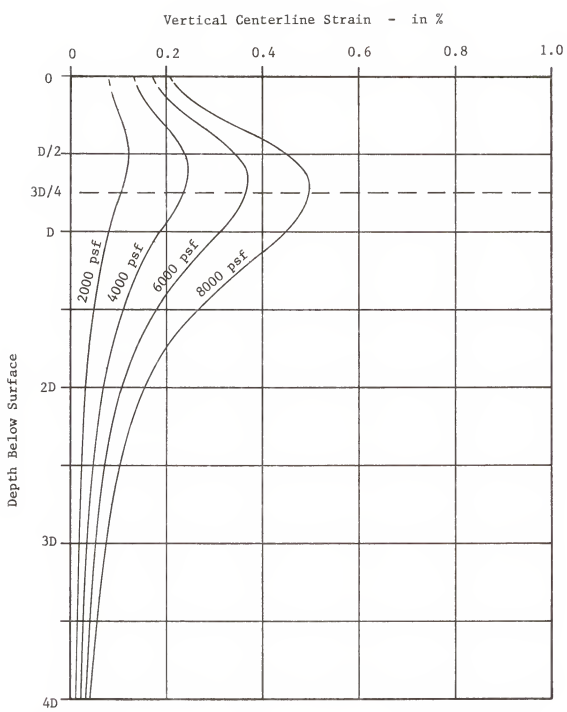


Figure 55. Vertical Centerline Strain Distribution for Plane Strain Loading of 20 Ft Wide Concrete Footing Using Minor Principal Stresses and Bulk Failure Condition; K = 60,000, ν = 0.40, and k_o = 0.50

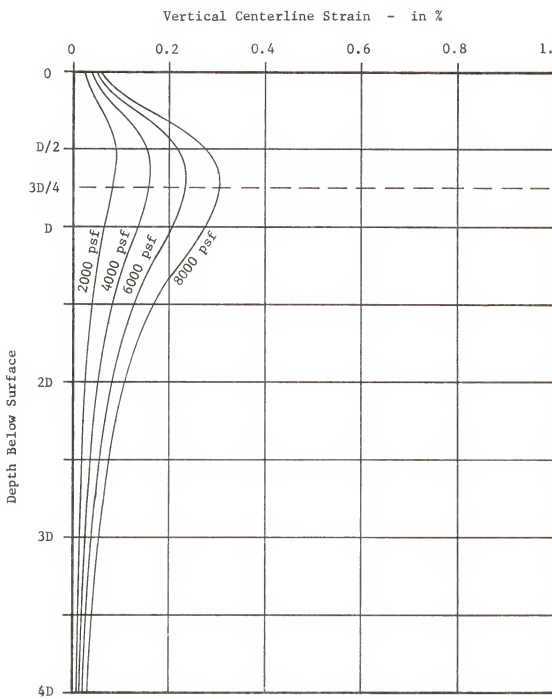


Figure 56. Vertical Centerline Strain Distribution for Plane Strain Loading of 20 Ft Wide Concrete Footing Using Minor Principal Stresses and Bulk Failure Condition; K = 60,000, ν = 0.48, and k_o = 0.50

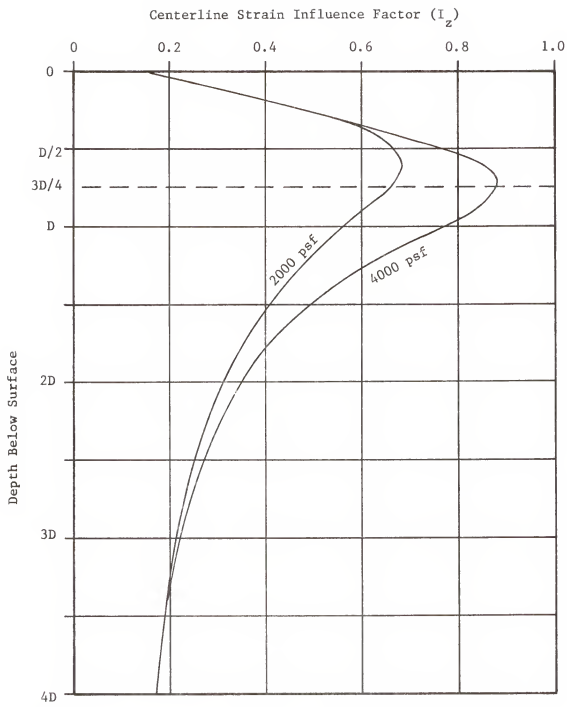


Figure 57. Centerline Vertical Strain Influence Factor for Plane Strain Loading of 20 Ft Wide Concrete Footing Using Minor Principal Stresses and Bulk Failure Condition; K = 60,000, ν = 0.30, and k_o = 0.50

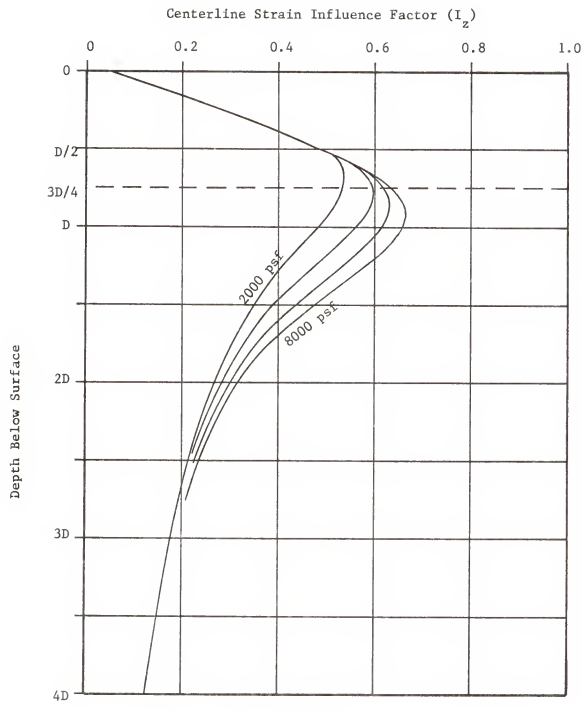


Figure 58. Centerline Vertical Strain Influence Factor for Plane Strain Loading of 20 Ft Wide Concrete Footing Using Minor Principal Stresses and Bulk Failure Condition; $K = 60{,}000$, $\nu = 0.40$, and $k_o = 0.50$

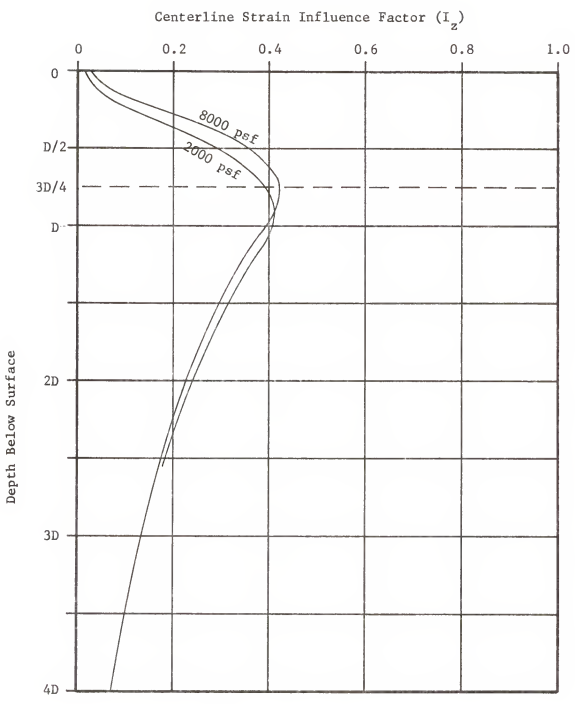


Figure 59. Centerline Vertical Strain Influence Factor for Plane Strain Loading of 20 Ft Wide Concrete Footing Using Minor Principal Stresses and Bulk Failure Condition; K = 60,000, ν = 0.48, and k_o = 0.50

influence factor value of 0.1 is not reached until an approximate depth of 4D. If a simplified triangular distribution were to be assumed, it appears that a depth of 4D would be more reasonable for the plane strain case, instead of 2D which was used for the axisymmetric case.

If the peak strain influence factor values from Figures 57 through 59 are plotted as a function of Poisson's ratio and the surface loading, the result is as shown in Figure 60. Additionally, if a similar plane strain analysis is made, only using flexible surface loading instead of the concrete footing on the nonlinear stress-dependent modulus material, and then the peak strain influence factors plotted, the result is as shown in Figure 61. The individual flexible loading strain distribution curves are not shown, but they are similar in form to those in Figures 57 through 59. On both Figures 60 and 61 the peak strain influence factor values for the classic plane strain analyses (from Figures 28 and 30) are also shown, as are the equal settlement contours.

As in the axisymmetric case, the complexity of using a single peak strain influence factor value in conjunction with an assumed triangular distribution is illustrated in Figures 60 and 61. If it is assumed that a Poisson ratio of 0.4 is reasonable for most average conditions and that loadings are typically 4000 psf or greater, then it appears from Figure 60 that a single peak strain influence factor value of 0.6 is reasonable for the case of a concrete footing, while a value of 0.7 (from Figure 61) appears more reasonable for the flexible case.

Another way of illustrating the effect of Poisson's ratio is

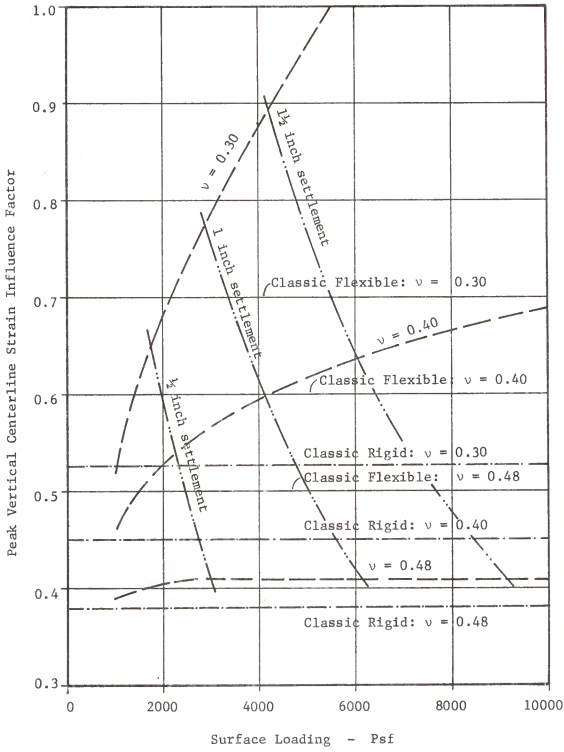


Figure 60. Peak Vertical Centerline Strain Influence Factor for Concrete Footing on Nonlinear Material under Plane Strain Loading as a Function of Surface Loading and Poisson's Ratio; K = 60,000, k_o = 0.50

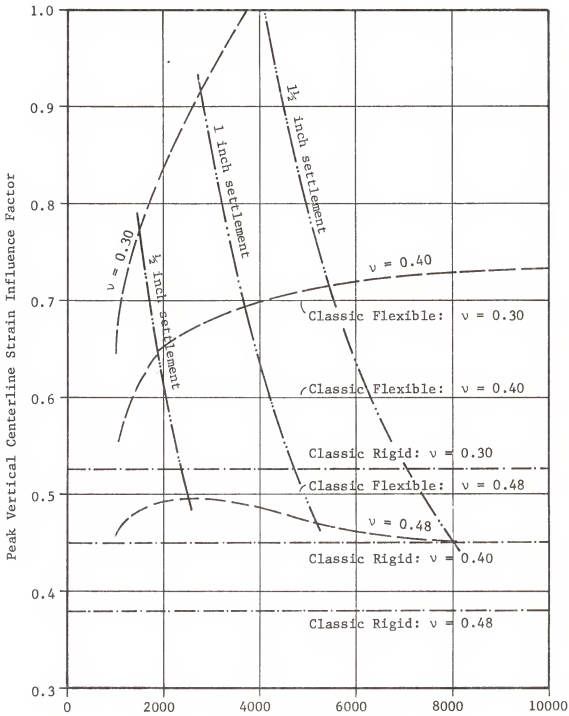


Figure 61. Peak Vertical Centerline Strain Influence Factor for Flexible Plane Strain Loading on Nonlinear Material as a Function of Surface Loading and Poisson's Ratio: K = 60,000, k_o = 0.50

shown in Figures 62 and 63 where the centerline strain influence factor is plotted for three different Poisson's ratios and for specific loads of 2000 and 4000 psf. The range in peak strain influence factor values is from 0.42 to 0.88 for the loads considered. At higher surface loadings the spread would be even greater, and especially for values of Poisson's ratio less than 0.4. This large spread for higher footing loadings has been shown in Figure 60.

Figure 64, similar to Figure 63, uses octahedral stresses instead of the minor principal stresses. As in the case of the axisymmetric analysis, the discrepancy is generally less than 20 percent and even less than this for higher Poisson's ratios. This discrepancy is minor and does not affect the general results of this study.

The effect of using a lower nonlinear modulus number (K) of 30,000 is illustrated by comparing Figures 65 and 62 which are for the 2000 psf footing load. For the range of Poisson's ratios considered, the range of peak strain influence factor values is from 0.42 to 0.68 for K = 60,000 (dense sand) and from 0.44 to 0.81 for K = 30,000 (medium dense sand). As in the axisymmetric case, the discrepancy increases for larger loads, and especially for Poisson's ratios less than 0.4.

If the peak centerline strain influence factor values from a series of runs using K = 30,000 (medium dense sand) and K = 15,000 (loose sand) are plotted as a function of Poisson's ratio and the surface loading, the results are as shown in Figures 66 and 67, which should be compared with Figure 60. As in the axisymmetric case, the effect of using a lower nonlinear modulus number is to decrease the

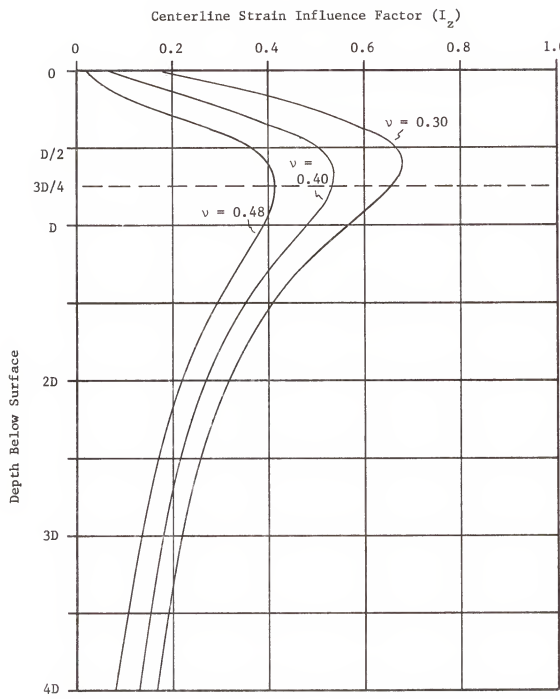


Figure 62. Centerline Vertical Strain Influence Factor for 2000 Psf Plane Strain Loading of 20 Ft Wide Concrete Footing Using Minor Principal Stresses and Bulk Failure Condition; K = 60,000, k_o = 0.50

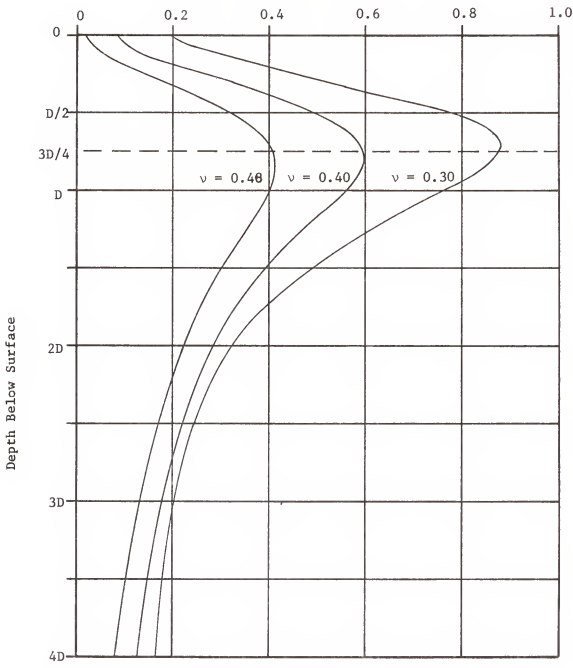


Figure 63. Centerline Vertical Strain Influence Factor for 4000 Psf Plane Strain Loading of 20 Ft Wide Concrete Footing Using Minor Principal Stresses and Bulk Failure Condition; K = 60,000, k_o = 0.50

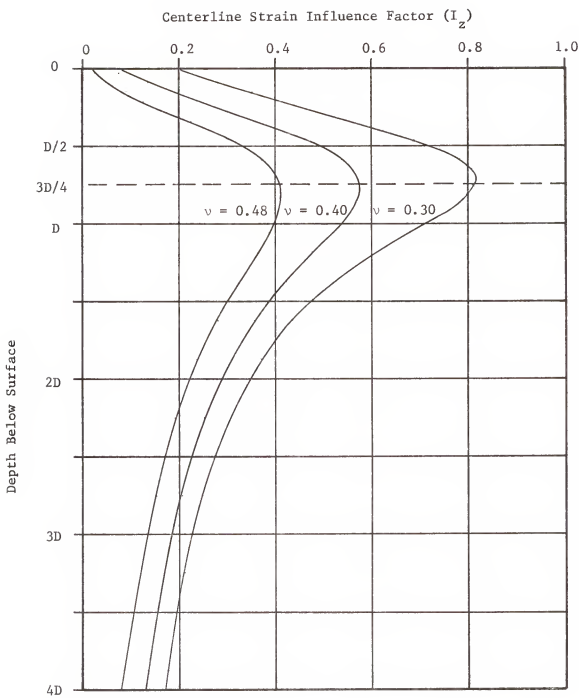


Figure 64. Centerline Vertical Strain Influence Factor for 4000 Psf Plane Strain Loading of 20 Ft Wide Concrete Footing Using Octahedral Stresses and Bulk Failure Condition; K = 60,000, k_o = 0.50

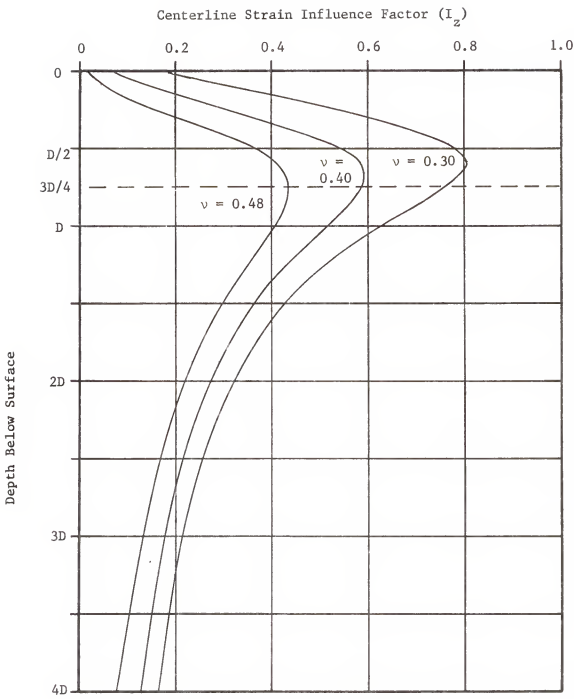


Figure 65. Centerline Vertical Strain Influence Factor for 2000 Psf Plane Strain Loading of 20 Ft Wide Concrete Footing Using Minor Principal Stresses and Bulk Failure Condition; K = 30,000, k_o = 0.50

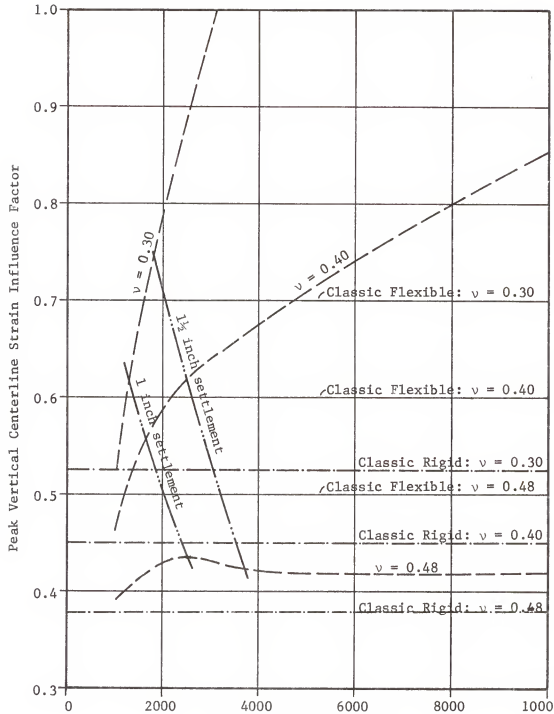


Figure 66. Peak Vertical Centerline Strain Influence Factor for Concrete Footing on Nonlinear Material under Plane Strain Loading as a Function of Surface Loading and Poisson's Ratio; K = 30,000, k_o = 0.50

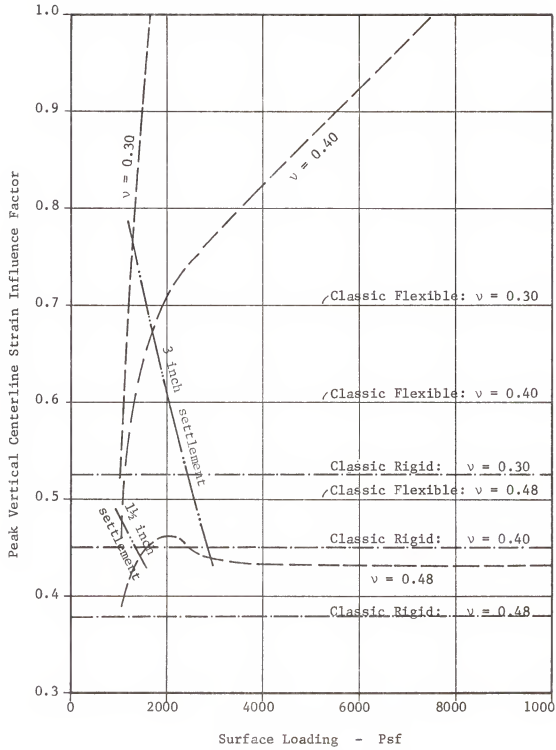


Figure 67. Peak Vertical Centerline Strain Influence Factor for Concrete Footing on Nonlinear Material under Plane Strain Loading as a Function of Surface Loading and Poisson's Ratio; K = 15,000, k_o = 0.50

peak strain influence factor value which might be used. The suggested plane strain depth of influence of 4D is not affected by the nonlinear modulus number value.

The results shown in Figures 66 and 67 are similar to those found for the axisymmetric analysis. For progressively less dense soils it requires a lower surface loading for the same total settlement. However, the peak centerline vertical strain influence factor should remain very similar. For the case of a Poisson ratio of 0.4 and 1 inch settlement, the peak vertical centerline strain influence factor from Figure 60 is 0.60 and the surface load 4100 psf. For the same settlement and Poisson ratio these values are 0.56 and 1600 psf from Figure 66. The settlements on the loose soil in Figure 67 are so large that a reasonable comparison cannot be made. Again the medium dense and dense cases compare somewhat favorably.

These studies were based on a 20 ft wide concrete footing, and, as in the axisymmetric case, it might be expected that there would be some variation due to varying footing width. Figure 68 shows the effect of varying the footing width for $K = 60{,}000$, $\nu = 0.40$, and 4000 psf surface loading. As in the axisymmetric case, a scaled down grid was used for the finite element studies.

The general trend affecting the strain influence factor for varying geometries for the plane strain case is similar to that for the axisymmetric case. The increased strain influence factors for the smaller geometries are as expected due to the low modulus values near the surface. The depth of influence of 4D is relatively unaffected by geometry as is the location of the peak strain influence factor at a depth of 3D/4. Again the question is what should be a

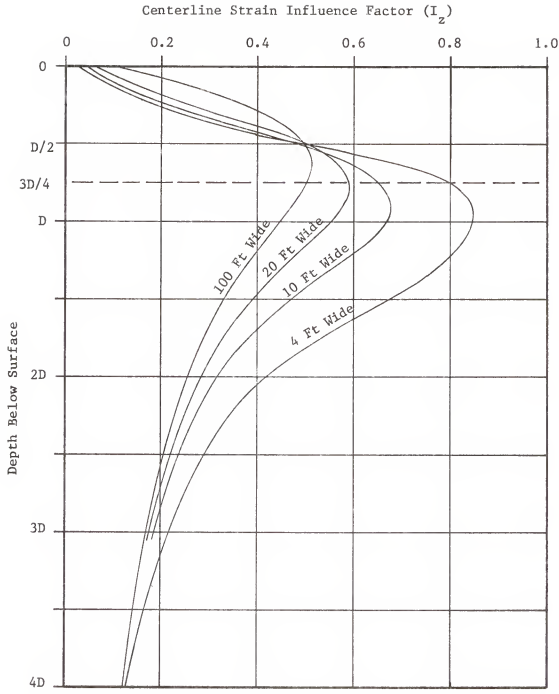


Figure 68. Centerline Vertical Strain Influence Factor Curves for Plane Strain Loading of Varying Width Concrete Footings and 4000 Psf Loading: K = 60,000, ν = 0.40

reasonable peak strain influence factor for use in a simplified triangular distribution.

In comparing settlements, it might be instructive to set up an analytical expression for the plane strain case, similar to that used for the axisymmetric case (Equation 80). Assuming a triangular distribution with a depth of influence of 4D, a surface intercept, I_s, and varying peak strain influence factor values, all located at a depth 3D/4, the settlement would be written

$$\rho = p \int_0^{3D/4} \frac{(I_s + \frac{4}{3}\{I_{zp} - I_s\})\frac{h}{D}\, dh}{\left[1 - R_f\left(\frac{1-\sin\phi}{\sin\phi}\right)\left(\frac{1-k_o}{k_o}\right)\right]^2 K\,(k_o\,\gamma\,h)^n} + p \int_{3D/4}^{4D} \frac{\left[-\left(\frac{I_{zp}}{4D-3D/4}\right)h + \frac{4D\ I_{zp}}{4D-3D/4}\right] dh}{\left[1 - R_f\left(\frac{1-\sin\phi}{\sin\phi}\right)\left(\frac{1-k_o}{k_o}\right)\right]^2 K(k_o\,\gamma\,h)^n} \quad (84)$$

where all terms have been previously defined. This equation can be simplified for n = 0.5, as well as include the I_{zp} function given by Equation 81, only using $\sigma_{3D/4}$ instead of $\sigma_{D/2}$. The result is

$$\rho = \frac{p\ D^{\frac{1}{2}}}{M_o}\ \{0.155\ I_s + 1.170(C_i + C_f\sqrt{\frac{p}{\gamma\ 3D/4}})\} \quad (85)$$

where M_o was defined by Equation 83.

Equation 81 for the peak strain influence factor, I_{zp}, was used for the plane strain studies as well as the axisymmetric. Additional trial and error studies indicated, however, that there should be some adjustment of the constant C_i for the plane strain case. The surface intercepts, I_s, were the same as before, 0.0, 0.1, and 0.2 for the

dense, medium dense, and loose sands, respectively. C_f was kept constant equal to 0.1.

A comparison between the results of the plane strain finite element computer runs and selected settlement relationships (using Equation 85) is given in Figures 69 through 71 for the 20 ft wide footing. Similar pressure-settlement curves for varying footing widths and sand densities are given in Figure 72.

Study of these figures indicates that Equation 81 is also reasonable for the plane strain case. The constant C_1, however, should be 0.3, 0.5, or 0.7 for the dense, medium dense, or loose sand conditions under plane strain loading.

These plane strain studies show that the use of a simplified triangular strain factor distribution is very reasonable, even when using a stress-dependent nonlinear modulus material. The peak strain influence factor to be used is given by Equation 81 where $C_f = 0.1$ for all sands and $C_i = 0.3$, 0.5, or 0.7 for dense, medium dense, or loose sands. The peak value should be located at a depth 3D/4 with a triangular depth of influence of 4D. A surface intercept value of 0.0, 0.1, or 0.2 is used for dense, medium dense, or loose sands.

4.3.3 Comparison of Axisymmetric and Plane Strain Cases

In Section 4.2 it was indicated that the settlements for plane strain loading on linear elastic materials varied from 2.5 to 4.3 times that for axisymmetric loading. Although this is true for linearly elastic materials, it does not necessarily follow for loading on the nonlinear stress-dependent modulus materials used in these analytical studies.

In Chapter 3.0 it was pointed out that the nonlinear modulus

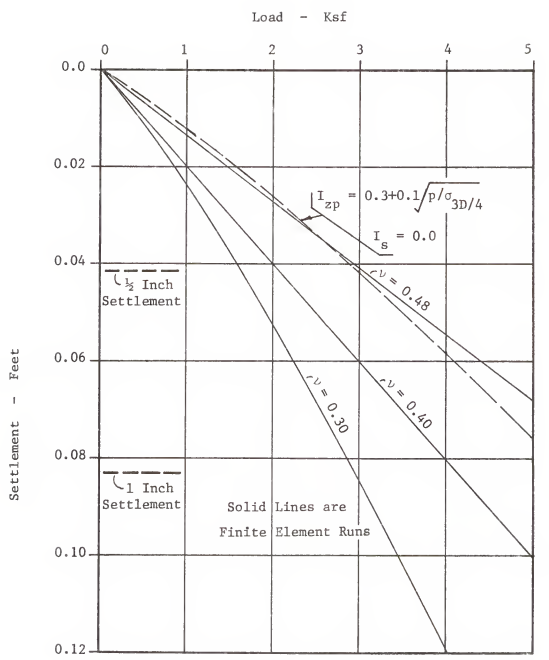


Figure 69. Load vs. Settlement Curves for 20 Ft Wide Concrete Footing on Dense Sand: K = 60,000

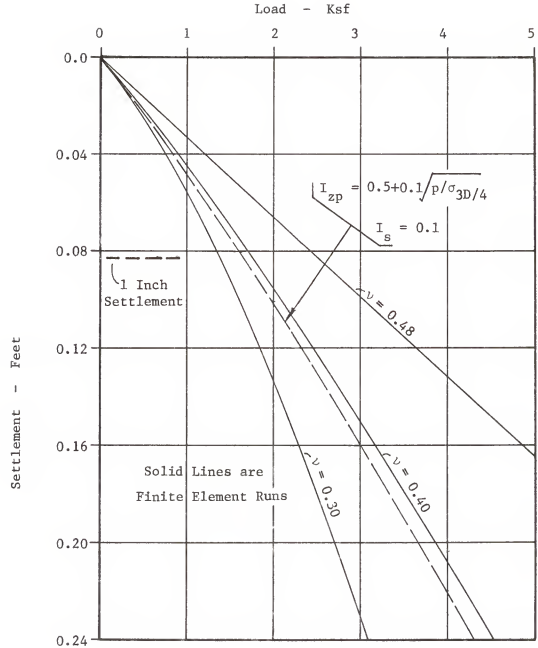


Figure 70. Load vs. Settlement Curves for 20 Ft Wide Concrete Footing on Medium Dense Sand: K = 30,000

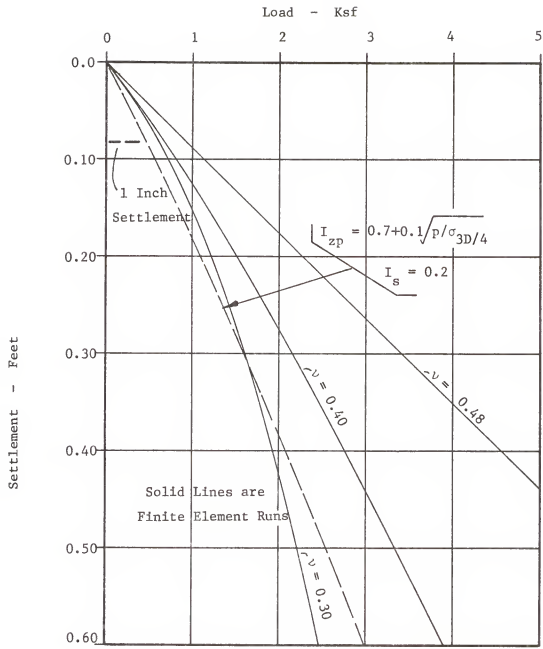


Figure 71. Load vs. Settlement Curves for 20 Ft Wide Concrete Footing on Loose Sand: K = 15,000

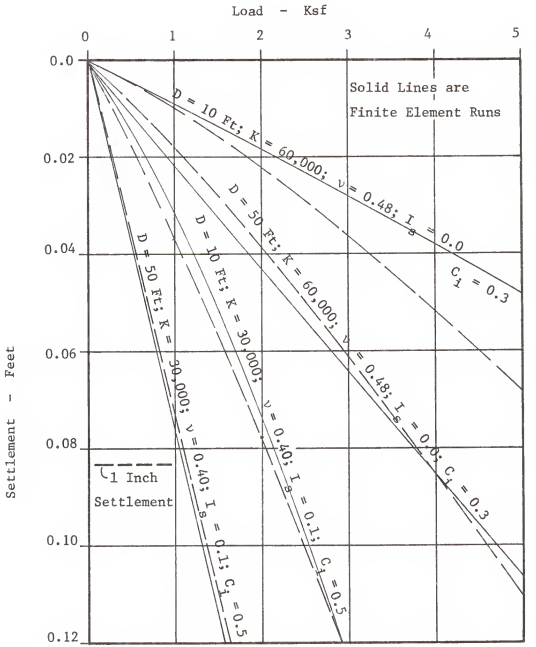


Figure 72. Load vs. Settlement Curves for Varying Width Concrete Footings

parameters are typically obtained from standard triaxial tests. Duncan and Chang (1970),who developed this analytical model, have also indicated that the nonlinear parameters could be obtained from plane strain tests, again assuming that the hyperbolic stress-strain relation is applicable.

The work of Lee (1970) in comparing the theoretical and experimental results of triaxial and plane strain testing was summarized in Section 3.2. The major results were presented in Table 3 which showed that although theoretically the moduli as obtained from plane strain and triaxial testing should vary by only 10 percent, Lee found them to vary by approximately 40 percent based on some limited laboratory testing. He also showed that Poisson's ratio and the angle of friction are also different, and are larger for plane strain testing. The plane strain angle of friction is generally taken as 10 percent greater than that for triaxial testing (Lee, 1970; Cornforth, 1964).

In these studies it has already been shown that Poisson's ratio is a very important variable in the analytical settlement estimates. In field testing, the specific exploration method will also influence the value of the in-situ modulus obtained. Results from cone testing and pressuremeter testing will give different modulus values which must then be correlated with laboratory testing methods or with other field methods. Schmertmann (1970) showed such a comparison between cone and plate bearing modulus values. This means that the engineer is generally faced with a great variety of modulus values and he must be able to use them properly and understand their applications as well as their limitations.

If the results of Lee's work were to be extended to these studies, it might be assumed that the nonlinear modulus number, as determined from plane strain testing, would be 40 percent greater than that from triaxial testing. The Poisson ratio would also be greater (see Table 3), and the angle of friction would be larger by approximately 10 percent (Cornforth, 1964). In making an analytical settlement comparison, therefore, it would be necessary to compare the $K = 30{,}000$, $\nu = 0.30$, $\phi = 37^{o}$ axisymmetric case with a $K = 42{,}000$, $\nu = 0.44$, $\phi = 40^{o}$ plane strain case. Another comparison might be made using the $K = 60{,}000$, $\nu = 0.30$, $\phi = 42^{o}$ axisymmetric case compared with the $K = 84{,}000$, $\nu = 0.44$, $\phi = 46^{o}$ plane strain case.

Load versus settlement curves from the analytical studies for the cases described are shown in Figures 73 and 74. In addition, the curves for the cases of identical nonlinear parameters, as well as various parameter combinations, are also shown for comparison. It is noted from these figures that when using the identical nonlinear parameters ($K = 30{,}000$, $\nu = 0.30$ and $K = 60{,}000$, $\nu = 0.30$) the plane strain settlement is approximately 1.5 times the axisymmetric settlement for the same loading sequence. However, when comparing the axisymmetric triangular distribution with the plane strain triangular distribution from the linear case (Figure 31), the plane strain to axisymmetric settlement ratio was 4.2. This latter ratio is in agreement with the settlement influence factors from Table 4 which indicated a plane strain to axisymmetric settlement ratio of approximately 3.40/0.79 or 4.3 for the linear case.

Some limited model footing laboratory tests which will be described in Chapter 6.0 also showed that the plane strain settlements were larger than the axisymmetric. The settlement ratio was approximately 3 or larger which is thus midway between the results of the linear and nonlinear analytical studies.

It should also be noted on Figures 73 and 74, however, that when using the larger plane strain parameters, the plane strain settlement is less than the axisymmetric. The increased nonlinear modulus number, K, does not affect the results as much as the increased value of Poisson's ratio, but this variation has already been well illustrated in Sections 4.3.1 and 4.3.2. There are perhaps several reasons for these discrepancies:

(1) The nonlinear stress-dependent model used in these studies is not as good for plane strain work as for axisymmetric. Duncan and Chang (1970) give excellent supporting data for its use in axisymmetric analyses, but limited supporting data for its use in plane strain analyses, other than the suggestion that it could be used for such analyses. Kulhawy et al. (1969), who give the most extensive listing of nonlinear modulus parameters, do not give any based on plane strain testing, and, in fact, use the triaxial test parameters for studies on large dams. Such studies, it might be argued, would be better analyzed using plane strain data. Of course, it should also be pointed out that there is a great deal of triaxial data available for study and analysis, while the plane strain data are quite limited. It can also be argued that perhaps a general hyperbola is not a good form for plane strain stress-strain data, and especially when applied to dense sands (Lee, 1970). This could

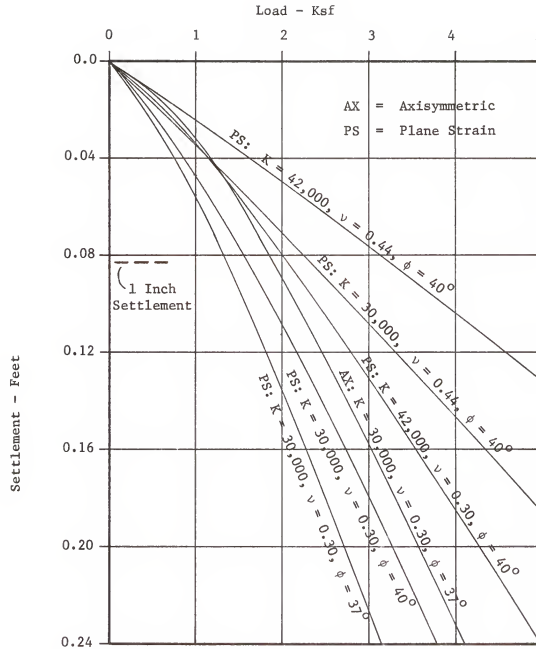


Figure 73. Comparison of Axisymmetric and Plane Strain Load vs. Settlement Curves on Medium Dense Sand: K = 30,000; D = 20 Ft

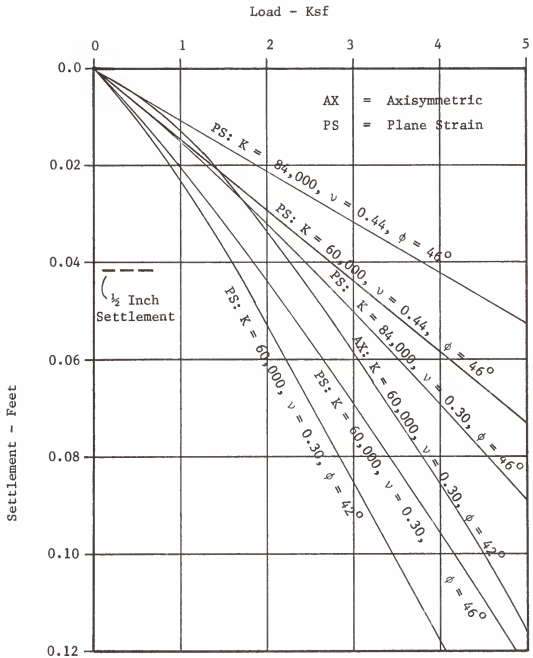


Figure 74. Comparison of Axisymmetric and Plane Strain Load vs. Settlement Curves on Dense Sand: K = 60,000; D = 20 Ft

be another weakness in using this particular analytical model for plane strain studies.

(2) Poisson's ratio, which has perhaps the greatest analytical effect in these studies, is no doubt one of the most difficult soil parameters to obtain and work with, primarily because of the dilatant nature of soils. A much better understanding of this particular parameter is necessary before one can state categorically why there are analytical inconsistencies and specifically how this parameter affects the results. No doubt Poisson's ratio is a nonisotropic parameter which changes during the loading process. Also the axisymmetric loading changes on Poisson's ratio would undoubtedly be different from those caused by plane strain loading. Some further comments will be made about this in Chapter 8.0.

These analytical studies give the most consistent results when one treats the nonlinear parameters as simply isotropic parameters which are based on a minor principal stress-dependent modulus approach, independent of the type of loading. This interpretation results in better agreement between the model tests (Chapter 6.0 - Figure 170) and the analyses shown in Figures 73 and 74. Such results do conflict with the modulus interpretation by Lee (1970), but some possible reasons for such discrepancies have already been noted above. It does appear that the plane strain to axisymmetric settlement ratio resulting from these nonlinear studies (1.5) is on the low side when compared with linear studies (4.3), and perhaps the 'answer' lies somewhere in the middle, or at least as a band of values in the middle. The limited model footing tests seem to indicate this as a possibility. Obviously there is a great

need for more correlative data between triaxial and plane strain testing, especially with regard to analytical models that might be used for the two cases.

4.3.4 Influence of Lateral Stresses

In a given field situation it is very possible for the lateral coefficient of earth pressure to be greater than the typical value of approximately 0.5. This increased lateral stress condition might be due to a variety of factors including static or dynamic over-consolidation.

If a deposit has greater lateral stresses, this means that the minor principal stress and the octahedral stress would be larger, as would be the initial in-situ modulus. This has been shown in Figures 32 through 34. For a given load, therefore, since the modulus is larger, the resulting strain will be lower than for the previous cases studied with $k_o = 0.5$. However, in normalizing the results to obtain the strain influence factor distribution, it might be expected that there would be very little change.

This strain influence factor for the case of $k_o = 1.00$ is plotted in Figure 75 for the axisymmetric loading under 4000 psf, and for various Poisson's ratios. Figure 75 should be compared with Figure 44, which was for identical conditions, only with $k_o = 0.5$. Study of these two figures shows that the higher lateral stress case gives a smaller variation due to Poisson's ratio and the peak is located at a depth of D/2 or slightly less. The general shape of the strain influence factor distribution curve is the same, with an approximate depth of influence for axisymmetric loading of 2D.

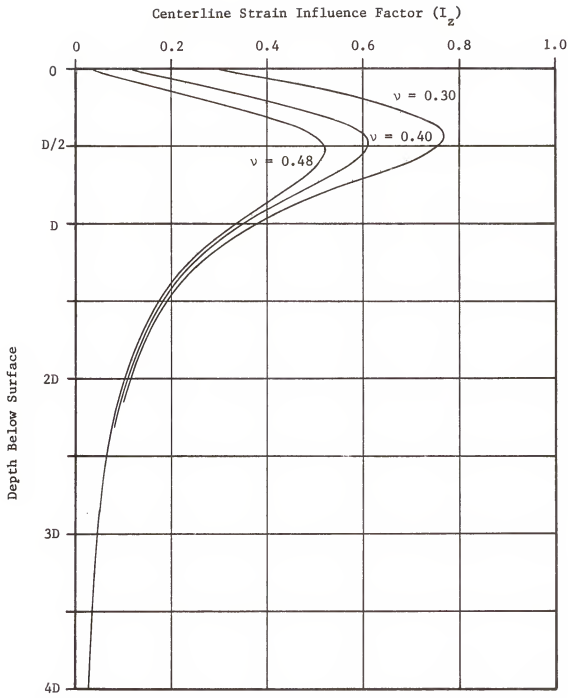


Figure 75. Centerline Vertical Strain Influence Factor for 4000 Psf Axisymmetric Loading of 20 Ft Diameter Concrete Footing Using Minor Principal Stresses and Bulk Failure Condition; K = 60,000, k_o = 1.00

If a series of runs are made and the peak vertical centerline strain influence factor values plotted as a function of Poisson's ratio and the surface loading, the results are as shown in Figure 76, which should be compared with Figure 41. Careful study of these two figures substantiates the previous general conclusions.

The effect of the increased lateral stresses on the nonlinear analytical model is to decrease the spread in the peak strain influence factor values for varying Poisson's ratios. In fact, for a Poisson ratio of 0.4, the curves are almost identical, and indicate a peak strain influence factor value of 0.67 and 5200 psf for 1 inch settlement in Figure 41, and 0.68 and 5200 psf for ½ inch settlement in Figure 76. Since the surface pressures and the peak strain influence factors are very similar, the settlements must therefore be inversely proportional to the modulus number, K. As seen in Figure 34, the in-situ tangent modulus for the $k_o = 1.00$ case is approximately double that for the $k_o = 0.5$ case. Thus the settlement for the $k_o = 1.00$ case should be approximately one-half that for the $k_o = 0.5$ case, which it was. These lateral stress results are reasonable, therefore, and indicate that the strain influence factor recommendations are not affected by an increase in the lateral stress coefficient.

A similar analysis can be made for plane strain loading conditions. Figure 77, which should be compared with Figure 63, compares the $k_o = 1.00$ case with the $k_o = 0.5$ case. The peak strain influence factor location is shifted to a depth of 3D/4 or less and the range of influence factor values for varying Poisson's ratios is also decreased.

If a series of runs are made to compare peak strain influence

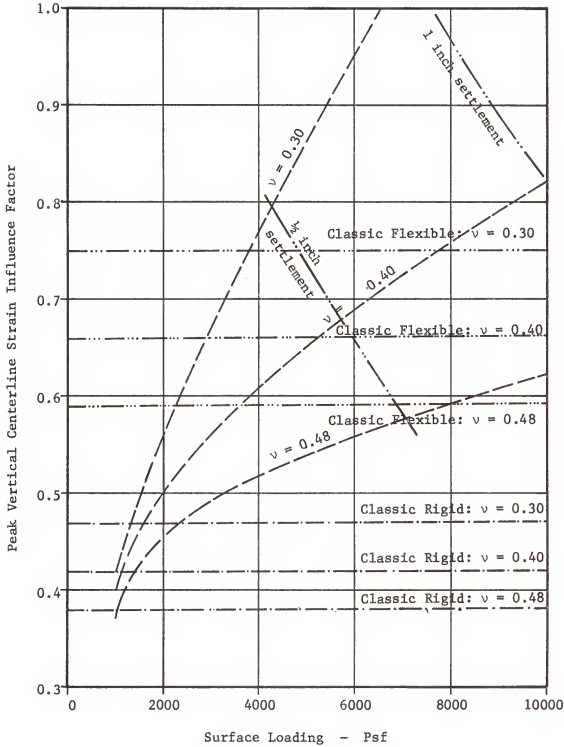


Figure 76. Peak Vertical Centerline Strain Influence Factor for Concrete Footing on Nonlinear Material under Axisymmetric Loading as a Function of Surface Loading and Poisson's Ratio; K = 60,000, k_o = 1.00

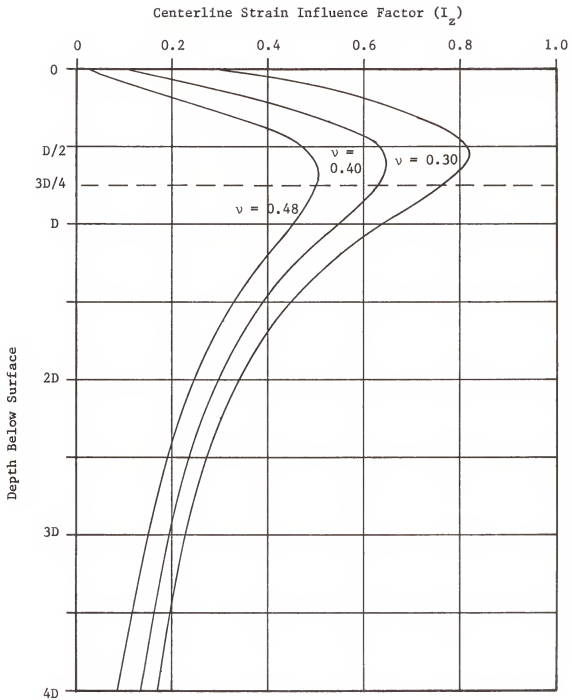


Figure 77. Centerline Vertical Strain Influence Factor for 4000 Psf Plane Strain Loading of 20 Ft Wide Concrete Footing Using Minor Principal Stresses and Bulk Failure Condition; K = 60,000, k_o = 1.00

factor values as a function of surface loading and Poisson's ratio, the results are as shown in Figure 78, which should be compared with Figure 60. The settlement comparison, as in the axisymmetric case, is favorable.

Another way to compare the effect of increased lateral stresses would be to compare the finite element settlement results with those predicted by using the analytical Equation 80 (for the axisymmetric case) and Equation 84 (for the plane strain case). Equation 81 for the peak strain influence factor, I_{zp}, should also be used. Such a comparison is shown in Figure 79 for the K = 60,000, $\nu = 0.48$ and K = 30,000, $\nu = 0.40$ cases. The comparisons shown in this figure are very reasonable and indicate that the previous recommendations for the $k_o = 0.50$ will not change. The peak strain formula and surface intercept values remain the same for the increased lateral stresses case, as would be expected.

Another case to consider with respect to increased lateral stresses is that condition where there is a variable k_o distribution with depth. This is a common occurrence in the field and can result from the removal of overburden. The finite element program was first tried using an unloading step, similar to what will be described in the next section. This resulted, however, in large tensile distortions with much "failure" in the elements near the surface. This approach was not pursued further at this time. The next attempt was to use a variety of materials giving a typical variation of the lateral stress coefficient, k_o, with depth, and then load the surface in a manner similar to previous studies.

Figure 80 shows the results of such a study for the

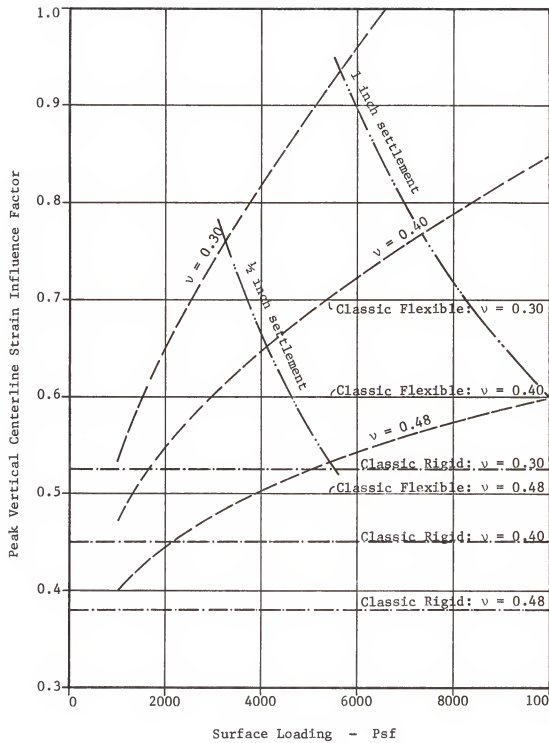


Figure 78. Peak Vertical Centerline Strain Influence Factor for Concrete Footing on Nonlinear Material under Plane Strain Loading as a Function of Surface Loading and Poisson's Ratio; K = 60,000, k_o = 1.00

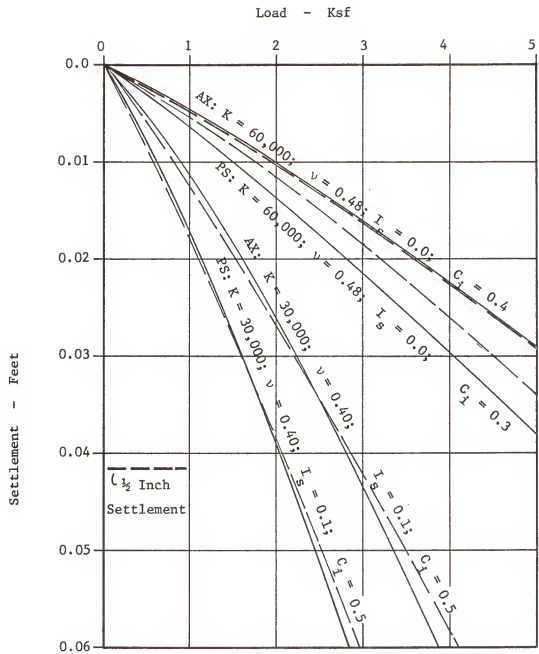


Figure 79. Load vs. Settlement Curves for Axisymmetric and Plane Strain Loading on Dense and Medium Dense Sand: D = 20 Ft; k_o = 1.00

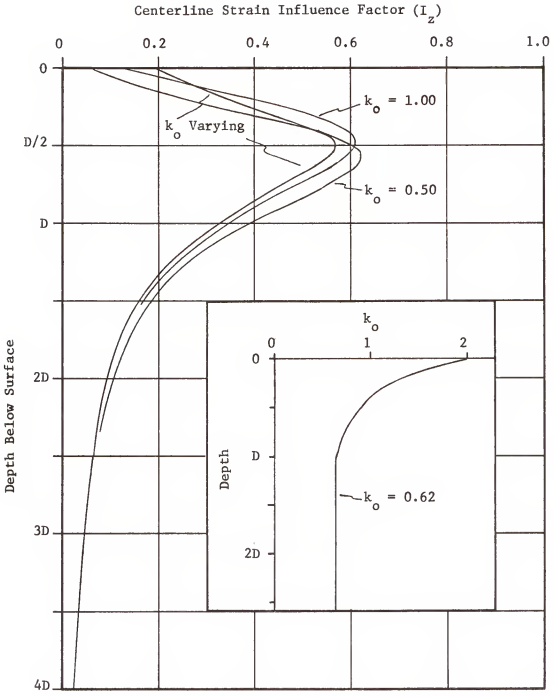


Figure 80. Comparison of Centerline Vertical Strain Influence Factor for 4000 Psf Axisymmetric Loading of 20 Ft Diameter Concrete Footing with Varying k_o Values; K = 60,000, ν = 0.40

axisymmertic case. The k_o variation with depth is indicated in the insert and varied from a value of 2.00 near the surface to a value of 0.62 at depth. The strain influence factor curve for 4000 psf surface loading is plotted and compared with the results from the constant $k_o = 0.5$ and $k_o = 1.00$ cases. It is seen that the general form of the curves is similar as would be expected because of the normalizing technique used to calculate the strain influence factor, as previously discussed.

Other possible variations and effects of a varying k_o parameter were not studied at this time. Future studies will be valuable in this area as more field information becomes available.

This brief study of the effects of increased lateral stresses shows that when using the normalized strain influence factor distribution approach, the effect of increased lateral stresses is minor. The previous recommendations with regard to the nature of assumed simplified triangular distributions and peak strain factor formulas remain the same, including the depth of influence, the surface intercept values, and the location of the peak vertical strain influence factor.

4.4 Influence of Depth to Rigid Layer

In many practical field problems, soil deposits do not extend to unlimited depths and in many cases there are relatively rigid layers at various depths. This study was undertaken to determine what the effects would be on the strain influence factor distribution due to a rigid layer at various depths.

It might be expected that theoretically there should be very

little effect on the strain distribution due to the includion of a rigid layer. Although the rigidity will impose lower displacements and thus lower strains for a given load, the normalization of this in obtaining the strain influence factor should give approximately the same strain factor values. There might be some redistribution of the influence factor results, however, due to the confining effect, especially for the nonlinear model.

When placing a rigid layer at shallow depths and using the finite element model in linear elastic analyses, the bottom boundary condition becomes more critical. Several approaches were considered and studied. One approach was to fix the nodal points at the interface between the nonrigid overlying layer and the rigid layer, thus allowing for no movement at that interface in any direction. For shallow layers (i.e., at depths of D or even 2D) the results of this type of fixed nodal points boundary condition on the strain and strain influence factors were not reasonable, especially near the boundary. The zero-displacement boundary condition often caused tension in elements near the boundary and, therefore, negative strains. Similar problems were encountered when using horizontal rollers along the bottom boundary.

Another approach was to place at the rigid boundary a layer of more rigid material with a modulus four or ten times greater than the material above it. For example, when using the linear elastic material with a modulus of 100 tsf, rigid materials with modulus values of 400 or 1000 tsf were used at the various depths being investigated. This approach gave more reasonable results and it was interesting to note that generally there was very little

difference in the strain factor distribution when using either the 400 or 1000 tsf modulus for the rigid layer. For uniformity in the linear analyses, the 400 tsf modulus was generally used.

For the nonlinear analyses, a rigid concrete layer was placed at the depth of interest and this proved to be a satisfactory solution, giving reasonable results.

4.4.1 Axisymmetric Loading

Initially the linear elastic material was loaded with the concrete footing under axisymmetric conditions and with depths to the rigid layer of 20, 40, and 60 ft. The strain influence factor was then calculated as described previously. The results for these cases are shown in Figures 81 through 83 which should be compared with the finite element solution in Figure 29 to determine the effect of the rigid layer. For comparison purposes, Figure 84 gives the influence factor curves from Figures 29, 81, 82, and 83 for a Poisson's ratio equal to 0.4.

It is noted that at a depth of 20 ft the value of the peak strain influence factor is approximately 10 percent greater than for the case with the rigid layer at 60 ft. The 40 and 60 ft depth cases are almost identical and compare well with Figure 29. For all three cases the peak value of the strain influence factor is at a depth of between 3D/8 and D/2.

If a single simplified triangular distribution were to be assumed based on the linear analyses, the rigid layer has only a slight effect on the value of the peak strain influence factor and its location. A peak located at a depth of D/2 is reasonable. The recommended depth of influence of 2D for the axisymmetric loading

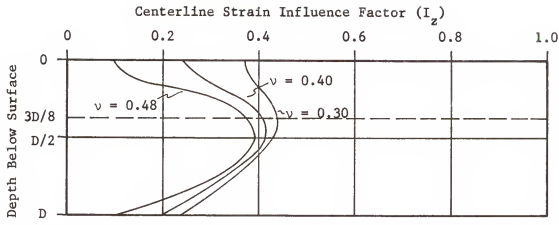


Figure 81. Centerline Vertical Strain Influence Factor for Axisymmetric Loading of 20 Ft Diameter Concrete Footing on Linear Elastic Material with Rigid Layer at a depth of 20 Ft

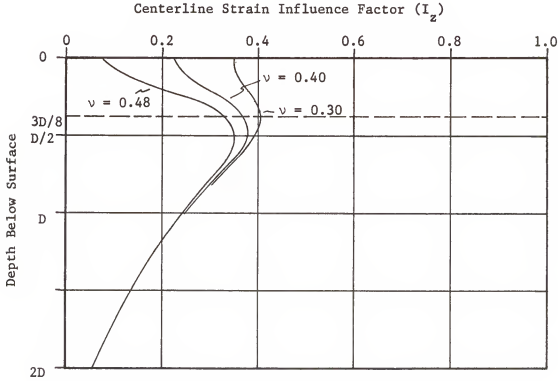


Figure 82. Centerline Vertical Strain Influence Factor for Axisymmetric Loading of 20 Ft Diameter Concrete Footing on Linear Elastic Material with Rigid Layer at a Depth of 40 Ft

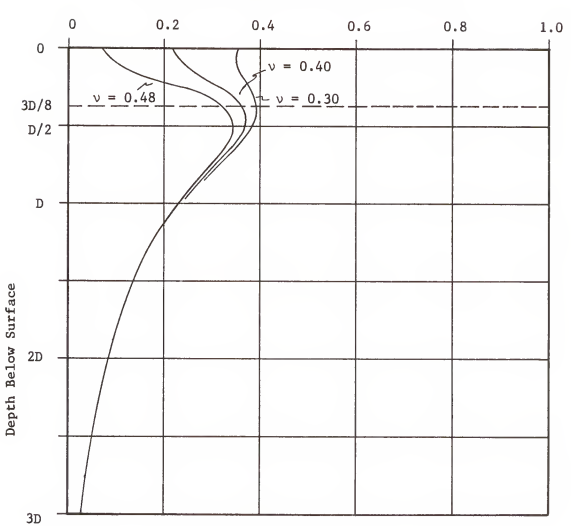


Figure 83. Centerline Vertical Strain Influence Factor for Axisymmetric Loading of 20 Ft Diameter Concrete Footing on Linear Elastic Material with Rigid Layer at a Depth of 60 Ft

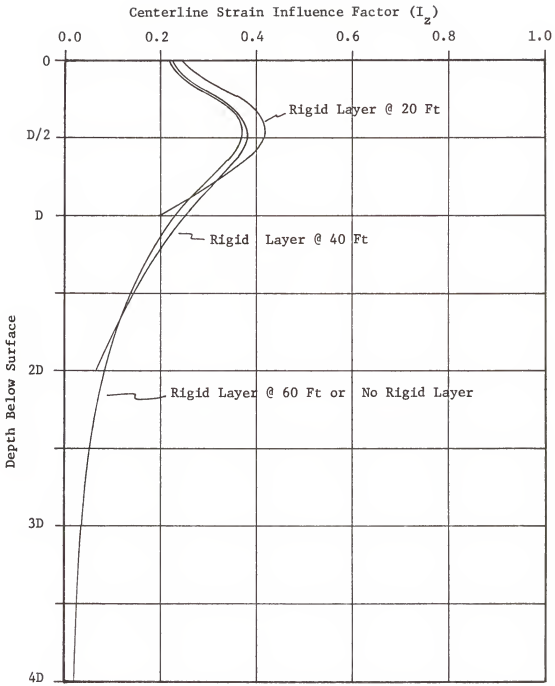


Figure 84. Comparison of Centerline Vertical Strain Influence Factor for Axisymmetric Loading of 20 Ft Diameter Concrete Footing on Linear Elastic Material with Rigid Layer at Varying Depths: $\nu = 0.40$

is also relatively unaffected by the rigid layer. Study of Figure 80 indicates that a reasonable triangular strain distribution could be obtained by using a depth of influence of 2D and then ignoring that part of the triangular distribution below the depth D. A surface intercept strain influence factor value of 0.2 also appears reasonable for the linear analyses.

The results of the nonlinear analyses are shown in Figures 85 through 87. The 4000 psf loading of the dense sand for varying Poisson's ratios is plotted in these figures, which should be compared with Figure 44. The general results are very similar to those for the linear analyses. For comparison purposes, Figure 88 gives the influence factor curves from Figures 44, 85, 86, and 87 for Poisson's ratio equal to 0.4. Figure 88 also includes the curve for the rigid layer at a depth of 10 ft under the same conditions.

When the rigid layer is at a depth D, the peak strain influence factor is increased slightly with the greatest effect for lower Poisson's ratios. Then, as the rigid layer depth increases, the peak strain influence factor values decrease and approach those for the case of no rigid layer. For the rigid layer depths of 40 and 60 ft, the results are very similar, as can be noted in Figures 86 and 87.

It is of interest to note from Figure 88 that the area beneath the strain influence factor curves is approximately the same above the rigid layer depth being studied. For example, the area under the influence curve for the rigid layer at 10 ft is approximately the same as the area above the D/2 depth for the 40 and 60 ft depth cases. Similarly, the area under the influence curve for the rigid

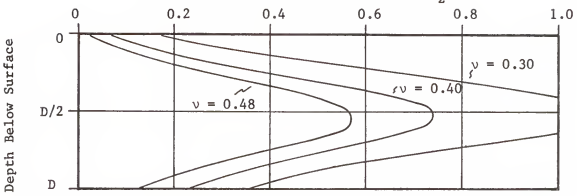


Figure 85. Centerline Vertical Strain Influence Factor for 4000 Psf Axisymmetric Loading of 20 Ft Diameter Concrete Footing Using Minor Principal Stresses and Bulk Failure Condition with Rigid Layer at a Depth of 20 Ft; K = 60,000

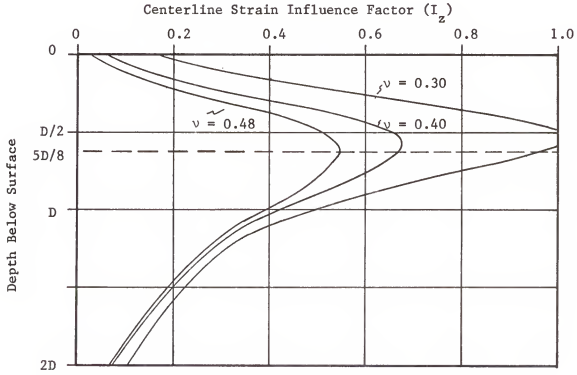


Figure 86. Centerline Vertical Strain Influence Factor for 4000 Psf Axisymmetric Loading of 20 Ft Diameter Concrete Footing Using Minor Principal Stresses and Bulk Failure Condition with Rigid Layer at a Depth of 40 Ft; K = 60,000

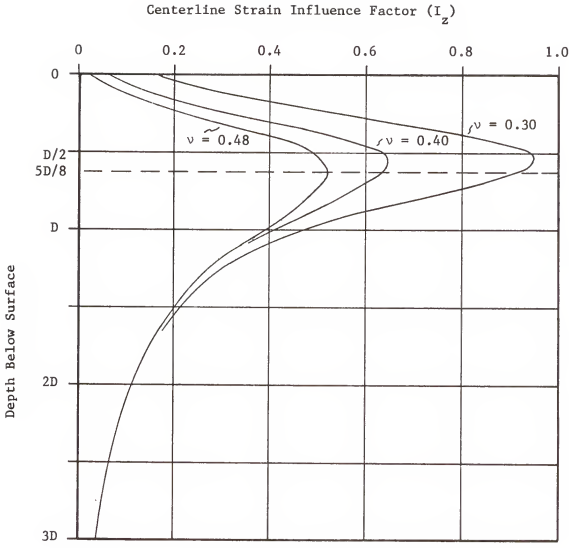


Figure 87. Centerline Vertical Strain Influence Factor for 4000 Psf Axisymmetric Loading of 20 Ft Diameter Concrete Footing Using Minor Principal Stresses and Bulk Failure Condition with Rigid Layer at a Depth of 60 Ft; K = 60,000

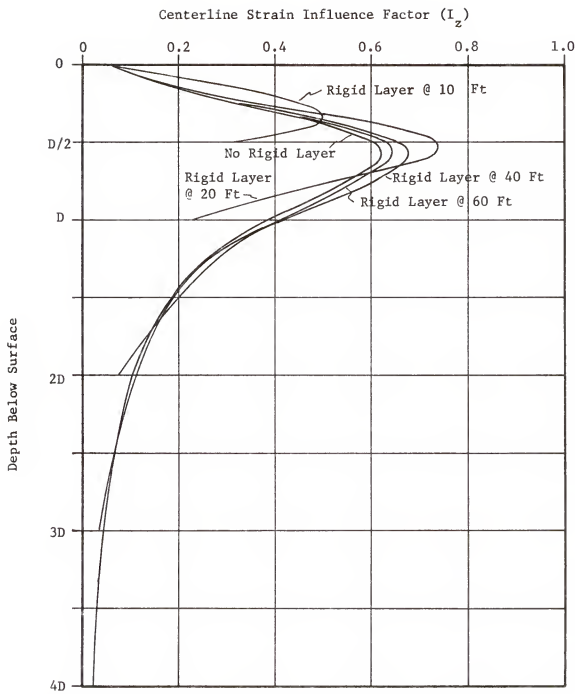


Figure 88. Comparison of Centerline Vertical Strain Influence Factor for 4000 Psf Axisymmetric Loading of 20 Ft Diameter Concrete Footing Using Minor Principal Stresses and Bulk Failure Condition with Rigid Layers at Varying Depths: K = 60,000; ν = 0.4

layer at 20 ft is approximately the same above the D depth as the 40 and 60 ft depth cases above this depth. This would imply that perhaps there might be very little error in using the previously recommended simplified strain factor distributions and equations and ignoring the effect of the rigid layer. Such an approximation would probably be least accurate for very shallow layers and smaller geometries.

Also, although the peak strain factor varies for the shallow rigid layer depths, this variation is less than that due to Poisson's ratio or using octahedral stresses or other possible analytical variations previously discussed. Therefore, it does not appear reasonable to make modifications for the effects of rigid layers under axisymmetric loading, based on these brief studies.

One way to indicate the relatively minor effect of the rigid layers under axisymmetric loading is shown in Figure 89. In this figure the finite element settlement relationships for the case of a 20 ft diameter footing with rigid layers at 10, 20, and 40 ft beneath the surface are plotted and compared with the analytical settlements that would be obtained from the use of Equations 80 and 81. In using Equation 80, the modulus values for the rigid concrete layer were used over the applicable depths. That is, when the rigid layer was at a depth of 10 ft, the integration used the nonlinear soil model from the surface to D/2 and then used a constant concrete modulus value from D/2 to 2D. The concrete settlements were negligible when compared to those of the soil, as would be expected. In agreement with previous discussions, the settlements in Figure 89 compare more favorably for the 20 and 40 ft

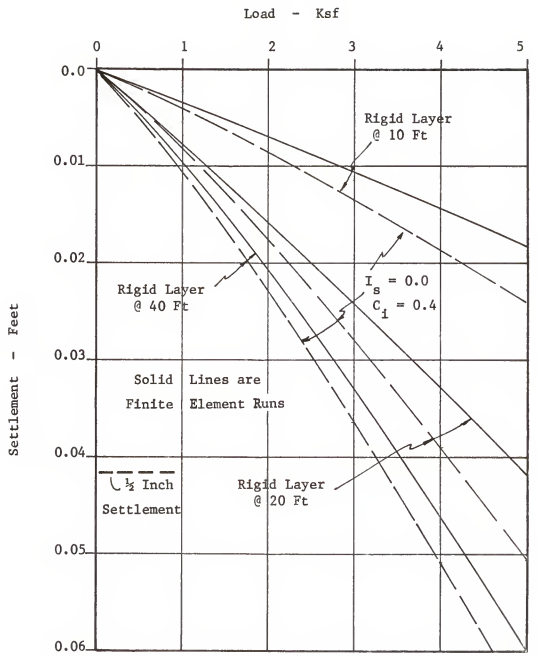


Figure 89. Load vs. Settlement Curves for 20 Ft Diameter Concrete Footing on Very Dense Sand with Rigid Layer at Varying Depths: K = 60,000, $\nu = 0.48$, $k_o = 0.5$

rigid layer depth cases, and less so for the 10 ft case.

Because of the parabolic in-situ modulus relationship previously discussed, it might be expected that there would be a variation due to the size of the axisymmetric foundation. This effect is illustrated in Figure 90. which gives the load vs. settlement curves for 10 and 50 ft diameter footings with depths to rigid layers of 5 ft for the 10 ft diameter case, and 25 and 50 ft for the 50 ft diameter case. In agreement with previous results, the comparison is most favorable for the larger geometry.

Still another way to show the effect of a rigid layer is shown in Figure 91. In this case a dense sand (K = 60,000) layer 10 ft thick was placed at the surface and at depths of 10 and 20 ft in a medium dense sand (K = 30,000). The normalized strain influence factor curves plotted in Figure 91 are only slightly affected by the rigid layer, even with the nonlinear modulus material. Although the peak locations are shifted slightly, the general shape of the curve is approximately the same as is the area enclosed by the strain influence factor curve with depth.

An additional way to consider the effect of a rigid layer is illustrated in Figure 92. In this figure, which is typical of many field conditions, a dense sand surface layer (K = 60,000, ν = 0.48) is located on the surface over a relatively loose deposit (K = 15,000, ν = 0.30). The surface "pavement" varies in thickness.

It is noted from the figure that generally the pavement layer has a minor effect on the shape of the strain factor distribution curve. There is, of course, some shifting of the curve due to the thickness of the top rigid layer, but generally the triangular shape

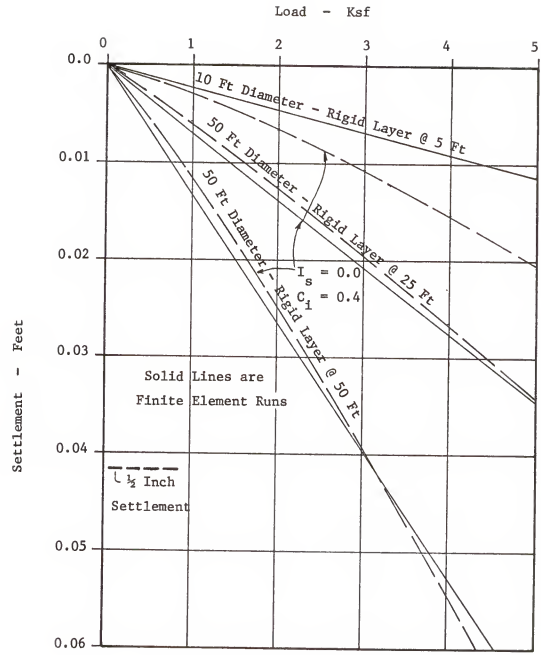


Figure 90. Load vs. Settlement Curves for 10 and 50 Ft Diameter Concrete Footings on Dense Sand with Rigid Layers at Varying Depths: K = 60,000; ν = 0.48; k_o = 0.5

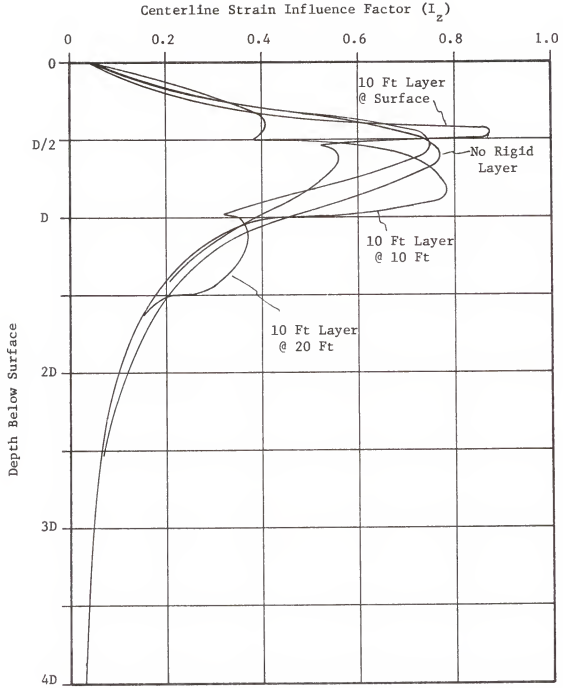


Figure 91. Centerline Vertical Strain Influence Factor for Axisymmetric Loading of 20 Ft Diameter Concrete Footing with 10 Ft Thick Dense Sand Layer (K = 60,000) at Various Depths and 4000 Psf Loading; K = 30,000, ν = 0.40, and k_o = 0.50

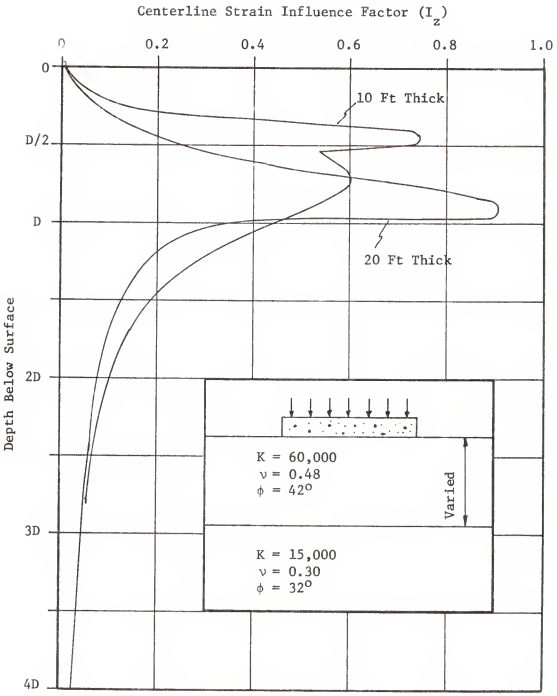


Figure 92. Effect of Rigid Surface Layer (K = 60,000) of Varying Thickness over Loose Deposit (K = 15,000) for 20 Ft Diameter Concrete Footing Under 4000 Psf Axisymmetric Loading

remains and it appears that little error would be involved in using the simplified strain factor distributions previously developed.

Obviously a much more thorough parametric study would be necessary to uncover all the subtleties of the effect of a rigid surface layer. Varying modulus combinations and thicknesses could be studied as well as the nature of the interfaces between the two materials. This is promising as an area of future research.

The studies in this section all indicate that the effect of a higher modulus layer is negligible, especially when compared with the many variables involved in an analysis. The general simplified triangular distribution approach previously developed should be used along with the appropriate modulus values for the materials involved.

4.4.2 Plane Strain Loading

The linear elastic modulus material was loaded with the 20 ft wide concrete footing under plane strain conditions and with depths to the rigid layer of 20, 40, and 60 ft. The strain influence factors for these cases are plotted in Figures 93 through 95, which should be compared with the finite element solutions in Figure 30. For comparison purposes, Figure 96 gives the influence factor curves from Figures 30, 93, 94, and 95 for a Poisson's ratio equal to 0.4.

It is noted that with the rigid layer at a depth of 20 ft the value of the peak strain influence factor is only slightly greater than for the case with the rigid layer at 60 ft. The 40 and 60 ft depth cases are almost identical and compare favorably with Figure 30. For all three cases the peak value of the strain influence factor is at a depth of approximately D/2. As in the axisymmetric case for the linear analysis, there is only a slight effect due to

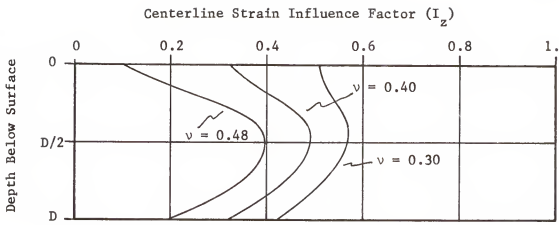


Figure 93. Centerline Vertical Strain Influence Factor for Plane Strain Loading of 20 Ft Wide Concrete Footing on Linear Elastic Material with Rigid Layer at a Depth of 20 Ft

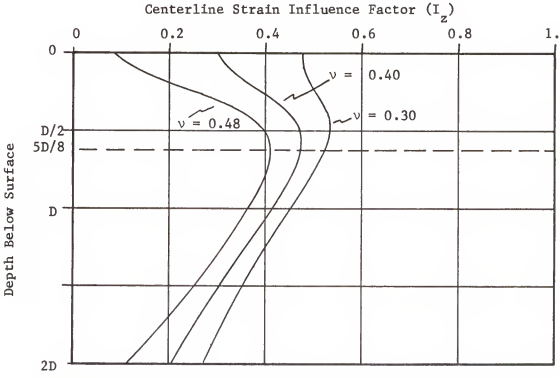


Figure 94. Centerline Vertical Strain Influence Factor for Plane Strain Loading of 20 Ft Wide Concrete Footing on Linear Elastic Material with Rigid Layer at a Depth of 40 Ft

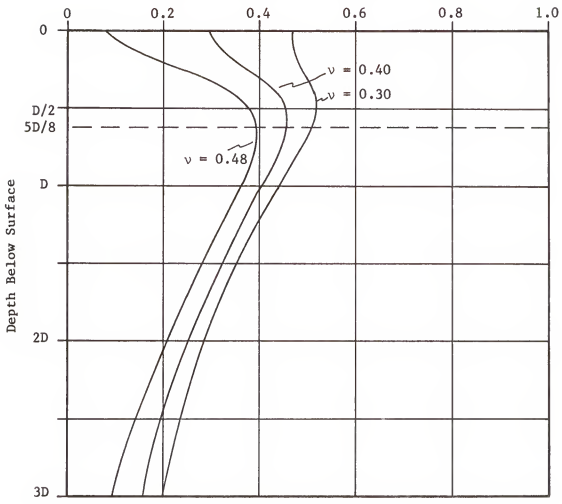


Figure 95. Centerline Vertical Strain Influence Factor for Plane Strain Loading of 20 Ft Wide Concrete Footing on Linear Elastic Material with Rigid Layer at a Depth of 60 Ft

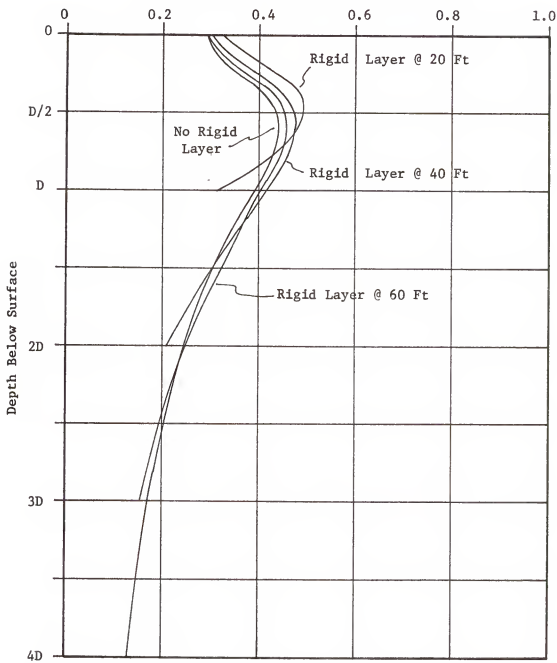


Figure 96. Comparison of Centerline Vertical Strain Influence Factor for Plane Strain Loading of 20 Ft Wide Concrete Footing on Linear Elastic Material with Rigid Layer at Varying Depths: $\nu = 0.40$

the rigid layers and it appears reasonable to use the same triangular strain distribution as developed for the general plane strain case, and ignore the effects of the rigid layer.

The results of the nonlinear analyses are shown in Figures 97 through 99 which are for the 4000 psf loading of the dense sand and should be compared with Figure 63. For comparison purposes, Figure 100 gives the strain influence factor curves from Figures 63, 97, 98, and 99 for the case of Poisson's ratio equal to 0.4, and includes the additional case when the depth to the rigid layer is 10 ft.

As in the axisymmetric studies, the general effect of the rigid layer is to modify slightly the individual strain influence factor distribution curves. However, as noted in Figure 100, the area beneath the strain influence factor curves is approximately the same above the rigid layer depth being studied. This would imply that there should be very little error involved in using the previously developed simplified triangular strain distribution and then ignoring the effects of the rigid layer.

This is further illustrated in Figure 101 for the 20 ft wide footing and in Figure 102 for 10 and 50 ft wide footings. The finite element settlement curves in these figures are compared with the settlement relationship which would result from integrating Equation 84 and using Equation 81 for I_{zp} with $\sigma_{3D/4}$ instead of $\sigma_{D/2}$. As in the axisymmetric studies, the modulus values for the rigid concrete layer were used over the applicable depths. In Figure 101 the settlements compare favorably for the 20 and 40 ft rigid layer depth cases, and less so for the 10 ft case. This is in general agreement

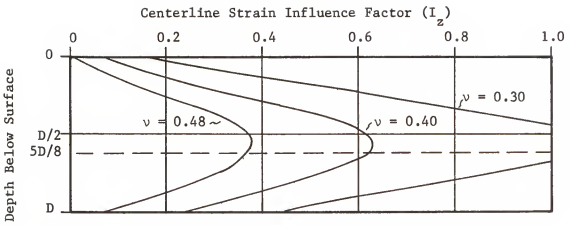


Figure 97. Centerline Vertical Strain Influence Factor for 4000 Psf Plane Strain Loading of 20 Ft Wide Concrete Footing Using Minor Principal Stresses and Bulk Failure Condition with Rigid Layer at a Depth of 20 Ft; K = 60,000

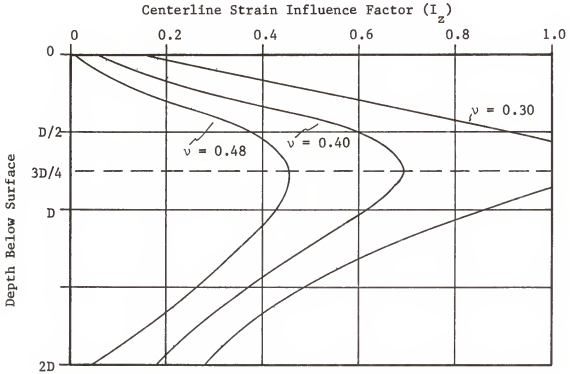


Figure 98. Centerline Vertical Strain Influence Factor for 4000 Psf Plane Strain Loading of 20 Ft Wide Concrete Footing Using Minor Principal Stresses and Bulk Failure Condition with Rigid Layer at a Depth of 40 Ft; K = 60,000

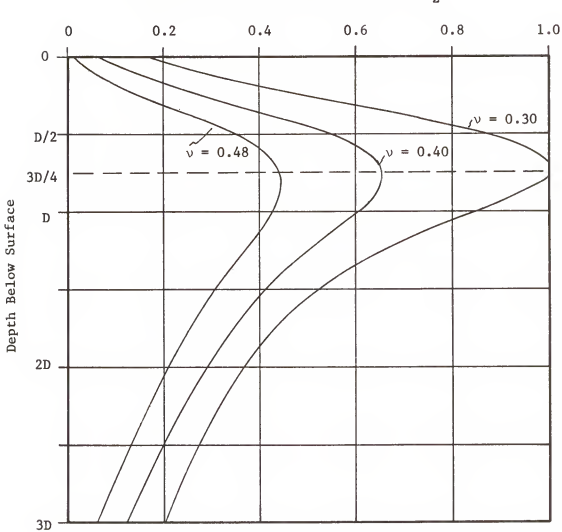


Figure 99. Centerline Vertical Strain Influence Factor for 4000 Psf Plane Strain Loading of 20 Ft Wide Concrete Footing Using Minor Principal Stresses and Bulk Failure Condition with Rigid Layer at a Depth of 60 Ft; K = 60,000

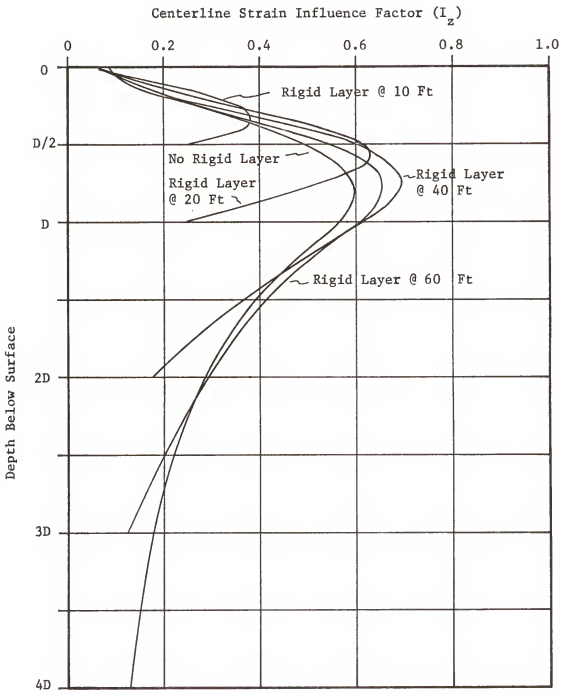


Figure 100. Comparison of Centerline Vertical Strain Influence Factor for 4000 Psf Plane Strain Loading of 20 Ft Wide Concrete Footing Using Minor Principal Stresses and Bulk Failure Condition with Rigid Layers at Varying Depths: K = 60,000; ν = 0.4

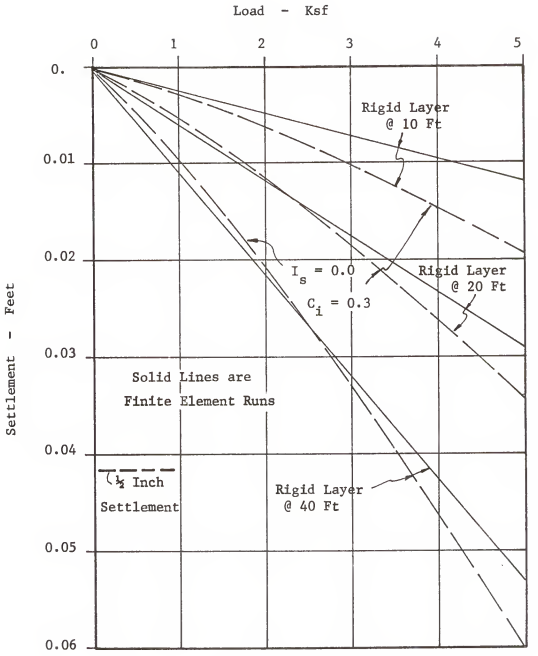


Figure 101. Load vs. Settlement Curves for 20 Ft Wide Concrete Footing on Dense Sand with Rigid Layer at Varying Depths: K = 60,000, ν = 0.48, k_o = 0.5

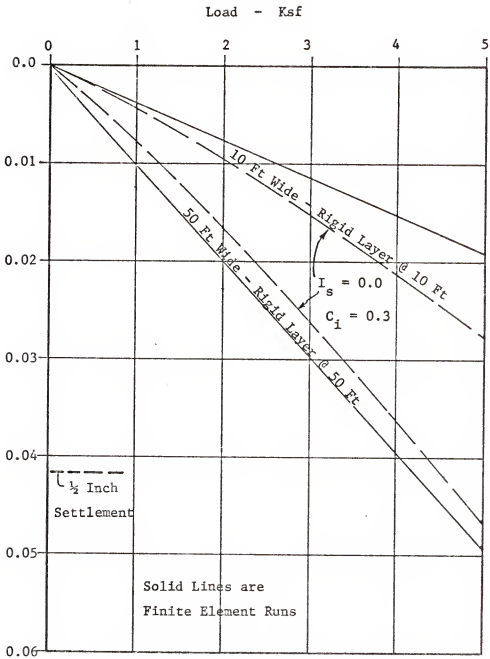


Figure 102. Load vs. Settlement Curves for 10 and 50 Ft Wide Concrete Footings on Dense Sand with Rigid Layers at Varying Depths: $K = 60{,}000$, $\nu = 0.48$, $k_o = 0.5$

with the results of the axisymmetric analysis and is to be expected, considering the parabolic distribution of the initial in-situ tangent modulus. In Figure 102, the 50 ft wide footing case therefore compares more favorably than the 10 ft wide case, for similar reasons.

Still another way to show the effect of a rigid layer is shown in Figure 103. In this figure a dense sand layer 10 ft thick was placed at 10 and 20 ft depths in medium dense sand. The normalized strain influence factor curves plotted in Figure 103 are only slightly affected by the rigid layer, even with the nonlinear modulus material. Although the peak locations are shifted slightly, the general shape of the curve is approximately the same, as is the total area enclosed by the strain influence factor curve with depth.

The rigid "pavement" case was not studied under plane strain loading, but it is felt that the results would be similar to those for the axisymmetric and indicate that generally the simplified strain distribution approach remains reasonable.

The studies in this section all indicate that the effect of a rigid layer is generally negligible, especially when compared with the many variables involved in the analysis. The simplified triangular strain factor distribution and peak strain factor formulas should be used for both axisymmetric and plane strain analyses, along with appropriate modulus values for the soil and the rigid materials. These results are further summarized in Section 4.7.

These recommendations are less accurate for very narrow footing geometries and very shallow depth rigid layers. More complete parametric studies would be necessary to further define all the variables and determine their effects for such cases.

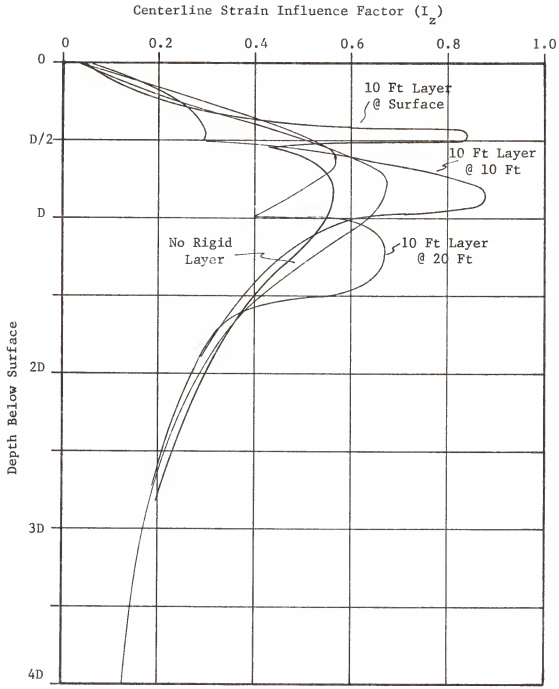


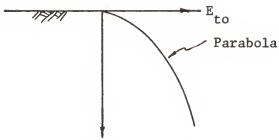
Figure 103. Centerline Vertical Strain Influence Factor for Plane Strain Loading of 20 Ft Wide Concrete Footing with 10 Ft Thick Dense Sand Layer (K = 60,000) at Various Depths and 4000 Psf Loading; K = 30,000, ν = 0.40, and k_o = 0.50

4.5 Influence of Embedment

In ordinary foundation construction, the footings are often placed at some depth beneath the surface. This usually means that there is an excavation, with a subsequent unloading of the soil due to removed material, followed by a reloading caused by the structure. To model this using the finite element method, the elements in the excavation were replaced with air and then the bottom and sides of the excavation were unloaded using existing in-situ stresses. After this step the concrete footing was placed in the bottom of the excavation and then loaded in increments. This procedure is shown in Figure 104.

The unload-reload modulus number, K_{ur}, was discussed in Section 3.2 and is a linear stress-dependent modulus, similar to the nonlinear modulus number, K. The unloading step was a single step. The value of K_{ur} was generally taken as one-third greater than the value of K, as indicated by the results of studies by Kulhawy et al. (1969).

The strain distribution for such an unloading case should, of course, differ from that of direct surface loading. The initial unloading causes a tension in the elastic material, and thus negative strains. Then the reloading reimposes positive strains. Any structural settlement will be based on reloading the unloaded material. Therefore, a meaningful strain influence factor distribution should be based on the unloaded condition as a starting point. The computer program was set up using this unloaded condition as the starting point for determining strains after



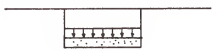
(a) Establish In-Situ Initial Tangent Modulus



(b) Remove Soil Elements



(c) Unload Using In-Situ Stresses



(d) Put Concrete Footing in Excavation and Load

Figure 104. Steps in Unloading and Reloading Foundation for Embedment Studies

structural loading. The modulus value used in the calculations for the strain influence factor was the initial in-situ tangent modulus prior to excavation, as previously discussed.

The cases studied were for 5, 10, and 15 ft embedment using a soil with a density of 100 pcf. Thus the vertical unloading pressures at the various depths were 500, 1000, and 1500 psf respectively. The first analyses were made using the linear elastic material, and then extended to the nonlinear cases.

4.5.1 Axisymmetric Loading

Figures 105 through 107 give the centerline vertical strain influence factor distribution beneath the 20 ft diameter concrete footing when placed in a linear elastic material at depths of 5, 10, and 15 ft beneath the surface. These figures should be compared with the finite element solution in Figure 29.

As would be expected, the peak strain influence factor decreases as the depth of embedment increases. It is interesting to note, however, that in all cases the depth to the peak strain influence factor is at a depth of from 3D/8 to D/2 beneath the bottom of the foundation, and the depth of influence is generally 2D beneath the base of the foundation.

Very similar results were obtained for the nonlinear analyses, which are plotted in Figures 108 through 110. These curves, which should be compared with Figure 44, are for the 4000 psf axisymmetric loading of the 2 ft thick concrete footing. As in the linear analysis, the peak strain influence factor value decreases with increasing embedment, although the location remains generally at a depth of D/2 beneath the bottom of the foundation. The depth of

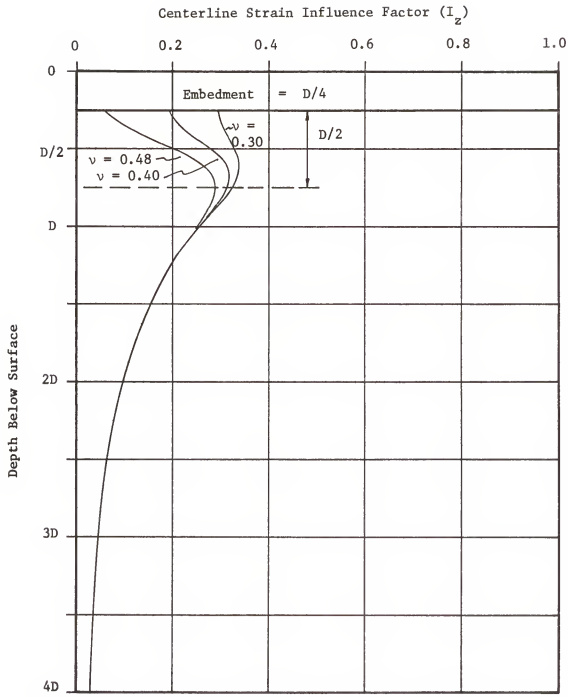


Figure 105. Centerline Vertical Strain Influence Factor for Axisymmetric Loading of 20 Ft Diameter Concrete Footing Embedded 5 Ft into Linear Elastic Material

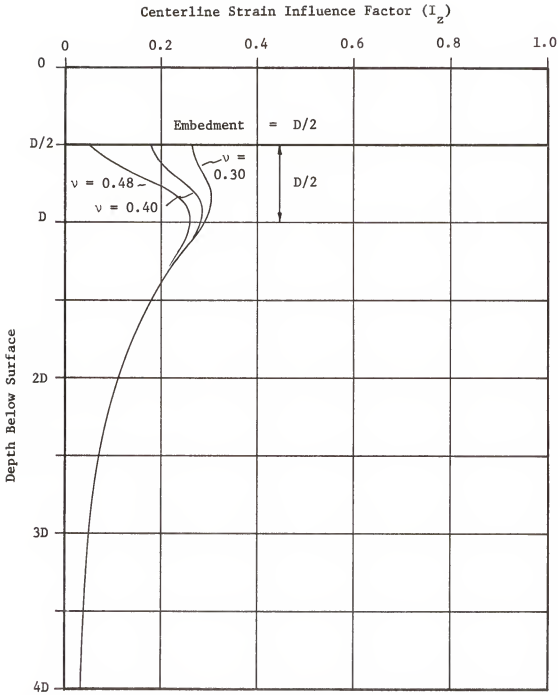


Figure 106. Centerline Vertical Strain Influence Factor for Axisymmetric Loading of 20 Ft Diameter Concrete Footing Embedded 10 Ft into Linear Elastic Material

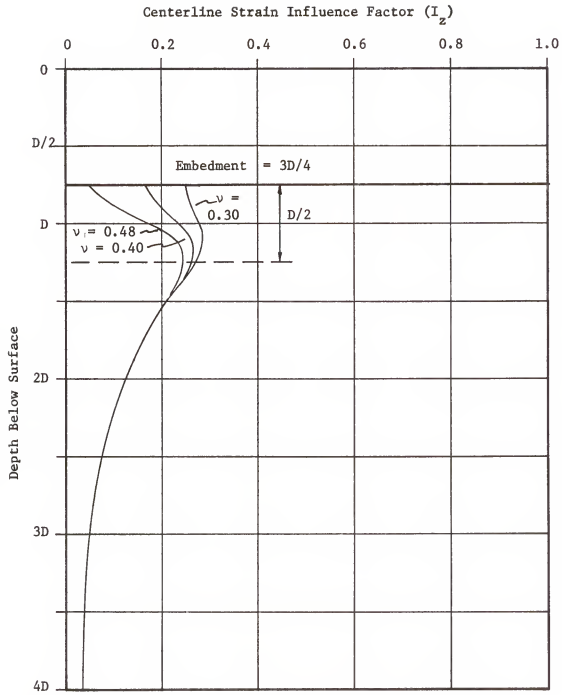


Figure 107. Centerline Vertical Strain Influence Factor for Axisymmetric Loading of 20 Ft Diameter Concrete Footing Embedded 15 Ft into Linear Elastic Material

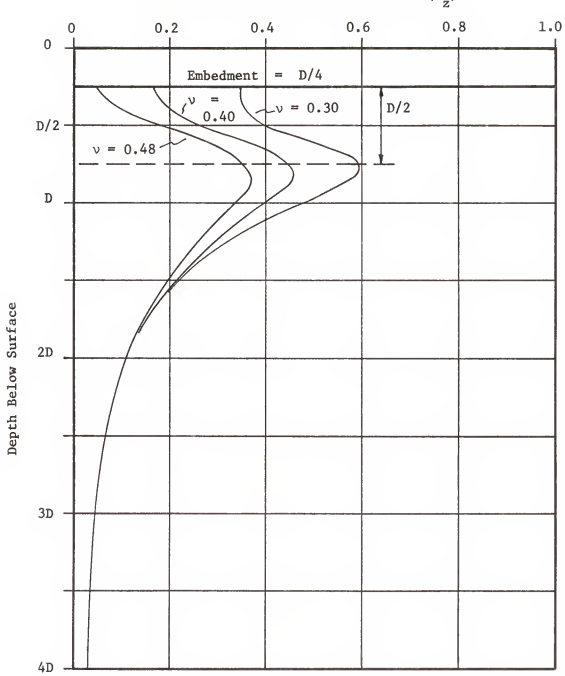


Figure 108. Centerline Vertical Strain Influence Factor for 4000 Psf Axisymmetric Loading of 20 Ft Diameter Concrete Footing Embedded 5 Ft into Nonlinear Elastic Material: K = 60,000

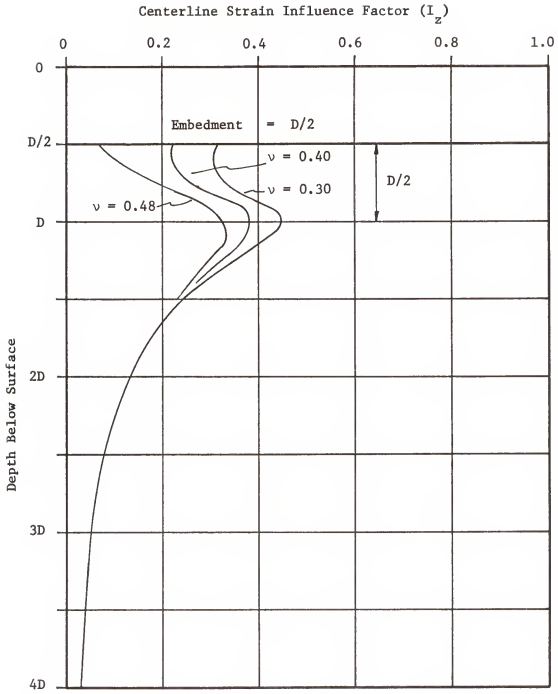


Figure 109. Centerline Vertical Strain Influence Factor for 4000 Psf Axisymmetric Loading of 20 Ft Diameter Concrete Footing Embedded 10 Ft into Nonlinear Elastic Material: K = 60,000

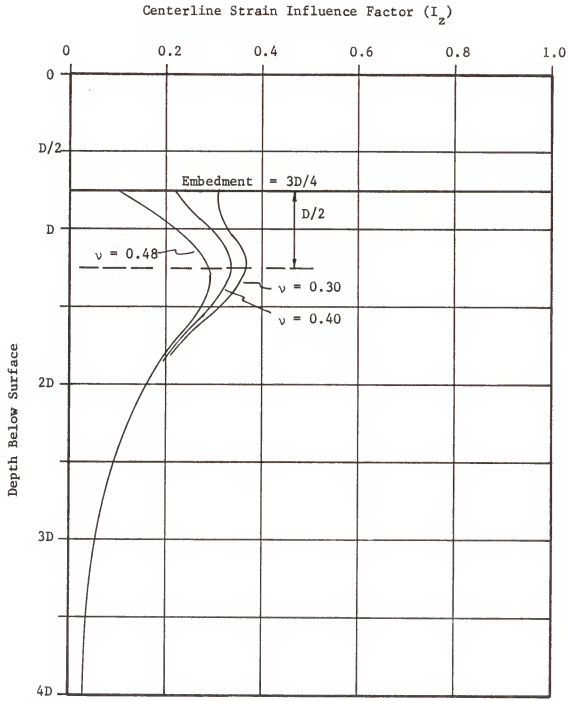


Figure 110. Centerline Vertical Strain Influence Factor for 4000 Psf Axisymmertic Loading of 20 Ft Diameter Concrete Footing Embedded 15 Ft into Nonlinear Elastic Material; K = 60,000

influence remains also at 2D, measured from the bottom of the foundation.

Based on these initial studies, it appears reasonable to retain the single simplified triangular strain factor distribution beneath the bottom of the foundation, regardless of embedment. This is in agreement with Schmertmann (1970). It also appears reasonable, however, to decrease the value of the peak centerline strain influence factor.

Schmertmann (1970) recommends an embedment correction factor, C_1, which is expressed as

$$C_1 = 1 - 0.5 \left(\frac{p_o}{\Delta p} \right) \tag{86}$$

where p_o is the in-situ vertical pressure at the depth in question and Δp is the difference between the foundation loading pressure and this in-situ pressure. The correction cannot be less than 0.5.

If Equation 86 is solved for the various conditions used in these embedment studies, the results can be tabulated as shown in Table 7. It is noted that because of the form of this correction equation, the settlements are most reduced (up to one-half) for the lower pressure loadings.

One way to consider the Schmertmann correction would be to apply it to the analytical settlement equations (Equations 80 and 81) as applied to axisymmetric loading and using the appropriate depths of integration. That is, for 5 ft embedment of the 20 ft diameter footing, the integration limits would be from D/4 to 3D/4 and from 3D/4 to 9D/4, thus retaining the 2D depth of influence, but measured from the foundation base.

Table 7. Schmertmann Embedment Correction Factor Values

Embedment	5 Ft		10 Ft		15 Ft	
P_o	500 Psf		1000 Psf		1500 Psf	
Load (Psf)	Δp (Psf)	C_1	Δp (Psf)	C_1	Δp (Psf)	C_1
1000	500	0.50	0	0.50	-500	0.50
2000	1500	0.83	1000	0.50	500	0.50
3000	2500	0.90	2000	0.75	1500	0.50
4000	3500	0.93	3000	0.83	2500	0.70
5000	4500	0.94	4000	0.88	3500	0.79

If the finite element settlements for K = 60,000, ν = 0.48, and various embedment depths are compared to the results using these equations (with and without the Schmertmann correction), the results are as shown in Figures 111 through 113. These three figures indicate that the uncorrected use of the analytical expressions predicts settlements which are too high, which is a reasonable result. The Schmertmann correction, however, is a reasonable one, but apparently predicts too low settlements at the lower pressures, when compared with the results of these studies. It is of additional interest to note that the U.S. Navy Design Manual, NAVFAC DM-7 (Department of the Navy, 1972) recommends no reduction for settlement estimates if the embedment is equal to or less than the footing dimension, D, which was the case for these studies.

Inspection of Figures 111 through 113 indicates that a more reasonable settlement comparison would result if the constant C_i were to be reduced. For comparison purposes, the results using modified Equation 80 and C_i values of 0.3 and 0.2 are also plotted on these figures. Study of these indicates that C_i can be reduced by 0.1 for D/4 embedment (Figure 111) and by 0.2 for D/2 and 3D/4 embedment (Figures 112 and 113). Perhaps a reasonable and general recommendation might be to reduce C_i by 0.1 for any shallow embedment (less than D) until further more complete parametric studies can be made. In using this approach, the triangular strain factor distribution should be measured from the base of the foundation. Schmertmann's correction is also reasonable, and could be used in place of the C_i reduction if desired.

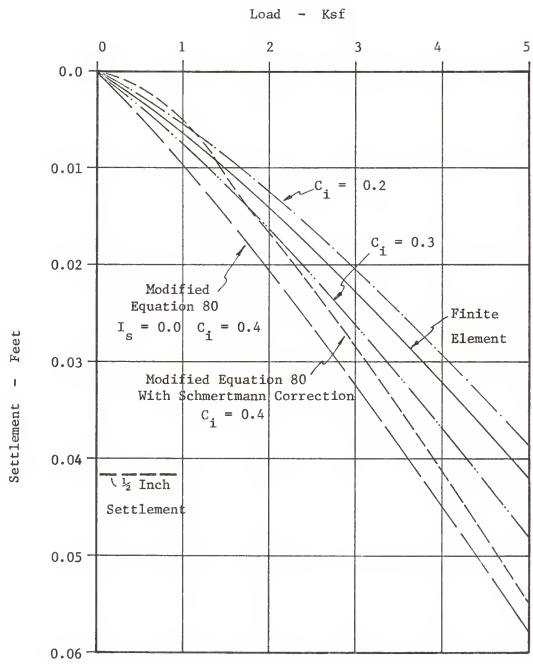


Figure 111. Load vs. Settlement Curves for 5 Ft Embedment of 20 Ft Diameter Concrete Footing in Dense Sand: K = 60,000, ν = 0.48, k_o = 0.5

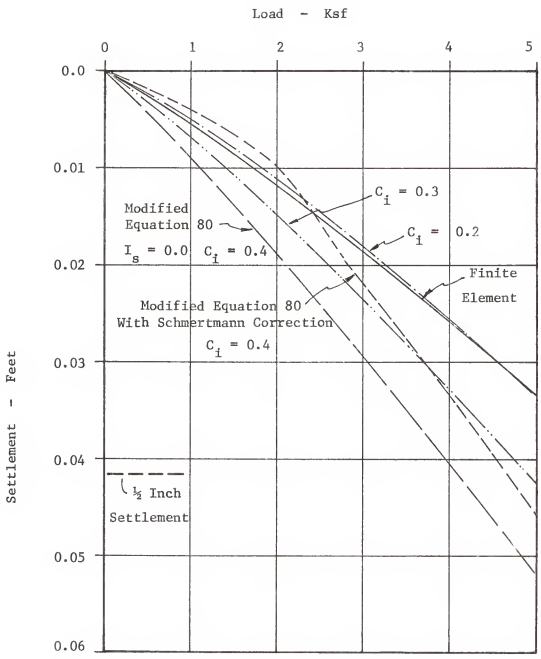


Figure 112. Load vs. Settlement Curves for 10 Ft Embedment of 20 Ft Diameter Concrete Footing in Dense Sand: K = 60,000, ν = 0.48, k_o = 0.5

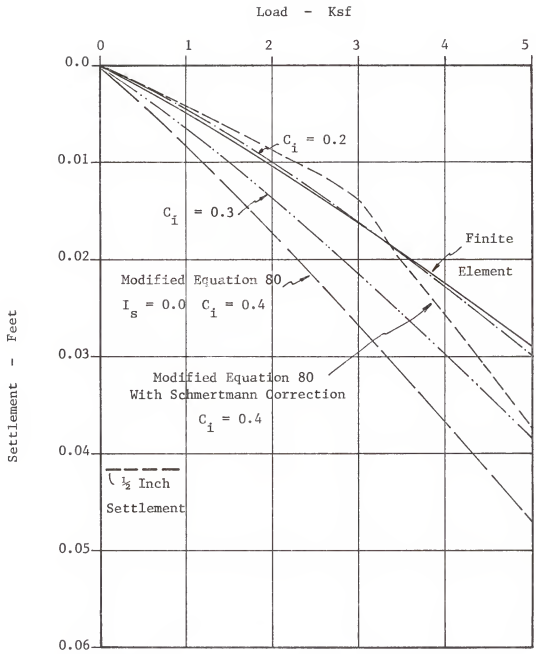


Figure 113. Load vs. Settlement Curves for 15 Ft Embedment of 20 Ft Diameter Concrete Footing in Dense Sand: K = 60,000, ν = 0.48, k_o = 0.5

4.5.2 Plane Strain Loading

Figures 114 through 116 give the centerline vertical strain influence factor distribution beneath the 20 ft wide concrete footing when placed in linear elastic material at depths of 5, 10, and 15 ft beneath the surface. The figures should be compared with the finite element solution in Figure 30.

The results for the plane strain analysis in the linear elastic material are very similar to those for the axisymmetric case. The peak strain influence factor decreases with increasing embedment, but for the linear analysis the peak location remains at approximately D/2 beneath the foundation base.

The nonlinear analysis results for the 4000 psf loading are shown in Figures 117 through 119 and should be compared with Figure 63. The peak strain influence factor location remains at a depth of 3D/4 beneath the foundation base and a depth of influence of 4D beneath this base also appears reasonable.

The settlement comparisons between the finite element studies and a modified Equation 84 (modified for appropriate limits of integration), both including and excluding the Schmertmann correction,are given in Figures 120 through 122.

As in the axisymmetric case, it appears that the Schmertmann correction gives too low settlement predictions, especially at the lower loading pressures, but the uncorrected analytical settlement as given by a modified Equation 84 predicts settlements too high. For comparison purposes, the results using the modified Equation 84 but with C_i values of 0.2 and 0.1 are included on the figures. Study of these figures indicates, as in the axisymmetric case, that

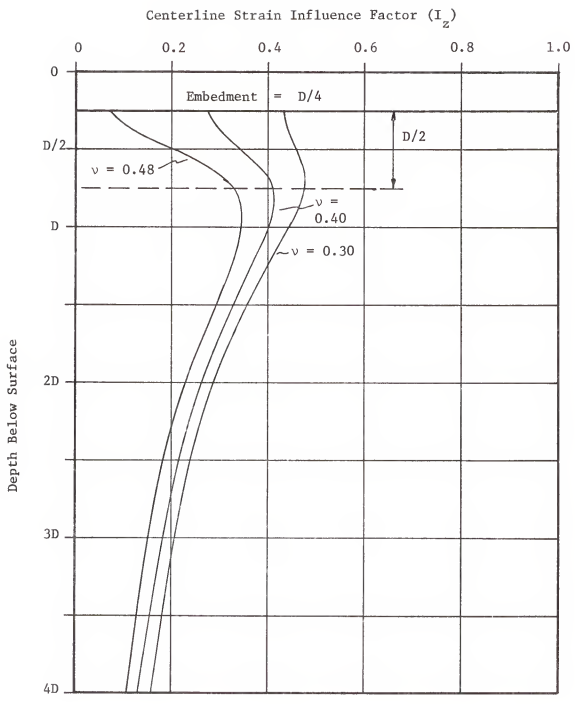


Figure 114. Centerline Vertical Strain Influence Factor for Plane Strain Loading of 20 Ft Wide Concrete Footing Embedded 5 Ft into Linear Elastic Material

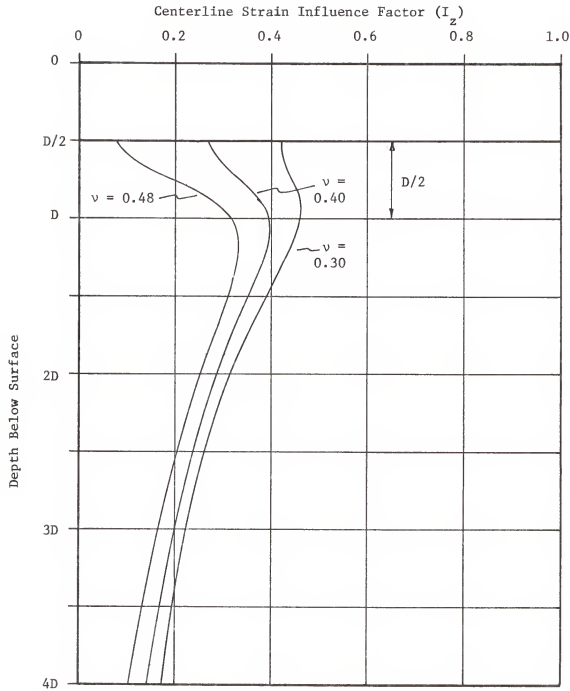


Figure 115. Centerline Vertical Strain Influence Factor for Plane Strain Loading of 20 Ft Wide Concrete Footing Embedded 10 Ft into Linear Elastic Material

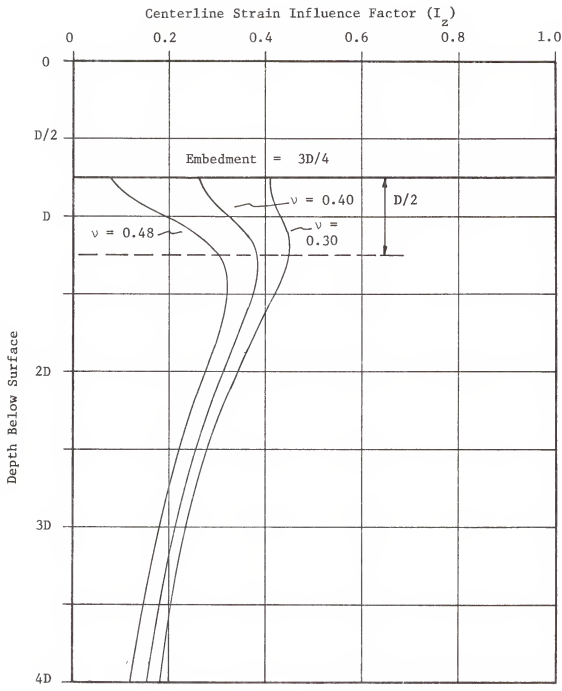


Figure 116. Centerline Vertical Strain Influence Factor for Plane Strain Loading of 20 Ft Wide Concrete Footing Embedded 15 Ft into Linear Elastic Material

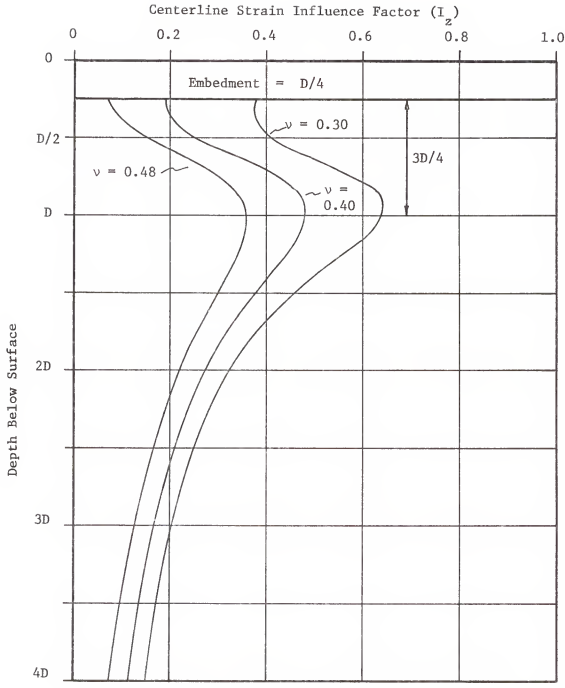


Figure 117. Centerline Vertical Strain Influence Factor for 4000 Psf Plane Strain Loading of 20 Ft Wide Concrete Footing Embedded 5 Ft into Nonlinear Elastic Material: K = 60,000

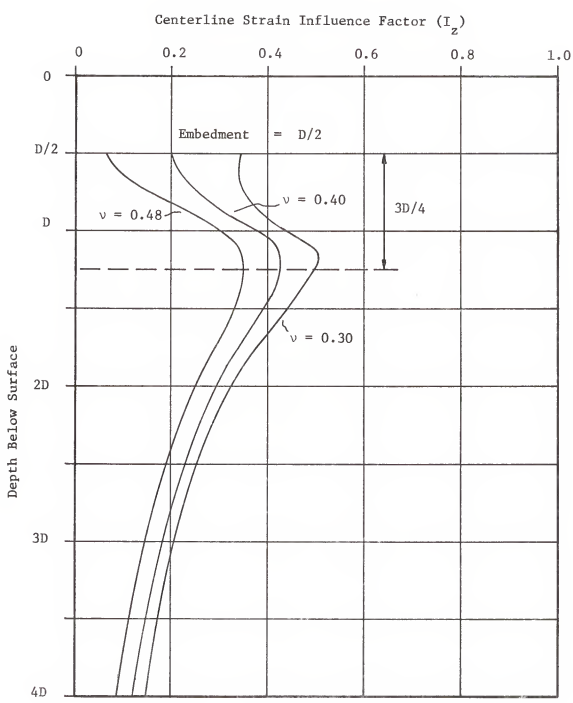


Figure 118. Centerline Vertical Strain Influence Factor for 4000 Psf Plane Strain Loading of 20 Ft Wide Concrete Footing Embedded 10 Ft into Nonlinear Elastic Material: K = 60,000

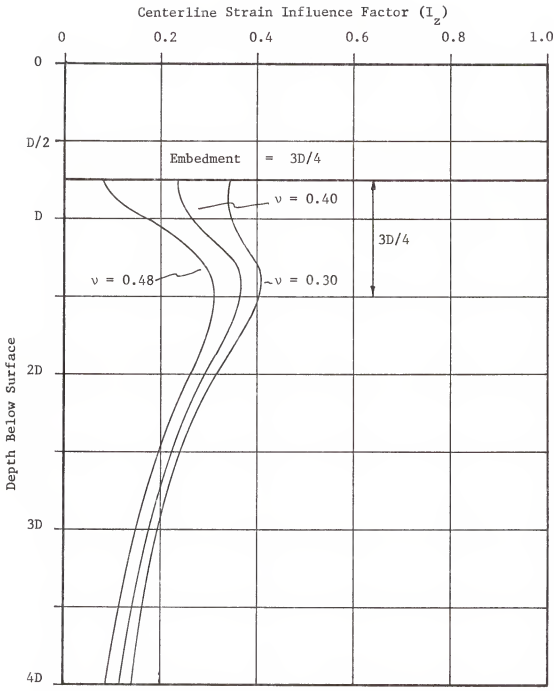


Figure 119. Centerline Vertical Strain Influence Factor for 4000 Psf Plane Strain Loading of 20 Ft Wide Concrete Footing Embedded 15 Ft into Nonlinear Elastic Material: K = 60,000

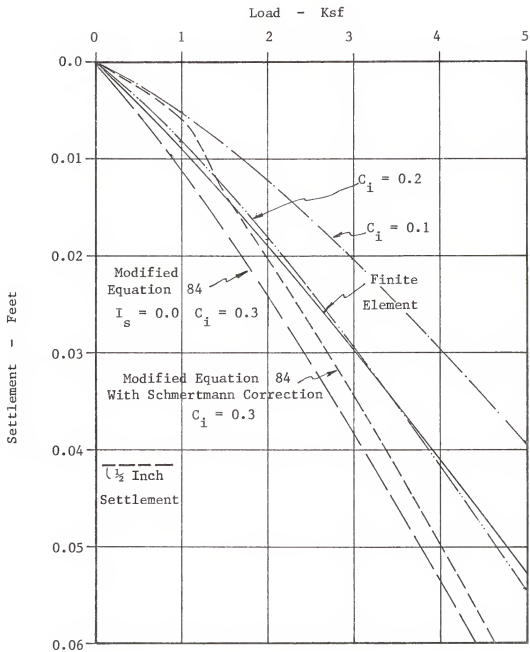


Figure 120. Load vs. Settlement Curves for 5 Ft Embedment of 20 Ft Wide Concrete Footing in Dense Sand: K = 60,000, ν = 0.48, k_o = 0.5

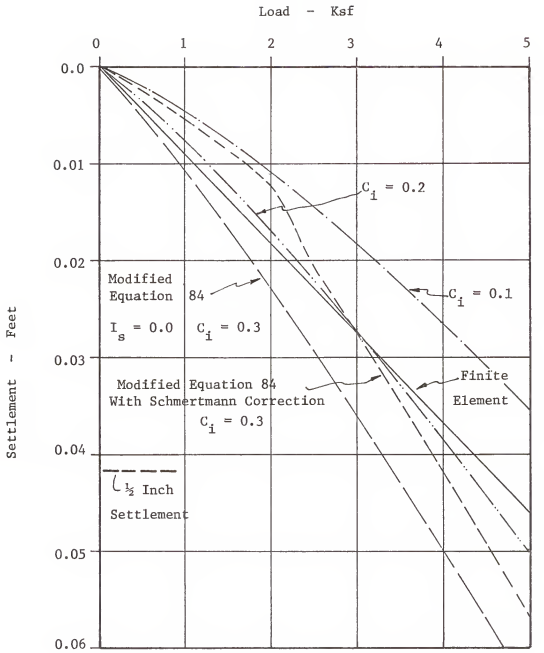


Figure 121. Load vs. Settlement Curves for 10 Ft Embedment of 20 Ft Wide Concrete Footing in Dense Sand: K = 60,000, ν = 0.48, k_o = 0.5

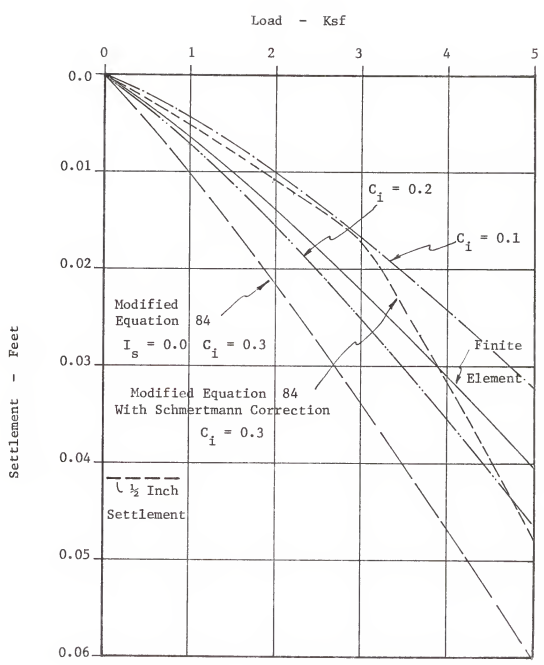


Figure 122. Load vs. Settlement Curves for 15 Ft Embedment of 20 Ft Wide Concrete Footing in Dense Sand: K = 60,000, ν = 0.48, k_o = 0.5

a reasonable recommendation would be to reduce C_i by 0.1 for shallow foundation embedment (less than D). In using this approach, the triangular strain factor distribution should be measured from the base of the foundation. Schmertmann's correction is also reasonable, and could be used in place of the C_i reduction if desired.

4.6 Variations Near Edge of Footing

It is well known that the pressure variation beneath rigid loading on a homogeneous, isotropic, linearly elastic material increases from the center to the edge with a theoretical value of infinity at the edge (Terzaghi, 1943). Since stress is proportional to strain, it should follow that at the edge of the rigid footing there should be a high strain and thus a high value of the strain influence factor. Figure 123 shows the vertical strain influence factor at the center and at the edge of a rigid axisymmetric footing on the linearly elastic material, using the finite element model. Inspection of these strain influence factor curves shows that the one at the edge decreases with depth, while the one at the centerline has the typical triangular shape with a peak at approximately D/2. Since the settlement at both points should be the same, the area beneath these curves (as a function of depth) should be the same, as it appears to be from the figure. A similar variation is illustrated in Figure 124 for the plane strain loading.

If a similar study is made for the nonlinear stress-dependent modulus material, then the results are as shown in Figures 125 and 126 for the axisymmetric and plane strain loadings. Because the

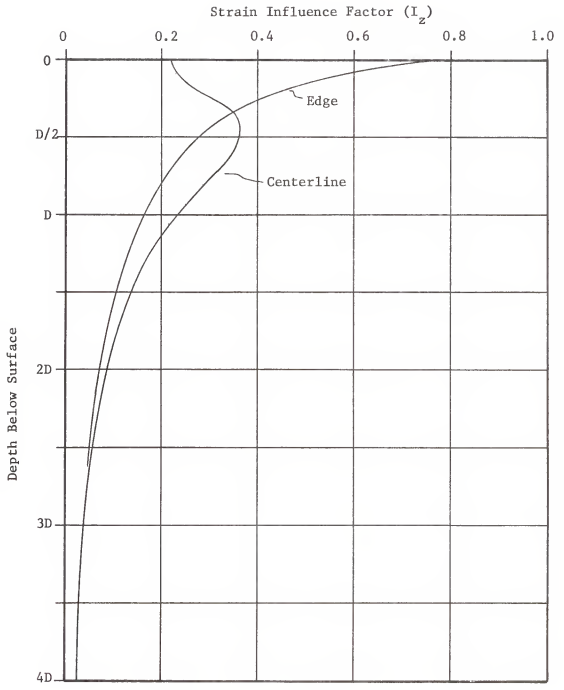


Figure 123. Comparison of Vertical Strain Influence Factor Beneath Center and Edge of Rigid Footing on Linear Elastic Material under Axisymmetric Loading: $\nu = 0.40$

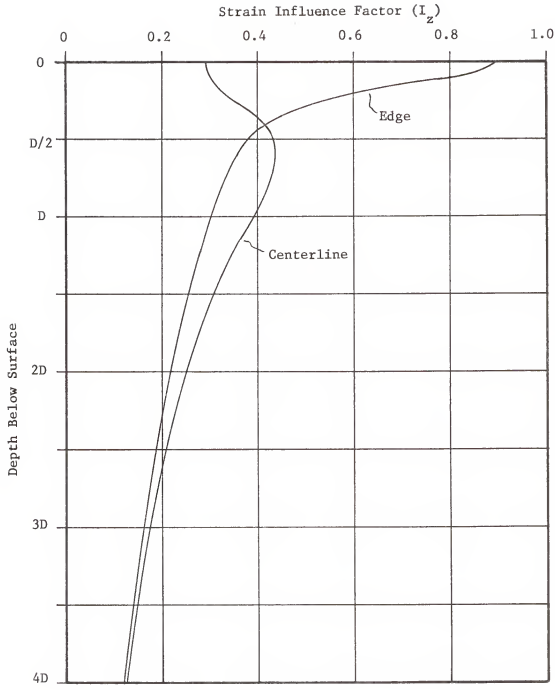


Figure 124. Comparison of Vertical Strain Influence Factor Beneath Center and Edge of Rigid Footing on Linear Elastic Material under Plane Strain Loading: $\nu = 0.40$

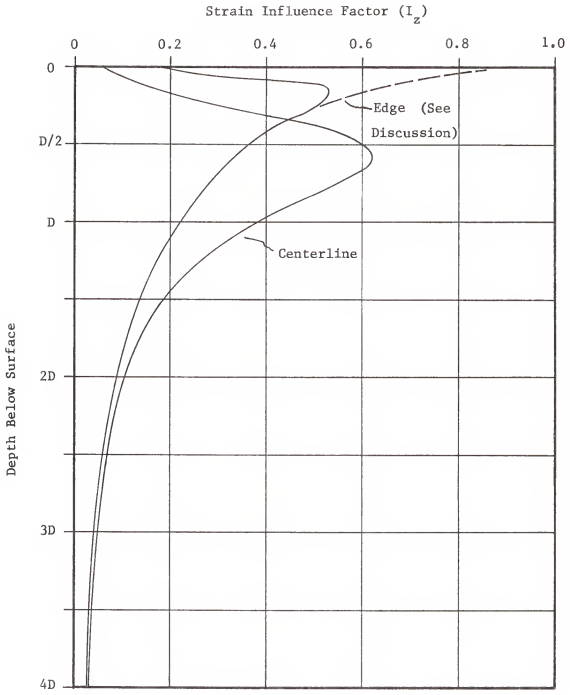


Figure 125. Comparison of Vertical Strain Influence Factor Beneath Center and Edge of Rigid Footing on Nonlinear Elastic Material under 4000 Psf Axisymmetric Loading: K = 60,000; ν = 0.40

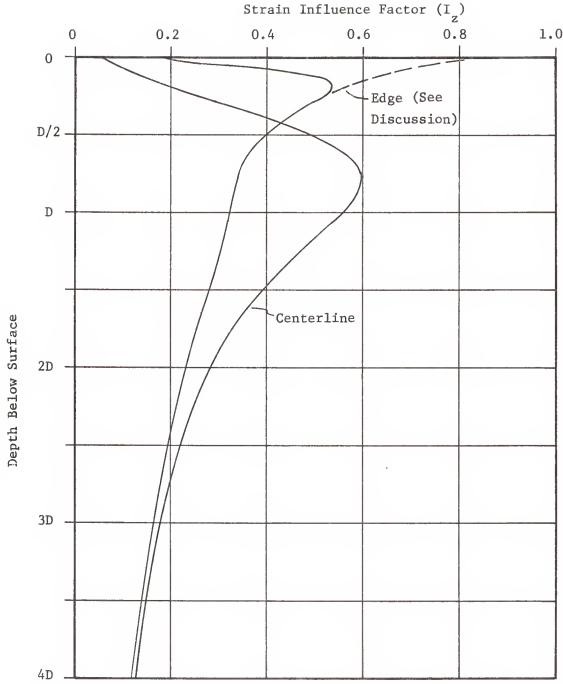


Figure 126. Comparison of Vertical Strain Influence Factor Beneath Center and Edge of Rigid Footing on Nonlinear Elastic Material under 4000 Psf Plane Strain Loading: $K = 60{,}000$; $\nu = 0.40$

finite element technique uses the equations of elasticity, there is some similarity with the linear elastic results. The discrepancies noted near the surface are primarily due to the fact, as noted previously, that some of the elements near the edge of the footing go into "failure." The bulk modulus failure approach used in these studies (shear modulus = 0 at failure) causes varying displacements and strains at such edge points with erratic numerical results.

These results are reasonable, but obviously a much more detailed analysis would be necessary to determine the many parameters which affect the strain and strain influence factor distribution variations, especially in the "failed" regions described.

4.7 Conclusions

The concept of a simplified triangular strain influence factor distribution, as originally suggested by Schmertmann (1970), can be used as an approximation to the strain distribution beneath foundations, even when using a nonlinear stress-dependent modulus, typical of sands. Although there are many variables involved in such an analysis, these studies indicate the following for such a simplified approach to settlement analysis:

(1) For axisymmetric loading of sands, use a strain influence factor triangle with a depth of influence of 2D and a peak strain influence factor located at a depth D/2. The peak strain influence factor and surface intercept values for loose, medium dense, and dense sands are as given in Figure 127.

(2) For plane strain loading of sands, use a strain influence

factor triangle with a depth of influence of 4D and a peak strain influence factor located at a depth 3D/4. The peak strain influence factor and surface intercept values for loose, medium dense, and dense sands are as given in Figure 127.

(3) For cases between the purely axisymmetric (L/D = 1) and the plane strain (L/D > 100) use a logarithmic interpolation for the depth of influence between 2D and 4D as well as for the peak strain values and locations. Thus for L/D = 10, use a depth of influence of 3D, thus giving a settlement in the middle between the L/D = 1 and the L/D = 100 cases. This is in agreement with the linear elastic results given in Table 4. For other L/D ratios the engineer should use a logarithmic scale for determining a reasonable depth of influence. This approach is further illustrated in more detail in Section 4.8.

(4) Ignore the effect of increased lateral stresses on the strain influence factor distribution. The field modulus values will be affected, but not the strain influence factor values or distribution.

(5) When using the simplified strain factor distribution approach with rigid layers, use the appropriate strain factor distribution triangle over the specific layer thickness. That is, use the dense sand I_z relations over the thickness of the dense sand and the loose or medium dense sand I_z relations over the thickness of the loose or medium dense sand. This approach, as originally

suggested by Schmertmann, is shown in Section 4.8.

(6) If the foundation is embedded, use the recommended strain factor distribution, only measured from the base of the foundation. Use the modulus values as indicated before the excavation. The load, p, should be that applied after the excavation, that is, the net load. For shallow embedment (between D/4 and D), reduce the constant C_i by 0.1 for both axisymmetric and plane strain loading.

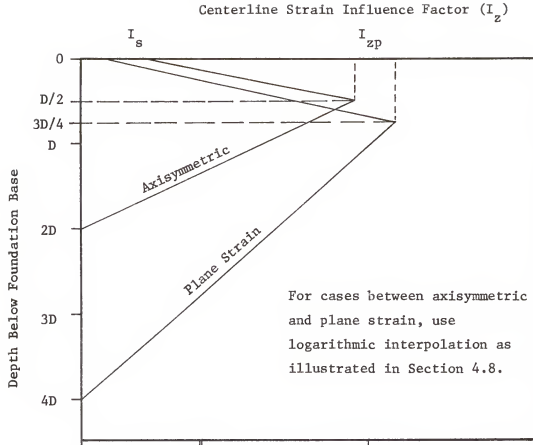
These recommendations give a ratio of plane strain settlement to axisymmetric settlement of 1.5 to 1.7 depending upon the loading pressure and relative density. These ratios are consistent with these analytical studies, but are low when compared to model tests.

When applied to relatively narrow footings (diameter or width less than 5 ft) these recommendations may predict too high a settlement, and the predictions will depend upon Poisson's ratio, as indicated by the relative density. This analytical model did not study in detail the local shear and punching type of settlement more typical of narrower footing geometries.

These conclusions are further illustrated in Figure 127. An example of a settlement prediction using these recommendations is given in the next section.

4.8 Example Settlement Problem

As an example of the procedure outlined in Section 4.7 using the strain influence factor approach for settlement calculations, consider the Test Case No. 1 used by Schmertmann (1970). In this example a 2.60 by 23.0 meter pier is placed at a depth of 2.0 meters



	AXISYMMETRIC		PLANE STRAIN	
I_{zp} Equation	$C_i + 0.1\sqrt{p/\sigma_{D/2}}$		$C_i + 0.1\sqrt{p/\sigma_{3D/4}}$	
Constants	I_s	C_i	I_s	C_i
Loose Sand	0.2	0.6	0.2	0.7
Medium Dense Sand	0.1	0.5	0.1	0.5
Dense Sand	0.0	0.4	0.0	0.3

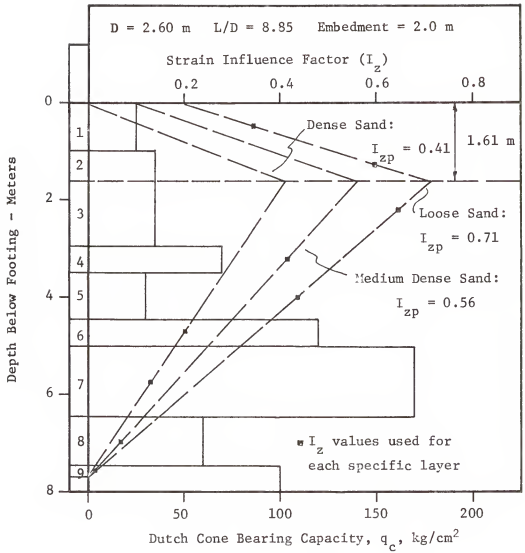
Figure 127. Recommended Triangular Strain Influence Factor Distribution for Sands (See Discussion for Use with Layering or Embedment cases)

beneath the surface on a layered sand whose Dutch cone bearing capacity values as a function of depth are as given in Figure 128. Schmertmann's settlement calculation results gave 1.60 inches over 5 years compared with actual measurements of from 1.02 to 1.53 inches. Using the method outlined in Section 4.7 and illustrated in Figures 128 and 129 and tabulated in Table 8 gives a larger settlement, 2.10 inches compared with 1.60 inches. Of course, this study does not include an expression for creep with time, which would then give an even larger settlement estimate.

This revised approach should give larger values when compared with Schmertmann's, primarily because the strain influence factor triangle is larger (has a depth of 3D for L/D = 10). Schmertmann's use of the Dutch cone bearing capacity assumes that $E_c = 2\ q_c$, based on comparison with screw plate load tests. Schmertmann does give a range of correlation for this recommended relation and it might be that it should be modified for plane strain cases. For example, if in the test case given in Figure 128 and Table 8 the relation $E_c = 2.5\ q_c$ is used, the settlement will be 1.68 inches, and if $E_c = 3\ q_c$, then the settlement estimate is 1.40 inches.

Small variations within the strain factor approach itself do not cause dramatic changes, but since the settlement is inversely proportional to the modulus value, its determination is more critical. For that matter, it may be that the functional relation between the cone bearing and the elastic modulus will itself vary depending on the sand density, as well as the type of loading.

This example does further support the strain factor approach as



NOTE: Specific calculations are given in Figure 129.

Figure 128. Example Settlement Problem

For depth of influence - logarithmic interpolation for L/D = 8.85

Depth of Influence = (2 + Log(L/D)) D = (2 + Log 8.85)(2.60)

= (2.947)(2.60) = 7.66 meters

For I_{zp} - reduce C_i by 0.1 for embedment - net load = 1.50 kg/cm^2

Axisymmetric - peak at D/2 depth

Loose: $I_{zp} = 0.5 + 0.1\sqrt{1.50/0.528} = 0.67$

Med. Dense: $I_{zp} = 0.4 + 0.1\sqrt{1.50/0.528} = 0.57$

Dense: $I_{zp} = 0.3 + 0.1\sqrt{1.50/0.528} = 0.47$

Plane Strain - peak at 3D/4 depth

Loose: $I_{zp} = 0.6 + 0.1\sqrt{1.50/0.632} = 0.75$

Med. Dense: $I_{zp} = 0.4 + 0.1\sqrt{1.50/0.632} = 0.55$

Dense: $I_{zp} = 0.2 + 0.1\sqrt{1.50/0.632} = 0.35$

Interpolating above peak values, use:

Loose Sand: $I_{zp} = 0.71$

Med. Dense Sand: $I_{zp} = 0.56$

Dense Sand: $I_{zp} = 0.41$

For depth to peak - logarithmic interpolation

Depth to peak = D/2 + (D/8)Log(L/D)

= 0.5 D + (0.947)(0.125) D

= 1.61 meters

Figure 129. Background Calculations for Figure 128

Table 8. Settlement Example Problem Calculations

$p = 1.82\ kg/cm^2$ $p_o = 0.32\ kg/cm^2$ $\Delta p = 1.50\ kg/cm^2$ $\rho = \Delta p \frac{I_z \Delta z}{E_c}$

Layer	z (cm)	q_c (kg/cm^2)	E_c (kg/cm^2)	I_z	$\frac{I_z}{E_c} \Delta z$ $\{\frac{cm}{kg/cm^2}\}$
1	100	25	50	0.35	0.70
2	61	35	70	0.60	0.52
3	139	35	70	0.65	1.29
4	50	70	140	0.42	0.15
5	100	30	60	0.44	0.73
6	50	120	240	0.20	0.04
7	150	170	340	0.13	0.06
8	100	60	120	0.07	0.06
9	16	100	200	0.02	0.00
					SUM = 3.55

$\rho = (1.50)(3.55) = 5.33\ cm = 2.10\ inches$

a reasonable method. The parametric studies in this dissertation now provide further understanding of several variables including sand density, plane strain vs. axisymmetric loading, and the effects of layering.

CHAPTER 5.0

PRESSUREMETER TEST FINITE ELEMENT STUDY

5.1 General Discussion

A major purpose of this study was to determine possible field pressuremeter test parameters which might be of value in estimating the settlement of sands. The writer has selected the strain influence factor settlement approach as suggested by Schmertmann (1970). This approach, which has been explained in Section 2.2.1, requires three major steps: (1) the selection of an appropriate simplified strain influence factor distribution, (2) the selection of appropriate elastic moduli as a function of depth, and (3) the numerical integration of estimated settlements for various vertical increments beneath the foundation.

Chapter 4.0 investigated the many factors involved in the strain influence factor distribution in sands and made recommendations with respect to certain simplified triangular distributions. Schmertmann (1970) had originally obtained the variation of the elastic modulus with depth by means of the cone penetrometer, and correlations made with screw-plate load tests. Since the pressuremeter is another in-situ testing device which can give elastic modulus information, its results might also be used with the strain influence factor distribution.

Analytically, the approach previously described is reasonable, and this chapter investigates the pressuremeter loading phenomenon in sands, with primary emphasis on the elastic modulus information which might be obtained from pressure-volume curves.

Using the nonlinear analytical sand model described previously, the writer, using the finite element method for parametric studies, investigated the various parameters involved in pressuremeter tests. These included the effects of the differential pressure, borehole unloading and disturbance, the effect of a disturbed "smear" zone, increased lateral stresses, and increased depth, as well as the effects of linear cross-anisotropy.

Because the finite element analysis method is very sensitive to displacements, great care was necessary in choosing a grid which would give reliable displacements, and thus reliable volume measurements. After much trial and error, a very complex grid with 817 nodal points and 756 elements was selected. One-fourth of this doubly symmetrical grid is illustrated in Figure 130. The grid shown is for the 0.1 ft diameter pressuremeter with a 12 inch central measuring cell and two 12 inch guard cells. The critical displacement analysis regions of the grid were at the loading boundaries, and it was especially important that the displacements be as accurate as possible over the measuring cell region. This is the primary reason for the general form of the grid selected.

Fortunately, because of the availability of the Tranter solution, as discussed in Section 2.1.2, it was possible to compare the results of the finite element analysis for a linear elastic material with the classical displacement solution. Figures 131 and 132 show the results

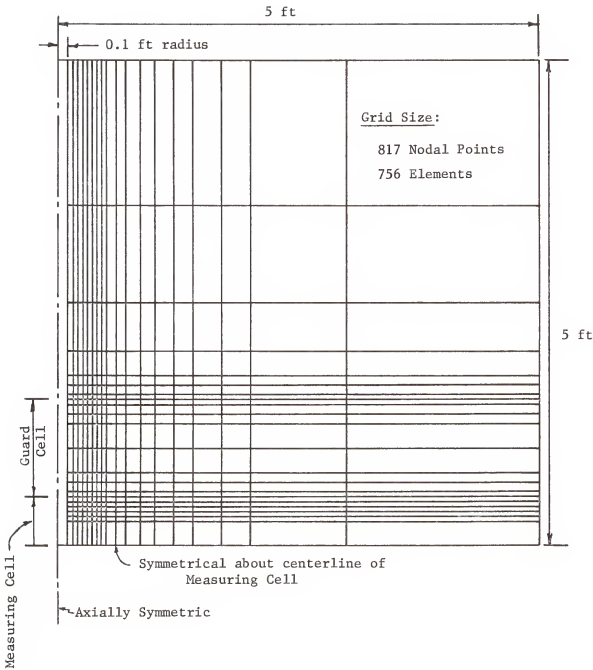


Figure 130. Typical Finite Element Grid for Pressuremeter Parametric Study

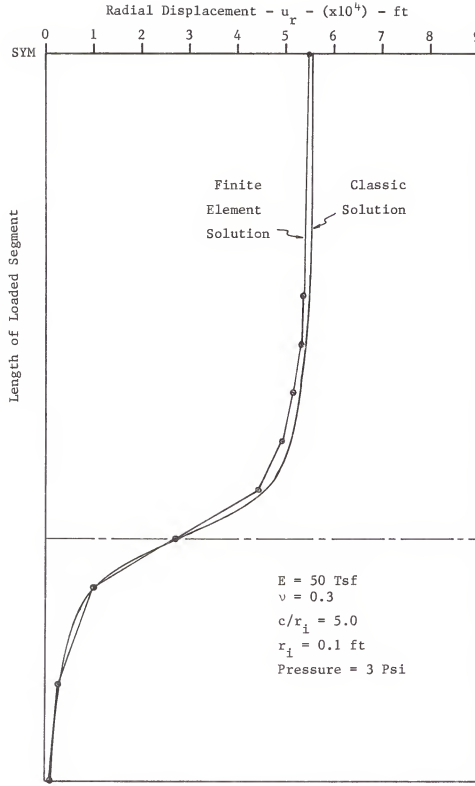


Figure 131. Comparison of Finite Element and Classic Pressuremeter Displacements; E = 50 Tsf, ν = 0.3

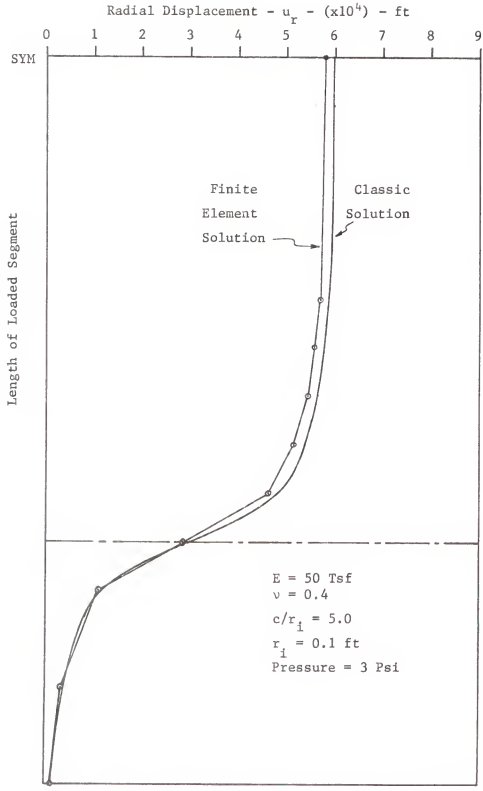


Figure 132. Comparison of Finite Element and Classic Pressuremeter Displacements; E = 50 Tsf, ν = 0.4

using this grid compared to the Tranter solution for a material with an elastic modulus of 50 Tsf and Poisson's ratios of 0.3 and 0.4. The comparison is quite favorable, although the reader will note that the finite element solution will give a volume measurement slightly less than that using the classical solution.

For higher Poisson's ratios the displacements were not as comparable. Further grid trials were not as successful for these higher Poisson's ratios either. This is an example of a case that is not as precise for high Poisson's ratios, no matter how fine the grid (Zienkiewicz, 1971). This displacement discrepancy at higher Poisson's ratios is further illustrated in Figure 133. This figure compares the displacement of the centerline nodal point for the infinite cylinder, Tranter's solution, and the finite element grid. Since reasonable values for Poisson's ratio of 0.3, 0.4, and 0.45 are commonly used for sands, this does not present a problem for this parametric study. However, if the studies and program were to be extended for a pressuremeter analysis of clays, with an assumed Poisson ratio of 0.5, then an entirely different approach to the equilibrium and stress-strain relationships would be necessary.

In the analytical study, the lengths of the measuring cell and guard cells were stipulated by noting the first and last nodal points to be used for either the measuring cell or the total pressuremeter. The differential pressure was first applied over the desired number of pressure increments over the length of the measuring cell. Then the entire pressuremeter was loaded to a specified pressure by the desired number of steps. This procedure had the effect of making the load on the central measuring cell continuously greater than that on the guard

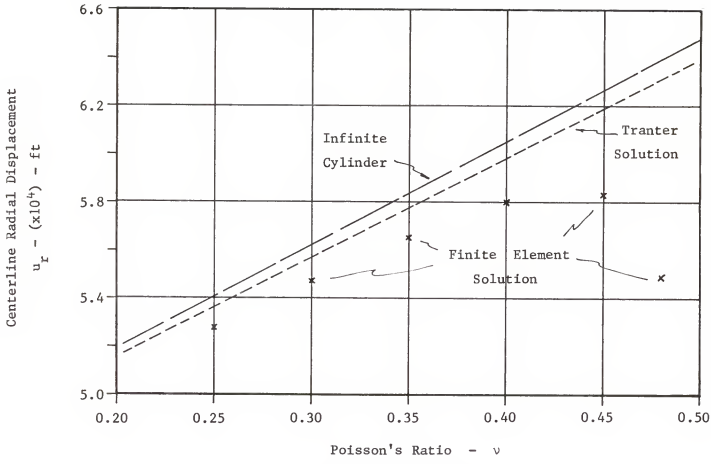


Figure 133. Comparison of Pressuremeter Centerline Displacements for Infinite Cylinder, Finite Element, and Classic Tranter Solutions: $c/r_i = 5$

cells by an amount equal to the differential pressure.

After each pressure step the total displacement of all the nodal points in the grid was known. The weighted average displacement of the nodal points adjacent to the measuring cell was then used to calculate the average volume of the measuring cell. The volumetric strain was also calculated using

$$\varepsilon_v = \frac{\Delta V}{V_o + \Delta V} \tag{87}$$

where ε_v is the volumetric strain and V_o and ΔV the initial volume and volume change of the measuring cell.

The many parameters which could be varied for the nonlinear analytical sand model have been discussed previously. There were several additional features incorporated into the pressuremeter finite element program which could also be varied. The borehole could be unloaded by using a geostatic pressure distribution duplicating the in-situ lateral stresses. This unloading was done by replacing the triangular geostatic distribution by uniform unloading over each grid section as illustrated in Figure 134. Various unloading moduli could be used also.

As described previously, Ménard (1965) recommends the use of an unloading modulus as obtained from field pressuremeter testing in order to assist in calculating settlements. An unloading sequence was built into the pressuremeter program which allowed for a single unloading step with a specified pressure and then reloading using the same pressure increment. This unloading could be done at any point in the incremental pressure loading sequence of the entire pressuremeter.

The Users'Manual for this program gives more of the details and is given in Appendix III along with the program listing.

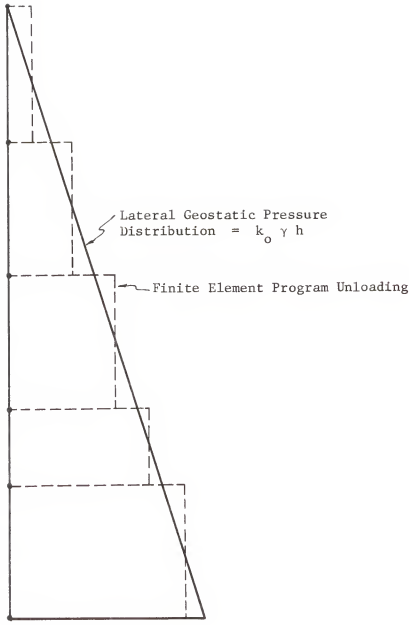


Figure 134. Example of Finite Element Program Unloading of Borehole

5.2 Parametric Study Using Linear Elastic Material

5.2.1 Introduction

An initial study was conducted using a linear elastic material to obtain a better understanding of the effects of varying various geometrical and material parameters. The finite element grid and the reliability of the displacements for such an analysis have been discussed previously. Using this study, several factors were investigated, including the effects of:

(1) Poisson's Ratio

(2) Differential Pressure

(3) Borehole Unloading

(4) Increased Lateral Stresses and Depth

(5) Linear Cross-Anisotropy

(6) a "Disturbed" Zone

(7) Unloading and Reloading the Pressuremeter

By using a linear elastic material it was possible to gain a better understanding of these effects without masking the analytical conclusions due to the variety of parameters involved in the nonlinear analysis. This also helped in the interpretation and understanding of the nonlinear analytical results.

5.2.2 Effect of Poisson's Ratio

Using a 100 pcf model sand at a pressuremeter centerline depth of 7 ft and a lateral stress coefficient (k_o) of 0.5, several computer runs investigated the pressure-volume response of a linear material with a constant elastic modulus of 50 tsf and varying Poisson's ratios.

A single step differential pressure of 3 psi was used on the

12-12-12 pressuremeter. Then the entire pressuremeter was loaded an additional 12 psi in 2 steps. The resulting pressure-volume curves are shown in Figure 135. The elastic moduli as calculated using the slope of these curves (E_{PMT}) are given in Table 9.

The results of the linear study are as expected. Below the differential pressure of 3 psi, when only the central 12 inch cell is being loaded, the modulus as calculated from the slope of the line is high over the assumed E = 50 tsf by about 10 to 15 percent, due to the edge effects previously discussed. Above the differential pressure, when the loading is applied over the entire pressuremeter length of 36 inches, the slope increases and the modulus calculation is within 2 to 5 percent with greater accuracy for the lower values of Poisson's ratio. There is theoretically no effect due to Poisson's ratio, the variations in Table 9 being due to the slight discrepancies in the finite element model displacements, especially as Poisson's ratio approaches a value of 0.5.

This linear study shows that the pressure-volume response is a reasonable method for calculating an elastic modulus for all values of Poisson's ratio, assuming that the loading length is sufficient to eliminate the edge effects. It also shows that there can be a slight break in the pressure-volume curve at the value of the differential pressure and a subsequent increase in the slope. This break would be sharper for short measuring cells, and will become indistinct as the length of the measuring cell increases.

5.2.3 Effect of Differential Pressure

It was noted previously that the modulus calculation based on the slope of the pressure-volume curve was most accurate after the

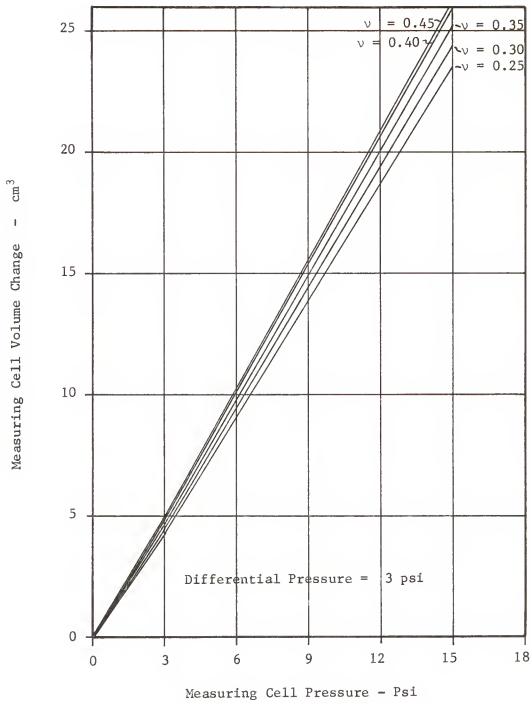


Figure 135. Pressuremeter Loading of Linear Elastic Material with E = 50 Tsf and Varying Poisson's Ratios

Table 9. Modulus Calculations Using Slope of Pressure-Volume Curves in Figure 135 and Equation 1: E = 50 Tsf

Poisson's Ratio (ν)	E_{PMT} (Tsf)	
	Below Differential Pressure	Above Differential Pressure
0.25	54.8	50.1
0.30	55.1	50.3
0.35	55.5	50.5
0.40	56.2	50.9
0.45	58.0	52.4

differential pressure was reached. This should be true no matter what the magnitude of the differential pressure. Figure 136 shows the pressure-volume response for the linear elastic material and a Poisson ratio of 0.3 for three different differential pressures, 0, 3, and 6 psi. The slopes are the same above the differential pressure and the modulus calculations would be identical to those given in Table 9 for the case of $\nu = 0.3$.

In most pressuremeter calculations the slope is taken over a portion of the pressure-volume curve well above the differential pressure. Although the slope should remain the same, no matter what the value of the differential pressure, the magnitude of the differential pressure does affect the location of the pressure-volume curve. This curve is shifted to lower volume changes for a given pressure as the magnitude of the differential pressure increases. This shift is very small, and almost negligible in this linear analysis.

5.2.4 Effect of Borehole Unloading

If the borehole is unloaded using the triangular approximation discussed in Section 5.1, the effect is to decrease the volume of the borehole. The subsequent reloading restores the initial volume and then increases the volume in the region being loaded.

Unloading of the 100 pcf ($k_o = 0.5$) linear elastic material at pressuremeter centerline depths of 7 and 20 ft is illustrated in Figure 137. The recovery of the volume change to 0 cc after the borehole unloading occurs above the value of the centerline in-situ lateral stresses of 2.43 and 6.94 psi. This is reasonable since the entire borehole was unloaded, but then pressuremeter loads were only imposed over a small segment of the borehole.

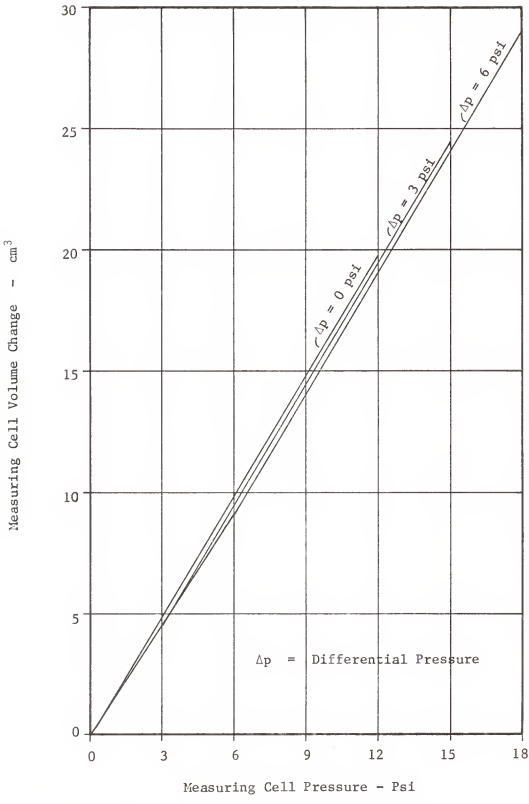


Figure 136. Pressuremeter Loading of Linear Elastic Material with E = 50 Tsf, ν = 0.3, and Varying Differential Pressures

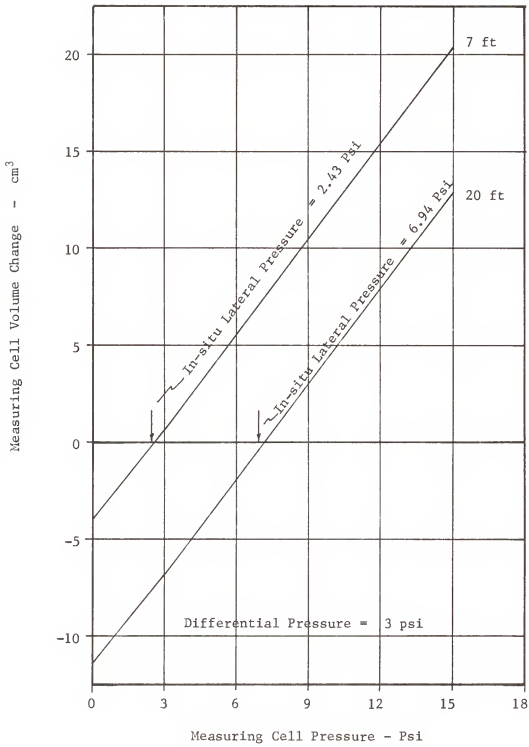


Figure 137. Pressuremeter Loading of Unloaded Linear Elastic Material with E = 50 Tsf, ν = 0.3, k_o = 0.5, and Varying Depths

The slopes used to calculate the linear elastic modulus are the same as those in previous sections and the modulus calculations are thus the same. For the linear analysis, therefore, there is no effect due to borehole unloading on the calculation of the elastic modulus.

5.2.5 Effect of Increased Lateral Stresses and Depth

Several runs were made to investigate the effects of both increased lateral stresses and depth. Since the result of an increased lateral stress coefficient (k_o) is to increase the lateral confinement, which is similar to placing the pressuremeter at a greater depth, these results on linear elastic materials should be similar.

Figure 138 gives the results of studies at the 7 ft depth, only with an increase in the lateral stress coefficient to 1.0. For comparison, the result of the $k_o = 0.5$ study (from Section 5.2.2) is also plotted. This study indicates clearly that the effect of increasing the lateral stress is to shift the pressure-volume curve parallel to the previous lower lateral stress curve, and also to cause a greater unloading value and increase the necessary pressure for returning to the initial zero volume change condition. The modulus calculation based on the slope is the same, however, as would be expected.

Figure 138 also gives the results of studies at the 20 ft depth compared to those at the 7 ft depth. The effect is as expected, namely a shift parallel to the pressure-volume results at the shallower depth with a new zero volume change pressure during the reloading phase. Again the modulus calculations based on the slope remain unchanged.

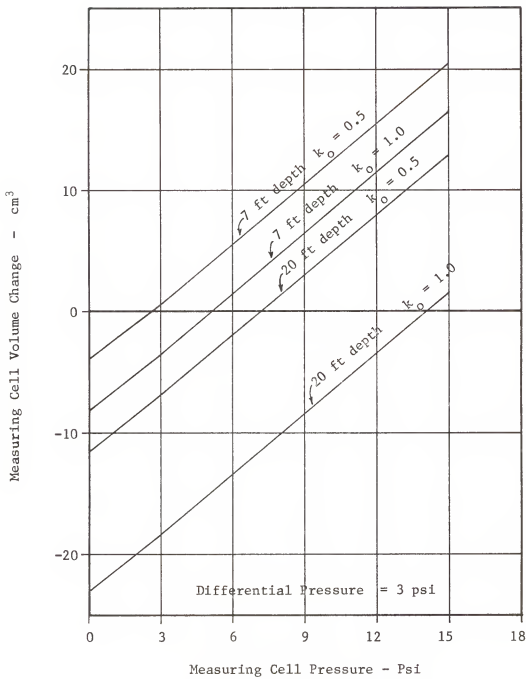


Figure 138. Pressuremeter Loading of Unloaded Linear Elastic Material with E = 50 Tsf, ν = 0.3, and Varying Depths for Lateral Stress Coefficients (k_o) of 0.5 and 1.0

5.2.6 Effect of Linear Cross-Anisotropy

It is well known that not only are soils not linearly elastic, they are also often not isotropic. In order to get an understanding for the possible consequences of anisotropy, the linear elastic model was also used to investigate the effects of linear anisotropy for a cross-anisotropic material.

Figure 139 gives the results of two computer runs. In one case the vertical elastic modulus (E_v) was 50 tsf and the horizontal elastic modulus (E_h) was 25 tsf. The values were reversed for the second case. In both cases Poisson's ratio was 0.3. Using the pressure-volume slope results as shown in Figure 139, the resulting values of E_{PMT} were within a few percent of the value of the horizontal modulus. This confirms the one-dimensional analysis of Livneh (1971) and is reasonable. Therefore, in cross-anisotropic materials the pressuremeter should measure the value of the horizontal modulus.

5.2.7 Effect of a "Disturbed" Zone

A very practical question in using the pressuremeter in the field is the effect of a "disturbed" or smear zone around the inside of the borehole. It is of interest to know what will be the effect on the pressure-volume curve of the pressuremeter.

To obtain an understanding of this with the linear elastic materials, the finite element model was set up using various widths of a lower elastic modulus material as a smear zone at the edge of the borehole. The pressuremeter radius was 0.1 ft and the widths of the smear zone were varied from 0 to 0.2 ft. The smear zone modulus was 25 tsf, while the material around the zone had a modulus of 50 tsf. The resulting pressure-volume curves are shown in Figure 140. A Poisson ratio of 0.3 was used for both materials.

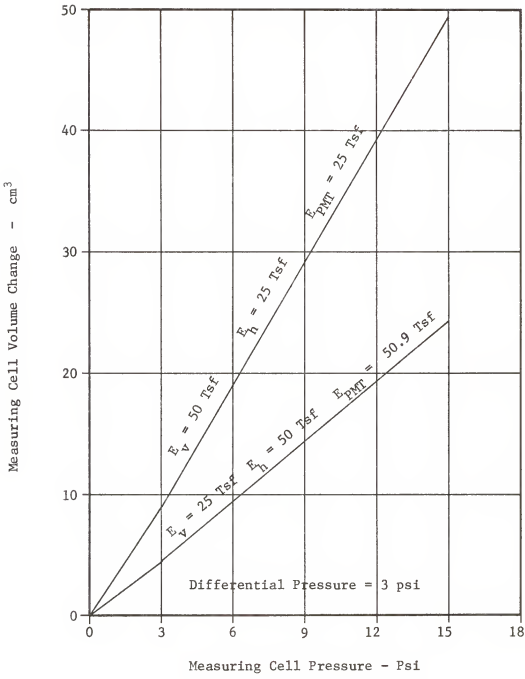


Figure 139. Pressuremeter Loading of Cross-Anisotropic Linear Elastic Materials with $\nu = 0.3$

It is noted that there is a distinct spread in the pressure-volume results as a function of the width of the smear zone. The slope increases as the smear zone width increases, and thus the modulus calculation will decrease as the width of the smear zone increases. For no smear the modulus should be 50 tsf, while as the smear zone width increases, the modulus calculation should approach the value of 25 tsf.

Using the modulus calculations from the slopes of Figure 140, the effect of the smear zone width is shown in Figure 141. This figure shows clearly that there is a very important effect due to a smeared zone. For the case considered, when the smear zone width is one-fourth of the borehole radius, the modulus as calculated from the pressure-volume curve is approximately 39 tsf which is 20 percent less than the modulus of the material surrounding the smear zone.

When the smear zone width is equal to the borehole radius, the modulus as calculated from the pressure-volume curve is 30 tsf, which is almost the value of the smear zone modulus, and much less than the modulus of the material around the smear zone. This figure also shows that if the smear zone width is approximately two times the radius of the borehole, then the pressuremeter is essentially measuring the response of the smear zone, and not the parent material.

This study shows that it is very important to minimize borehole disturbance as much as possible. Of course, it can also be argued that there is an unknown variation in modulus calculations as determined by laboratory tests on field samples which have been strained by sampling and then unloaded, and thus are "disturbed" in their transfer from the field to the laboratory. Since it is

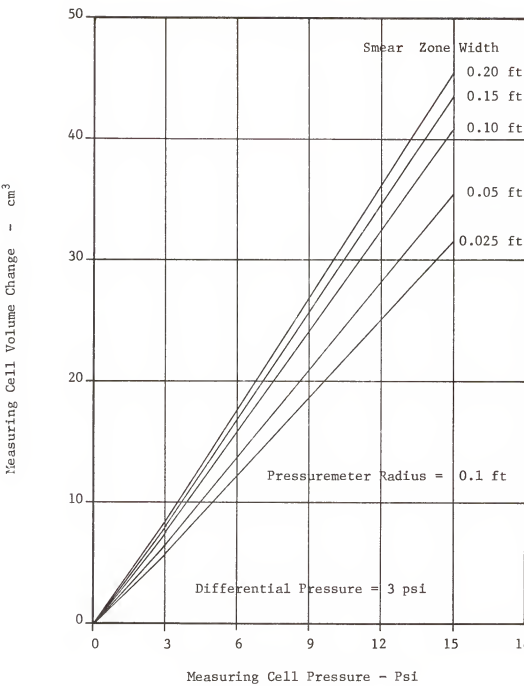


Figure 140. Pressuremeter Loading of Linear Elastic Material with E = 50 Tsf, ν = 0.3, and Varying Widths of a Smear Zone with E = 25 Tsf

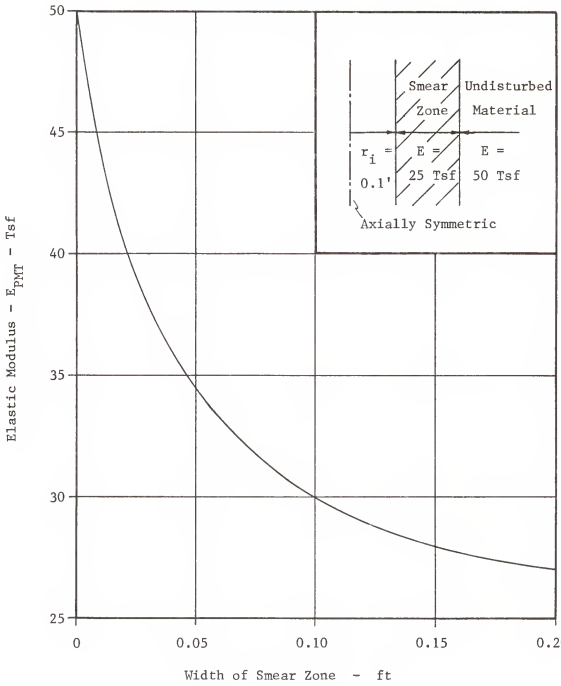


Figure 141. Modulus Calculations as a Function of Width of Smear Zone in Linear Elastic Material with $\nu = 0.3$

impossible to completely eliminate disturbance, it is important to understand its possible effects and minimize disturbance as much as possible.

It can also be noted from Figure 140 that there is no apparent way to study the linear pressure-volume curve and determine if the material is disturbed, or the possible degree of disturbance. The pressure-volume response is typical of a linear elastic material, even when not disturbed, and has the characteristic break at the differential pressure.

5.2.8 Effect of Unloading and Reloading the Pressuremeter

Since the determination of various moduli as used in pressuremeter calculations is based on occasional unloading and then reloading of the pressuremeter, this feature was built into the finite element program.

For a linear elastic material the result of unloading and then reloading the pressuremeter should have no effect on the slope of the pressure-volume curve. This is illustrated in Figure 142 which shows clearly that the unload-reload feature of the finite element program gives the proper results when applied to a linear elastic material. Therefore, this feature of the program may be expected to provide a reasonable analysis capability when applied to the analysis of a nonlinear material.

5.2.9 Conclusions Based on Linear Elastic Analysis

This study of the pressuremeter loading of a linear elastic material has provided many valuable conclusions:

(1) As long as the loading length is sufficiently long so as to reduce edge effects (see Section 2.1.2), the slope of the

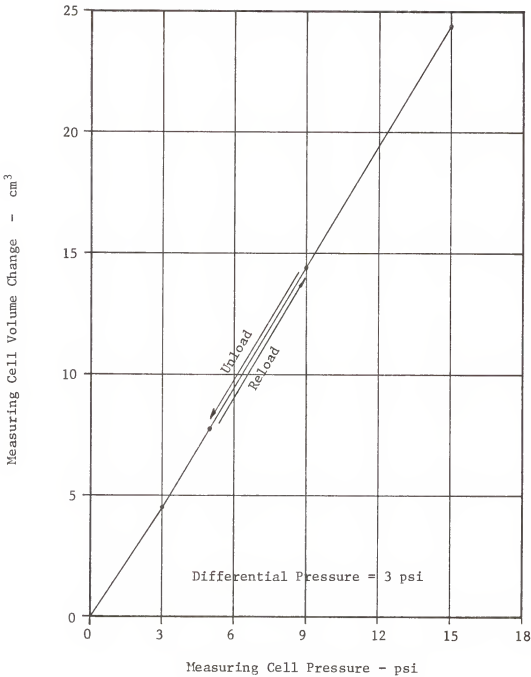


Figure 142. Effect of Unloading and Reloading Pressuremeter in Linear Elastic Material with E = 50 Tsf, ν = 0.3

pressure-volume curve is an excellent way to obtain the elastic modulus of a linear elastic material and is independent of (i) Poisson's ratio, (ii) the magnitude of the differential pressure, (iii) the lateral stresses or the depth, (iv) the unloading of the borehole, and (v) the unloading or reloading of the pressuremeter.

(2) The pressuremeter test measures the horizontal elastic modulus (E_h) when used in a linear cross-anisotropic material.

(3) A smear zone around the pressuremeter will affect the slope and therefore the modulus results. Assuming the modulus of the smear zone is less than that of the surrounding material, the increased width of the smear zone causes a decrease in the modulus calculations with the modulus of the smear zone as a lower limit. The pressure-volume curve considering the smear zone remains linear. There is apparently no way to determine disturbance by inspection of the linear pressure-volume curve itself. Any break point on this linear curve is a function of the differential pressure, and not the degree of disturbance or width of smear zone. The effect of smear zone width on modulus calculation is illustrated in Figure 141.

Based on the reasonable results of this linear elastic analysis, it is now possible to apply this same analytical technique and finite element program to the nonlinear model sand material as described in Chapter 3.0.

5.3 Parametric Study Using Nonlinear Sand Model

5.3.1 Introduction

The nonlinear analysis used the same model geometry and unloading, loading, and reloading geometries as described previously and included in more detail in the Users' Manual in Appendix III.

The study using the nonlinear material was considerably more complex and involved than the linear analysis. In addition, because of the incremental nature of the nonlinear analysis, coupled with the need for the large grid as previously described, the nonlinear analysis was much more costly. As an added problem, because the nonlinear analysis had so many complex and variable parameters, it was often difficult to isolate any one parameter as being of prime significance.

The general features of a field pressure-volume curve have been discussed in Section 2.1.1 and illustrated in Figure 2. Field results are definitely not linear, although occasionally the elastic region is approximately linear, at least over a small pressure range. Thus, the linear analyses previously discussed, although informative and useful, do not correctly model any field test.

It should be noted from Figure 2 that most field tests have an initial high slope (low modulus) pressure-volume response, followed by a relatively linear elastic response. This is typically followed by a nonlinear increasing slope (decreasing modulus) region referred to as the plastic region. This initial portion has been identified as being due to reloading to initial stresses by Gibson and Anderson (1961). According to Ménard (1965) and as noted in Figure 14, the initial portion is a high modulus linear region. This is not typical of many field data, however.

The first studies using the nonlinear material used the dense and very dense sands at a depth of 7 ft, with a lateral coefficient (k_o) of 0.5 and direct pressuremeter loading, without unloading the borehole. This relatively straightforward nonlinear model was used to investigate the effects due to the value of the pressure increment used, the effect of using minor principal and octahedral stresses, and the effects of using the bulk and failure modulus criteria.

Figure 143 shows the pressure-volume response of the 12-12-12 pressuremeter at a depth of 7 ft using minor principal stresses, K = 60,000, k_o = 0.5, and a Poisson ratio of 0.4. The effect of using 1, 2, or 3 psi pressure increments is noted by studying curves B, C, and D. Obviously curve B, which uses 1 psi increments, is much better defined and easier to interpret than curves C and D which require considerable judgement in plotting. Curve D, which uses 3 psi increments, is the most difficult to interpret.

It is noted that the pressure and volume ranges in Figure 143 and following figures are relatively small when compared to many available field data. These nonlinear studies are analytically consistent, however, as will be seen in the next few sections. More realistic pressure-volume variations occur when considering the effects of borehole unloading as will be discussed in Section 5.3.6.

Of additional interest is the pressure increment where "failure" in one or more of the elements first occurs. Each pressure step is noted where failure occurs on the next loading increment in one or more elements. Curves A and B, which are identical except for the failure criterion used, show that after the 10 psi load is reached, the next step includes the effect of loading against some failed

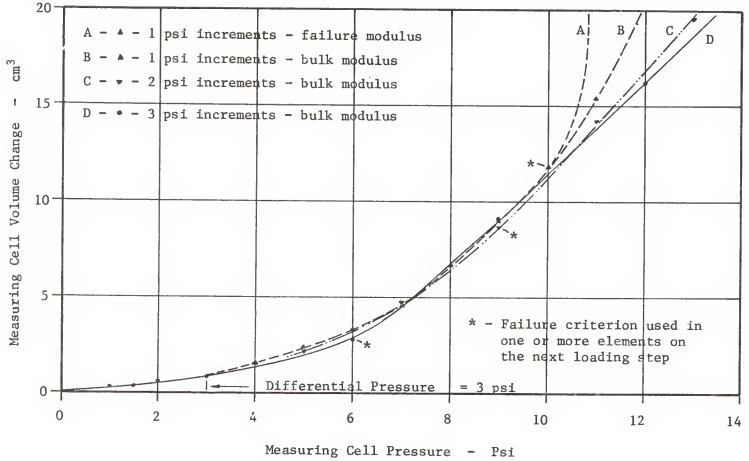


Figure 143. Comparison of Effect of Pressure Increment and Failure Modulus in Pressuremeter Loading of Nonlinear Material Using Minor Principal Stresses: K = 60,000, ν = 0.4, k_o = 0.50, Depth = 7 ft

elements. When the bulk modulus failure criterion is used (Curve B), the general shape of the curve is not greatly affected and continues in a reasonable manner. However, when the low failure modulus approach is used (Curve A), the volume change literally blows up and provides no more useful interpretation.

The nature of "failure" when noted in this analytical model was not particularly dramatic. It was noted that generally failure would occur in one or more of the elements immediately adjacent to the pressuremeter, and often in the elements adjacent to the top of the measuring cell and bottom of the top guard cell (see Figure 130). As more elements failed in successive steps, these elements (0.05 ft wide) were also adjacent to the measuring and guard cells and there was sort of a failure smear in the elements along the pressuremeter edge. The nonlinear pressure-volume response was quite reasonable, including this small failure region. As more and more pressure steps were used to higher pressures, the failure zone spread laterally into the nonlinear continuum, but in very small increments.

It appears, therefore, that typically the curved shape of the pressure-volume curve in field tests is a better indication of the general nonlinear stress-strain response of the soil than a clear indication of the elastic and plastic regions. This will be shown in later sections to be especially true for higher Poisson's ratios. This conclusion may not be true for clays, but for this sand analysis it was very evident.

It is concluded from this work that the 1 psi increment is to be preferred in the analytical studies. Also, the bulk modulus failure condition provides a more reasonable pressure-volume response when the

stress conditions within the mass approach failure in one or more of the elements. It should be noted, however, that in using the 1 psi increment a large amount of computer time and money is necessary, even for one run. When possible, the 1 psi increment was used in these studies.

Figure 144 shows the results of using the minor principal stress compared to the octahedral stress. Since the octahedral stress is higher than the minor principal stress, the corresponding modulus value should be higher for each step in the loading process. This is shown in Figure 144, since the pressure-volume curve for the octahedral case would give consistently higher modulus values using the slope calculation approach. Since the original analytical model as proposed by Duncan and Chang (1970) was based on the minor principal stress approach, this was retained for the majority of the nonlinear studies.

It has already been noted that pressuremeter loading of soil is quite complex. Initially, under gravity stress conditions, the soil is loaded under vertical major principal stresses (γh) and horizontal minor principal stresses ($k_o \gamma h$). As the soil is loaded by the pressuremeter, the material adjacent to the loading cell undergoes an increase in the horizontal stress. As loading progresses the lateral stress will soon reach the value of the vertical stress. Additional loading will further increase the lateral stress such that it becomes the major principal stress. The tangential stress (σ_θ) which originally was equal to the minor principal stress (and the radial stress), becomes the minor principal stress, while the vertical stress (σ_z) becomes the intermediate principal stress.

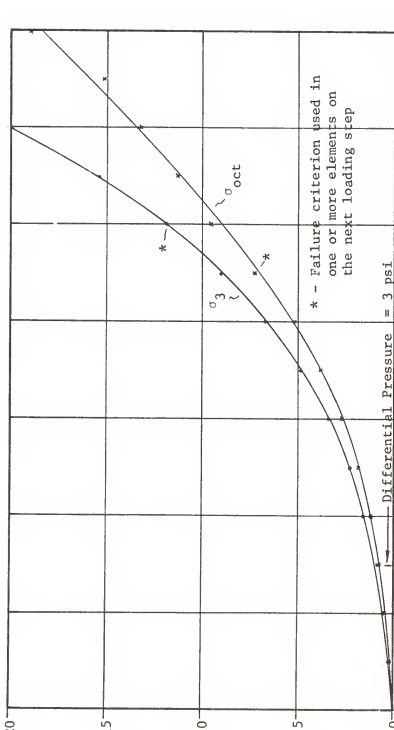


Figure 144. Comparison of Effect of Using Minor Principal and Octahedral Stresses in Pressuremeter Loading of Nonlinear Material: K = 60,000, ν = 0.4, k_o = 0.50

This loading sequence is shown in Figure 145 for elements adjacent to the centerline of a pressuremeter. The initial in-situ conditions are shown by the single Mohr circle. The stress conditions at 11 psi pressuremeter loading are shown by the usual three-dimensional representation, using three circles. On the next incremental pressure step this centerline element will go into the failure condition, since at 11 psi it is tangent to the Mohr-Coulomb failure line.

Another stress condition which might be considered is that of the maximum shear stress (τ_{max}). In terms of the major and minor principal stresses, τ_{max} is written

$$\tau_{max} = \frac{\sigma_1 - \sigma_3}{2} \tag{88}$$

Initially under in-situ conditions the constant maximum shear stress contours will be horizontal lines. As the loading is applied these contours will build up in a fashion shown in Figures 146 through 148, which are typical of the buildup of the maximum shear contours using the nonlinear stress-dependent modulus material.

The maximum shear stress contours initially concentrate around the measuring cell while the differential pressure is applied. Then as the guard cells are also loaded, the contours spread laterally, but the maximum values remain adjacent to the measuring cell. Any hardware anomalies that would affect the perfectly flexible loading used for this analysis would, of course, affect the distribution of these contours. They show, however, that the loading and stress distribution is reasonable for the nonlinear stress-dependent modulus material, including the effects of gravity stresses.

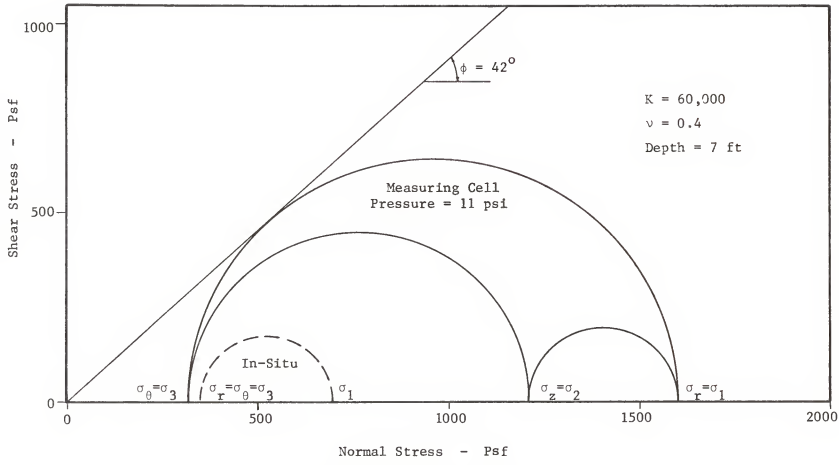


Figure 145. Mohr's Circle Representations of Stresses in Soil at Centerline of Pressuremeter Initially and After Loading: K = 60,000; ν = 0.4

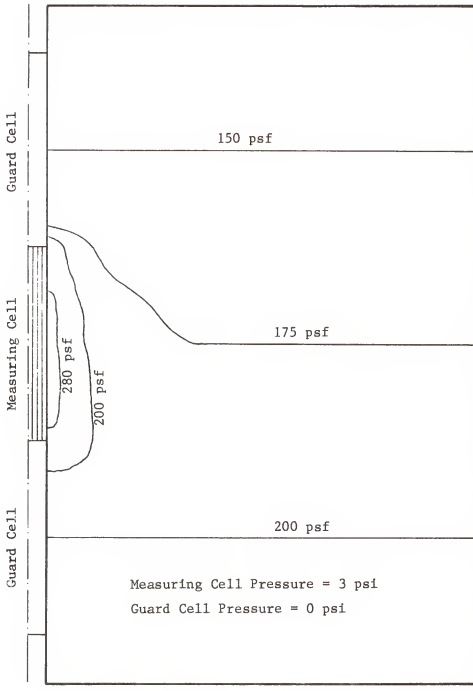


Figure 146. Maximum Shear Stress Contours Under Measuring Cell Pressure of 3 psi; K = 60,000; ν = 0.4; Depth = 7 Ft

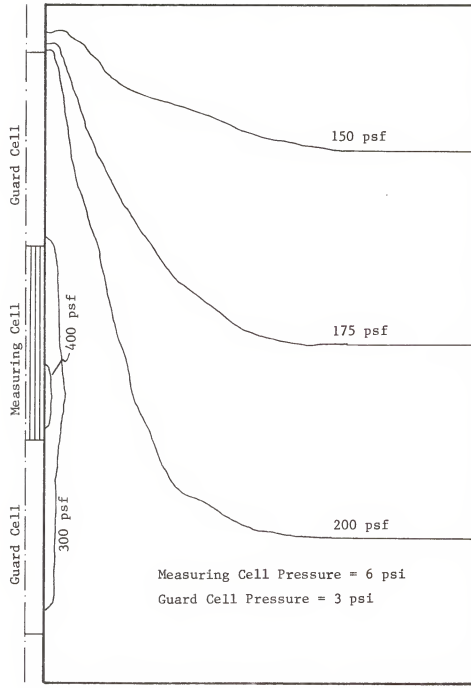


Figure 147. Maximum Shear Stress Contours Under Measuring Cell Pressure of 6 psi; K = 60,000; ν = 0.4; Depth = 7 Ft

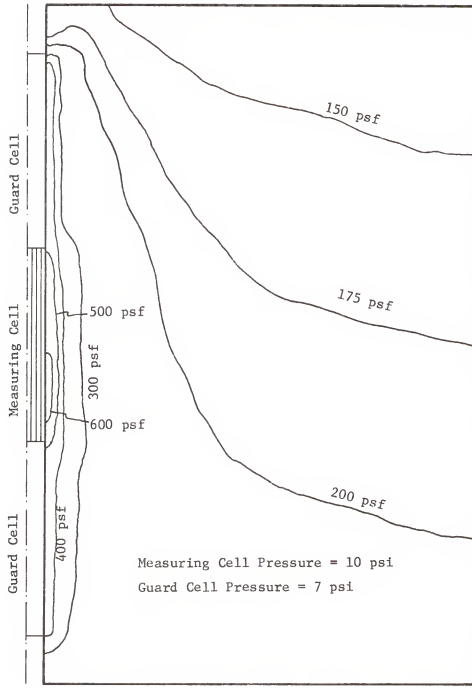


Figure 148. Maximum Shear Stress Contours Under Measuring Cell Pressure of 10 psi; K = 60,000; ν = 0.4; Depth = 7 Ft

The nonlinear studies in this chapter were concentrated on a better understanding of the elastic modulus determination, since this is a crucial part of the strain influence factor distribution approach to settlement calculations. As in the linear elastic analyses, the specific parameters studied included the effects of differential pressure, nonlinear analysis parameters, lateral stresses, depth, borehole disturbance, and unloading and reloading of the pressuremeter. These factors will be discussed in the following sections.

5.3.2 Effect of Differential Pressure Magnitude

In the linear analysis the effect of varying the differential pressure was to cause a slight shift in the pressure-volume curve, but it did not affect the slope and the modulus calculation. However, if the differential pressure is varied in the nonlinear analysis, there is a more noticeable variation, as illustrated in Figure 149.

The effect of using higher differential pressures is to shift the pressure-volume curve in such a manner that the modulus calculation, as determined from the judgement of the slope of the nonlinear pressure-volume curve, would generally be higher for higher differential pressures. This shift would also cause a shift in the response of the pressuremeter in the plastic or failure region, and thus could cause a variation in the interpretation of the limit pressure. These variations are all illustrated in Figure 149.

On Figure 149 is illustrated another problem with regard to the interpretation of the nonlinear pressuremeter data. Two lines have been drawn to indicate the modulus range that might be estimated using these data and the slope calculation method. It is noted that there is a wide variation, and the two values are both quite different from

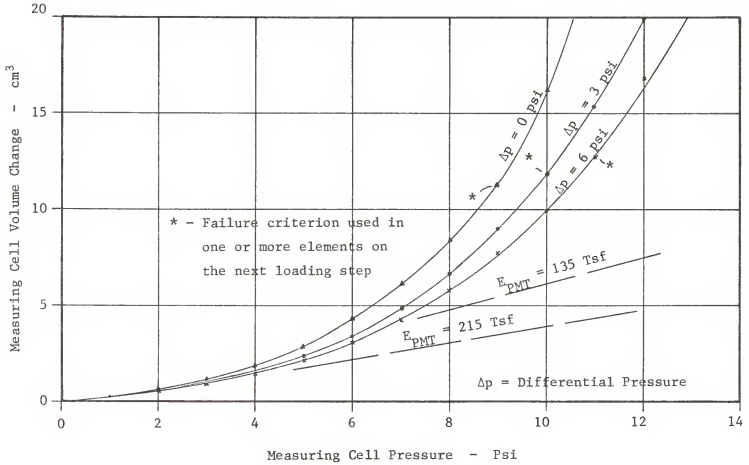


Figure 149. Comparison of Effect of Varying Differential Pressure Using Minor Principal Stresses and Bulk Failure Condition; K = 60,000; ν = 0.40

the initial in-situ tangent modulus which is shown in Figure 34 to be 350 tsf. The two slope moduli are one-third to two-thirds of this in-situ value.

The additional complexity of the nonlinear response is shown by calculating the modulus using the linear slope between each of the 1 psi pressure increments. If this is done for the three cases shown in Figure 149, the results can be tabulated as in Table 10. For comparison the initial in-situ tangent modulus from Figure 34 and Equation 73 is also given. This table shows clearly that the initial slope of the 0 differential pressure curve most closely equals the initial in-situ tangent modulus. For the 3 and 6 psi differential pressure cases, the initial slope gives a slightly high modulus. This is primarily due to edge effects and the slight volume discrepancy of the finite element model (see Figures 131 and 132). Since only the central cell is being loaded up to 3 psi in the one case, the initial modulus variation of 13 percent on the high side is reasonable based on the results of the linear analysis. As the pressure is increased, the slope also increases, such that the modulus decreases. This is reasonable and generally typical of field data.

Another way to consider modulus information from a pressure-volume curve is to use a secant modulus approach. A secant modulus is determined from the slope of a line connecting two points on the pressure-volume curve. The major problem involved in using a secant modulus is the selection of the two points on the curve that should be used. In materials work, the secant modulus is often taken between the origin and some percent of strain, or some stress level, or some other fixed point. In this work, however, even the origin is not

Table 10. E_{PMT} Calculations for Varying Differential Pressures; K = 60,000; ν = 0.4; Depth = 7 Ft ; k_o = 0.5

Case \ Interval	E_{PMT} (Tsf) 0 - 1 psi	1 - 2 psi	2 - 3 psi	3 - 4 psi	4 - 5 psi	*Initial In-Situ Tangent Modulus
Differential Pressure = 0 psi	364	261	174	120	91	350
Differential Pressure = 3 psi	394	298	217	153	108	350
Differential Pressure = 6 psi	394	298	217	163	131	350

* From Figure 34 and Equation 73 (Isotropic Modulus)

a meaningful starting point, since most pressuremeter field data have a poorly defined starting volume condition.

This initial nonlinear study does not account for borehole unloading, and the only analytically consistent comparison that can be made is between the initial in-situ tangent modulus and the moduli as calculated from the pressure-volume curves. Since the initial in-situ tangent modulus was the modulus used in the normalizing of the strain data in Chapter 4.0 (to determine a strain influence factor), this initial tangent modulus should best be used for settlement estimates using the strain factor distribution approach.

About the only additional conclusion that can be made when considering these nonlinear pressure-volume curves (without accounting for borehole unloading) is that any secant modulus that might be drawn between any two points, including the origin (which is well defined in these analytical studies) will be less than the initial in-situ tangent modulus and the value will vary depending upon the two points chosen. Some further comments about a secant modulus will be discussed when considering the effects of borehole unloading in Section 5.3.6.

In a field application, the actual pressure on the soil, as well as the true value of the differential pressure, are both difficult to determine. Pressure monitoring equipment is not usually as precise as that used under controlled laboratory conditions, and certainly not as precise as can be used in theoretical analyses such as these. The results of this differential pressure study on the nonlinear stress-dependent modulus material are reasonable, but it might be extremely difficult and costly to undertake as precise a study in the laboratory due to the many hardware factors previously discussed.

These studies show that a carefully controlled pressuremeter test, with a low or negligible differential pressure, should be able to measure the initial in-situ tangent modulus over the initial portion of the pressure-volume curve. After the pressure of 2 or 3 psi is reached, however, all the slope calculations will yield lower modulus values. Unfortunately, due to membrane inertia and other hardware difficulties, as well as borehole disturbance, it is this initial portion of the pressure-volume curve which is the most difficult to determine accurately in the field. It appears from this study, however, that any attempts to use sophisticated hardware, minimize disturbance, accurately determine precise loading pressures and borehole volumes, and minimize the effects of the differential pressure, might be well worthwhile for future research with respect to pressuremeter hardware.

5.3.3 Effect of Nonlinear Analysis Parameters

Since the studies as shown in Section 5.3.1 give reasonable results for the nonlinear response of sands to pressuremeter loading, a major problem to be investigated is the interpretation of these pressure-volume curves in terms of the known nonlinear analysis parameters used in the analytical study. Again, the borehole was not unloaded, so that any effects due to disturbance or borehole unloading were not included in these initial nonlinear studies.

The loose, medium dense, and dense sand was loaded at a depth of 7 ft with a lateral coefficient (k_o) of 0.5. The pressure increment was 1 psi, and the differential pressure 3 psi. The only variables were the nonlinear modulus numbers (K) and the angle of friction (ϕ), both of which depended on the loose, medium dense, or dense nature of

the soil. The pressure-volume curves for these three cases are shown in Figure 150. The general response of the curves is reasonable in that there is a consistently greater modulus as determined from the slope as the nonlinear modulus number increases.

Modulus calculations using the slope between each 1 psi increment are tabulated in Table 11. The results are similar to those in Section 5.3.2. The best measure of the initial in-situ tangent modulus can be determined using the initial portion of the pressure-volume curve, but this value is slightly on the high side. Thereafter, the slope method will yield continuously lower moduli, as expected.

Another variable which should be considered is the effect of Poisson's ratio. It was shown in the linear elastic analyses that the effect of Poisson's ratio was negligible in calculating the elastic modulus from the slope, assuming the proper Poisson ratio was used.

In the field Poisson's ratio is not known, and generally in sandy soils a Poisson ratio of 0.3 to 0.4 is assumed. It is not as critical a parameter as might be expected since in the E_{PMT} equation (Equation 1) the effect of using 0.4 instead of 0.3 is to increase the modulus calculation by 1.4/1.3 or 8 percent. This is a minor discrepancy considering all the factors involved in the field test.

The medium dense and dense sand was loaded at the 7 ft depth with a lateral coefficient (k_o) of 0.5, and Poisson's ratios of 0.3, 0.4, and 0.48. The results are shown in Figures 151 and 152, while modulus calculations using the slope between each 1 psi pressure increment are tabulated in Table 12. The results using a Poisson ratio of 0.48 are slightly less reliable than the others, but in general they are quite reasonable, indicating the general effect of increasing Poisson's ratio.

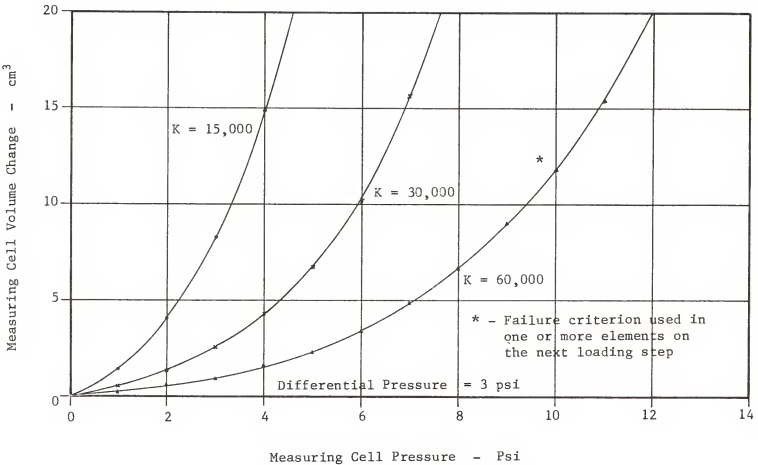


Figure 150. Comparison of Effect of Varying Nonlinear Modulus Numbers in Pressuremeter Loading: $\nu = 0.40$; Depth = 7 Ft

Table 11. E_{PMT} Calculations Using Varying Nonlinear Modulus
Number Conditions: $\nu = 0.40$; Depth = 7 Ft

	E_{PMT} (Tsf)					*Initial In-Situ Tangent Modulus
Interval / Case	0 - 1 psi	1 - 2 psi	2 - 3 psi	3 - 4 psi	4 - 5 psi	
K = 15,000 Loose	61	34	21	14	10	55
K = 30,000 Dense	163	111	74	51	37	145
K = 60,000 Very Dense	394	298	217	163	131	350

* From Figures 32 through 34 and Equation 73

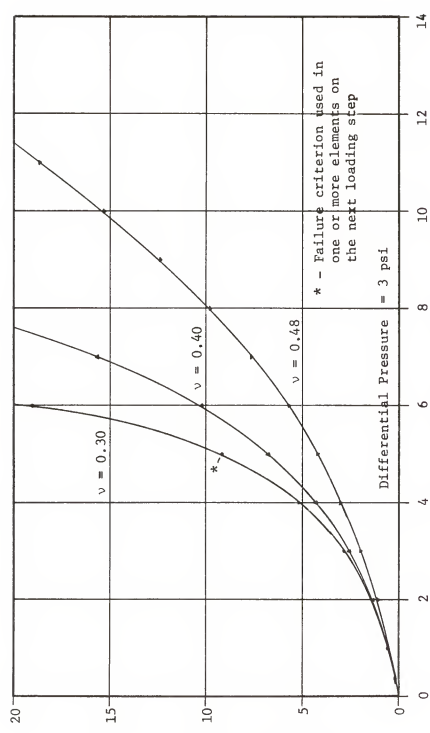


Figure 151. Comparison of Effect of Varying Poisson's Ratio in Pressuremeter Loading; K = 30,000; Depth = 7 Ft

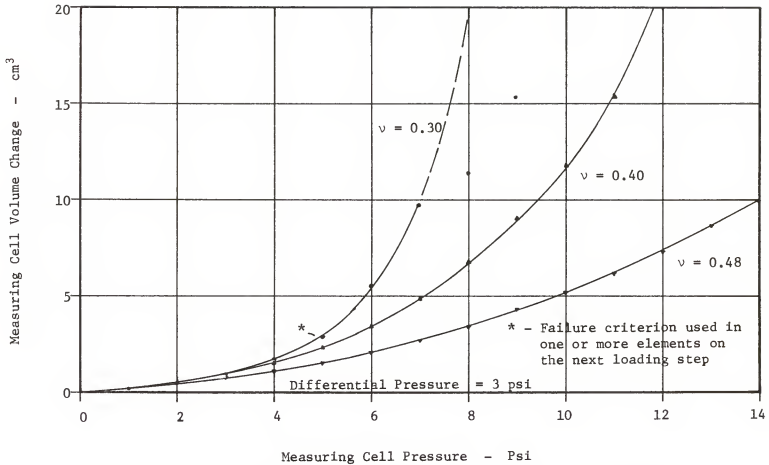


Figure 152. Comparison of Effect of Varying Poisson's Ratio in Pressuremeter Loading: K = 60,000; Depth = 7 Ft

Table 12. E_{PMT} Calculations Using Varying Poisson's Ratios: Depth = 7 Ft

Case \ Interval	E_{PMT} (Tsf) 0 – 1 psi	1 – 2 psi	2 – 3 psi	3 – 4 psi	4 – 5 psi	*Initial In-Situ Tangent Modulus
K = 60,000 ν = 0.48	387	332	285	229	193	350
K = 60,000 ν = 0.40	394	298	217	163	131	350
K = 60,000 ν = 0.30	386	282	186	112	72	350
K = 30,000 ν = 0.48	160	130	106	82	67	145
K = 30,000 ν = 0.40	163	111	74	51	37	145
K = 30,000 ν = 0.30	160	103	59	34	21	145

* From Figures 33 and 34 and Equation 73

These calculations again indicate that the initial portion of the pressure-volume curve is the best indication of the measurement of the initial in-situ tangent modulus. The modulus as calculated from the initial portion of the curves is relatively insensitive to Poisson's ratio as is indicated by examining the 0-1 psi increment column in Table 12. However, after the initial portion, the nonlinear response is greatly affected by Poisson's ratio. This also appears to affect the interpretation of the limit pressure. This might indicate that there would be a possible correlation between the limit pressure and Poisson's ratio, but other factors also affect this limit pressure, including the nonlinear modulus number, the differential pressure magnitude, and the lateral stresses, among others.

Another variable which can affect the shape of the pressure-volume curve, including the limit pressure, is the angle of friction, ϕ. This is illustrated in Figure 153 which shows the results of three runs using the same nonlinear modulus number (K = 60,000), but varying the angle of friction. Since the nonlinear modulus, even below failure, is a function of the angle of friction (see Equation 46), the general shape of the pressure-volume curve is affected. However, the initial in-situ tangent modulus will also be affected. The consistency of the analytical model used is illustrated in Table 13, which gives the modulus calculations. Again it is noted that the initial slope of the pressure-volume curve is the best indication of the in-situ tangent modulus.

It is important to note that it is possible for two analytical pressure-volume curves to resemble each other, and yet use different parameters. This is illustrated in Figure 154, which compares the

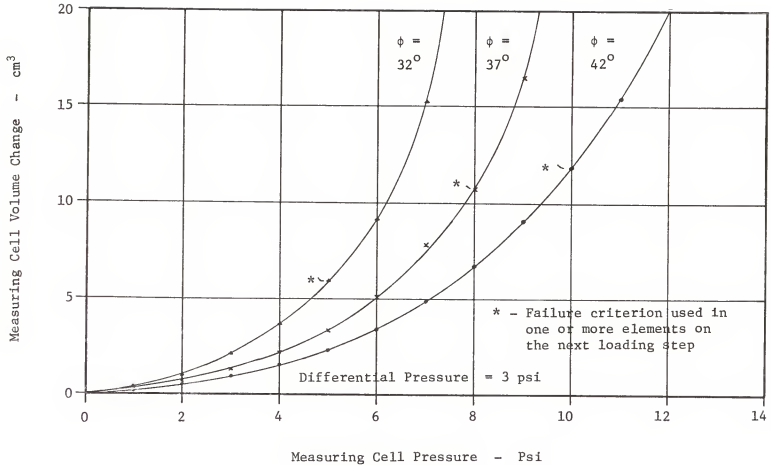


Figure 153. Effect of Varying the Angle of Friction in Pressuremeter Loading: K = 60,000; ν = 0.40; Depth = 7 Ft

Table 13. E_{PMT} Calculations for Varying Angles of Friction in Pressuremeter
Loading: K = 60,000; ν = 0.40; Depth = 7 Ft

Case \ Interval	E_{PMT} (Tsf) 0 - 1 psi	1 - 2 psi	2 - 3 psi	3 - 4 psi	4 - 5 psi	*Initial In-Situ Tangent Modulus
K = 60,000 $\phi = 42^{o}$	394	298	217	163	131	350
K = 60,000 $\phi = 37^{o}$	326	222	148	103	74	290
K = 60,000 $\phi = 32^{o}$	245	137	84	59	39	217

* From Figure 34 and Equation 73

K = 60,000, ν = 0.40, ϕ = 32^{o} case from Figure 153 with the K = 30,000, ν = 0.30, ϕ = 37^{o} case from Figure 151. The curves are very similar, but the parameters used to obtain them are appreciably different.

This indicates the many problems involved in a simplified interpretation of a single pressure-volume curve. It should be emphasized, however, that each of these curves is consistent with the analytical model, and the use of the initial slope will give the best indication of the initial in-situ tangent modulus used for each case.

These studies with respect to the various nonlinear parameters involved in pressuremeter testing indicate that the major effect of increasing nonlinear modulus numbers (K), Poisson's ratios (ν), and friction angles (ϕ), is to shift the pressure-volume curve in such a manner that the modulus as calculated from the slope of this curve increases, as does the limit pressure. The study also shows that it is extremely difficult to determine from a single pressure-volume curve just what these individual parameters are. In all cases, a reasonable approximation of the initial in-situ tangent modulus is calculated by using the initial slope of the pressure-volume curve.

It is of additional interest to note that in most analyses of clays (Ladanyi, 1972; Palmer, 1972), two of the three variables noted in this section are not considered. For studies in clays, Poisson's ratio is usually taken as 0.5, and, since the angle of friction is 0, the failure condition is a constant cohesion value, c. Clay studies also use a constant stress-strain curve, but include strain-softening.

As will be seen in following sections, the interpretation is further complicated by consideration of lateral stresses, depth (which is at least a known condition), and borehole unloading.

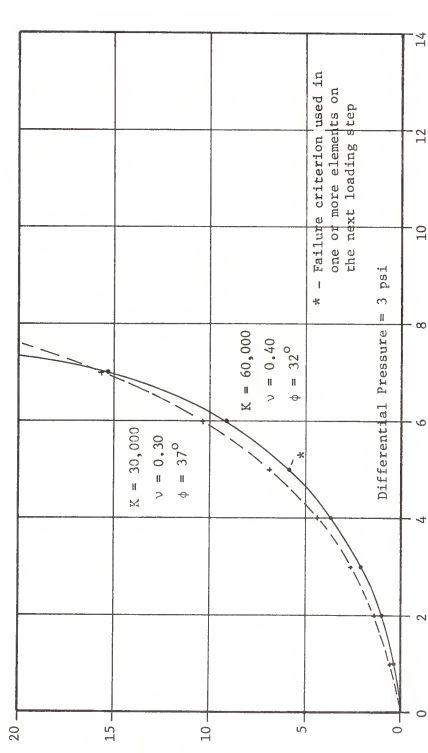


Figure 154. Comparison of Similar Pressure-Volume Curves in Pressuremeter Loading Using Different Nonlinear Analysis Parameters

5.3.4 Effect of Increased Lateral Stresses

The effect of increasing the lateral stress coefficient (k_o) from 0.5 to 1.0 is illustrated in Figure 155 for the dense and very dense sands. There is a dramatic flattening in the pressure-volume curves with an attendant increase in the modulus as calculated from the slope. The incremental moduli for the 1 psi increments are given in Table 14. As before, the initial slope gives the best indication of the initial in-situ tangent modulus.

It should be noted that there is no specific indication from the pressure-volume curve, other than the very high initial modulus calculation, to indicate higher lateral stresses. In fact, the trend of the pressure-volume curves at higher lateral stresses is very similar to those for increasing Poisson's ratios or increasing nonlinear modulus numbers, both of which result from an increase in density. This can be noted by comparing the results in Figure 155 with those in Figures 150 and 152.

5.3.5 Effect of Depth

The effect of increasing the depth of loading in the very dense sand is illustrated in Figure 156, while the moduli as calculated for the 1 psi pressure increments are tabulated in Table 15. For these cases the lateral stress coefficient was 0.5. The effect of depth is to decrease the slope of the pressure-volume curve and thus increase the modulus. The initial slope again gives the best indication of the initial in-situ tangent modulus.

The effect of increasing depth is very similar to increasing the lateral stress, as would be expected. This similarity can be seen by noting the K = 60,000, k_o = 1.0 curve at the 7 ft depth in Figure 155

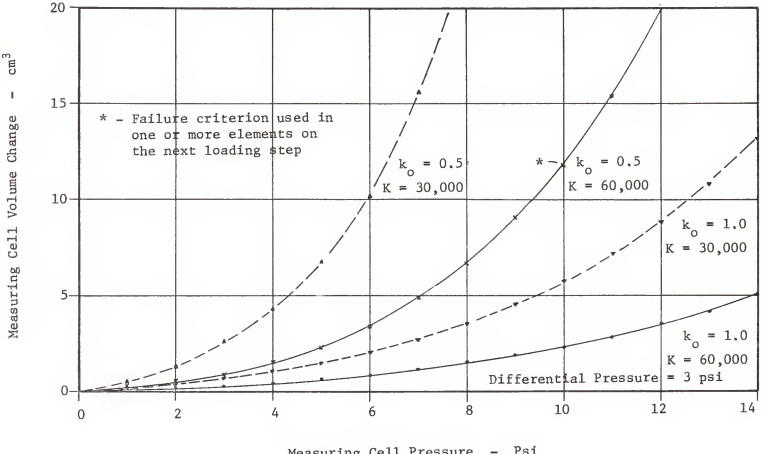


Figure 155. Effect of Increasing Lateral Stress Coefficient in Pressuremeter Loading: $\nu = 0.40$; Depth = 7 Ft

Table 14. E_{PMT} Calculations for Varying Lateral Stresses in Pressuremeter Loading: $\nu = 0.40$; Depth = 7 Ft

Case \ Interval	E_{PMT} (Tsf) 0 - 1 psi	1 - 2 psi	2 - 3 psi	3 - 4 psi	4 - 5 psi	*Initial In-Situ Tangent Modulus
K = 60,000 k_o = 0.5	394	298	217	163	131	350
K = 60,000 k_o = 1.0	888	801	701	572	478	794
K = 30,000 k_o = 0.5	163	111	74	51	37	145
K = 30,000 k_o = 1.0	447	389	331	260	210	397

* From Figures 33 and 34 and Equation 73

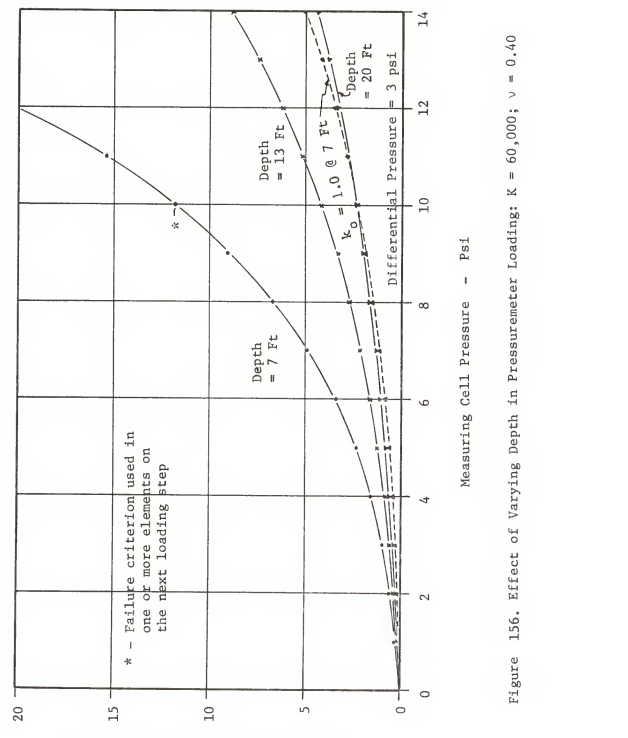


Figure 156. Effect of Varying Depth in Pressuremeter Loading: K = 60,000; ν = 0.40

Table 15. E_{PMT} Calculations for Varying Depths in Pressuremeter Loading: $K = 60{,}000$; $\nu = 0.40$; $k_o = 0.5$

Case \ Interval	E_{PMT} (Tsf) 0 - 1 psi	1 - 2 psi	2 - 3 psi	3 - 4 psi	4 - 5 psi	*Initial In-Situ Tangent Modulus
K = 60,000 Depth = 7 Ft	394	298	217	163	131	350
K = 60,000 Depth = 13 Ft	538	468	404	331	267	477
K = 60,000 Depth = 20 Ft	665	610	562	473	422	592

* From Figure 34 and Equation 73

compared to the K = 60,000, k_o = 0.5 curve at the 20 ft depth in Figure 156. This curve from Figure 155 has been added to Figure 156. The curves are very similar, even with this precise analysis. Under field conditions it would be very difficult to differentiate between the two.

Since the depth is known in field testing, this at least is not an unknown compared to the lateral stress coefficient, Poisson's ratio, and the friction angle. The depth is an important factor in interpreting the pressure-volume curve in materials whose modulus is a function of depth, such as sands.

5.3.6 Effect of Borehole Disturbance

The initial studies of the possible effects due to borehole disturbance were similar to those described in Section 5.2.7. A thin smear of sand with K = 30,000 was placed in varying thicknesses at the edge of the borehole which was in the dense sand material (K = 60,000). A Poisson ratio of 0.4 was used for both materials.

The resulting pressure-volume curves for this smear zone study are shown in Figure 157. These results are reasonable, since as the thickness of the smear zone increases, the initial slope increases, and the modulus decreases. Modulus calculations based on the slope over the 1 psi increments are tabulated in Table 16. Again the initial portion of the pressure-volume curve is the best indication of the in-situ tangent modulus. It is also noted that as the thickness of the smear zone increases, the modulus approaches the modulus of the smear zone, in a manner similar to that previously shown in Figure 141 for the linear elastic analyses.

Although this smear zone approach gives reasonable analytical

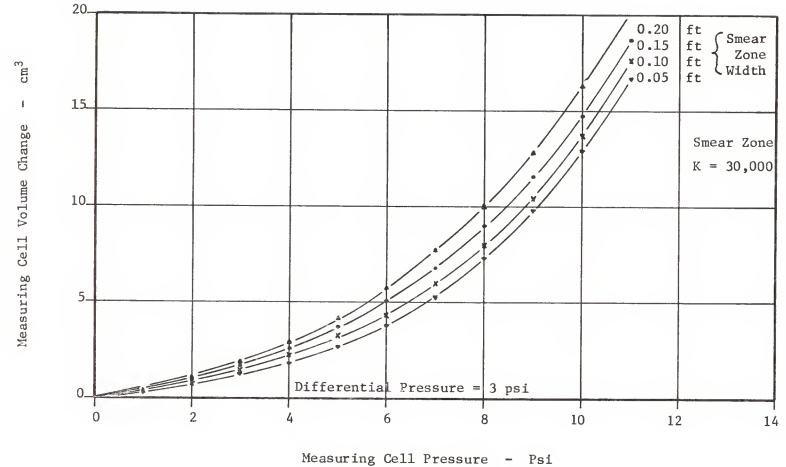


Figure 157. Effect of Smear Zone Width on Pressuremeter Loading in Nonlinear Elastic Material: K = 60,000; ν = 0.40; Depth = 7 Ft

Table 16. E_{PMT} Calculations for Varying Widths of Smear Zones in Pressuremeter Loading of Nonlinear Elastic Material: $\nu = 0.40$; Depth = 7 Ft; $k_o = 0.5$

	E_{PMT} (Tsf)					*Initial In-Situ Tangent Modulus
Case \ Interval	0 - 1 psi	1 - 2 psi	2 - 3 psi	3 - 4 psi	4 - 5 psi	
No Smear Zone	394	298	217	163	131	350
0.05 Ft Wide Smear Zone	255	218	184	141	111	350 (145)**
0.10 Ft Wide Smear Zone	213	179	150	118	97	350 (145)
0.15 Ft Wide Smear Zone	195	157	128	100	83	350 (145)
0.20 Ft Wide Smear Zone	185	144	114	88	73	350 (145)

* From Figure 34 and Equation 73
** Initial In-Situ Tangent Modulus of Smear Zone Material

results, it does not correctly model the initial low modulus region typical of most field data and illustrated in Figure 2. Most engineers consider the low initial modulus region to be due to seating conditions in the field test, and, as previously noted, Gibson and Anderson (1961) consider that it represents a reloading to the initial horizontal in-situ conditions.

Another approach to the investigation of the effects of borehole disturbance would be to first unload the borehole. This stress relief occurs in the field and it would be of interest to determine what its effect might be on the pressure-volume curve. The borehole was unloaded using the geostatic distribution previously shown in Figure 134.

The effect of borehole unloading is to cause a decrease in the lateral stress followed by reloading due to the pressuremeter. In the finite element model it was found that for the grid selected the unloading caused a failure condition in the elements immediately adjacent to the borehole due to the lowering of the lateral stress. Again the use of the bulk failure criterion gave more reasonable results than the use of a low failure modulus.

When the pressuremeter then reloaded the soil, including the thin (0.05 ft thick) smear of bulk modulus elements, the resulting pressure-volume curve was shown in Figure 158, which includes the similar curve for the case of no borehole unloading (from Figure 150). After the lateral reloading the elements adjacent to the borehole returned to a nonfailure stress condition and remained in this state until the lateral pressuremeter loading itself induced failure in the element.

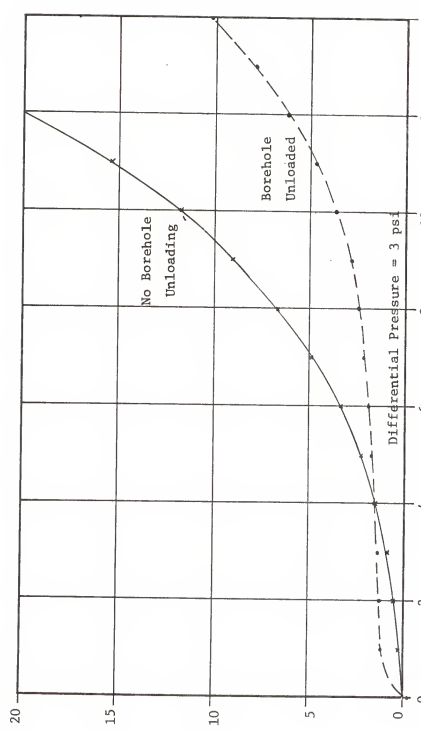


Figure 158. Effect of Borehole Unloading on Pressuremeter Loading:
K = 60,000; ν = 0.40; Depth = 7 Ft

This unloading and reloading sequence is shown in Figure 159 for the elements adjacent to the centerline of the pressuremeter. The original in-situ condition was as previously shown in Figure 145. After borehole unloading the lateral stress in the element decreased and the element went into the bulk failure condition. Subsequent reloading then restored the nonlinear elastic response of the soil. Mohr's circles for the borehole unloading and for the measuring cell loading pressure of 11 psi are shown in Figure 159. These results compare favorably with the case for no borehole unloading which was shown in Figure 145.

The pressure-volume curve in Figure 158, which includes the effects of borehole unloading, is in a very reasonable form when compared to field data. The results of this analysis indicate that the initial pressure-volume curve low modulus region is due to the reloading of the thin smear of failed elements at the edge of the borehole. This smear was caused by stress relief due to borehole unloading. These analytical results substantiate the reloading opinion of Gibson and Anderson (1961).

It is also noted from Figure 158 that the reloaded pressure-volume curve has an extremely flat slope with a high modulus. Tabulated calculations of the slope modulus are given in Table 17. Study of this table indicates that the moduli as calculated from the slope of the reloaded portion of the pressure-volume curve are considerably higher than the initial in-situ tangent modulus. This is significant because it implies that any problem in obtaining the initial portion of the pressure-volume curve for the case of no borehole unloading may be compensated for due to borehole unloading.

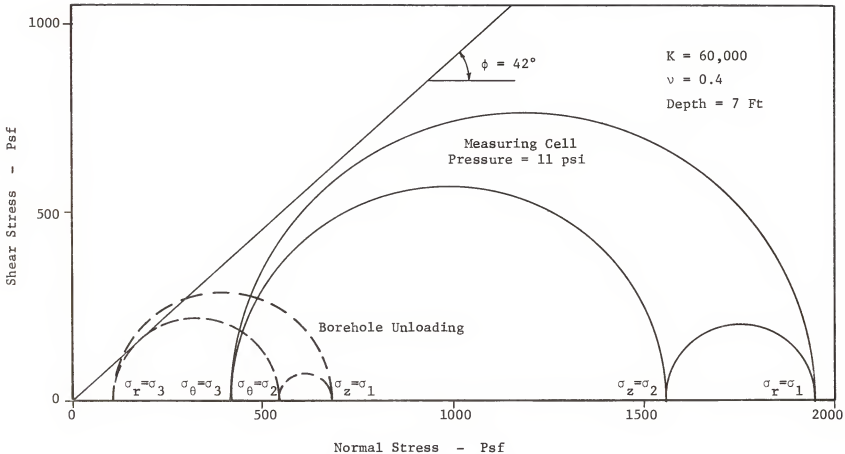


Figure 159. Mohr's Circle Representations of Stresses in Soil at Centerline of Pressuremeter After Borehole Unloading and Pressuremeter Loading: K = 60,000; ν = 0.40

Table 17. E_{PMT} Calculations Including Effect of Borehole Unloading: $K = 60{,}000$; $\nu = 0.40$; Depth = 7 Ft

Case \ Interval	E_{PMT} (Tsf) 0 - 1 psi	1 - 2 psi	2 - 3 psi	3 - 4 psi	4 - 5 psi	*Initial In-situ Tangent Modulus
$K = 60{,}000$ $\nu = 0.4$ No Borehole Unloading	394	298	217	163	131	350
$K = 60{,}000$ $\nu = 0.4$ Borehole Unloading	64	558	620	579	301	350

* From Figure 34 and Equation 73

With no borehole unloading the slope moduli (after the first pressure increment) tend to be too low, while with borehole unloading they tend to be too high. Practical field testing may thus involve a series of compensating factors which tend toward a reasonable average modulus value very close to the initial in-situ tangent modulus. In Table 17 the average of the high modulus calculation values is 590 tsf which is slightly less than twice the value of the initial in-situ tangent modulus value of 350 tsf.

The value of the reloading modulus used had a very slight effect. The borehole unloading used the nonlinear unloading modulus number (K_{ur}) discussed in Chapter 3.0, which was typically assumed to be one-third greater than the nonlinear modulus number, K. For reloading, this same modulus, or some fraction of it, could be used. If a nonlinear unloading modulus number 25 percent of that used for the case in Figure 158 is used, the resulting pressure-volume curve is almost identical to that in Figure 158. This indicates that the value of the reloading modulus number itself is not too critical. The reloading against the bulk failed elements is an important analytical sequence, however, in order to get the low modulus initial portion of the typical field pressure-volume curves.

The size of the pressure increments was noted in Section 5.3.1 to be of great importance in the analytical model. This is also shown in Figure 160. On the reloading of the borehole, the first pressure increment will load against the failed elements. Obviously, then, the first pressure increment is critical since that step will load against the failed elements no matter what the numerical size of the step. The following pressure steps will then load against the

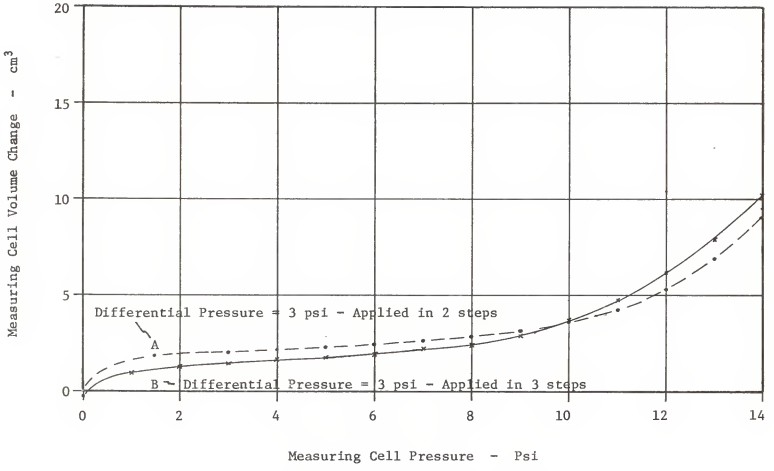


Figure 160. Effect of Initial Pressure Increment on Pressuremeter Loading:
K = 60,000; ν = 0.40; Depth = 7 Ft

unfailed nonlinear elastic elements. This means that analytically it is possible to make the initial portion of the pressure-volume curve bend the way the analyst wants by means of the choice of steps. Additionally, the size of the first increments will affect the entire pressure-volume curve. This is shown in Figure 160.

In Curve A the initial reloading to 3 psi was done in two steps, while in Curve B it was done in three steps. Analytically it would be possible to make the curve bend at any location. Gibson and Anderson (1961) felt that the curve would break at the point of the original horizontal in-situ pressure, but this is not indicated by this particular modeling of the unloading and subsequent reloading of the borehole. It is of interest to note that the relatively linear portion of Curves A and B (between 2 and 4 psi) have approximately the same slope and would thus give the same modulus value. For consistency within this study the 1 psi increments were maintained.

Because this analytical model can use so many alternatives with varying, but reasonable, results, it is possible to obtain almost any initial pressure-volume curve the engineering analyst has the time and money to pursue. However, it is possible to make some conclusions based on these studies of possible borehole disturbance effects.

The initial low modulus region, typical of most field pressure-volume data, is most likely due to a reloading against some failed region which can be reasonably analyzed using the bulk failure condition. This failed region could be due to the lateral stress relief caused in drilling the borehole, or perhaps to the effects of the drilling process itself.

Although it seems reasonable to believe that the break in the pressure-volume curve after this initial reloading occurs at the value of the in-situ horizontal pressure, this analytical study shows that this is not necessarily true. This is not to say that it isn't true, but rather to indicate that combinations of pressure increments and unloading and reloading moduli can produce almost any initial pressure-volume curve desired. To study the possible combinations and intricacies involved in just this initial condition alone would be an extensive study by itself and it is questionable whether the large quantity of time and computer money would be justified.

This study also indicates quite conclusively that the use of a lower modulus smear zone with a fixed thickness around the borehole will not give the typical low modulus initial region of the typical field pressure-volume curve.

It has been noted previously that the nonlinear pressuremeter curves obtained by direct loading against the borehole, but not including the effect of unloading the borehole, gave pressure and volume changes which were quite low when compared to field data in sandy type soils. The borehole unloading phenomenon, however, in addition to providing an explanation for the original low modulus region of the typical pressuremeter curve, also causes the rest of the pressure-volume curve to assume a much more reasonable form, which is more comparable to field data.

To unload the borehole and then use small pressure increments up to large pressures requires a great deal of computer time. As an indication, however, of the more reasonable nature of the pressure-volume curve when including both the borehole unloading and the

necessary calculations to higher pressures, consider Figure 161. This figure shows the case for reloading an unloaded borehole at depths of 7 and 20 ft for K = 60,000, k_o = 0.50, and Poisson's ratios of 0.40 and 0.48. Additionally the case for k_o = 1.00 at the 7 ft depth is included for comparison. The scatter in the data points is due to some of the analytical elements going into the bulk failure condition. The general shape of the curves is quite reasonable, however.

A study of the failure conditions and limit pressures of pressuremeter loading using the finite element technique would require parametric curves of the type shown in this figure. Since each curve requires a large amount of computer time to calculate, such a study would be extremely costly.

Perhaps the most interesting conclusion that can be made from a study of Figure 161 is the very similar nature of the pressure-volume curves in their initial portion. It has already been shown that the analytical model is consistent, and that the modulus as determined from the slope of the reloaded curve is generally higher than that of the initial in-situ tangent modulus. It has also been shown that analytically it is possible to make the reloading of the unloaded borehole follow any steps the analyst desires. But, regardless of these facts, all of these studies, on both the natural and unloaded boreholes, have indicated the large variation of the pressure-volume curves as a function of Poisson's ratios and lateral stresses. Perhaps there is a great deal more information to be obtained concerning these parameters in sands from a study of pressure-volume curves. Although some possible correlations have been mentioned in the pressuremeter literature (see Section 2.1.3),

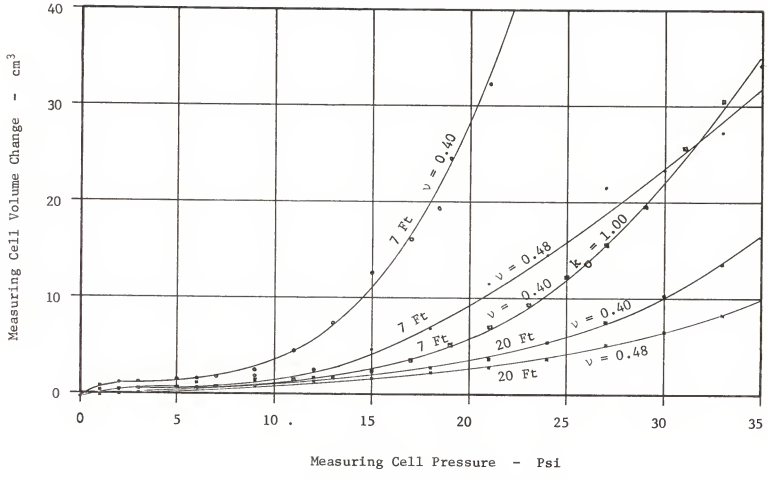


Figure 161. Pressuremeter Loading Curves for Varying Poisson's Ratios and Depths Including Effect of Borehole Unloading, Minor Principal Stresses, and Bulk Failure Condition: K = 60,000; k_o = 0.50

these analytical studies indicate that Poisson's ratio and lateral stresses are very important variables in the interpretation of the nonlinear pressure-volume curve.

5.3.7 Effect of Unloading and Reloading the Pressuremeter

The linear elastic studies discussed in Section 5.2.8 showed that the analytical model correctly unloaded and then reloaded the pressuremeter from a given point on the pressure-volume curve. The nonlinear model could also use this feature, which is illustrated in Figures 162 and 163. Figure 162 shows the unloading from selected points on a pressure-volume curve which does not include the effect of borehole unloading, while Figure 163 shows a similar result for the case including borehole unloading.

The results of modulus calculations for these cases are included on the figures. The unloading results shown in Figure 162 are very typical in form to what has been suggested by Ménard (1965) and previously illustrated in Figure 14. In the analytical model, however, E^+ is larger than E_a, which is not typical of field data. The reason for this in the nonlinear analysis is as follows. During the pressure unloading the minor principal stress decreases which means that a lower reloading modulus (E^+) would be expected. However, the decrease in the strain means that the tangent modulus to be used on reloading is higher than before, and generally this effect is dominant.

In Figure 162 it is noted that the unloading and reloading moduli have generally the same values no matter what the initial unloading point. Also, their average is slightly greater than twice the initial in-situ tangent modulus value of 350 tsf. It is also noted

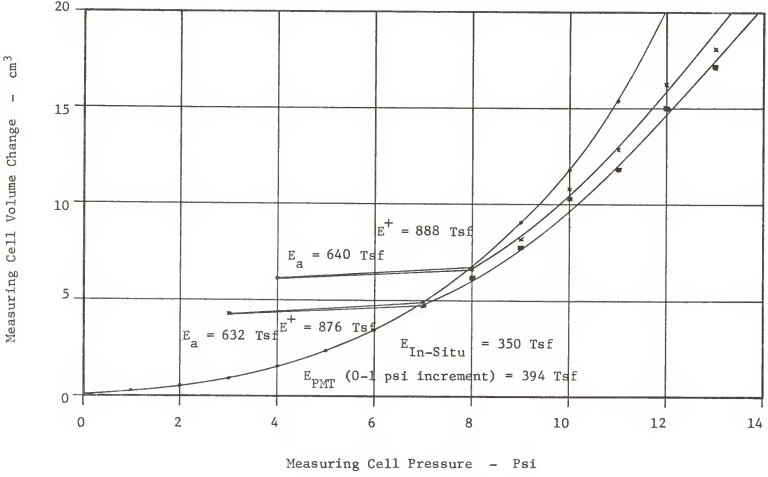


Figure 162. Effect of Unloading and Reloading the Pressuremeter Test: Borehole Not Unloaded: K = 60,000; ν = 0.40; Depth = 7 Ft

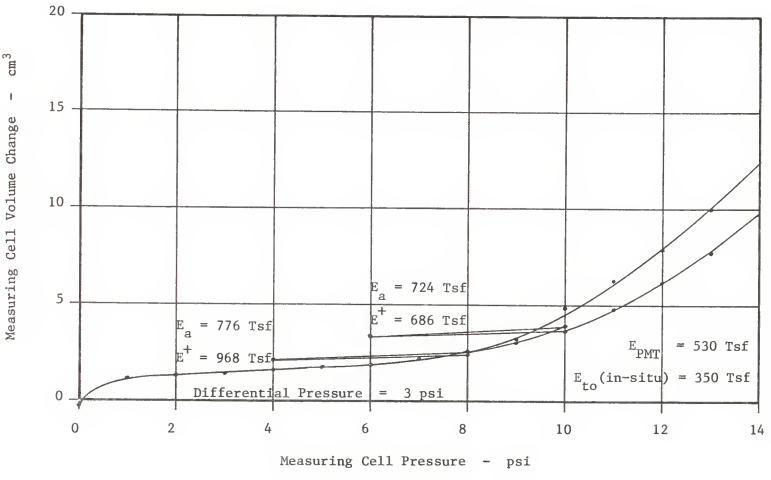


Figure 163. Effect of Unloading and Reloading the Pressuremeter Test: Borehole Unloaded: K = 60,000; ν = 0.40; Depth = 7 Ft

that the pressure-volume curves are different after the unloading-reloading sequence. This is because numerically there was a single large pressure reloading step used which gives slightly different modulus values when using the incremental pressure approach compared to using a series of steps all using the smaller increment.

The effect of unloading the borehole was generally to flatten the pressure-volume curve. This will also tend to flatten the unloading and reloading segments of the curve as seen in Figure 163. It is also to be noted in Figure 163 that the unloading and reloading moduli are affected by the initial unloading point, but are still approximately two times greater than the initial in-situ tangent modulus for this case. The relatively linear portion of the pressure-volume curve itself gives a modulus value higher than the in-situ value, but less than the unload-reload values.

Perhaps the major conclusion to be drawn from these brief studies is that it is possible to model the unloading and reloading sequence using a nonlinear elastic material. As would be expected, the unloading and reloading moduli are greater than both the relatively linear portion of the pressure-volume curve in an unloaded borehole as well as the analytical initial in-situ tangent modulus. It appears that the use of an unload-reload modulus could be promising for use with strain distribution settlement studies, but much more extensive studies would be needed first to determine the effects of all the parameters such as Poisson's ratio, varying unload-reload moduli, the precise unload-reload mechanism (number of steps), etc.

5.4 Use of Pressuremeter Moduli in Settlement Prediction

A major purpose of this study was to determine possible field pressuremeter test parameters which might be of value in estimating the settlement of sands using the strain distribution approach. Analytically such an approach is reasonable, and this chapter has shown that the initial portion of an "undisturbed" pressure-volume curve can be a good measure of the initial in-situ tangent modulus. Additionally, a secant modulus would be difficult to define on such an undisturbed pressure-volume curve. Since such a curve is not very practical when compared to field data, this form of a secant modulus on an "undisturbed" pressure-volume curve was not studied further.

There are many practical field problems to consider when applying pressuremeter results to this settlement technique:

(1) The pressuremeter test is very time-consuming when compared to the cone penetrometer and does not give an extensive amount of data with depth. For example, to take pressuremeter tests at 5 ft increments down a 40 ft hole would probably take at least a day, assuming there were no problems. Cone penetrometer tests to a similar depth could be obtained in a few hours or less. In addition, to conduct thorough pressuremeter testing down several boreholes over a site would be quite time-consuming and expensive. When compared to laboratory testing, of course, the pressuremeter test is relatively cheap which is a major reason why it is important to gain a better understanding of this test.

(2) In sands, whose elastic moduli are definitely nonlinear and stress-dependent, it has been shown in this study that the in-situ modulus can be very difficult to obtain using the slope calculation method. The initial portion of the pressure-volume curve is the most important with respect to determining the initial in-situ tangent modulus, and is most difficult, if not impossible, to obtain in practical field testing.

(3) It has also been noted that the pressure-volume curve can be greatly affected by reloading against an unloaded borehole and in such cases gives an average slope modulus greater than the initial in-situ tangent modulus. Compensating errors may cause the average slope modulus to approach the value of the initial in-situ tangent modulus, but there are many unknowns. This average slope modulus is, however, the one typically obtained by field testing and thus by necessity would need to be used for settlement analysis. It is a form of secant modulus since it is essentially the straight-line portion of the typical reverse curvature field pressure-volume curve (see Figure 2).

(4) The unload-reload modulus obtained from pressuremeter testing appears to be a fairly consistent and reproducible type of parameter which could be of value in determining moduli for this type of settlement analysis. These initial studies indicate that such a modulus appears to be in the range of twice the initial

in-situ tangent modulus, but again many variables remain not investigated.

(5) This study has also shown that many factors influence the shape of the pressure-volume curve in sands and they cannot be independently ascertained from the inspection of one single pressure-volume curve at a given depth.

Although the pressuremeter test in sands can theoretically be used in conjunction with the strain influence factor distribution approach to calculate settlements, it appears based on the above discussion that a great quantity of testing data would be needed in conjunction with field settlement studies. Ménard (1971) has done some work along these lines, but has not used the strain factor approach.

The cone penetrometer currently furnishes a great many data in much less time and at much less expense. Of course, it is also necessary to get a large number of cone data since it is also a very complex test, with much less of a theoretical basis for understanding than the pressuremeter test. These conclusions are based on these studies with regard to a sand model and do not apply to clays.

CHAPTER 6.0

COMPARISON BETWEEN ANALYTICAL MODEL AND LABORATORY TESTING

6.1 Introduction

These analytical studies have been based on work originally done by Duncan and Chang (1970). Although the studies have been helpful in understanding many of the factors involved in the strain influence factor approach to settlement, as well as the interpretation of pressuremeter tests in sands, the general applicability of the analytical model can best be shown by comparison with controlled test results.

The University of Florida has a unique testing chamber which can be used to make carefully controlled cone penetrometer, pressuremeter, and plate load tests in sand soils.

In this section a comparison will be made between the results of such tests and the analytical model. The results show that the analytical model gives reasonable results when compared to the laboratory tests, although there should be additional research in the future with respect to additional testing and correlation studies.

6.2 Description of Test Chamber

The University of Florida testing chamber was designed by Holden (1971) who describes some of its basic features in conjunction with

his work studying the cone penetrometer in sands. The chamber was also used by Laier (1973) for pressuremeter testing.

The chamber, a simplified sketch of which is shown in Figure 164, is essentially a 4 ft diameter, 4 ft deep stress-controlled volume which can be used to test laboratory-deposited soils. Testing is done with dry sands which are rained into the chamber from a moving shutter plate at a fixed elevation above the chamber. The speed of deposition and size of the shutter plate help to control the relative density of the sand.

Lateral pressure is exerted by water placed around the large rubber membrane inside the steel chamber. The lateral pressure can be varied to duplicate various depths and/or lateral stress constraints. At the bottom of the chamber is a piston which can be loaded to a prescribed vertical pressure. The piston can be locked to provide zero vertical displacement, or it can be maintained at a constant pressure and allowed to move.

Further information about this testing chamber may be found in the references cited (Holden, 1971; Laier, 1973).

6.3 Triaxial Tests on Edgar Sand

The sand used for the laboratory tests was a uniform, sub-angular quartz sand from Edgar, Florida. The sand had a coefficient of uniformity (C_u) of 2 and an effective diameter (D_{10}) of 0.3 mm. The maximum and minimum densities as determined from laboratory tests were 107.2 and 86.4 pcf respectively.

Triaxial tests were conducted using carefully placed saturated samples. The tests were saturated in order to determine volume change

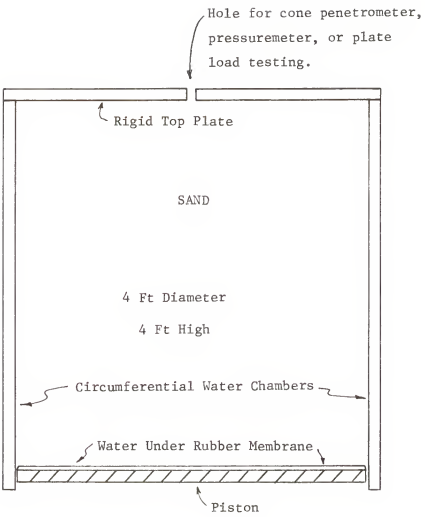


Figure 164. Simplified Sketch of University of Florida Sand Testing Chamber

characteristics during testing and used confining pressures of 0.5, 1.0, and 2.0 kg/cm^2. Great care was taken to try to make the samples as similar as possible with regard to structure as well as density.

There were two sets of tests, one at a high density and one at a lower density. The high density tests turned out to be over 100 percent relative density, while the lower density tests were in the range of 75 to 80 percent. Attempts to make lower density samples under saturation conditions to measure volume change were not successful.

The stress-strain and volume change curves from the triaxial tests, the resulting Mohr circles at failure, and the data for determining the nonlinear analysis parameters are given in Appendix IV. The engineer must use considerable judgement in interpreting laboratory data for use in the analytical model. The results based on this limited series of tests are given in Table 18, and are reasonable for a sand of this type.

6.4 Experimental and Analytical Pressuremeter Test Results

Four of the pressuremeter tests (numbers 1, 7, 8, and 9) made by Laier (1973) were studied using the finite element model. The test probe consisted of three 16 inch long cells, with an outer radius of 0.06 ft. Two of the tests were conducted at relative densities of 57 percent, while two were at 97 percent relative density. For additional comparison, cone penetrometer testing data were also available (Holden, 1971). The various modulus values obtained from tests in the University of Florida testing chamber are tabulated in Table 19.

Table 18. Nonlinear Analysis Parameters for Edgar Sand

Relative Density	K	n (Assumed)	G	F	j	ϕ
100+%	53,600	0.5	0.84	0.12	20	42°
75%	41,100	0.5	0.60	0.06	19	36°

Table 19. University of Florida Testing Chamber Modulus Results

Approximate Relative Density	*Laier Test No.	$*E_{PMT}$ (tsf)	$*E_a$ (Tsf)	$*E^+$ (Tsf)	**E(chamber) (Tsf)	***E(cone) (Tsf)
57%	1	27	---	---	100	48
	7	21	352	122	107	
97%	8	90	260	157	193	130
	9	97	---	---	180	

* Laier (1973)

** Based on One-Dimensional Compression (Laier, 1973)

*** Holden (1971) - Based on $E = 2\ q_c$ (q_c = Cone Bearing Capacity)

The finite element grid used is shown in Figure 165 and is an adaptation of the grid used for the parametric studies. These chamber finite element studies used the same program that was used for the parametric studies. In this regard it was necessary to experiment to obtain the best possible results based on the various boundary conditions. The program was not rewritten to duplicate the unique loading conditions of the testing chamber itself, including the circumferential hydrostatic pressure and either a stress or displacement controlled base. Should further more thorough studies be made in this testing chamber it might be worthwhile to develop a finite element program uniquely adaptable to the chamber.

The most reasonable results were generally achieved when the top and bottom of the chamber were placed on rollers and the outside kept free to displace. For the low pressures studied, the effect of the gravity stresses helped to make the displacement solutions generally reasonable until large displacements were reached.

Comparison of the results of the selected chamber pressuremeter tests and the finite element analyses are shown in Figures 166 and 167. Although the comparison appears reasonable at first glance, it is noted that there are distinct discrepancies in the values of the various elastic moduli. The finite element model gives much higher values of E_{PMT}, E_a, and E^+. The general shape of the curves compares favorably, however. The precise numerical discrepancies could be due to a variety of factors including

(1) The finite element model could be reconstructed to more precisely model the chamber boundary conditions. This would require a complete redevelopment of the PRESMETR

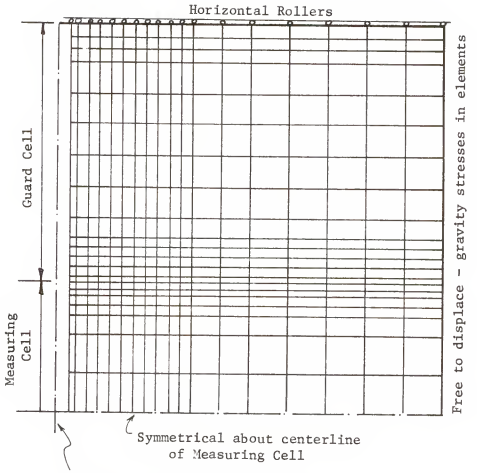


Figure 165. Finite Element Grid for Chamber Pressuremeter Study

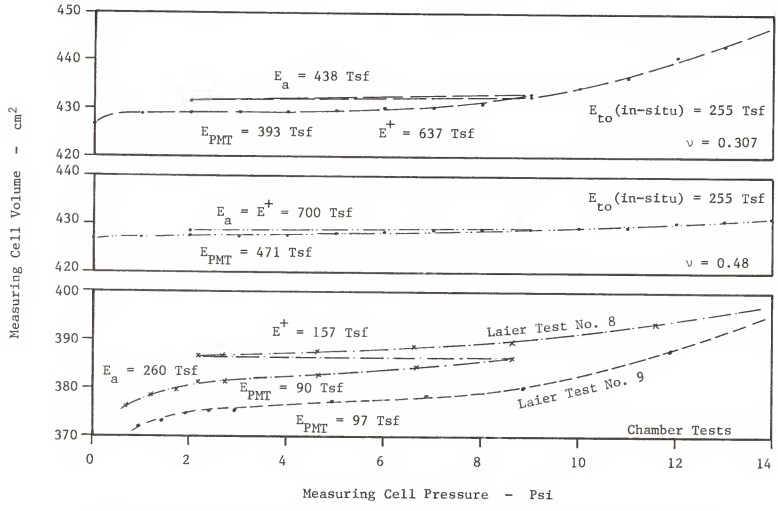


Figure 166. Comparison of Finite Element and Laboratory Pressuremeter Tests in Dense Edgar Sand: K = 53,600; $\phi = 42^{\circ}$; $k_o = 0.444$; Depth = 7 Ft; Differential Pressure = 1 psi

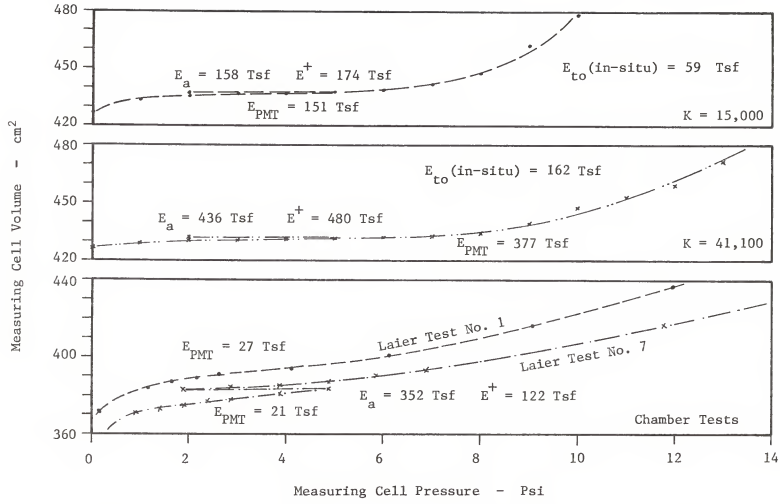


Figure 167. Comparison of Finite Element and Laboratory Pressuremeter Tests in Medium Dense Edgar Sand: $\phi = 36^o$; $k_o = 0.467$; $\nu = 0.318$; Depth = 7 Ft; Differential Pressure = 1 psi

program described in Appendix III, for specific application to the test chamber.

(2) The discrepancies could be due to the fact that sand is not an elastic continuum and the field data measure this response, while the finite element model is geometrically and mathematically constrained.

(3) The volume discrepancies introduce a small problem. In comparing field tests with analytical results, it is always necessary to adjust for the initial volume conditions. Analytically it is easy to determine precisely the initial volume prior to loading. In field tests, however, the volume of the measuring cell is a function of the end constraints, the membrane thickness, and any unevenness at the borehole surface. The original modulus equation (Equation 12) is based on a theoretical initital volume (V_o). In field work, Laier (1973) recommends an extrapolated value of V_o based on the apparent location of the initial portion of the elastic region. This initial volume is different from that used in the analytical studies, as can be noted in Figures 166 and 167.

(4) The analytical parameters could be better defined. The triaxial tests were for a relative density of approximately 75 percent, while the chamber tests were for a relative density of 57 percent. The one analytical run using a low nonlinear modulus number (K = 15,000) and shown in Figure 167 attempted to account for this. More extensive triaxial tests, especially at lower confining pressures, might give

better correlation. These data are very difficult to obtain in sands, however. Correlation with the results of plane strain testing may be more accurate for pressuremeter loading, due to the vertical confinement, instead of the minor principal stress model used in this study.

(5) Although several Poisson's ratios were tried, none gave completely satisfactory results. Although the analytical model attempts to model the dilatant effects of the soil, it is not as sensitive as originally hoped. In fact, the nonlinear parameters listed in Table 18 usually calculated Poisson's ratios greater than 0.48, so that 0.48 was used in the analyses. This is noted on some of these figures. Perhaps a completely fresh and entirely different approach for dilatant materials would give a better comparison.

In Chapter 5.0, some studies dealt with the effects of unloading and then reloading the pressuremeter. Figure 163 showed two such cases and the average unload-reload moduli were approximately two times the initial in-situ tangent modulus (E_{to}). The analytical results in Figures 166 and 167 also give unload-reload moduli greater than E_{PMT} and E_{to}. The average unload-reload moduli range from an average of two to three times E_{to} and 1.1 to 1.5 times E_{PMT}. It should be noted that the unload-reload case is exceedingly sensitive analytically and is a function of many variables, as has been discussed. Because of these variables, it is possible, as in the case of the borehole unloading and reloading, to analytically obtain almost any result one desires. The cases illustrated in Figure 163 are reasonable based on the analytical variables.

In the laboratory tests illustrated in Figures 166 and 167, the average of the unload-reload moduli is 10 times E_{PMT} for the medium dense sand (Figure 167) and 2 times E_{PMT} for the dense sand (Figure 166). The specific values are tabulated in Table 19 which shows the spread in modulus values using various testing methods.

It appears from both the analytical and the chamber pressuremeter tests that perhaps the unload-reload moduli could be of value in engineering calculations. An advantage is that such a testing result could remove some of the initial borehole disturbance factors and initial "seating" uncertainties. Two chamber tests are not sufficient, of course, to warrant major conclusions, but certainly tests including the unload-reload testing mechanism should be incorporated in future research. It is of interest to note from Figures 166 and 167 that the E_{PMT} values from the chamber tests were reasonably reproducible. It also appears, however, that the initial point used for the unloading and reloading as well as the magnitude of the unloading pressure increment could be major factors affecting the results of chamber tests.

Based on this limited series of tests and comparisons, the general conclusion is that the finite element model gives reasonable analytical results and is consistent within itself. However, it does not compare as favorably as hoped with controlled laboratory pressuremeter tests, which could be due to a variety of factors. More favorable comparisons of finite element models and chamber tests is a promising area of future research, especially as more testing data are obtained. It should also be pointed out that the sophisticated pressuremeter finite element runs which use borehole

unloading as well as unload-reload features are very expensive. Depending on the size of the pressure steps and, of course, the specific computer charging algorithm, such runs can easily cost several hundred dollars each.

6.5 Experimental and Analytical Plate Load Test Results

Plate bearing tests were another means of comparing the analytical models with actual laboratory tests. Two plate load tests, one at the high density and one at the low, were conducted in the test chamber. The chamber was filled to within approximately 6 inches of the top and a conventional 1 square foot area circular steel plate placed and leveled in the center.

After completing the filling and sealing of the chamber, the loading rods were placed and the plate movement during chamber pressurization noted. The plate load was then applied by means of a hydraulic jack loaded against a reaction beam and measured by a load cell. Data sheets for the two plate load tests in the chamber are included in Appendix V.

The finite element grid used for the analysis is shown in Figure 168. The load was applied through the steel rod and plates as shown. The program used was an adaptation of SOILSTRN which is described further in Appendix II. The elements above the plate would generally fail due to tension, but the analytical failure approach used did not affect the results appreciably. Again the centerline of the chamber was placed at an assumed depth of 7 ft to duplicate the pressure chamber conditions, and the outside boundary was allowed to displace.

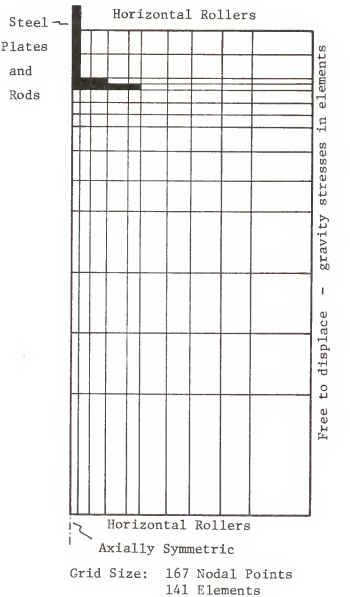


Figure 168. Finite Element Grid for Analysis of Plate Load Test in Chamber

Comparison of the plate load tests and the finite element model is shown in Figures 169 and 170. The comparison is generally quite favorable although there are some discrepancies, especially at the initial loading. It would be necessary to try various combinations of nonlinear analytical parameters to determine a better fit. Some of the factors which could cause such discrepancies have been discussed in the previous section. Specific correlation studies between additional plate load tests and a redeveloped finite element model should be promising future research.

If the chamber testing results from Figures 166 and 167, as well as Table 19, are used with the settlement techniques suggested in Section 2.2, it is possible to compare the Schmertmann and Menard methods. For the very dense sand, using E_{PMT} = 93.5 tsf, ν = 0.307, and a plate diameter of 13.3 inches, the Ménard settlement equations (Equations 28, 29, and 30) reduce to

$$\rho = 0.047\ p \qquad \text{for} \quad \alpha = 1 \tag{89}$$

and

$$\rho = 0.051\ p \qquad \text{for} \quad \alpha = 1/3 \tag{90}$$

where all symbols and units have been defined. From the very dense pressuremeter test in the chamber, $\alpha = (93.5/260)^{\frac{1}{2}} = 0.6$, so Equations 89 and 90 are reasonable bounds.

For the Schmertmann method it is necessary to use the results of cone testing given in Table 19, and then his settlement relation reduces to:

$$\rho = 0.0614\ p \tag{91}$$

The very dense settlement relationships given in Equations 89, 90, and 91 are linear. Since the plate was buried in the testing chamber, perhaps some effect due to embedment must be taken into account. However, this is not truly a classic case of embedment, since there was no excavation and no stress relief. The effect of depth was included by means of the circumferential confining pressure in the chamber tests and by means of the gravity stresses in the finite element model.

For the recommended triangular axisymmetric influence factor distribution and peak strain factor given in Figure 127, the settlement would be given by

$$\rho = \frac{p\,D}{E_c} \left\{ 0.3 + 0.1\sqrt{p/\sigma_{D/2}} \right\} \qquad (92)$$

which includes a 0.1 reduction in C_i for embedment as well as a surface intercept value, I_s, of 0.0. The term $\sigma_{D/2}$ is the vertical pressure approximately ½ foot beneath the settlement plate. This result is plotted on Figure 169.

Doing a similar analysis for the dense sands, and using E_{PMT} = 24 tsf, E_c = 48 tsf, and α = 0.318 ($\alpha = \{24/352\}^{\frac{1}{2}} = 0.26$), the settlement equations reduce to

$$\rho = 0.166\ p \qquad (93)$$

using Schmertmann's distribution, and

$$\rho = 0.183\ p \quad \text{for} \quad \alpha = 1 \qquad (94)$$

and

$$\rho = 0.201\ p \quad \text{for} \quad \alpha = 1/3 \qquad (95)$$

for the Ménard case.

Using the recommendations from Figure 127 for the dense sand,

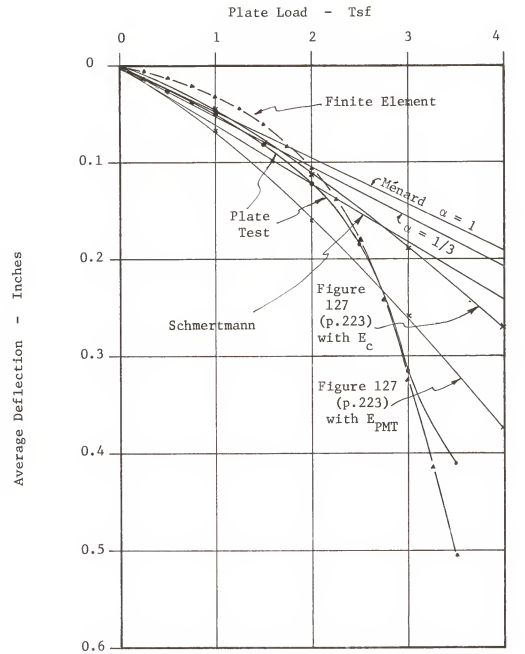


Figure 169. Comparison of Finite Element, Analytical Settlement, and Plate Load Test Results in Dense Sand: K = 53,000, ν = 0.48

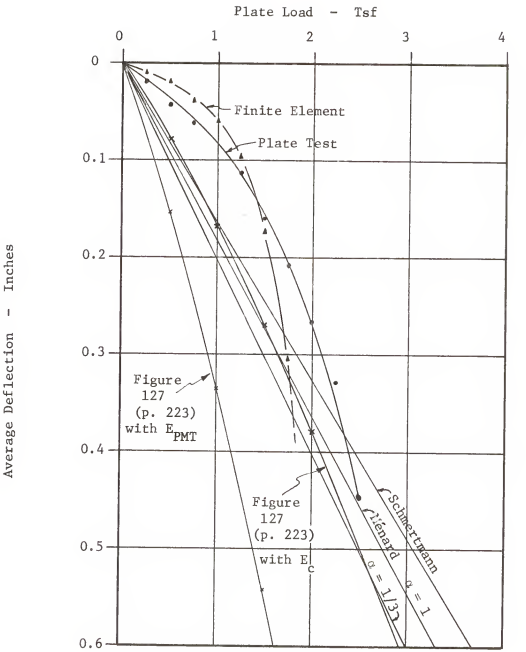


Figure 170. Comparison of Finite Element, Analytical Settlement, and Plate Load Test Results in Medium Dense Sand: K = 41,000, ν = 0.48

including the C_i reduction and using $I_s = 0.1$, the settlement is

$$\rho = \frac{p\,D}{E_c} \{ 0.425 + 0.1 \sqrt{p/\sigma_{D/2}} \} \quad (96)$$

which is plotted in Figure 170. If the modulus values from the chamber pressuremeter tests are used with Figure 127, instead of the cone modulus values, then the predicted settlements would be greater. These results are also shown on Figures 169 and 170 and indicate that the cone modulus comparison is more favorable for these data.

It is apparent from a study of these two figures that the three recommended settlement calculation techniques compare fairly well among themselves. All three methods are strongly dependent upon the modulus value, and this is especailly true for the simplified triangular strain influence factor distribution approaches. The method recommended in Figure 127 does provide a means for introducing nonlinearity into the settlement estimates and is apparently more reasonable at the lower loading pressures.

There are many possible reasons for the spread in comparisons between the settlement estimates and the plate bearing tests shown in Figures 169 and 170. Two plate bearing tests are the minimum that might be considered and an extensive late bearing test program would give more reliable data for comparison and analysis. Since these were the first plate bearing tests conducted using this unique testing chamber, there may be some problems in conducting such tests that only an extensive test program would uncover.

There may have been some problems with the pressuremeter tests, especially at the lower densities. The E_{PMT} for the medium dense case was 24 tsf and for the dense case it was 93.5 tsf, a ratio of

1 to 4. The laboratory plate settlement curves from Figures 169 and 170 are not in a 4 to 1 ratio, although the analytical settlement estimate curves are. The cone moduli were in a ratio of approximately 2½ to 1, and gave more reasonable settlement estimates, as has been previously noted.

One of the major advantages of the simplified triangular strain influence factor approach to settlement calculations is that it provides a simplified distribution for use when considering a great many varying modulus data, such as is obtained from cone penetrometer testing. In these tests there was just one modulus value considered with just one strain distribution, and perhaps this is carrying the simplified analysis approach too far.

Obviously it would be possible to back-figure the necessary simplified triangular strain influence factor distribution factors such as C_i and C_f which might give better comparisons. The writer does not feel that this would be meaningful, however, because of the limited number of field data, and because of all the variables involved in sand settlement, even under controlled laboratory testing.

These results do indicate, however, that the simplified strain influence factor distribution approach is reasonable, especially considering all the variables. The recommendations given in Figure 127 provide a reasonable means for introducing nonlinearity into settlement estimates.

6.6 Model Footing Settlement Tests

As indicated in Chapter 4.0, these analytical studies show that

for linear modulus materials the settlement due to plane strain loading should be greater than that for axisymmetric. Table 4 indicates a plane strain to axisymmetric settlement ratio for rigid foundations of 2.10/0.79 = 2.7 for L/D = 10 and 3.40/0.79 = 4.3 for L/D = 100.

Because the precise variation between plane strain and axisymmetric soil parameters still requires further study, the nonlinear studies using varying nonlinear modulus numbers could give a variety of settlement ratios, depending on the nonlinear modulus number (K) or Poisson's ratio (ν). When using identical nonlinear modulus numbers, the plane strain settlements were analytically greater that the axisymmetric by a ratio of approximately 1.5.

To investigate this settlement variation further, some model footing tests were conducted. The model footings were rigid steel bars 7.6 cm wide with lengths of 7.6, 26.8, and 45.9 cm, which gave length to width ratios of 1:1, 1:3.5, and 1:6. The sand used was a uniform Ottawa sand at an approximate relative density of 80 percent. The testing container was a 46 cm by 46 cm, 40 cm deep lucite box. The depth of sand was approximately 30 cm to give a depth of 4D for these rectangular footings. The 1:6 footing was an approximation of a plane strain test since the footing went the full length of the container and the sand was thus constrained on the ends. The loads were applied by using standard laboratory weights and the deflections measured by 0.0001 inch accuracy dials.

The laboratory test results are given in Appendix VI, and they are plotted in Figure 171. Study of this figure substantiates the

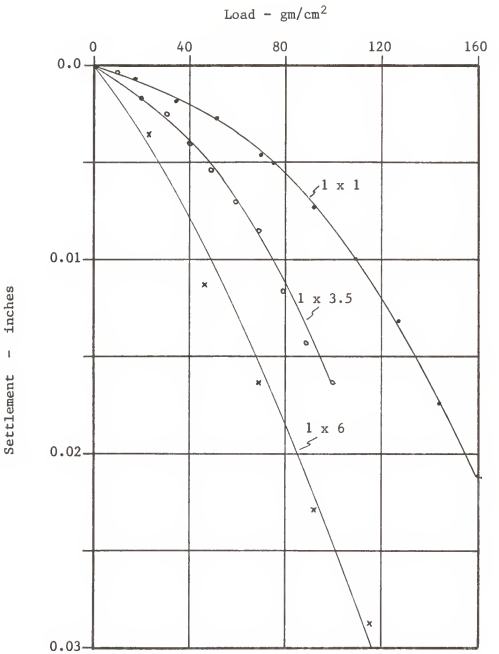


Figure 171. Results of Laboratory Model Footing Settlement Tests on Ottawa Sand

general conclusions that plane strain settlements should be greater than axisymmetric. In the model tests, the 1:6 footing settled approximately 3 times greater than the 1:1 footing. This compares with the linear settlement ratio of 2.7 for L/D = 10, but is less than the 4.3 ratio for true plane strain. The ratio of 3 is, of course, greater by a factor of 2 than the analytical nonlinear settlement results. The writer's recommendations in Figure 127 give plane strain to axisymmetric settlement ratios of approximately 1.5 to 1.7 which is analytically consistent with these results but might predict too low settlements for plane strain loading. Obviously a great deal more testing work and field data analysis are necessary to investigate further the nature of the plane strain to axisymmetric settlement ratio.

CHAPTER 7.0

CONCLUSIONS

In Chapter 1.0 it was stated that there were two major purposes of this study: (1) To determine analytically the factors involved in using the vertical strain distribution approach for settlement prediction in sands and how to determine the best vertical strain distribution; (2) To determine how the pressuremeter test can be best interpreted for use in using this vertical strain distribution approach. This summary will discuss the conclusions in these two areas.

Based on the analysis of the simplified vertical strain factor distribution approach for settlement prediction in sands, the following conclusions were evident:

(1) The concept of a simplified triangular strain factor distribution, as originally suggested by Schmertmann (1970), can be used as a reasonable approximation to the strain distribution beneath foundations, even when using a nonlinear stress-dependent modulus, typical of sands.

(2) The major factors affecting the peak strain influence factor values are Poisson's ratio and loading pressure. A simplified triangular strain influence factor distribution including equations for varying I_{zp} as a function of loading pressure, geometry, and sand density is given in Figure 127.

(3) For axisymmetric loading of sands, use a strain influence factor triangle with a depth of influence of 2D and a peak strain influence factor located at a depth D/2. The peak strain influence factor and surface intercept values for loose, medium dense, and dense sands are as given in Figure 127 (p. 223).

(4) For plane strain loading of sands, use a strain influence factor triangle with a depth of influence of 4D and a peak strain influence factor located at a depth 3D/4. The peak strain influence factor and surface intercept values for loose, medium dense, and dense sands are as given in Figure 127 (p. 223).

(5) For cases between the purely axisymmetric (L/D = 1) and the plane strain (L/D > 100) use a logarithmic interpolation for the depth of influence between 2D and 4D as well as for the peak strain values and locations. Thus for L/D = 10, use a depth of influence of 3D, thus giving a settlement in the middle between the L/D = 1 and the L/D = 100 cases. For other L/D ratios the engineer should use a logarithmic scale for determining a reasonable depth of influence as well as other parameters (see Section 4.8).

(6) Ignore the effect of increased lateral stresses on the strain influence factor distribution. The field modulus values will be affected, but not the strain influence factor values or distribution.

(7) When using the simplified strain factor distribution approach with rigid layers, use the appropriate strain

factor distribution triangle over the specific layer thickness. That is, use the dense sand I_z relations over the thickness of the dense sand and the loose or medium dense sand I_z relations over the thickness of the loose or medium dense sand layers.

(8) If the foundation is embedded, use the recommended strain factor distribution, only measured from the base of the foundation. Use the modulus values as indicated before the excavation. The load, p, should be that applied after the excavation, that is, the net load. For shallow embedment (between D/4 and D), reduce the constant C_i by 0.1 for both axisymmetric and plane strain loading.

(9) These recommendations give a ratio of plain strain settlement to axisymmetric settlement of 1.5 to 1.7 depending upon the loading pressure and sand density. These ratios are consistent with the analytical studies, but are low when compared to model tests (ratio of 3) or linear analyses (ratio of 4.3).

(10) When applied to relatively narrow footings (diameter or width less than 5 ft) these recommendations may predict too high a settlement, and the magnitude of the variation will depend upon Poisson's ratio, as indicated by the relative density.

In the interpretation of pressuremeter tests in general as well as specifically in sands, I reached the following conclusions.

(1) Because of edge effects, if a single cell finite probe is used, the ratio of the cell length to diameter should be a

minimum of 8 in order to keep the volume change measurements within 5 percent of those for an infinite cylinder (see Figure 12).

(2) Interpretation of the pressuremeter test using a linear elastic material is helpful, but completely unrealistic for application to granular soils.

(3) In a linear elastic material the elastic modulus as obtained from the slope of the pressure-volume curve was shown to be independent of (i) Poisson's ratio, (ii) the magnitude of the differential pressure, (iii) the depth or lateral stress, (iv) the unloading of the borehole, and (v) the unloading or reloading of the pressuremeter.

(4) Based on a linear elastic analysis, the pressuremeter test measures the horizontal elastic modulus when used in a linear cross-anisotropic material.

(5) Based on a linear elastic analysis, the effect of a smear zone of lower modulus is to give a lower slope modulus calculation. This slope modulus is a function of the width of the smear zone, with the value of the smear zone modulus as a lower limit (see Figures 140 and 141).

(6) The nonlinear stress-dependent analytical model developed by Duncan and Chang (1970) gives reasonable pressuremeter pressure-volume responses for sands.

(7) Study of the nonlinear stress-dependent analytical model indicates that the slope of the initial portion of an "undisturbed" pressure-volume curve gives the best indication of the initial in-situ tangent modulus, but

this is the most difficult portion of the pressure-volume curve to obtain in practical field testing.

(8) The slope of the nonlinear pressure-volume curve decreases, and thus the calculated modulus increases, for (i) increasing differential pressure, (ii) increasing Poisson's ratio, (iii) increasing lateral stresses, (iv) increasing nonlinear modulus numbers, (v) increasing depth, and (vi) increasing friction angle.

(9) The slope of the nonlinear pressure-volume curve increases, and thus the calculated modulus decreases, for the case of a lower nonlinear modulus material placed, in varying thickness, along the inner edge of the borehole.

(10) The initial low modulus region of a nonlinear pressure-volume curve can best be explained as being due to the reloading of an unloaded borehole. These studies do not show that the break point in such a curve necessarily occurs at the value of the horizontal in-situ pressure.

(11) The effect of borehole unloading and reloading is to decrease the slope of the pressure-volume curve and thus increase the calculated modulus. The slope modulus for this case is generally higher than the initial in-situ tangent modulus. This is essentially the modulus that is obtained from field testing.

(12) The modulus obtained from unloading and then reloading the pressuremeter is greater than the modulus obtained from the slope of the pressure-volume curve. The value of the average unload-reload modulus depends upon (i) the initial

unloading point on the pressure-volume curve, (ii) the value of the unloading pressure, and (iii) the analytical parameters and steps used. As in the case of borehole unloading, the analysis of the unload-reload procedure can give varying results depending upon the combinations of parameters previously discussed.

In the interpretation of pressuremeter tests with regard to predicting sand settlements, I reached the following conclusions.

(1) Theoretically the initial "undisturbed" pressuremeter slope modulus can be used in conjunction with the strain influence factor approach to predict sand settlements. However, this is very difficult to obtain practically.

(2) The analytical studies (assuming the proper analytical parameters can be determined) generally gave E_{PMT} values higher than the controlled laboratory tests. The general curve shapes compare favorably, but the precise calculations for the analytical studies yield higher results than for the laboratory tests. This could be because of the difficulty in determining the proper analytical parameters, or because of inaccuracies in trying to use elastic analyses and equations on a nonelastic particulate medium like sand.

(3) One reasonable modulus value to use from field pressuremeter test results is the relatively linear portion of the pressure-volume curve, which follows the reloading of the unloaded borehole. The analytical studies showed that this was generally higher than the initial in-situ

tangent modulus, which had been used as a basis for the simplified strain influence factor distributions.

(4) The unload-reload modulus obtained from pressuremeter tests appears promising for determining a more consistent elastic modulus since it gets away from some of the initial borehole disturbance. Much more extensive testing of this phenomenon in sands is needed to determine the many practical variables. This modulus value is greater than both the analytical initial in-situ tangent modulus and the slope of the pressure-volume curve modulus.

(5) Both the Ménard and the simplified settlement calculation approaches (Figures 13 and 127) gave reasonable settlement predictions when compared to results from two laboratory plate load tests. Using E_{cone} with the simplified strain factor approach was more reasonable than using E_{PMT} with this approach. The many possible reasons for these variations were discussed in Chapter 6.0.

CHAPTER 8.0

RECOMMENDATIONS FOR FURTHER RESEARCH

There are many areas of future research indicated by this study. These include:

1. In the area of hardware investigation, it appears that some future work might be profitable in understanding just precisely how the field pressuremeter is loading the soil. Although it is recognized that any field data cannot be as precisely determined as analytical techniques, the field data are the most important data for practical engineering purposes. An understanding of the precise nature of the field loading including the membrane expansion characteristics, initial volume and volume change precision, and other hardware factors is extremely important.

2. It is very important from this study that there must be developed a much clearer role of Poisson's ratio in soil mechanics' analyses. This problem is no doubt coupled with that of modeling a discontinuum. Engineers think generally in terms of the classic approach to stress-strain relations using Poisson's ratio. Perhaps an entirely different approach is needed for dilatant materials. The work being done in England (Schofield and Wroth, 1968) may be profitable for future work along these lines. It should be pointed out, however, that even if better and more sophisticated techniques are developed, these techniques will not be used unless they are

generally understood and put in practical form such that the practising engineer considers them a practical, useful technique.

3. In the laboratory it would be most informative to extend the plate bearing tests mentioned in this study and consider the many influences and chamber constraints on the plate bearing tests on sands. This should be profitable in the correlation of plate bearing, cone penetrometer, and pressuremeter test results. Additional sand triaxial and plane strain testing should be done in conjunction with these chamber tests to provide and develop additional correlations. If possible, some variable geometry plate settlement tests should also be conducted.

4. A more detailed finite element model could be constructed of the University of Florida sand testing chamber. This would provide a better and more specific capability in analyzing chamber tests. This would be more worthwhile as more and more chamber testing is done. Specifically the bottom piston displacement loading and the lateral confinement pressure steps might be included.

5. In addition to the further testing chamber comparisons between pressuremeter and cone modulus determinations, it is recommended that a careful experimental study of the unload-reload modulus be undertaken. Some factors that should be considered include (i) the starting point for the unloading, (ii) the value of the unloading pressure, and (iii) other chamber parameters including lateral pressures, density, etc.

6. In the area of analytical studies, there are three distinct problems which should be further investigated. One is the settlement

relations for the narrow plane strain and axisymmetric loadings, especially in the 2 to 3 foot diameter or width range. Of course, as three-dimensional models become more common, the relations between circumferential footing settlement compared to areal or mat type foundation settlements should also be studied. Another area which could be further pursued analytically is that of deep embedment, and determining recommendations for a more complete spectrum of embedment geometries. A third area for further study is that dealing with the effects of surface geometry. The writer feels that the depth of influence recommendations made in this study are reasonable. However, a three-dimensional analytical model would be of value in studying in more detail the effects of varying L/D ratios on footing settlements.

APPENDIX I

FORTRAN LISTING FOR SOLUTION OF TRANTER'S TWO-DIMENSIONAL DISPLACEMENT EQUATION

University of Florida
Department of Civil Engineering

TRANTER
April 1973

I. Identification: Fortran IV Computer Program for Solution of Displacements due to Localized Hydrostatic Pressure on Cylindrical Hole

II. Programmer: J.P. Hartman, University of Florida, 1972

III. Description: This Fortran IV computer program solves for the displacements due to the hydrostatic loading of a localized region inside a cylindrical hole. The original solution was presented by C.J. Tranter in 1946 ("On the Elastic Distortion of a Cylindrical Hole by a Localized Hydrostatic Pressure," Quarterly of Applied Mathematics, Vol. 4, No. 3, 1946, pp. 298-302). The program additionally obtains the ratio of the displacement at each point to that for an infinite cylinder under the same loading conditions. The weighted average displacement is calculated in order to get an indication of the volume of displacement.

IV. Data Input:

Heading Card (20A4):

Columns 1-80 contain any desired problem description

Data Card (8F10.0):

Columns	
1-10	ratio of half-loaded length to radius (c/r_i)
11-20	ratio of length over which calculations desired to half-loaded length (z/c)
21-30	Poisson's ratio
31-40	Modulus of Elasticity (Psf)
41-50	Pressure (Psf)
51-60	Radius of hole (Ft)
61-70	Number of increments of length over which calculations desired
71-80	Number of length increments in going from centerline to end of loaded length

V. Data Output:

For each step the program lists the c/r_i ratio, the z/c location, the value of the integral in the Tranter expression, the value of the displacement at that point in feet, and the ratio of that displacement to that of an infinite cylinder under the same loading conditions. At the end of each set of calculations it then lists the average displacement over the loaded length, both ignoring and then considering higher order algebraic terms.

```
C*************************************************************************
C TRANTER SOLUTION OF LOCALIZED HYOROSTATIC PRESSURE ON CYLINORICAL HOLE
C  * * * THIS CASE USES 0.05 INTEGRATION INCREMENTS * * *
C*************************************************************************
      REAL KOA,KOA2,K1A,K1A2
      OIMENSION HED(20),URU(30),URU1(30)
      OIMENSION Y(401),Z(401)
C*************************************************************************
  100 READ  (5,1000) HED,CA,ZCI,POIR,E,PR,R1,STEPS,OO
      WRITE (6,2000) HED,R1,PR,E,POIR
      FINK=(2.0*E)/((1.0-POIR)*PR)
      WRITE (6,2002)
      ZCI=0.0
      LENO=STEPS+1
      OELZC=(ZCE-ZCI)/STEPS
      OO 66 L=1,LENO
      IF(L-1) 6,5,6
    5 ZC=ZCI
      GO TO 7
    6 W=L-1
      ZC=W*OELZC+ZCI
C     ESTABLISH FUNCTION TABLE
    7 ALPHA=0.0001
      OO 55 K=1,401
      X=ALPHA
      N=0
      CALL BESK (X,N,BK,IER)
      KOA=BK
      KOA2=KOA*KOA
      N=1
      CALL BESK (X,N,BK,IER)
      K1A=BK
      K1A2=K1A*K1A
      FNUM=K1A2*SIN(CA*ALPHA)*COS(ZC*CA*ALPHA)
      OENOM=ALPHA*((ALPHA**2+2.0*(1.0-POIR))*K1A2-ALPHA**2*KOA2)
      Y(K)=FNUM/OENOM
      ALPHA=ALPHA+0.05
   55 CONTINUE
C     INTEGRATE TRANTER EXPRESSION
      H=0.05
      NOIN=401
      CALL QSF (H,Y,Z,NOIN)
      QUAO=Z(NOIN)
      RATIO=((1.0-POIR)*4.0*QUAO)/3.14159654
      UTR=(4.0*PR*R1*(1.0-POIR**2)*QUAO)/(E*3.14159654)
      IF (ZC-LE-1.0) GO TO 64
      IF (ZC-GT-1.0) GO TO 65
   64 URU(L)=RATIO
   65 WRITE (6,2001) CA,ZC,QUAO,UTR,RATIO
   66 CONTINUE
C     OBTAIN AVERAGE OISPLACEMENT RATIO
      LINO=OO+1.0
      OENUMP=2.0*OO
      URUSE=0.0
      OO 88  L=1,LINO
      URU1(L)=0.0
   88 CONTINUE
      OO 820  L=1,LINO
      IF (L.EQ.LINO) GO TO 813
      IF (L.GT.1) GO TO 812
      URU1(L)=URU(L)/OENUMP
      GO TO 814
  812 URU1(L)=(2.0*URU(L))/OENUMP
      GO TO 814
  813 URU1(L)=URU(L)/OENUMP
  814 URUSE=URUSE+URU1(L)
  820 CONTINUE
      UBET=URUSE*(URUSE+FINK)/(1.0+FINK)
      WRITE (6,2004) URUSE
      WRITE (6,2005) UBET
      WRITE (6,2003)
      GO TO 100
C*************************************************************************
 1000 FORMAT (20A4/8F10.0)
 2000 FORMAT (1H1 20A4//
     1 32H  INSIDE RADIUS IN FT ---------      F10.2/
     2 32H  PRESSURE IN PSF ---------------    F10.2/
     3 32H  ELASTIC MODULUS IN PSF ------      F10.2/
     4 32H  POISSONS RATIO ----------------    F10.2///)
 2001 FORMAT (2F10.2,2F12.8,1F10.3)
 2002 FORMAT (1H0,*      C/A         Z/C   INTEGRAL     UR(FT)        RATIO
     1 */)
 2003 FORMAT (1H1)
 2004 FORMAT (30H0AVERAGE OISPLACEMENT RATIO =       F10.3)
 2005 FORMAT (38H0BETTER AVERAGE OISPLACEMENT RATIO =       F10.3//)
C*************************************************************************
      END
C*************************************************************************
      SUBROUTINE BESK (X,N,BK,IER)
C*************************************************************************
      OIMENSION T(12)
      BK=0.0
      IF(N) 10,11,11
   10 IER=1
      RETURN
   11 IF(X) 12,12,20
   12 IER=2
      RETURN
   20 IF(X-170.0) 22,22,21
   21 IER=3
      RETURN
   22 IER=0
      IF(X-1.0) 36,36,25
   25 A=EXP(-X)
      B=1.0/X
```

```
      C=SQRT(B)
      T(1)=B
      DO 26 L=2,12
   26 T(L)=T(L-1)*B
      IF(N-1) 27,29,27
C     COMPUTE K0 USING POLYNOMIAL APPROXIMATION
   27 GO=A*(1.25331414+-.1566644*T(1)+.08811127*T(2)+-.09139095*T(3)
     2+.1344596*T(4)+-.2299853*T(5)+.3792497*T(6)+-.524727*T(7)
     3+.557536*T(8)+-.4262629*T(9)+.2184518*T(10)+-.066809*T(11)
     4+.0091893*T(12))*C
      IF(N) 20,28,29
   28 BK=GO
      RETURN
C     COMPUTE K1 USING POLYNOMIAL APPROXIMATION
   29 G1=A*(1.253314+.4659927*T(1)+-.1468584*T(2)+.1280426*T(3)
     2+-.1736431*T(4)+.2847618*T(5)+-.4594362*T(6)+.628338*T(7)
     3+-.663229*T(8)+.5050238*T(9)+-.2581303*T(10)+.0788001*T(11)
     4+-.0108*T(12))*C
      IF(N-1) 20,30,31
   30 BK=G1
      RETURN
C     FROM K0,K1 COMPUTE KN USING RECURRENCE RELATION
   31 DO 35 J=2,N
      GJ=2.0*(FLOAT(J)-1.0)*G1/X+GO
      IF(GJ-1.0E30) 33,33,32
   32 IER=4
      GO TO 34
   33 GO=G1
   35 G1=GJ
   34 BK=GJ
      RETURN
   36 B=X/2.0
      A=0.57721566+ALOG(B)
      C=B*B
      IF(N-1) 37,43,37
C     COMPUTE K0 USING SERIES EXPANSION
   37 GO=-A
      X2J=1.0
      FACT=1.0
      HJ=0.0
      DO 40 J=1,16
      RJ=1.0/FLOAT(J)
      X2J=X2J*C
      FACT=FACT*RJ*RJ
      HJ=HJ+RJ
   40 GO=GO+X2J*FACT*(HJ-A)
      IF(N) 43,42,43
   42 BK=GO
      RETURN
C     COMPUTE K1 USING SERIES EXPANSION
   43 X2J=B
      FACT=1.0
      HJ=1.0
      G1=1.0/X+X2J*(0.5+A-HJ)
      DO 50 J=2,8
      X2J=X2J*C
      RJ=1.0/FLOAT(J)
      FACT=FACT*RJ*RJ
      HJ=HJ+RJ
   50 G1=G1+X2J*FACT*(0.5+(A-HJ)*FLOAT(J))
      IF(N-1) 31,52,31
   52 BK=G1
      RETURN
C*******************************************************************
      SUBROUTINE QSF (H,Y,Z,NO1M)
C*******************************************************************
      DIMENSION Y(401),Z(401)
      HT=0.33333333333*H
      SUM1=Y(2)+Y(2)
      SUM1=SUM1+SUM1
      SUM1=HT*(Y(1)+SUM1+Y(3))
      AUX1=Y(4)+Y(4)
      AUX1=AUX1+AUX1
      AUX1=SUM1+HT*(Y(3)+AUX1+Y(5))
      AUX2=HT*(Y(1)+3.875*(Y(2)+Y(5))+2.625*(Y(3)+Y(4))+Y(6))
      SUM2=Y(5)+Y(5)
      SUM2=SUM2+SUM2
      SUM2=AUX2+HT*(Y(4)+SUM2+Y(6))
      Z(1)=0.0
      AUX=Y(3)+Y(3)
      AUX=AUX+AUX
      Z(2)=SUM2-HT*(Y(2)+AUX+Y(4))
      Z(3)=SUM1
      Z(4)=SUM2
C     INTEGRATION LOOP
      DO 4 I=7,NO1M,2
      SUM1=AUX1
      SUM2=AUX2
      AUX1=Y(I-1)+Y(I-1)
      AUX1=AUX1+AUX1
      AUX1=SUM1+HT*(Y(I-2)+AUX1+Y(I))
      Z(I-2)=SUM1
      IF(I-NO1M)3,6,6
    3 AUX2=Y(I)+Y(I)
      AUX2=AUX2+AUX2
      AUX2=SUM2+HT*(Y(I-1)+AUX2+Y(I+1))
    4 Z(I-1)=SUM2
      Z(NO1M-1)=AUX1
      Z(NO1M)=AUX2
      RETURN
    6 Z(NO1M-1)=SUM2
      Z(NO1M)=AUX1
      RETURN
      END
C*******************************************************************
```

APPENDIX II

FORTRAN LISTING FOR FINITE ELEMENT STRAIN STUDY PROGRAM (SOILSTRN)

University of Florida
Department of Civil Engineering

SOILSTRN
December 1972

I. Identification: Finite Element Computer Program for Solution of Axisymmetric and Plane Strain Stress-Deformation Problems in Cross-Anisotropic Soils

II. Programmers: E.L. Wilson, University of California, 1966
J.M. Duncan, University of California, 1968
J.P. Hartman, University of Florida, 1971-72

III. Description: This Fortran IV finite element computer program, which consists of a main program and 8 subroutines, was written by E.L. Wilson. Modifications were made by J.M. Duncan to (1) generate element and nodal point data automatically for systems consisting of elements bounded entirely by horizontal and vertical lines; (2) calculate gravity stresses; and (3) solve problems involving stress-dependent modulus values in a series of steps, applying part of the load in each step.

J.P. Hartman made additional modifications to (1) use cross-anisotropic stress-dependent modulus values; (2) allow for the unloading of a rectangular segment of material (symmetrical about the centerline) using unloaded gravity stresses and unloading moduli; (3) allow for the subsequent reloading of material placed in the excavation; and (4) calculate the percent strain vertically down the centerline and the 4 adjacent columns for each pressure increment.

IV. Data Input:

Heading Card (20A4):

Columns 1-80 contain any desired problem description

Control Card I (8I10):

Columns 1-10	Number of nodal points (600 maximum)
11-20	Number of elements (550 maximum)
21-30	Number of materials (10 maximum)
31-40	Number of boundary pressure cards (20 maximum)
41-50	Number of approximations
51-60	Number of specified boundary displacements (NBC)
61-70	Number of specified element materials (NEC)

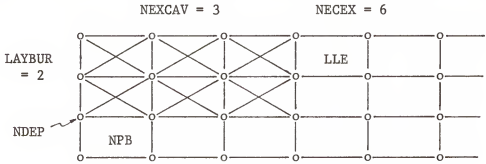
Control Card II (2I10,6F10.0):

Columns 1-10	0 for axisymmetric analysis; 1 for plane strain
11-20	0 for using minor principal stresses 1 for using octahedral stresses
21-30	0.0 for using failure modulus in failed elements 1.0 for using bulk modulus in failed elements
31-40	0.0 for right hand vertical boundary on rollers 1.0 for right hand vertical boundary free

Control Card III (8I10): (See sketch below)

Columns 1-10 Number of element at the centerline beneath the excavation (NPB)
11-20 Number of nodal point at the centerline beneath the excavation (NDEP)
21-30 Number of layers excavated (LAYBUR)
31-40 Number of columns excavated (NEXCAV)
41-50 Number of element at the surface adjacent to the excavation (LLE)
51-60 Total number of elements excavated (NECEX)
61-70 Total number of elements to be placed into the excavation (NFCAR)
71-80 Number of nodal points with changed support condition at side of footing (NFRIC)

NOTE: If there is no unloading, the 8 columns should all be zeros.



Loaded Area Card (8F10.0):

Columns 1-10 Axisymmetric: Radius of loaded area
Plane Strain: Half-width of loaded area
11-20 Loading Pressure

Material Property Cards:

First Card - One for each material (I10,7F10.0)

Columns 1-10 Material number
11-20 Unit weight
21-30 Lateral coefficient of earth pressure
31-40 COAD (MTYPE)
COAD = 0.0 for materials for which $E_i = K(\sigma)^n$ (where $\sigma = \sigma_3$ or σ_{oct} - this is for drained conditions in sand or clay).
COAD = 1.0 for materials for which E_i = (Consolidation Pressure)^n - (this is undrained clays).
COAD = 2.0 for constant modulus materials
41-50 Consolidation pressure - required only for COAD = 1.0 - otherwise 0.0.

Second Card - Vertical Properties - One for each material (8E10.3):

Columns	1-10	Cohesion, c
	11-20	Angle of Friction, ϕ, in degrees
	21-30	Failure Ratio, R_f
	31-40 K, 41-50 n	where $E_i = K(\sigma)^n$
	51-60	Modulus value after failure
	61-70	Tangent Poisson ratio factor, G
	71-80	Poisson ratio factor F

Third Card - Vertical Properties (continued) - (8E10.3):

Columns	1-10	Poisson ratio factor j
	11-20	Tensile strength of the material
	21-30	K_{ur} for unloading and reloading soils

Fourth Card - Horizontal Properties - One for each material (8E10.3):

Identical to Second Card (above) only for the horizontal properties.

Fifth Card - Horizontal Properties (continued) - (8E10.3):

Identical to Third Card (above) only for the horizontal properties.

Pressure Boundary Cards (2I10,6F10.0):

Columns	1-10	First nodal point (I)
	11-20	Second nodal point (J)
	21-30	Pressure on boundary between

Cards are required for each boundary loaded (20 maximum). The boundary loaded should be at the left when proceeding from the first nodal point to the second.



Plate, Column, and Row Card (4I10,4F10.0):

Columns	1-10	Number of elements in plate on surface
	11-20	Number of columns of elements
	21-30	Number of rows of elements including plate
	31-40	Number of nodal point at centerline right at buried plate-soil interface (NSIG) - buried plate analysis.
	41-50	Vertical gravity stress at top boundary of rectangular grid (SIGDEP) - used for buried plate analysis.
	51-60	Radius of buried plate

Circumferential Element Boundary Cards (I10,7F10.0):

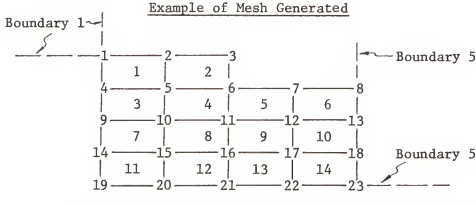
Columns 1-10 Boundary number (increases out)
11-20 Radial distance to boundary (increases out)

Horizontal Element Boundary Cards (2I10,6F10.0):

Columns 1-10 Boundary number (increases down)
11-20 Number of material below boundary
21-30 Elevation of boundary (increases up)

NOTE: The first and last boundaries must be specified. Intermediate boundaries, if omitted, will be generated at equal intervals between those specified.

Example of Mesh Generated



Number of nodal points = 23; Number of elements = 14

Number of elements in plate = 2; Number of columns of elements = 4; Number of rows of elements = 4

Individual Nodal Point Cards (I10,7F10.0):

Columns 1-10 Nodal point number
11-20 Code (0.0, 1.0, 2.0, or 3.0 - see below)
21-30 UR
31-40 UZ
Loads or displacements - see below

NBC cards are required. The purpose of these cards is to provide greater flexibility to the program, permitting alteration of the boundary conditions while retaining the mesh generation feature.

Code	UR	UZ	Condition
0.0	Radial load	Axial Load	Free
1.0	Radial displacement	Axial load	
2.0	Radial load	Axial displacement	
3.0	Radial displacement	Axial displacement	Hinged

Individual Element Cards (2I10,6F10.0):

Columns		
1-10	Element number
11-20	Material number
21-30	Vertical gravity stress at center of element
31-40	Horizontal stress at center of element
41-50	Vertical stress at center of element
51-60	Horizontal stress at center of element
61-70	Horizontal (and vertical) shear stress at center of element

NEC cards are required. The purpose of these cards is to provide greater flexibility to the program, permitting the change of material type for individual elements. Otherwise, all elements in any row will have the same material.

Excavation Material Cards (2I10,6F10.0): (For unloading only)

Columns	
1-10	Element number
11-20	Material number - usually use air
21-30	0.0
31-40	0.0
41-50	0.0
51-60	0.0
61-70	0.0

NECEX cards are required.

Placing Footing in Excavation Cards (2I10,6F10.0):

Columns	
1-10	Element number
11-20	Material number - typically concrete
21-30	0.0
31-40	0.0
41-50	0.0
51-60	0.0
61-70	0.0

NFCAR cards are required.

Change of Footing Edge Boundary Condition Cards (I10,7F10.0):

Columns	
1-10	Nodal point number
11-20	Code (0.0, 1.0, 2.0, or 3.0)
21-30	UR
31-40	UZ

NFRIC cards are required. This enables one to change the boundary conditions on the footing after it has been placed into the excavation - if desired.

V. Data Output

The program output is quite complete and gives the following information for each step in the successive approximation technique:

(1) Displacement at each nodal point.

(2) Percent strain calculations down the centerline and down 4 adjacent nodal point columns.

(3) Element number and center coordinates (r,z) or (x,z).

(4) Vertical and horizontal moduli of elasticity and Poisson's ratios used for each element.

(5) The values of the following stresses for the center of each element:

Axisymmetric: σ_r σ_z τ_{rz} $\sigma_{1_{rz}}$ $\sigma_{3_{rz}}$ τ_{max} σ_θ

Plane Strain: σ_x σ_z τ_{xz} σ_1 σ_3 τ_{max} σ_y

(6) The value of the angle α to the critical plane and the ratio of σ_1 to σ_3.

```
C*****************************************************************
C
C  AXISYMMETRIC OR PLANE STRAIN LOADING OF ANISOTROPIC SOIL
C
C*****************************************************************
      COMMON/INTGR/NUMNP,NUMEL,NUMMAT,NUMPC,NP,IBC(20),JBC(20),NPLATE,
     1 NUMCOL,NUMROW,IX(550,5),NEQ(20),NPP1,NPP2,NPB,MTYPE,NSTEP,NDEP,
     2 NUNLOO,IBCE(20),JBCE(20),LAYBEN,NSIG,SIGDEP,RPLATE
      COMMON/PROP/MATYP(34),E(11,10),RO(10),AKO(10),EE(7),ET(11),
     1 COA(10),CP(10),EH(11,10),EV(7),ETH(11)
      COMMON/LOAD/CODE(600),PR(20),ANGLE(4),PRE(20)
      COMMON/GEOM/R(600),Z(600),UR(600),UZ(600),DISP(600,2),
     1 RADIST(25),ELEV(34)
      COMMON/STRSS/SIGMA(4,550),SIG(11),PZERO,RZERO,GSTRSS(550)
      COMMON/BULK/ESVB(550),ESHR(550),POHB(550),POVB(550),BLK
      COMMON/PLOCT/NPP,NOCT
      COMMON /ARG/ RR9(5),ZZZ(5),S(10,10),P(10),TT(4),LM(4),DO(3,3),
     1 HH(6,10),RR(4),ZZ(4),C(4,4),H(6,10),D(6,6),F(6,10),TP(6),XI(10)
      COMMON /BANARG/ MBAND,NUMBLK,B(108),A(108,54)
C*****************************************************************
C     READ AND PRINT OF CONTROL INFORMATION AND MATERIAL PROPERTIES
C*****************************************************************
   50 READ  (5,1000) MED,NUMNP,NUMEL,NUMMAT,NUMPC,NP,NRC,NEC
      WRITE (6,2000) MED,NUMNP,NUMEL,NUMMAT,NUMPC,NP,NRC,NEC
      READ  (5,1001) NPP,NOCT,BLK,RIFREE
      READ  (5,1003) NPB,NDEP,LAYBUR,NEXCAV,LLE,NECEX,NFCAR,NFRIC
      APP=NP
      STOP=0.0
C*****************************************************************
C     READ AND PRINT OF RADIUS AND PRESSURE
C*****************************************************************
      READ  (5,1005) RZERO,PZERO
      WRITE (6,2012) RZERO,PZERO
      PZERO=PZERO/APP
C*****************************************************************
C     READ AND PRINT MATERIAL PROPERTY VALUES
C*****************************************************************
      IF (BLK.EQ.0.0) WRITE (6,2042)
      IF (BLK.GT.0.0) WRITE (6,2043)
      IF (NOCT) 65,64,65
   65 WRITE (6,2034)
      GO TO 53
   64 WRITE (6,2035)
   53 IF (NPP) 55,54,55
   55 WRITE (6,2029)
      GO TO 57
   54 WRITE (6,2030)
   57 WRITE (6,2033)
   56 DO 59 M=1,NUMMAT
      READ  (5,1002) MTYPE,RO(MTYPE),AKO(MTYPE),COA(MTYPE),CP(MTYPE)
      WRITE (6,2011) MTYPE,RO(MTYPE),AKO(MTYPE),COA(MTYPE),CP(MTYPE)
      READ  (5,1007)  (EJ,MTYPE),J=1,11)
      WRITE (6,2010)
      WRITE (6,2015)  (E(J,MTYPE),J=1,11)
      READ  (5,1007) (EH(J,MTYPE),J=1,11)
      WRITE (6,2010)
      WRITE (6,2015) (EH(J,MTYPE),J=1,11)
   59 CONTINUE
C*****************************************************************
C     READ AND PRINT PRESSURE BOUNDARY CONDITIONS
C*****************************************************************
      IF (NUMPC) 290,310,290
  290 WRITE (6,2005)
      DO 300 L=1,NUMPC
      READ  (5,1001) IBC(L),JBC(L),PR(L)
      WRITE (6,2007) IBC(L),JBC(L),PR(L)
  300 PR(L)=PR(L)/APP
  310 CONTINUE
C*****************************************************************
C     READ POSITIONS OF BOUNDARIES BETWEEN ELEMENTS
C*****************************************************************
      WRITE (6,2004)
      READ  (5,1009) NPLATE,NUMCOL,NUMROW,NSIG,SIGDEP,RPLATE
      L=0
  101 READ  (5,1002) N,RADIST(N)
      DELTN=N-L
      DELTR=(RADIST(N)-RADIST(L))/DELTN
  102 L=L+1
      IF (L.EQ.NUMCOL+1) GO TO 103
      IF (L.EQ.N) GO TO 101
      RADIST(L)=RADIST(L-1)+DELTR
      GO TO 102
  103 L=0
  104 READ  (5,1001) N,MATYP(N),ELEV(N)
      DELTN=N-L
      DELTE=(ELEV(N)-ELEV(L))/DELTN
  105 L=L+1
      IF (L.EQ.NUMROW+1) GO TO 106
      IF (L.EQ.N) GO TO 104
      ELEV(L)=ELEV(L-1)+DELTEL
      MATYP(L)=MATYP(L-1)
      GO TO 105
C*****************************************************************
C     GENERATE NODAL POINT DATA
C*****************************************************************
  106 NCP1=NUMCOL+1
      NRP1=NUMROW+1
      NPP1=NPLATE+1
      NPPP=NPP1+1
      NCOL=0
      NROW=0
      DO 107 N=1,NUMNP
      NCOL=NCOL+1
      NROW=NROW+1
      CODE(N)=0.0
      IF (NCOL.EQ.NCP1) CODE(N)=1.0
      IF (NCOL.EQ.NCP1.AND.RIFREE.GT.0.0) CODE(N)=0.0
      IF (NROW.EQ.1.AND.SIGDEP.EQ.0.0) CODE(N)=0.0
      IF (NROW.EQ.2.AND.SIGDEP.NE.0.0) CODE(N)=2.0
      IF (NCOL.EQ.1.AND.SIGDEP.NE.0.0) CODE(N)=0.0
      IF (NROW.EQ.NRP1) CODE(N)=3.0
      R(N)=RADIST(NCOL)
      Z(N)=ELEV(NROW)
      UR(N)=0.0
      UZ(N)=0.0
      IF (NCOL.LT.NCP1) NROW=NROW-1
      IF (N.EQ.NPP1.AND.N.GT.1) NROW=NROW+1
      IF (NCOL.EQ.NCP1) NCOL=0
```

```
      IF (N.EQ.NPP1.AND.N.GT.1) NCOL=0
  107 CONTINUE
      IF(NBC.EQ.0) GO TO 5000
      DO 108 N=1,NBC
      READ(5,1006) NPN,CODE(NPN),UR(NPN),UZ(NPN)
  108 CONTINUE
 5000 DO 109 N=1,NUMNP
      WRITE (6,2002) N,CODE(N),R(N),Z(N),UR(N),UZ(N)
  109 CONTINUE
C*****************************************************************
C     GENERATE ELEMENT DATA
C*****************************************************************
      WRITE (6,2013)
      NROW=0
      NCOL=0
      DO 100 N=1,NUMEL
      NCOL=NCOL+1
      NROW=NROW+1
      IX(N,1)=N+NROW-1
      IX(N,2)=IX(N,1)+NUMCOL+1
      IF (N.LE.NPLATE) IX(N,2)=IX(N,1)+NPLATE+1
      IX(N,3)=IX(N,2)+1
      IX(N,4)=IX(N,1)+1
      IX(N,5)=MATYP(NROW)
      IF(NCOL.LT.NUMCOL) NROW=NROW-1
      IF (N.EQ.NPLATE) NROW=NROW+1
      IF(NCOL.EQ.NUMCOL) NCOL=0
      IF (N.EQ.NPLATE) NCOL=0
  100 CONTINUE
      DO 111 N=1,NUMEL
  111 WRITE (6,2003) N,(IX(N,I),I=1,5)
C*****************************************************************
C     PRINT NODAL POINT AND ELEMENT MESH
C*****************************************************************
      WRITE (6,2020)
      IF (NPLATE) 113,114,113
  113 WRITE (6,2018) (ND,ND=1,NPP1)
      WRITE (6,2019) (NE,NE=1,NPLATE)
      NRW=NUMROW-1
      NFNP=NPP2
      NFE=NPP1
      GO TO 115
  114 NRW=NUMROW
      NFNP=1
      NFE=1
  115 DO 116 N=1,NRW
      NLNP=NFNP+NUMCOL
      NLE=NFE+NUMCOL-1
      WRITE (6,2018) (ND,ND=NFNP,NLNP)
      WRITE (6,2019) (NE,NE=NFE,NLE)
      NFNP=NLNP+1
      NFE=NLE+1
  116 CONTINUE
      NFNP=NUMNP-NUMCOL
      WRITE (6,2018) (ND,ND=NFNP,NUMNP)
C*****************************************************************
C     DETERMINE BAND WIDTH
C*****************************************************************
      J=0
      DO 340 N=1,NUMEL
      DO 340 I=1,4
      DO 325 L=1,4
      KK=IABS(IX(N,I)-IX(N,L))
      IF (KK-J) 325,325,320
  320 J=KK
  325 CONTINUE
  340 CONTINUE
      MBAND=2*J+2
      WRITE (6,2023)  MBAND
C*****************************************************************
C     INITIALIZE DISPLACEMENTS AND STRESSES IN PLATE
C*****************************************************************
      DO 3 N=1,NUMNP
      DO 3 I=1,2
      DISP(N,I)=0.0
    3 CONTINUE
      IF(NPLATE.EQ.0) GO TO 7
      DO 4 N=1,NPLATE
      GSTRSS(N)=0.0
      DO 4 I=1,4
      SIGMA(I,N)=0.0
    4 CONTINUE
    7 CONTINUE
C*****************************************************************
C     CALCULATE GRAVITY STRESSES FOR A LAYER
C*****************************************************************
      NLMAX=NUMEL-NUMCOL+1
      DO 6 NL=NPP1,NLMAX,NUMCOL
      IL=IX(NL,1)
      JL=IX(NL,2)
      MTYPE=IX(NL,5)
      IF(NL.EQ.NPP1) GSTRSS(NL) =0.5*(RO(MTYPE))*(Z(IL)-Z(JL)) + SIGDEP
      NBFOR=NL-NUMCOL
      IF(NBFOR.LE.0) GO TO 5
      ILL=IX(NBFOR,1)
      MTYPEE=IX(NBFOR,5)
      IF(NL.GT.NPP1) GSTRSS(NL)=GSTRSS(NBFOR)+(0.5*(RO(MTYPE))
     1 *(Z(ILL)-Z(IL)))+(0.5*(RO(MTYPEE))*(Z(IL)-Z(JL)))
    5 NP=NL+NUMCOL-1
C*****************************************************************
C     SET GRAVITY STRESSES EQUAL FOR ALL ELEMENTS IN LAYER
C*****************************************************************
      DO 6 N=NL,NP
      GSTRSS(N)=GSTRSS(NL)
    6 CONTINUE
      IF(NEC.EQ.0) GO TO 5001
      DO 110 N=1,NEC
      READ  (5,1001) NEL,IX(NEL,5),GSTRSS(NEL),(SIGMA(I,NEL),I=1,4)
  110 CONTINUE
 5001 WRITE (6,1997)
      WRITE (6,1998)
      DO 20 N=NPP1,NUMEL
      MTYPE=IX(N,5)
      GSZ=GSTRSS(N)
      GSR=GSZ*AKO(MTYPE)
      GST=GSR
      GSRZ=0.0
      WRITE (6,1999) N,GSR,GSZ,GST,GSRZ
```

```
   20 CONTINUE
      IF(SIGDEP,NE,0,0) GO TO 459
      IF(NPR,EQ,0) GO TO 999
C     SET MATERIAL IN EXCAVATION TO AIR
      NSTEP=0
      NUNLDO=I
      DO 88  L=I,+NECEX
      READ  (5,1001) NLK,IX(NLK+5),+GSTRSS(NLK),+(SIGMA(I,+NLK),I=I,+4)
   88 CONTINUE
C*****************************************************************
C     DETERMINE THE UNLDAOING PRESSURES
C*****************************************************************
      PRELB=0,0
      DO 455  LLL=1,+LAYBUR
      IBCE(LLL) = IX(LLE,1)
      ILE = IX(LLE,1)
      JBCE(LLL) = IX(LLE,2)
      JLE = IX(LLE,2)
      MTYPE = IX(LLE,5)
      PRE(LLL) = -0,5*(AKD(MTYPE))*(RD(MTYPE))*(Z(ILE)-Z(JLE)) - PRELB
      PRELB = (AKD(MTYPE))*(RD(MTYPE))*(Z(ILE)-Z(JLE)) + PRELB
      LLE=LLE+NUMCDL
  455 CONTINUE
      LAYB1=LAYBUR+1
      LAYBEN=LAYBUR+NEXCAV
      LLE=LLE-1
      DO 456  LLL=LAYB1,+LAYBEN
      IBCE(LLL) = IX(LLE,4)
      ILE = IX(LLE,4)
      JBCE(LLL) = IX(LLE,1)
      JLE = IX(LLE,1)
      MTYPE = IX(LLE,5)
      PRE(LLL) = -(RO(MTYPE))*(Z(I)-Z(ILE))
      LLE=LLE-1
  456 CONTINUE
      WRITE (6,2024)
      DO 458  NN=1,+LAYBEN
      WRITE (6,2007) IBCE(NN),+JBCE(NN),+PRE(NN)
  458 CONTINUE
C     SET INITIAL STRESSES EQUAL TO GRAVITY STRESSES
  459 DO 21 N=NPP1,+NUMEL
      MTYPE=IX(N,5)
      SIGMA(2,+N)=GSTRSS(N)
      SIGMA(1,+N)=GSTRSS(N)*AKD(MTYPE)
      SIGMA(3,+N)=SIGMA(1,+N)
      SIGMA(4,+N)=0,0
   21 CONTINUE
      IF(SIGDEP,NE,0,0) GO TO 474
C*****************************************************************
C     UNLOAD EXCAVATION
C*****************************************************************
C     FORM STIFFNESS MATRIX
      CALL STIFF
C     SOLVE FOR DISPLACEMENTS
      CALL BANSOL
      WRITE (6,2025)
      WRITE (6,2022)
      DO 32 N=I,+NUMNP
      DISP(N,1)=DISP(N,1)+B(2*N-1)
      DISP(N,2)=DISP(N,2)+B(2*N)
      WRITE (6,2006) N,+DISP(N,1),+DISP(N,2)
   32 CONTINUE
C     STRAIN CALCULATIONS IN PERCENT
      WRITE (6,2025)
      WRITE (6,2008)
      WRITE (6,2016)
      NEND=NUMNP-2*NUMCDL-1
      NCTR=NUMCDL+1
      IF( NPLATE,EQ,0) NPP2=1
      NSEN=NPP2+4
      NSTR=NPP2
      NST1=NSTR
      DO 468  L=NSTR,+NSEND
      DO 467 N=NST1,+NEND,+NCTR
      NNEX=N+NCTR
      DIFDIS=-(DISP(NNEX,2)-DISP(N,2))
      OENDIS=Z(N)-Z(NNEX)
      PERSTR=100,0*(DIFDIS/OENDIS)
      WRITE (6,1008)  N,+NNEX,+PERSTR
      IF (PERSTR,GT,20,0)  STOP=1,0
  467 CONTINUE
      NST1=NST1+1
      NEND = NEND + 1
      WRITE (6,2026)
  468 CONTINUE
C     COMPUTE STRESSES
      CALL STRESS
C     RE-INITIALIZE DISPLACEMENTS
      DO 6000  N=1,+NUMNP
      DO 6000  I=1,2
      DISP(N,I)=0,0
 6000 CONTINUE
      IF (STOP) 77,+78,+77
   77 CALL EXIT
C     PUT MATERIAL INTO THE EXCAVATION
   78 DO 85  L=I,+NFCAR
      READ  (5,+1001) KLN,+IX(KLN,5),+GSTRSS(KLN),+(SIGMA(I,+KLN),+I=I,+4)
   85 CONTINUE
C     CHANGE BOUNDARY CONDITIONS NEAR FOOTING
      IF(NFRIC,EQ,0)  WRITE (6,+2027)
      IF(NFRIC,EQ,0) GO TO 474
      WRITE (6,+2028)
      DO 473  L=1,+NFRIC
      READ  (5,+1006) NBF,+CDOE(NBF),+UR(NBF),+UZ(NBF)
  473 CONTINUE
C     CALCULATE APPROXIMATE LOAD STRESSES
  474 IF(SIGDEP,NE,0,0) NPR=NSIG
      IF(SIGDEP,NE,0,0) NOEP=IX(NSIG+1)
      IF(SIGDEP,NE,0,0) PZERO=((RZERO**2)/(RPLATE**2))*PZERO
      IF(SIGDEP,NE,0,0) RZERO=RPLATE
      DO 13 N=NNP8,+NUMEL
      IK=IX(N,1)
      KK=IX(N,3)
      MTYPE=IX(N,5)
      ZDIST=Z(NNEP)-((Z(IK)+Z(KK))/2,0)
      RDIST=(R(IK)+R(KK))/2,0
      SFACT=(RZERO**2)/((RZERO+ZDIST)**2)
      IF(ZDIST,LT,(RDIST-RZERO)) SFACTR=0,0
```

```
      S1GMA(2,N)=PZERO*SFACTR+S1GMA(2,N)
      S1GMA(1,N)=PZERO*SFACTR*AKO(MTYPE)+S1GMA(1,N)
      IF (NPP) 367,368,367
  367 S1GMA(3,N)= 0.48*(S1GMA(1,N)+S1GMA(2,N))+S1GMA(3,N)
   13 CONTINUE
      WRITE (6,1996)
      WRITE (6,1998)
      DO 17 N=NPP1,NUMEL
      WRITE (6,1999) N,(S1GMA(I,N),I=1,4)
   17 CONTINUE
      GO TO 777
C*****************************************************************
C     CALCULATE APPROXIMATE LOAD STRESSES
C*****************************************************************
  999 DO 10 N=NPP1,NUMEL
      IK=IX(N,1)
      KK=IX(N,3)
      MTYPE=IX(N,5)
      ZD1ST=Z(NPP2)-((Z(IK)+Z(KK))/2.0)
      RD1ST=(R(IK)+R(KK))/2.0
      SFACTR=(RZERO**2)/((RZERO+ZD1ST)**2)
      IF(ZD1ST.LT.(RD1ST-RZERO)) SFACTR=0.0
      S1GMA(2,N)=PZERO*SFACTR
      S1GMA(1,N)=S1GMA(2,N)*AKO(MTYPE)
      IF (NPP) 357,358,357
  357 S1GMA(3,N)= 0.48*(S1GMA(1,N)+S1GMA(2,N))
      GO TO 8
  358 S1GMA(3,N)=S1GMA(1,N)
    8 S1GMA(4,N)=0.0
   10 CONTINUE
      WRITE (6,1996)
      WRITE (6,1998)
      DO 11 N=NPP1,NUMEL
      WRITE (6,1999) N,(S1GMA(I,N),I=1,4)
   11 CONTINUE
C*****************************************************************
C     ADD GRAVITY STRESSES TO LOAD STRESSES
C*****************************************************************
      DO 30 N=NPP1,NUMEL
      MTYPE=IX(N,5)
      S1GMA(2,N)=S1GMA(2,N)+GSTRSS(N)
      S1GMA(1,N)=S1GMA(1,N)+GSTRSS(N)*AKO(MTYPE)
      IF (NPP) 377,378,377
  377 S1GMA(3,N)=S1GMA(3,N)+GSTRSS(N)*AKO(MTYPE)
      GO TO 30
  378 S1GMA(3,N)=S1GMA(1,N)
   30 CONTINUE
C*****************************************************************
C     SOLVE NON-LINEAR STRUCTURE BY SUCCESSIVE APPROXIMATIONS
C*****************************************************************
  777 NUNLOD=0
      NSTEP=1
      DO 500 NNN=1,NP
      PUSE=NNN*PZERO
C     FORM STIFFNESS MATRIX
      CALL STIFF
C     SOLVE FOR DISPLACEMENTS
      CALL BANSOL
      WRITE (6,2014) NSTEP
      WRITE (6,2022)
      DO 31 N=1,NUMNP
      D1SP(N,1)=D1SP(N,1)+B(2*N-1)
      D1SP(N,2)=D1SP(N,2)+B(2*N)
      WRITE (6,2006) N,D1SP(N,1),D1SP(N,2)
   31 CONTINUE
C     STRAIN CALCULATIONS IN PERCENT
      WRITE (6,2014) NSTEP
      WRITE (6,2008)
      WRITE (6,2016)
      NEND=NUMNP-2*NUMCOL-1
      NCTR=NUMCOL-1
      IF( NPLATE.EQ.0) NPP2=1
      NSTR=NPP2
      NSEND=NPP2+4
      NST1=NSTR
      DO 401  L=NSTR,NSEND
      DO 400 N=NST1,NEND,NCTR
      NNEX=N+NCTR
      D1FD1S=(D1SP(NNEX,2)-D1SP(N,2))
      DEND1S=Z(N)-Z(NNEX)
      PERSTR=100.0*(D1FD1S/DENDIS)
      IF (NPLATE.GT.0) 1I=NPP2
      IF (NPLATE.EQ.0) 1I=1
      HD1S=Z(1I)-((Z(N)+Z(NNEX))/2.0)
      NKJ=NPP1+(NUMROW-((NEND+NUMCOL+1-N)/NCTR)-1)*NUMCOL
      MTYPE=IX(NKJ,5)
      POWR=F(5,MTYPE)
      E1I=E(4,MTYPE)*(AKO(MTYPE)*RO(MTYPE)*HDIS)**POWR
      PHI=E(2,MTYPE)/57.28
      RENUM=E(3,MTYPE)*(1.0-S1N(PH1))*(1.0-AKO(MTYPE))*RO(MTYPE)*HD1S
      DE=2.*E(1,MTYPE)*COS(PH1)+2.*AKO(MTYPE)*S1N(PH1)*RO(MTYPE)*HD1S
      ET1=(1.0-(RENUM/DE))**2.0*E1I
      CORR=((2.0*AKO(MTYPE)+1.0)/(3.0*AKO(MTYPE)))**POWR
      IF (NOCT.GT.0)  ET1=ET1*CORR
      SCHI=(D1FD1S/DENDIS)*(ET1/PUSE)
      WRITE (6,1006)  N,NNEX,PERSTR,SCHI
      IF (PERSTR.GT.20.0)  STOP=1.0
  400 CONTINUE
      WRITE (6,2026)
      NST1=NST1+1
      NEND = NEND + 1
  401 CONTINUE
C     COMPUTE STRESSES
      CALL STRESS
      NSTEP=NSTEP+1
      IF (STOP) 499,500,499
  499 CALL EXIT
  500 CONTINUE
      GO TO 50
C*****************************************************************
 1000 FORMAT (20A4/A110)
 1001 FORMAT (2I10,6FI0.0)
 1002 FORMAT (I10,7FI0.0)
 1003 FORMAT (A110)
 1004 FORMAT (8F10.0/8F10.0)
 1005 FORMAT (8F10.0)
 1006 FORMAT (I10,7FI0.0)
 1007 FORMAT (8FI0.3/8EI0.3)
```

```
1008 FORMAT (2I10,3F15,6)
1009 FORMAT (4I10,4F10,0)
1996 FORMAT (38H1APPROXIMATE FIRST CYCLE LOAD STRESSES)
199T FORMAT (1TH1GRAVITY STRESSES)
1998 FORMAT (TH0EL,NO,,11X,4HSIGR,11X,4HSIGZ,TX,8HSIGTHETA,10X,5HTAURZ)
1999 FORMAT (I7,4F15,2)
2000 FORMAT (1H1 20A4//
     1 30H0 NUMBER OF NODAL POINTS----- I10 /
     2 30H0 NUMBER OF ELEMENTS--------- I10 /
     3 30H0 NUMBER OF DIFF. MATERIALS--- I10 /
     4 30H0 NUMBER OF PRESSURE CARDS---- I10 /
     5 30H0 NUMBER OF APPROXIMATIONS---- I10 /
     6 30H0 NUM SPEC BOUND DISP--------- I10 /
     T 30H0 NUM SPEC ELEM MATS---------- I10 )
2001 FORMAT (49HIELEMENT NO.      I      J      K      L     MATERIAL  )
2002 FORMAT (1I2,3F12,2,2E24,4,F12,2)
2003 FORMAT (1I13,4I6,1I13)
2004 FORMAT (1H1,'      NODAL POINT     TYPE      R-ORDINATE   Z-ORDINATE
     1R LOAD OR DISPLACEMENT  Z LOAD OR DISPLACEMENT')
2005 FORMAT (29H0PRESSURE BOUNDARY CONDITIONS/ 24H      I      J      PRESS
     1URE )
2006 FORMAT (1I12,2E20,7)
2007 FORMAT (2I6,F12,2)
2008 FORMAT (1H0,'STRAIN CALCULATIONS IN PERCENT')
2009 FORMAT (26H0NODAL POINT CARD ERROR N= I5)
2010 FORMAT (1H0,2X,8HCONESIZ,2X,8HFRICTION,2X,
     110HFAIL-RATIO,5X,1HK,6X,1HN,3X,11HFAILED MOD,,2X,9HPOISSON G,
     22X,9HPOISSON F,2X,9HPOISSON D,2X,8HTENS STR,2X,3HKUR)
2011 FORMAT (1H0,6HMTYPE=,I3,3X,8HTENSITY=,F9,2,3X,6HKZERO=,F6,2,3X,
     19HMAT CODE=,F4,1,3X,7HCONS P=,F8,2)
2012 FORMAT (30H0 RADIUS OF LOADED AREA ------=,F10,2/
     130H0 SURFACE PRESSURE ----------=,F10,2/)
2013 FORMAT (1H0,5X,7HELEMENT,5X,1HI,5X,1HJ,5X,1HK,5X,1HL,5X,8HMATERIAL)
2014 FORMAT (12H1STEP NUMBER   I3)
2015 FORMAT (1H ,1P11E10,2,//)
2016 FORMAT (1H0,8X,1HN,6X,4HNNEX,8X,6HSTRAIN,7X,10HINF FACTOR/)
2017 FORMAT (29H0BAND WIDTH EXCEEDS ALLOWABLE )
2018 FORMAT (1H0,2216)
2019 FORMAT (1H0,1I9,2I16)
2020 FORMAT (1H1,25HNODAL POINTS AND ELEMENTS )
2021 FORMAT (22H0TIME SINCE BEGINNING=F10,3,2X,3HSEC )
2022 FORMAT (12H0N,P, NUMBER 18X 2HUR 18X 2HUZ )
2023 FORMAT (8H0NBAND = I5)
2024 FORMAT (30H0UNLOADING BOUNDARY CONDITIONS/24H      I      J      PRESS
     1URE )
2025 FORMAT (1H1,'EXCAVATION UNLOADING')
2026 FORMAT (1H )
2027 FORMAT (1H0,'FULL FRICTION ALONG SIDE OF FOOTING')
2028 FORMAT (1H0,'NO FRICTION ALONG SIDE OF FOOTING')
2029 FORMAT (1H0,'PLANE STRAIN ANALYSIS')
2030 FORMAT (1H0,'AXISYMMETRIC ANALYSIS')
2033 FORMAT (1H0,'VERTICAL MATERIAL PROPERTIES ARE LISTED FIRST ')
2034 FORMAT (1H0,'OCTAHEDRAL STRESSES USED')
2035 FORMAT (1H0,'MINOR PRINCIPAL STRESS USED')
2042 FORMAT (1H0,'FAILURE MODULUS USED IN FAILED ELEMENTS')
2043 FORMAT (1H0,'BULK MODULUS USED IN FAILED ELEMENTS')
C*************************************************************************
      END
C*************************************************************************
      SUBROUTINE STRESS
C*************************************************************************
      COMMON/INTGR/NUMNP,NUMEL,NUMMAT,NUMPC,NP,IBC(20),JBC(20),NPLATE,
     1 NUMCOL,NUMROW,IX(550,5),HED(20),NPP1,NPP2,NPB,MTYPE,NSTEP,NDEP,
     2 NUNLOD,IBCE(20),JBCE(20),LAYREN,NSIG,SIGDEP,RPLATE
      COMMON/PRNP/MK,TYP(34),E(11,10),RO(10),AKO(10),EE(T),ET(11),
     1 COAD(10),CP(10),EH(11,10),EEH(T),ETH(11)
      COMMON/LOAD/CODE(600),PR(20),ANGLE(4),PRE(20)
      COMMON/GEOM/R(600),Z(600),UR(600),UZ(600),DISP(600,2),
     1 RADIST(20),ELEV(34)
      COMMON/STRSS/SIGMA(4,550),SIG(11),PZERO,RZERO,GSTRSS(550)
      COMMON/BULK/ESVB(550),ESHB(550),POHB(550),POVB(550),BLK
      COMMON/PPLNCT/NNOCT
      COMMON /ARG/ RRR(5),ZZZ(5),S(10,10),P(10),TT(4),WM(4),DD(3+3),
     1 HH(6,10),RR(4),ZZ(4),C(4,4),H(6,10),D(6,6),F(6,10),TP(6),XI(10)
      COMMON /BANARG/ MBAND,NUMBLK,B(108),A(108,54)
C*************************************************************************
      IF (NPLATE.EQ.0) GO TO 2
      DO 1 N=1,NPP1
      IX(N,5)=IABS(IX(N,5))
    1 CONTINUE
C     COMPUTE ELEMENT STRESSES
    2 NPRINT=0
      DO 300 M=NPP1,NUMEL
      N=M
      IX(N,5)=IABS(IX(N,5))
      MTYPE=IX(N,5)
      CALL QUAD(N,VOL)
      IX(N,5)=MTYPE
      DO 120 I=1,4
      II=2*I
      JJ=2*IX(N,I)
      P(II-1)=B(JJ-1)
  120 P(II)=B(JJ)
      DO 150 I=1,2
      RR(I)=R(I+8)
      DO 150 K=1,8
  150 RR(I)=RR(I)-S(I+8,K)*P(K)
      COMM=S(9,9)*S(10,10)-S(9,10)*S(10,9)
      IF (COMM) 155,160,155
  155 P(9)=(S(10,10)*RR(1)-S(9,10)*RR(2))/COMM
      P(10)=(-S(10,9)*RR(1)+S(9,9)*RR(2))/COMM
  160 DO 170 I=1,6
      TP(I)=0.0
      DO 170 K=1,10
  170 TP(I)=TP(I)+HH(I,K)*P(K)
  171 RR(1)=TP(2)
      RR(2)=TP(6)
      RR(3)=(TP(1)+TP(2)*RRR(5)+TP(3)*ZZZ(5))/RRR(5)
      RR(4)=TP(3)+TP(5)
C     CALCULATE STRESSES DUE TO STRAINS
   10 DO 5 K=1,3
    5 SIG(K)=0.0
      DO 6 I=1,3
      DO 6 K=1,3
    6 SIG(I)=SIG(I)+C(I,K)*RR(K)
      SIG(4)=C(4,4)*RR(4)
C SUBTRACT APPROXIMATE LOAD STRESSES FIRST CYCLE ONLY
      IF (NSTEP.GT.1) GO TO T
```

```
      IK=IX(N,I)
      KK=IX(N,3)
      ZDIST=Z(NPP2)-((Z(IK)+Z(KK))/2,0)
      RDIST=(R(IK)+R(KK))/2,0
      SFACTR=(RZERO**2)/((RZERO+ZDIST)**2)
      IF(ZDIST.LT.(.001*ZDIST-RZERO)) SFACTR=0,0
      SIGMA(2,N)=SIGMA(2,N)-RZERO*SFACTR
      SIGMA(1,N)=SIGMA(1,N)-AKO(MTYPE)*RZERO*SFACTR
      IF (NPP) 377,378,377
  377 SIGMA(3,N)=SIGMA(3,N)-EE(2)*(SIGMA(1,N)+SIGMA(2,N))
      GO TO 7
  378 SIGMA(3,N)=SIGMA(3,N)-AKO(MTYPE)*PZERO*SFACTR
C     ADD STRESS INCREMENTS TO PREVIOUS STRESSES
C     NEGATIVE SIGN IS FOR SOIL MECHANICS POSITIVE COMPRESSION
    7 CONTINUE
      DO 9 I=1,4
      SIG(I)=SIGMA(I,N)-SIG(I)
    9 CONTINUE
      DO 8 I=1,4
      SIGMA(I,N)=SIG(I)
    8 CONTINUE
      NPR=0
C*****************************************************************
C     OUTPUT STRESSES
C*****************************************************************
C     CALCULATE PRINCIPAL STRESSES
C*****************************************************************
   88 CC=(SIG(1)+SIG(2))/2,0
      BB=(SIG(1)-SIG(2))/2,
      CR=SQRT(BB**2+SIG(4)**2)
      SIG(5)=CC+CR
      SIG(6)=CC-CR
      SIG(7)=2B,64B*ATAN2(SIG(4),BB)
      RATIO=SIG(5)/SIG(6)
      SIG(8)=EE(I)
      SIG(9)=EE(2)
      SIG(10)=EEH(1)
      SIG(11)=EEH(2)
      IF (NPP,NE,0)   SIG(3)=EE(2)*(SIG(1)+SIG(2))
      ESV8(N)=SIG(8)
      POV8(N)=SIG(9)
      ESH8(N)=SIG(10)
      POH8(N)=SIG(11)
  104 IF (MPRINT) 110,105+110
  105 IF(NUNLOO,EQ,1)  GO TO 111
      WRITE (6+2004) NSTEP
      GO TO 107
  111 WRITE (6+2005)
  107 IF (NPP,EQ,0)  WRITE (6+2001)
      IF (NPP,NE,0)  WPITE (6+2006)
      MPRINT = 52
  110 MPRINT=MPPINT-1
      WPITE(6+2002)N+PPR(5)+ZZZ(5)+SIG(8)+SIG(9)+SIG(10)+SIG(11)+SIG(1)+
     1SIG(2)+SIG(4)+SIG(5)+SIG(6)+CP+SIG(3)+SIG(7)+RATIO
  300 CONTINUE
  320 RETURN
C*****************************************************************
 2000 FORMAT (4SHOFIRST LINE WITH GRAVITY+ SECONO LINE WITHOUT )
 2001 FORMAT (5HOELEM+3X+1HP+5X+1HZ+4X+7HVEP MOO+2X+4HVPOI+1X+7HHOR MOO+
     12X+4HHPOI+3X+4HSIGR+5X+4HSIGZ+4X+5HTAURZ+4X+6HSIGIRZ+3X+
     23X+6HTAUMA*4X+3X+5HSIGTH+3X+5HANGLE+1X+5HRATIO/)
 2002 FORMAT (IH +I3+2F7,2+1PE9,2+0PF5,2+1PF9,2+0PF5,2+1P7E9,2+0PF6,1+
     10PF6,2)
 2003 FORMAT (1H )
 2004 FORMAT (12H1STEP NUMBER  I3)
 2005 FORMAT (21H1EXCAVATION UNLOADING  )
 2006 FORMAT (5HOELEM+3X+1HR+5X+1HZ+4X+7HVER MOO+2X+4HVPOI+1X+7HHOR MOO+
     12X+4HHPOI+3X+4HSIGX+5X+4HSIGZ+4X+5HTAUXZ+5X+4HSIGI+5X+4HSIG3+4X+
     26HTAUMAX+4X+4HSIGY+3X+5HANGLE+1X+5HRATIO/)
 2021 FORMAT (22H0TIME SINCE BEGINNING=F10,3+2X+3HSEC )
C*****************************************************************
      END
C*****************************************************************
      SUBROUTINE STIFF
C*****************************************************************
      COMMON/INTGR/NUMNP+NUMEL+NUMMAT+NUMPC+NP+IBC(20)+JBC(20)+NPLATE+
     I NUMCOL+NUMROW+IX(550+5)+HEO(20)+NPP1+NPP2+NPR+MTYPE+NSTEP+NOEP+
     2 NUNLOD+IRCE(20)+JBCE(20)+LAYREN+NSIG+SIGNEP+RPLATE
      COMMON/PROP/MATYP(34)+E(I1+10)+RO(I0)+AKO(10)+EE(7)+ET(11)+
     I COAO(10)+CP(10)+EH(11+10)+EFH(7)+ETH(II)
      COMMON/LOAD/CCOOE(600)+PR(20)+ANGLE(4)+PRE(20)
      COMMON/GENM/R(600)+Z(600)+UR(600)+UZ(600)+OISP(600+2)+
     I PAOIST(25)+ELEV(34)
      COMMON/STRSS/SIGMA(4+550)+SIG(11)+PZERO+RZERO+GSTPSS(SSO)
      COMMON/RULK/ESV8(550)+ESH8(550)+POH8(550)+POV8(550)+RLK
      COMMON/PLOCT/NPP+NOCT
      COMMON/ARGG/ RRR(5)+ZZZ(5)+S(10+10)+P(10)+TT(4)+LW(4)+OO(3+3)+
     I HH(6+10)+RR(4)+ZZ(4)+C(4+4)+H(6+10)+D(6+6)+F(6+10)+TP(6)+XI(10)
      COMMON /BANARG/ MBANO+NUMBLK+B(108)+A(108+54)
C*****************************************************************
C     INITIALIZATION
C*****************************************************************
      NB=27
      NO=2*NB
      NO2=2*NO
      STOP=0,0
      NUMBLK=0
      DO 50 N=1+NO2
      B(N)=0,0
      DO 50 M=1+NO
   50 A(N+M)=0,0
C*****************************************************************
C     FORM STIFFNESS MATRIX IN BLOCKS
C*****************************************************************
   60 NUMBLK=NUMBLK+1
      NH=NB*(NUMBLK+1)
      NM=NH-NB
      NL=NH-NB+1
      KSHIFT=2*NL-2
      DO 210 N=1+NUMEL
      IF (IX(N+5)) 210,210+65
   65 DO 80 I=1,4
      IF (IX(N+I)-NL) 80+70+70
   70 IF (IX(N+I)-NH) 90,90+80
   80 CONTINUE
      GO TO 210
   90 CALL QUAD(N+VOL)
      IF(VOL) 142+142+144
```

```
  142 WRITE (6,2003) N
      STOP=1.0
  144 IF(IX(N-3)-IX(N-4)) 145,165,145
  145 DO 150 II=1,9
      CC=S(II+10)/S(10,10)
      P(II)=P(II)-CC*P(10)
      DO 150 JJ=1,9
  150 S(II+JJ)=S(II+JJ)-CC*S(10+JJ)
      DO 160 II=1,8
      CC=S(II+9)/S(9,9)
      P(II)=P(II)-CC*P(9)
      DO 160 JJ=1,8
  160 S(II+JJ)=S(II+JJ)-CC*S(9+JJ)
C     ADD ELEMENT STIFFNESS TO TOTAL STIFFNESS
  165 DO 166 I=1,4
  166 LM(I)=2*IX(N+I)-2
      DO 200 I=1,4
      DO 200 K=1,2
      II=LM(I)+K-KSHIFT
      KK=2*I-2+K
      B(II)=B(II)+P(KK)
      DO 200 J=1,4
      DO 200 L=1,2
      JJ=LM(J)+L-II+1-KSHIFT
      LL=2*J-2+L
      IF(JJ) 200,200,175
  175 IF(ND-JJ) 180,195,195
  180 WRITE (6,2004) N
      STOP=1.0
      GO TO 210
  195 A(II+JJ)=A(II+JJ)+S(KK+LL)
  200 CONTINUE
  210 CONTINUE
C     ADD CONCENTRATED FORCES WITHIN BLOCK
      DO 250 N=NL+NM
      K=2*N-KSHIFT
      B(K)=B(K)+UZ(N)
  250 B(K-1)=B(K-1)+UR(N)
C*****************************************************************************
C     BOUNDARY CONDITIONS
C*****************************************************************************
C         1. PRESSURE B.C.
      IF (NUNLOD.EQ.1) GO TO 251
      IF (NUMPC) 260,310,260
  260 DO 300 L=1,NUMPC
      I=IBC(L)
      J=JBC(L)
      PP=PR(L)/6.
      DZ=(Z(I)-Z(J))*PP
      DR=(R(J)-R(I))*PP
      RX=2.0*R(I)+R(J)
      ZX=R(I)+2.0*R(J)
      IF (NPP) 262,264,262
  262 RX=3.0
      ZX=3.0
  264 II=2*I-KSHIFT
      JJ=2*J-KSHIFT
      IF (II) 280,280,265
  265 IF (II-ND) 270,270,280
  270 SINA=0.0
      COSA=1.0
  272 B(II-1)=B(II-1)+RX*(COSA*DZ+SINA*DR)
      B(II)=B(II)+RX*(SINA*DZ-COSA*DR)
  280 IF (JJ) 300,300,285
  285 IF (JJ-ND) 290,290,300
  290 SINA=0.0
      COSA=1.0
  292 B(JJ-1)=B(JJ-1)+ZX*(COSA*DZ+SINA*DR)
      B(JJ)=B(JJ)+ZX*(SINA*DZ-COSA*DR)
  300 CONTINUE
      GO TO 310
  251 DO 259 L=1,LAYREN
      I=IBCE(L)
      J=JBCE(L)
      PP=PRE(L)/6.0
      DZ=(Z(I)-Z(J))*PP
      DR=(R(J)-R(I))*PP
      RX=2.0*R(I)+R(J)
      ZX=R(I)+2.0*R(J)
      IF (NPP) 122,124,122
  122 RX=3.0
      ZX=3.0
  124 II=2*I-KSHIFT
      JJ=2*J-KSHIFT
      IF (II) 255,255,252
  252 IF (II-ND) 253,253,255
  253 SINA=0.0
      COSA=1.0
  254 B(II-1)=B(II-1)+RX*(COSA*DZ+SINA*DR)
      B(II)=B(II)+RX*(SINA*DZ-COSA*DR)
  255 IF (JJ) 259,259,256
  256 IF (JJ-ND) 257,257,259
  257 SINA=0.0
      COSA=1.0
  258 B(JJ-1)=B(JJ-1)+ZX*(COSA*DZ+SINA*DR)
      B(JJ)=B(JJ)+ZX*(SINA*DZ-COSA*DR)
  259 CONTINUE
C         2. DISPLACEMENT B.C.
  310 DO 400 M=NL,NM
      IF (M-NUMNP) 315,315,400
  315 U=UR(M)
      N=2*M-1-KSHIFT
      IF (CODE(M)) 390,400,316
  316 IF (CODE(M)-1.) 317,370,317
  317 IF (CODE(M)-2.) 318,390,318
  318 IF (CODE(M)-3.) 390,380,390
  370 CALL MODIFY(A,B,ND2*MBAND,N,U)
      GO TO 400
  380 CALL MODIFY(A,B,ND2*MBAND,N,U)
  390 U=UZ(M)
      N=N+1
      CALL MODIFY(A,B,ND2*MBAND,N,U)
  400 CONTINUE
C     WRITE BLOCK OF EQUATIONS ON TAPE AND SHIFT UP LOWER BLOCK
      WRITE (2) (B(N),(A(N+M),M=1,MBAND),N=1,ND)
      DO 420 N=1,ND
      K=N+ND
      B(N)=B(K)
```

```
      B(K)=0.0
      DO 420 MM=1,ND
      A(N+M)=A(K+M)
  420 A(K+M)=0.0
C     CHECK FOR LAST BLOCK
      IF (NN-NUMNP) 60,480,480
  480 CONTINUE
      IF(STOP) 490,500,490
  490 CALL EXIT
  500 REWIND 2
      RETURN
C*****************************************************************************
 2003 FORMAT (2H0NEGATIVE AREA ELEMENT NO. I4)
 2004 FORMAT (29H0BAND WIDTH EXCEEDS ALLOWABLE I4)
C*****************************************************************************
      END
C*****************************************************************************
      SUBROUTINE QUAD(N,VOL)
C*****************************************************************************
      COMMON/INTGR/NUMNP,NUMEL,NUMMAT,NUMPC,NP,IBC(20),JBC(20),NPLATE,
     1 NUMCOL,NUMROW,IX(550,5),HED(20),NPP1,NPP2,NPR,MTYPE,NSTEP,NDEP,
     2 NUMLOD,IRCE(20),JBCE(20),LAYREN,NSIG,SIGDEP,RPLATE
      COMMON/PROP/MATYP(34),E(11,10),RO(10),AKO(10),EE(7),ET(11),
     1 COA0(10),CP(10),EH(11,10),EEH(7),ETH(11)
      COMMON/LOAD/CODE(600),PR(20),ANGLE(4),PRE(20)
      COMMON/GEOM/R(600),Z(600),UR(600),UZ(600),DISP(600,2),
     1 RADIST(25),ELEV(34)
      COMMON/STRSS/SIGMA(4,550),SIG(11),PZERO,RZERO,GSTRSS(550)
      COMMON/BULK/ESYB(550),ESHB(550),POHB(550),POVB(550),BLK
      COMMON/PLOCT/NPP,NOCT
      COMMON /ARG/ RR(15),ZZZ(5),S(10,10),P(10),TT(4),LM(4),OD(3,3),
     1 HH(6,10),RR(4),ZZ(4),C(4,4),H(6,10),O(6,6),F(6,10),TP(6),XI(10)
      COMMON /BANARG/ MBAND,NUMBLK,MB(108),A(108,54)
C*****************************************************************************
   90 I=IX(N,1)
      J=IX(N,2)
      K=IX(N,3)
      L=IX(N,4)
      MTYPE=IX(N,5)
      IX(N,5)=-IX(N,5)
C     FORM STRESS-STRAIN RELATIONSHIP
      CC=(SIGMA(1,N)+SIGMA(2,N))/2.0
      BB=(SIGMA(1,N)-SIGMA(2,N))/2.0
      CR=SQRT(SIGMA(4,N)*SIGMA(4,N)+BB*BB)
      SIG3=CC-CR
      SIG1=CC+CR
      IF (NPP) 17,16,17
   16 IF(SIGMA(3,N).LT.SIG3)SIG3 = SIGMA(3,N)
      IF(SIGMA(3,N).GT.SIG1)SIG1 = SIGMA(3,N)
      CR=(SIG1 - SIG3)/2.0
   17 DO 20 MM=1,11
      ET(MM) = E(MM,MTYPE)
      ETH(MM) = EH(MM,MTYPE)
   20 CONTINUE
C     COMPUTE MODULI AND POISSONS RATIOS
      IF(NPP.EQ.0)  SIG2=SIGMA(3,N)
      IF(NPP.NE.0)  SIG2=0.48*(SIGMA(1,N)+SIGMA(2,N))/2.0
      SIGOCT=(SIG1+SIG2+SIG3)/3.0
      ET(2)=ET(2)/57.28
      ETH(2) = FTH(2)/57.28
      RCS=2.0*(ET(1)*COS(ET(2))-SIG3*SIN(ET(2)))/(1.0-SIN(ET(2)))
      RCS=2.0*(ETH(1)*COS(ETH(2))-SIG3*SIN(ETH(2)))/(1.0-SIN(ETH(2)))
      HCS=RCS/ET(3)
      HCSH = RCSH/ETH(3)
      SHBFOR=(GSTRSS(N)-AKO(MTYPE)*GSTRSS(N))/2.0
      IF(COAD(MTYPE),EQ.0.0)F(1,1)=SIG3
      IF(COAD(MTYPE),EQ.0.0.AND.NOCT.NE.0)F(1,1)=SIGOCT
      IF(COAD(MTYPE),EQ.1.0)F(1,1)=CP(MTYPE)
      IF(COAD(MTYPE),FQ.2.0)F(1,1)=PT(1)
      IF (F(1,1).LE.0.0) F(1,1) = 1.0
      EI=ET(4)*(F(1,1)**ET(5))
      EE(1)=ET*(1.0-(2.0*CR/HCS))*(1.0-(2.0*CR/HCS))
      IF(COAD(MTYPE),EQ.2.0)  EF(1)=ET(4)
      IF (CR.LT.SHBFOR.AND.COAD(MTYPE),EQ.0.0)  EE(1)=ET(11)*(F(1,1)
     1 **ET(5))
      IF (NUNLOD.EQ.1.AND.COAD(MTYPE).EQ.0.0)  EE(1)=ET(11)*(F(1,1)
     1 **ET(5))
      EIH = ETH(4)*(F(1,1)**ETH(5))
      EEH(1)=EIH*(1.0-(2.0*CR/HCSH))*(1.0-(2.0*CR/HCSH))
      IF(COAD(MTYPE),EQ.2.0)  EEH(1)=ETH(4)
      IF (CR.LT.SHBFOR.AND.COAD(MTYPE),EQ.0.0) EEH(1)=ETH(11)*(F(1,1)
     1 **ETH(5))
      IF (NUNLOD.EQ.1.AND.COAD(MTYPE).EQ.0.0)  EEH(1)=ETH(11)*(F(1,1)
     1 **ETH(5))
      SIGT = SIG3
      IF(SIGT.LE.1.0)SIGT=1.0
      STRAIN=2.0*CR/(EI*(1.0-(2.0*CR/HCS)))
      PRAT=ET(7)-ET(8)*ALOG10(SIGT)
      EE(2)=PRAT/((1.0-ET(9)*STRAIN)*(1.0-ET(9)*STRAIN))
      HORST  =2.0*CR/(EIH*(1.0-(2.0*CR/HCSH)))
      PRATH=ETH(7) - ETH(8)*ALOG10(SIGT)
      EEH(2)=PRATH/((1.0-ETH(9)*HORST)*(1.0-ETH(9)*HORST))
      IF(BB.GE.0.0) GO TO 37
      IF(2.0*CR.GE.RCS.AND.BLK.GT.0.0) GO TO 498
      IF(2.0*CR.GE.RCS.AND.BLK.EQ.0.0) GO TO 35
      IF(SIG3.LE.0.0.AND.ABS(SIG3).GE.ABS(FT(10)))GO TO 30
      IF (F(1,1).LE.1.0)  GO TO 30
      GO TO 50
   30 EE(1)=ET(6)
      EF(2)=ET(7)
      GO TO 50
   35 WRITE (6,2002) N
      EF(1) = 1.1*ET(6)
      EE(2) = ET(7)-0.01
      GO TO 50
   37 IF (2.0*CR.GE.RCSH.AND.BLK.GT.0.0) GO TO 498
      IF (2.0*CR.GE.RCSH.AND.BLK.EQ.0.0) GO TO 39
      IF(SIG3.LE.0.0.AND.ABS(SIG3).GE.ABS(ETH(10))) GO TO 38
      IF (F(1,1).LE.1.0) GO TO 38
      GO TO 50
   38 EFH(1) = FTH(6)
      EEH(2) = ETH(7)
      GO TO 50
   39 WRITE (6,2003) N
      EFH(1) = 1.1*ETH(6)
      EFH(2) = FTH(7)-0.01
      GO TO 50
   50 IF(EE(2),GT.0.48)EE(2)=0.48
```

```
      IF (EEH(2).GT.0.48)  EEH(2) = 0.48
  400 EE(3)=EE(1)
      EE(4)=EE(2)
      EEH(3) = EEH(1)
      EEH(4) = EEH(2)
      IF (NPP) 85,86,85
   85 C(1,1)=1.0/EEH(1)
      C(1,2)=-EE(4)/EE(3)
      C(1,3)=-EEH(2)/EEH(1)
      C(2,1)=C(1,2)
      C(2,2)=1.0/EE(1)
      C(2,3)=C(1,2)
      C(3,1)=C(1,3)
      C(3,2)=C(2,3)
      C(3,3)=C(1,1)
      CALL SYMINV(C,3)
      C(4,4)=EE(1)/(1.0 + EE(1)/EEH(1) + 2.0*EE(2))
      DO 83 M=1,3
   83 C(3,M)=0.0
      C(1,3)=0.0
      C(2,3)=0.0
      GO TO 500
   86 C(1,1)=1.0/EEH(1)
      C(1,2)=-EE(2)/EE(1)
      C(1,3)=-EEH(4)/EEH(3)
      C(2,1)=C(1,2)
      C(2,2)=1.0/EE(1)
      C(2,3)=-EE(2)/EE(1)
      C(3,1)=C(1,3)
      C(3,2)=C(2,3)
      C(3,3)=1.0/EEH(3)
      CALL SYMINV(C,3)
      C(4,4)=EE(1)/(1.0 + EE(1)/EEH(1) + 2.0*EE(2))
      GO TO 500
C     FORM BULK MATRIX FOR FAILURE CONDITION
  498 IF(EE(2).GT.0.48) EE(2)=0.48
      IF (EEH(2).GT.0.48)  EEH(2) = 0.48
      WRITE (6,2001) N
      ENRAT = ESVB(N)/ESHB(N)
      DENKR=1.0+2.0*ENRAT-4.0*POVB(N)-2.0*POHB(N)*ENRAT
      KB=ESVB(N)/DENKB
      DO 77  III=1,3
      DO 78    JJJ=1,3
      C(III,JJJ)=KB
   78 CONTINUE
   77 CONTINUE
      C(4,4)=0.0
      IF (NPP) 179,500,179
  179 DO 180 M=1,3
  180 C(3,M)=0.0
      C(1,3)=0.0
      C(2,3)=0.0
C     FORM QUADRILATERAL STIFFNESS MATRIX
  500 RRR(5)=(R(II)+R(J)+R(K)+R(L))/4.0
      ZZZ(5)=(Z(I)+Z(J)+Z(K)+Z(L))/4.0
      DO 94 M=1,4
      MM=IX(N,M)
      IF (R(MM).EQ.0.0) COOE(MM)=1.0
      IF (NPP.EQ.0.AND.R(MM).EQ.0.0)  R(MM)=0.01*RRR(5)
      RRR(M)=R(MM)
      ZZZ(M)=Z(MM)
      DO 96  II=1,10
      P(II)=0.0
      DO 95 JJ=1,6
   95 HH(JJ,II)=0.0
      DO 96  JJ=1,10
   96 S(II,JJ)=0.0
      DO 119 II=1,4
      JJ=IX(N,II)
  119 ANGLE(II)=COOE(JJ)/57.3
      IF (K-L) 125,120,125
  120 CALL TRISTF(1,2,3)
      RRR(5)=(RRR(1)+RRR(2)+RRR(3))/3.0
      ZZZ(5)=(ZZZ(1)+ZZZ(2)+ZZZ(3))/3.0
      VOL=XI(1)
      GO TO 130
  125 VOL=0.0
      CALL TRISTF(4,1,5)
      VOL=VOL+XI(1)
      CALL TRISTF(1,2,5)
      VOL=VOL+XI(1)
      CALL TRISTF(2,3,5)
      VOL=VOL+XI(1)
      CALL TRISTF(3,4,5)
      VOL=VOL+XI(1)
      DO 140 II=1,6
      DO 140 JJ=1,10
  140 HH(II,JJ)=HH(II,JJ)/4.0
  130 RETURN
C*****************************************************************
 2001 FORMAT (34HOBULK MODULUS USED IN ELEMENT NO.    I4)
 2002 FORMAT (44HOFAILED VERTICAL MODULUS IN ELEMENT NO.    I4)
 2003 FORMAT (42HOFAILED HORIZONTAL MOOULUS IN ELEMENT NO.   I4)
C*****************************************************************
      END
C*****************************************************************
      SUBROUTINE TRISTF(II+JJ+KK)
C*****************************************************************
      COMMON/INTGR/NUMNP+NUMEL+NUMMAT+NUMPC+NP+IBC(20)+JBC(20)+NPLATE+
     1 NUMCOL+NUMROW+IX(550+5)+HED(20)+NPP1+NPP2+NPR+MTYPE+N5TEP+NDEP+
     2 NUNLOD+IBCE(20)+JBCE(20)+LAYBEN+NSIG+SIGDEP+RPLATE
      COMMON/PROP/MATYP(34)+E(11+10)+RO(10)+AKO(10)+EE(7)+ET(11)+
     1 COAD(10)+CP(10)+EH(11+10)+EEH(7)+ETH(11)
      COMMON/LOAD/COOE(600)+PR(20)+ANGLE(4)+PRE(20)
      COMMON/GEOM/R(600)+Z(600)+UR(600)+UZ(600)+DISP(600+2)+
     1 RAD1ST(25)+ELEV(34)
      COMMON/STRSS/SIGMA(4+550)+SIG(11)+PZERO+RZERO+GSTRSS(550)
      COMMON/BULK/ESVB(550)+ESHB(550)+POHB(550)+POVB(550)+BLK
      COMMON/PLOCT/NPP+NOCT
      COMMON /ARG/ RRA(5)+ZZZ(5)+S(10+10)+P(10)+TT(4)+LM(4)+DD(3+3)+
     1 HH(6+10)+RR(4)+ZZ(4)+C(4+4)+H(6+10)+O(6+6)+F(6+10)+TP(6)+XI(10)
      COMMON /BANARG/ HRAND+NUMBLK+B(108)+A(108+54)
C*****************************************************************
C       1. INITIALIZATION
      LM(1)=II
      LM(2)=JJ
      LM(3)=KK
      RR(1)=RRR(II)
```

```
      RR(2)=RRR(JJ)
      RR(3)=RRR(KK)
      RR(4)=RRR(II)
      ZZ(1)=ZZZ(II)
      ZZ(2)=ZZZ(JJ)
      ZZ(3)=ZZZ(KK)
      ZZ(4)=ZZZ(II)
   85 DO 100 I=1,6
      DO 90 J=I,10
      F(I,J)=0.0
   90 M(I,J)=0.0
      DO 100 J=1,6
  100 D(I,J)=0.0
C        2. FORM INTEGRAL(G)T*(C)*(G)
      CALL INTER(XI,RR,ZZ)
      D(2,6)=XI(1)*C(1,2)+C(2,3))
      D(3,5)=XI(1)*C(4,4)
      D(5,5)=XI(1)*C(4,4)
      D(6,6)=XI(1)*C(2,2)
      IF (NPP) 104,106,104
  104 D(2,2)=XI(1)*C(1,1)
      D(3,3)=XI(1)*C(4,4)
      GO TO 108
  106 D(1,1)=XI(3)*C(3,3)
      D(1,2)=XI(2)*(C(1,3)+C(3,3))
      D(1,3)=XI(5)*C(3,3)
      D(1,6)=XI(2)*C(2,3)
      D(2,2)=XI(1)*(C(1,1)+2.0*C(1,3)+C(3,3))
      D(2,3)=XI(4)*(C(1,3)+C(3,3))
      D(3,3)=XI(6)*C(3,3)+XI(1)*C(4,4)
      D(3,6)=XI(4)*C(2,3)
  108 DO 110 I=1,6
      DO 110 J=1,6
  110 D(J,I)=D(I,J)
C        3. FORM  COEFFICIENT=DISPLACEMENT TRANSFORMATION MATRIX
      COMM=RR(2)*(ZZ(3)-ZZ(1))+RR(1)*(ZZ(2)-ZZ(3))+RR(3)*(ZZ(1)-ZZ(2))
      DD(1,1)=(RR(2)*ZZ(3)-RR(3)*ZZ(2))/COMM
      DD(1,2)=(RR(3)*ZZ(1)-RR(1)*ZZ(3))/COMM
      DD(1,3)=(RR(1)*ZZ(2)-RR(2)*ZZ(1))/COMM
      DD(2,1)=(ZZ(2)-ZZ(3))/COMM
      DD(2,2)=(ZZ(3)-ZZ(1))/COMM
      DD(2,3)=(ZZ(1)-ZZ(2))/COMM
      DD(3,1)=(RR(3)-RR(2))/COMM
      DD(3,2)=(RR(1)-RR(3))/COMM
      DD(3,3)=(RR(2)-RR(1))/COMM
      DO 120 I=1,3
      J=2*LM(I)-1
      M(I,J)=DD(1,I)
      M(2,J)=DD(2,I)
      M(3,J)=DD(3,I)
      M(4,J)=DD(1,I)
      M(5,J+1)=DD(2,I)
  120 M(6,J+1)=DD(3,I)
C        4.  ROTATE UNKNOWNS IF REQUIRED
      DO 125 J=1,2
      I=LM(J)
      IF (ANGLE(I)) 122,125,125
  122 SINA=SIN(ANGLE(I))
      COSA=COS(ANGLE(I))
      IJ=2*I
      DO 124 K=1,6
      TEMM=M(K,IJ-1)
      M(K,IJ-1)=TEM*COSA+M(K,IJ)*SINA
  124 M(K,IJ)= -TEM*SINA+M(K,IJ)*COSA
  125 CONTINUE
C        5. FORM ELEMENT STIFFNESS MATRIX (M)T*(D)*(M)
      DO 130 J=1,10
      DO 130 K=1,6
      IF (M(K,J)) 128,130,128
  128 DO 129 I=1,6
  129 F(I,J)=F(I,J)+D(I,K)*M(K,J)
  130 CONTINUE
      DO 140 I=1,10
      DO 140 K=1,6
      IF (M(K,I)) 138,140,138
  138 DO 139 J=1,10
  139 S(I,J)=S(I,J)+M(K,I)*F(K,J)
  140 CONTINUE
C        6.  FORM STRAIN TRANSFORMATION MATRIX
  400 DO 410 I=1,6
      DO 410 J=1,10
  410 MM(I,J)=MM(I,J)+M(I,J)
      RETURN
      END
C*******************************************************************************
      SUBROUTINE MODIFY(A,B,NEQ,MBAND,N,U)
C*******************************************************************************
      DIMENSION A(10,54),B(108)
      DO 250 N=2,MBAND
      K=N-1
      IF(K) 235,235,230
  230 B(K)=B(K)-A(K,N)*U
      A(K,N)=0.0
  235 K=N+M-1
      IF(NEQ-K) 250,240,240
  240 B(K)=B(K)-A(N,N)*U
      A(N,N)=0.0
  250 CONTINUE
      A(N,1)=1.0
      B(N)=U
      RETURN
      END
C*******************************************************************************
      SUBROUTINE INTER(XI,RR,ZZ)
C*******************************************************************************
      DIMENSION RR(4),ZZ(4),XI(10),XM(6),R(6),Z(6),XX(6)
      COMMON/PLOCT/NPP,NOCT
      DATA XX/1.0,1.0,1.0,3.0,3.0,3.0/
      COMM=RR(2)*(ZZ(3)-ZZ(1))+RR(1)*(ZZ(2)-ZZ(3))+RR(3)*(ZZ(1)-ZZ(2))
      COMM=COMM/2.0
      R(1)=RR(1)
      R(2)=RR(2)
      R(3)=RR(3)
      R(4)=(R(1)+R(2))/2.
      R(5)=(R(2)+R(3))/2.
      R(6)=(R(3)+R(1))/2.
      Z(1)=ZZ(1)
      Z(2)=ZZ(2)
```

```
      Z(3)=ZZ(3)
      Z(4)=(Z(1)+Z(2))/2.
      Z(5)=(Z(2)+Z(3))/2.
      Z(6)=(Z(3)+Z(1))/2.
      IF (NPP) 10+30+10
   10 DO 20 I=1+6
   20 XM(I)=XX(I)
      GO TO 40
   30 DO 35 I=1+6
   35 XM(I)=XX(I)*R(I)
   40 DO  50 I=1+10
   50 X1(I)=0.0
      DO 100 I=1+6
      X1(1)=X1(1)+XM(I)
      X1(7)=X1(7)+XM(I)*R(I)
      X1(8)=X1(8)+XM(I)*Z(I)
      X1(9)=X1(9)+XM(I)*R(I)**2
      X1(10)=X1(10)+XM(I)*R(I)*Z(I)
      IF (NPP.NE.0)  GO TO 100
      X1(2)=X1(2)+XM(I)/R(I)
      X1(3)=X1(3)+XM(I)/(R(I)**2)
      X1(4)=X1(4)+XM(I)*Z(I)/R(I)
      X1(5)=X1(5)+XM(I)*Z(I)/(R(I)**2)
      X1(6)=X1(6)+XM(I)*Z(I)**2/(R(I)**2)
  100 CONTINUE
      DO 150 I=1+10
  150 X1(I)=X1(I)*CDMM
      RETURN
      END
C*****************************************************************************
      SUBROUTINE SYMINV(A+NMAX)
C*****************************************************************************
      DIMENSION A(4+4)
      DO 200 N=1+NMAX
      O=A(N+N)
      DO 100 J=1+NMAX
  100 A(N+J)=-A(N+J)/D
      DO 150 I=1+NMAX
      IF(N-I) 110+150+110
  110 DO 140 J=1+NMAX
      IF(N-J) 120+140+120
  120 A(I+J)=A(I+J)+A(I+N)*A(N+J)
  140 CONTINUE
  150 A(I+N)=A(I+N)/D
      A(N+N)=1.0/D
  200 CONTINUE
      RETURN
      END
C*****************************************************************************
      SUBROUTINE BANSOL
C*****************************************************************************
      COMMON /BANARG/ MM+NUMBLK+B(108)+A(10A+54)
      NN=54
      NL=NN+1
      NH=NN+NN
      NB=0
      GO TO 150
C     REDUCE EQUATIONS BY BLOCKS
C     1. SHIFT BLOCK OF EQUATIONS
  100 NB=NB+1
      DO 125 N=1+NN
      NM=NN+N
      B(N)=B(NM)
      R(NM)=0.0
      DO 125 M=1+MM
      A(N+M)=A(NM+M)
  125 A(NM+M)=0.0
C     2. READ NEXT BLOCK OF EQUATIONS INTO CORE
      IF (NUMBLK-NB) 150+200+150
  150 READ (2) (B(N)+(A(N+M)+M=1+MM)+N=NL+NH)
      IF (NB) 200+100+200
C     3. REDUCE BLOCK OF EQUATIONS
  200 DO 300 N=1+NN
      IF (A(N+1)) 225+300+225
  225 B(N)=B(N)/A(N+1)
      DO 275 L=2+MM
      IF (A(N+L)) 230+275+230
  230 C=A(N+L)/A(N+1)
      I=N+L-1
      J=0
      DO 250 K=L+MM
      J=J+1
  250 A(I+J)=A(I+J)-C*A(N+K)
      B(I)=B(I)-A(N+L)*B(N)
      A(N+L)=C
  275 CONTINUE
  300 CONTINUE
C     4. WRITE BLOCK OF REDUCED EQUATIONS ON TAPE 2
      IF (NUMBLK-NB) 375+400+375
  375 WRITE (1) (B(N)+(A(N+M)+M=2+MM)+N=1+NN)
      GO TO 100
C     BACK-SUBSTITUTION
  400 DO 450 N=1+NN
      NN=N-1+M
      DO 425 K=2+MM
      L=N+K-1
  425 B(N)=B(N)-A(N+K)*B(L)
      NM=N+NN
      B(NM)=B(N)
  450 A(NM+NB)=B(N)
      NB=NB-1
      IF (NB) 475+500+475
  475 BACKSPACE 1
      READ (1) (B(N)+(A(N+M)+M=2+MM)+N=1+NN)
      BACKSPACE 1
      GO TO 400
C     ORDER UNKNOWNS IN B ARRAY
  500 K=0
      DO 600 NB=1+NUMBLK
      DO 600 N=1+NN
      NM=N+NN
      K=K+1
  600 B(K)=A(NM+NB)
      REWIND 1
      REWIND 2
      RETURN
      END
```

APPENDIX III

FORTRAN LISTING FOR FINITE ELEMENT PRESSUREMETER PROGRAM (PRESMETR)

University of Florida
Department of Civil Engineering

PRESMETR
May 1972

I. Identification: Finite Element Computer Program for Solution of Axisymmetric Pressuremeter Stress-Deformation Problems in Cross-Anisotropic Soils

II. Programmers: E.L. Wilson, University of California, 1966
J.M. Duncan, University of California, 1968
J.P. Hartman, University of Florida, 1971-72

III. Description: This Fortran IV finite element computer program, which consists of a main program and 8 subroutines, was written by E.L. Wilson. Modifications were made by J.M. Duncan to (1) generate element and nodal point data automatically for systems consisting of elements bounded entirely by horizontal and vertical lines; (2) calculate gravity stresses; and (3) solve problems involving stress-dependent modulus values in a series of steps, applying part of the load in each step.

J.P. Hartman made additional modifications to (1) use cross-anisotropic stress-dependent modulus values; (2) allow for the unloading of a centerline borehole; (3) allow for the loading of a central pressuremeter cell placed in the borehole as well as the calculation of its average volume change for each pressure applied; (4) allow for the full-length loading of the pressuremeter unit and the calculation of the average volume change of the measuring cell for each pressure applied; and (5) allow for the unloading and reloading of the pressuremeter at some specified stage in the loading process.

IV. Data Input:

Heading Card (20A4):

Columns 1-80 contain any desired problem description

Control Card I (8I10):

Columns 1-10	Number of nodal points (900 maximum)
11-20	Number of elements (850 maximum)
21-30	Number of materials (10 maximum)
31-40	Number of boundary pressure cards for central cell loading only (20 maximum) - the program automatically generates these.
41-50	Number of steps in loading central cell only
51-60	Number of boundary pressure cards for full-length pressuremeter loading (30 maximum) - the program automatically generates these.
61-70	Number of pressure steps in loading full-length pressuremeter

Control Card II (3I10,5F10.0):

Columns		
	1-10	Number of specified boundary displacements (NBC)
	11-20	Number of specified element materials (NEC)

Control Card III (2I10,6F10.0):

Columns		
	1-10	Number of pressure step for unloading the pressuremeter (NUNS)
	11-20	Number of pressure step for reloading the pressuremeter (should be NUNS + 1)
	21-30	Value of pressuremeter unloading pressure in psf
	31-40	0.0 for using minor principal stresses 1.0 for using octahedral stresses
	41-50	Number of steps in loading the central cell through which the unload-reload modulus is to be used
	51-60	Maximum volume change of measuring cell in cc (When this value is exceeded the program will stop)
	61-70	0.0 for using failure modulus in failed elements 1.0 for using bulk modulus in failed elements
	71-80	0.0 allows unloading of the borehole 1.0 for no unloading of the borehole

Control Card IV (8F10.0):

Columns		
	1-10	Initial volume of measuring cell in cc
	11-20	Initial borehole radius in ft
	21-30	0.0 for right hand vertical boundary on vertical rollers 1.0 for right hand vertical boundary free
	31-40	0.0 for using unload-reload modulus in reloading the unloaded borehole. If not 0.0 is taken as the value (decimal) that is multiplied times the unload-reload modulus and used for reloading the unloaded borehole.
	41-50	Length of pressuremeter measuring cell in ft

Material Property Cards:

First Card - One for each material (I10,7F10.0):

Columns		
	1-10	Material number
	11-20	Unit weight
	21-30	Lateral coefficient of earth pressure
	31-40	COAD (MTYPE) COAD = 0.0 for materials for which $E_i = K(\sigma)^n$ (where $= \sigma_3$ or σ_{oct} - this is for drained conditions in sand or clay) COAD = 1.0 for materials for which E_i =(Consolidation Pressure)^n - (undrained clays). COAD = 2.0 for constant modulus materials

41-50 Consolidation pressure - required only for COAD = 1.0 - otherwise 0.0.

Second Card - Vertical - One for each material (8E10.3):

Columns 1-10 Cohesion, c
11-20 Angle of friction, ϕ, in degrees
21-30 Failure Ratio, R_f
31-40 K where $E_i = K (\sigma)^n$
41-50 n
51-60 Modulus value after failure
61-70 Tangent Poisson ratio factor, G
71-80 Poisson ratio factor F

Third Card - Vertical (continued) - (8E10.3):

Columns 1-10 Poisson ratio factor j
11-20 Tensile strength of the material
21-30 K_{ur} for unloading and reloading

Fourth Card - Horizontal - One for each material (8E10.3):

Identical to Second Card (above) only for horizontal properties.

Fifth Card - Horizontal (continued) - (8E10.3):

Identical to Third Card (above) only for horizontal properties.

Central Cell Pressure Boundary Card (3I10,5F10.0):

Columns 1-10 First nodal point for loading central cell
11-20 Last nodal point for loading central cell
21-30 Number of columns in rectangular grid
31-40 Pressure (psf) to be applied by central cell only

Full-Length Pressure Boundary Card (3I10,5F10.0):

Columns 1-10 First nodal point for loading full-length pressuremeter
11-20 Last nodal point for loading full-length pressuremeter
21-30 Number of columns in rectangular grid
31-40 Pressure (psf) to be applied by full-length pressuremeter loading

Geometry Control Card (2I10,6F10.0):

Columns 1-10 Number of columns of elements (NUMCOL)
11-20 Number of rows of elements (NUMROW)
21-30 Vertical gravity stress at top boundary of rectangular grid (SIGDEP) in psf

Circumferential Element Boundary Cards (I10,7F10.0):

Columns		
1-10	Boundary number (increases out)
11-20	Radial distance to boundary (increases out)

Horizontal Element Boundary Cards (2I10,6F10.0):

Columns	
1-10	Boundary number (increases down)
11-20	Number of material below boundary
21-30	Elevation of boundary (increases up)

NOTE: The first and last boundaries must be specified. Intermediate boundaries, if omitted, will be generated at equal intervals between those specified.

Individual Nodal Point Cards (I10,7F10.0) - NBC required:

Columns		
1-10	Nodal point number
11-20	Code (0.0, 1.0, 2.0, or 3.0 - see SOILSTRN)
21-30	UR	Loads or displacements - see SOILSTRN
31-40	UZ	

Individual Element Cards (2I10,6F10.0) - NEC required):

Columns	
1-10	Element number
11-20	Material number
21-30	Vertical gravity stress at center of element
31-40	Horizontal stress at center of element
41-50	Vertical stress at center of element
51-60	Horizontal stress at center of element
61-70	Horizontal (and vertical) shear stress at center of element

V. Data Output

The program output is quite complete and gives the following information for each step in the successive approximation technique:

(1) Displacement at each nodal point.

(2) Average radial displacement and volume change of the measuring cell.

(3) Element number and center coordinates (r,z).

(4) Vertical and horizontal moduli of elasticity and Poisson's ratios used for each element.

(5) The values of the following stresses for the center of each element: σ_r, σ_z, τ_{rz}, σ_{1rz}, σ_{3rz}, τ_{max}, σ_θ.

(6) The value of the angle α to the critical plane and the ratio of σ_1 to σ_3.

```
C*****************************************************************
C
C  PRESSUREMETER ANALYSIS - ANISOTROPIC SOIL - RECTANGULAR GRID
C
C*****************************************************************
      COMMON/INTGR/NUMNP,NUMEL,NUMMAT,NUMPC,NP,IBC(40),JBC(40),NXPAN,
     1 IX(850,5),MED(20),NPP,MTYPE,N5TEP,NUMCOL,NUMROW,NPPP,NUMPCP,NPPN,
     2 NPRES,IBCP(50),JBCP(50),IBCE(50),JBCE(50),URU(51),URU1(51),VOL,
     3 URU2(51),NUN5,NRE5,UNPRE5,OCT,RE5T,VCONT,BLK,VOLINT,RINT,BNO,OI5T
      COMMON/BULK/E5V8(850),E5H8(850),POH8(850),POV8(850)
      COMMON/PROP/MATYP(50),E(11,10),RO(10),AKO(10),EE(7),ET(11),
     1 CDAO(10),CP(10),EH(11,10),EEH(7),ETH(11)
      COMMON/LOAD/CODE(900),PR(40),ANGLE(4),PRP(50),PRE(50)
      COMMON/GEOM/R(900),Z(900),UR(900),UZ(900),DISP(900,2),
     1 RADIST(30),ELEV(50)
      COMMON/5TR55/SIGMA(4,850),5IG(I1),SIGMAD(4,850),05TR55(850),SIGDEP
      COMMON /ARG/ RRR(5),ZZZ(5),5(I0,I0),P(I0),TT(4),LM(4),DD(3,3),
     1 HH(6,10),RR(4),ZZ(4),C(4,4),W(6,10),O(6,6),F(6,10),TP(6),XI(I0)
      COMMON /BANARG/ MBAND,NUMBLK,B(108),A(108,54)
C*****************************************************************
C     READ AND PRINT CONTROL INFORMATION AND MATERIAL PROPERTIES
C*****************************************************************
   50 READ  (5,1000) NEQ,NUMNP,NUMEL,NUMMAT,NUMPC,NP,NUMPCP,NPPP
      WRITE (6,2000) NEQ,NUMNP,NUMEL,NUMMAT,NUMPC,NP,NUMPCP,NPPP
      READ  (5,1009) NBC,NEC
      READ  (5,1002) NUN5,NRE5,UNPRE5,OCT,RF5T,VCONT,BLK,BNO
      PUNP=UNPRE5/144.0
      IF (UNPRE5) 51,52,51
   51 WRITE (6,2031)  NUN5,NRE5,PUNP
      GO TO 53
   52 WRITE (6,2032)
   53 APPNP
      APPUNPPP
      5TOP=0.0
      READ  (5,1010)  VOLINT,RINT,RIFREE,OI5T,ZINT
      IF (OCT.EQ.0.0) WRITE (6,2035)
      IF (OCT.EQ.1.0) WRITE (6,2034)
      IF (OI5T.EQ.0.0)  WRITE (6,2049)
      IF (OI5T.NE.0.0)  WRITE (6,2050) OI5T
      IF(BNO) 531,532,531
  531 WRITE (6,2046)
      GO TO 533
  532 IF (RE5T.EQ.0.0) WRITE (6,2039)
      IF (RE5T.GT.0.0) WRITE (6,2040) REST
   55 WRITE (6,2044) VOLINT
      WRITE (6,2045) RINT
      WRITE (6,2041) VCONT
      IF (BLK.EQ.0.0) WRITE (6,2042)
      IF (BLK.GT.0.0) WRITE (6,2043)
      WRITE (6,2033)
   56 DO 59 M=1,NUMMAT
      READ  (5,1001) MTYPE,RO(MTYPE),AKO(MTYPE),CDAO(MTYPE),CP(MTYPE)
      WRITE (6,2011) MTYPE,RO(MTYPE),AKO(MTYPE),CDAO(MTYPE),CP(MTYPE)
      READ  (5,1007)  (E(J,MTYPE),J=1,11)
      WRITE (6,2010)
      WRITE (6,2015)  (E(J,MTYPE),J=1,11)
      READ  (5,1007) (EH(J,MTYPE),J=1,11)
      WRITE (6,2010)
      WRITE (6,2015) (EH(J,MTYPE),J=1,11)
   59 CONTINUE
C*****************************************************************
C     READ AND PRINT PRESSURE BOUNDARY CONDITIONS
C*****************************************************************
      IF (NUMPC) 290,310,290
  290 WRITE (6,2005)
      READ  (5,1009) NRE6,N5TOP,NUMCOL,PRE55
      DO 300 L=1,NUMPC
      IBC(L) = NBE6
      JBC(L) = NBE6+NUMCOL*I
      PR(L) = PRE55
      WRITE (6,2007) IBC(L),JBC(L),PR(L)
      PR(L) = PR(L)/APP
      NBE6 = NBE6+NUMCOL*1
      IF (NBE6.FQ.N5TOP) GO TO 310
  300 CONTINUE
  310 CONTINUE
      IF (NUMPCP) 312,316,312
  312 WRITE (6,2005)
      READ  (5,1009) NRE61,N5TOP1,NUMCOL,PRF55I
      DO 314 L=1,NUMPCP
      IBCP(L) = NBE61
      JBCP(L) = NBE61+NUMCOL*1
      PRP(L) = PRE551
      WRITE (6,2007) IBCP(L),JBCP(L),PRP(L)
      PRP(L)=PRP(L)/APPN
      NBE61 = NBE61+NUMCOL*1
      IF (NBE61.EQ.N5TOP1)  GO TO 316
  314 CONTINUE
  316 CONTINUE
C*****************************************************************
C   READ POSITIONS OF BOUNDARIES BETWEEN ELEMENTS
C*****************************************************************
      WRITE (6,2004)
      READ  (5,1002)  NUMCOL,NUMROW,SIGDEP
      L=0
  101 READ  (5,1001)  N,RADIST(N)
      DELTN=N-L
      DELTR=(RADIST(N)-RADIST(L))/DELTN
  102 L=L+1
      IF(L.EQ.NUMCOL+1) GO TO 103
      IF(L.EQ.N) GO TO 101
      RADIST(L)=RADIST(L-1)+DELTR
      GO TO 102
  103 L=0
  104 READ  (5,1002) N=MATYP(N),ELEV(N)
      DELTN=N-L
      DELTEL=(ELEV(N)-ELEV(L))/DELTN
  105 L=L+1
      IF(L.EQ.NUMROW+1) GO TO 106
      IF(L.EQ.N) GO TO 104
      ELEV(L)=ELEV(L-1)+DELTEL
      MATYP(L)=MATYP(L-1)
      GO TO 105
C*****************************************************************
C   GENERATE NODAL POINT DATA
C*****************************************************************
  106 NCP1=NUMCOL+1
      NRP1=NUMROW+1
```

```
      NCOL=0
      NROW=0
      DO 107 N=1,NUMNP
      NCOL=NCOL+1
      NROW=NROW+1
      CODE(N)=0.0
      IF(NCOL.EQ.NCP1) CODE(N)=1.0
      IF(RIFREE.GT.0.0.AND.NCOL.EQ.NCP1) CODE(N)=0.0
      IF(NROW.EQ.1.AND.SIDEP.EQ.0.0) CODE(N)=0.0
      IF(NROW.EQ.1.AND.SIDEP.NE.0.0) CODE(N)=2.0
      IF(NROW.EQ.NRP1) CODE(N)=2.0
      R(N)=RADIST(NCOL)
      Z(N)=ELEV(NROW)
      UR(N)=0.0
      UZ(N)=0.0
      IF(NCOL.LT.NCP1) NROW=NROW-1
      IF(NCOL.EQ.NCP1) NCOL=0
  107 CONTINUE
      IF(NBC.EQ.0) GO TO 5000
      DO 108 N=1,NBC
      READ  (5,1006) NPN,CODE(NPN),UR(NPN),UZ(NPN)
  108 CONTINUE
 5000 DO 109 N=1,NUMNP
      WRITE (6,2002) N,CODE(N),R(N),Z(N),UR(N),UZ(N)
  109 CONTINUE
C*********************************************************************
C     GENERATE ELEMENT DATA
C*********************************************************************
      WRITE (6,2013)
      NROW=0
      NCOL=0
      DO 100 N=1,NUMEL
      NCOL=NCOL+1
      NROW=NROW+1
      IX(N,1)=N-NROW+1
      IX(N,2)=IX(N,1)+NUMCOL+1
      IX(N,3)=IX(N,2)+1
      IX(N,4)=IX(N,1)+1
      IX(N,5)=MATYP(NROW)
      IF(NCOL.LT.NUMCOL) NROW=NROW-1
      IF(NCOL.EQ.NUMCOL) NCOL=0
  100 CONTINUE
  110 CONTINUE
      DO 111 N=1,NUMEL
  111 WRITE (6,2012) N,(IX(N,I),I=1,5)
C*********************************************************************
C     PRINT NODAL POINT AND ELEMENT MESH
C*********************************************************************
      WRITE (6,2020)
  114 NRM=NUMROW
      NFNP=1
      NFE=1
  115 DO 116 N=1,NRM
      NLNP=NFNP+NUMCOL
      NLE=NFE+NUMCOL-1
      WRITE (6,2018) (NO,NO=NFNP,NLNP)
      WRITE (6,2019) (NE,NE=NFE,NLE)
      NFNP=NLNP+1
      NFE=NLE+1
  116 CONTINUE
      NFNP=NUMNP-NUMCOL
      WRITE (6,2018) (NO,NO=NFNP,NUMNP)
C*********************************************************************
C     DETERMINE BAND WIDTH
C*********************************************************************
      J=0
      DO 340 N=1,NUMEL
      DO 340 I=1,4
      DO 325 L=1,4
      KK=IABS(IX(N,I)-IX(N,L))
      IF (KK-J) 325,325,320
  320 J=KK
  325 CONTINUE
  340 CONTINUE
      MBAND=2*J+2
      IF (MBAND.GT.54) WRITE(6,2017)
      IF (MBAND.GT.54) GO TO 50
C*********************************************************************
C     INITIAL DISPLACEMENTS
C*********************************************************************
      DO 3 N=1,NUMNP
      DO 3 I=1,2
      DISP(N,I)=0.0
    3 CONTINUE
C*********************************************************************
C     CALCULATE INITIAL STRESSES FOR A LAYER
C*********************************************************************
      NLMAX=NUMFL*NUMCOL+1
      DO 6 NL=1,NLMAX,NUMCOL
      IL=IX(NL,1)
      JL=IX(NL,2)
      MTYPE=IX(NL,5)
      IF(NL.EQ.1)  GSTRSS(NL)=0.5*(RO(MTYPE))*(Z(IL)-Z(JL)) + SIGOEP
      NBFOR=NL+NUMCOL
      IF(NBFOR.LE.0) GO TO 5
      ILL=IX(NBFOR,1)
      MTYPEE=IX(NBFOR,5)
      IF(NL.GT.1)   GSTRSS(NL)=GSTRSS(NBFOR)+(0.5*(RO(MTYPE))
     1*(Z(ILL)-Z(IL)))+(0.5*(RO(MTYPE))*(Z(IL)-Z(JL)))
    5 NR=NL+NUMCOL-1
C*********************************************************************
C     SET INITIAL STRESSES EQUAL FOR ALL ELEMENTS IN LAYER
C*********************************************************************
      DO 6 N=NL,NR
      GSTRSS(N)=GSTRSS(NL)
    6 CONTINUE
      IF(NEC.EQ.0) GO TO 5001
      DO 9000 N=1,NEC
      READ  (5,1002) NEL,IX(NEL,5),GSTRSS(NFL),(SIGMA(I,NEL),I=1,4)
 9000 CONTINUE
 5001 WRITE (6,1997)
      WRITE (6,1998)
      DO 20 N=1,NUMEL
      MTYPE=IX(N,5)
      SIGMAO(1,N) = GSTRSS(N)*AKO(MTYPE)
      SIGMAO(2,N) = GSTRSS(N)
      SIGMAO(3,N) = SIGMAO(1,N)
      SIGMAO(4,N) = 0.0
```

```
      WRITE(6,1999) N,(SIGMAO(J,N),J=1,4)
   20 CONTINUE
      DO 18 N=1,NUMEL
      DO 17 I=1,4
      SIGMA (I,N) = SIGMAO (I,N)
   17 CONTINUE
   18 CONTINUE
      IF (BNO.GT.0.0) GO TO 777
C*****************************************************************
C     DEVELOP ZERO STRESS CONDITION ON BOREHOLE SIDE
C     UNLOAD BOREHOLE WITH K=ZERO STRESSES
C*****************************************************************
      PRELB = 0.0
      LLE = 1
      DO 455  LLL = 1,NUMROW
      IBCE(LLL) = IX(LLE,1)
      ILE = IX(LLE,1)
      JBCE(LLL) = IX(LLE,2)
      JLE = IX(LLE,2)
      MTYPE = IX(LLE,5)
      PPE(LLL) = -0.5*(AKO(MTYPE))*(RO(MTYPE))*(Z(ILE)-Z(JLE)) + PRELB
     1 - (AKO(MTYPE))*SIGDEP
      PRELB = (AKO(MTYPE))*(RO(MTYPE))*(Z(ILE)-Z(JLE)) + PRELB
      LLE = 1 + LLL*NUMCOL
  455 CONTINUE
      WRITE (6,2016)
      DO 458  NN = 1,NUMROW
      WRITE (6,2007) IBCE(NN),JBCE(NN),PPE(NN)
  458 CONTINUE
      NXPAN = 1
C     FORM STIFFNESS MATRIX
      CALL STIFF
C     SOLVE FOR DISPLACEMENTS
      CALL BANSOL
      WRITE (6,2024)
      WRITE (6,2022)
      DO 29 N=1,NUMNP
      DISP(N,1)=DISP(N,1)+B(2*N-1)
      DISP(N,2)=DISP(N,2)+B(2*N)
      WRITE (6,2006) N,DISP(N,1),DISP(N,2)
   29 CONTINUE
      URUSE=0.0
      DO 801 L=1,NUMPC
      URU(L)=0.0
  801 CONTINUE
      DO 810 L=1,NUMPC
      LUSE=IBC(L)
      MUSE=JBC(L)
      URU(L)=(((DISP(LUSE,1)+DISP(MUSE,1))/2.0)*(Z(LUSE)-Z(MUSE)))/ZINT
  804 URUSE=URUSE+URU(L)
  810 CONTINUE
      WRITE (6,2001) URUSE
      VOLCC = 2.0*VOLINT*URUSE/RINT
      WRITE (6,2027) VOLCC
C     CALCULATE RADIAL STRAINS IN PERCENT
      WRITE (6,2024)
      WRITE (6,2025)
      WRITE (6,2026)
      ISP = IBC(1)
      ISPEND = ISP + NUMPC
      IROW = ISP+NUMCOL-1
 3002 LNNN=ISP
      DO 701 LN=LNNN,ISPEND
      DO 700 KN=ISP,IPOW
      INEX = KN+1
      OIFOIS = DISP(INEX,1) - DISP(KN,1)
      OENDIS = R(INEX) - R(KN)
      PEPSTP =-100.0*(OIFOIS/OENOIS)
      WRITE (6,1008) KN,INEX,PEPSTP
      IF (PERSTR,GT,20.0)  STOP
  700 CONTINUE
      WRITE (6,2028)
      ISP=ISP+1*NUMCOL
      IROW = ISP+NUMCOL-1
      IF(ISP.LT.ISPEND) GO TO 3002
  701 CONTINUE
C     COMPUTE STRESSES
      CALL STPESS
C*****************************************************************
C     APPLY INITIAL DIFFEPENTIAL PRESSUPE
C*****************************************************************
  777 NXPAN=0
      NPPES=0
      NSTEP=1
      DO 500 NNN=1,NP
C     FORM STIFFNESS MATRIX
      CALL STIFF
C     SOLVE FOR DISPLACEMENTS
      CALL BANSOL
      WRITE (6,2014) NSTEP
      WRITE (6,2022)
      DO 31 N=1,NUMNP
      DISP(N,1)=DISP(N,1)+B(2*N-1)
      DISP(N,2)=DISP(N,2)+B(2*N)
      WRITE (6,2006) N,DISP(N,1),DISP(N,2)
   31 CONTINUE
      URUSE=0.0
      DO 811 L=1,NUMPC
      URU1(L)=0.0
  811 CONTINUE
      DO 820 L=1,NUMPC
      LUSE=IBC(L)
      MUSE=JBC(L)
      URU1(L)=(((DISP(LUSE+1)+DISP(MUSE+1))/2.0)*(Z(LUSE)-Z(MUSE)))/ZINT
  814 URUSE=URUSE+URU1(L)
  820 CONTINUE
      WRITE (6,2037) NSTEP
      WRITE (6,2001) URUSE
      VOLCC = 2.0*VOLINT*URUSE/PINT
      WRITE (6,2027) VOLCC
      VDEN = VOLINT + VOLCC
      WRITE (6,2047)  VDEN
      VOLSTR=VOLCC/VDEN
      WRITE (6,2036)  VOLSTR
C     CALCULATE RADIAL STRAINS IN PERCENT
      WRITE (6,2014) NSTEP
      WRITE (6,2025)
      WRITE (6,2026)
```

```
      1SR = 1BC(1)
      ISREND = 1SR + NUMPC
      1ROW = 1SR*NUMCOL-1
 3001 LNNN=ISR
      DO 711 LN=LNNN,1SREND
      DO 710 KN=1SR,1ROW
      1NEX = KN+1
      DIFDIS = D1SP(1NEX,1) - D1SP(KN,1)
      DENDIS = R(1NEX) - R(KN)
      PERSTR =-100.0*(DIFDIS/DENDIS)
      WRITE (6,1008) KN,1NEX,PERSTR
  710 CONTINUE
      WRITE (6,2028)
      ISR=1SR+1+NUMCOL
      1ROW = 1SR+NUMCOL-1
      IF(1SR.LT.ISREND) GO TO 3001
  711 CONTINUE
C     COMPUTE STRESSES
      CALL STRESS
      NSTEP=NSTEP+1
      1F (STOP) 499,500,499
  499 CALL EXIT
  500 CONTINUE
C*****************************************************************
C     APPLY PRESSURES ALONG LENGTH OF PRESSUREMETER
C     SOLVE NON-LINEAR STRUCTURE BY SUCCESSIVE APPROXIMATIONS
C*****************************************************************
      NPRES=1
      DO 600  NNNN=1,NPPP
C     FORM STIFFNESS MATRIX
      CALL STIFF
C     SOLVE FOR DISPLACEMENTS
      CALL BANSOL
      WRITE (6,2023) NPRES
      1F (NPRES.EQ.NUNS) WRITE (6,2029)
      1F (NPRES.EQ.NRES) WRITE (6,2030)
      WRITE (6,2022)
      DO 33 N=1,NUMNP
      DISP(N+1)=DISP(N,1)+8(2*N-1)
      D1SP(N+2)=DISP(N+2)+8(2*N)
      WRITE (6,2006) N,D1SP(N+1),D1SP(N+2)
   33 CONTINUE
      URUSE=0.0
      DO 821 L=1,NUMPC
      URU2(L)=0.0
  821 CONTINUE
      DO 830 L=1,NUMPC
      LUSE=1BC(L)
      MUSE=JBC(L)
      URU2(L)=(((DISP(LUSE+1)+DISP(MUSE+1))/2.0)*(Z(LUSE)-Z(MUSE)))/ZINT
  824 URUSE=URUSE+URU2(L)
  830 CONTINUE
      WRITE (6,2038) NPRES
      1F (NPRES.EQ.NUNS) WRITE (6,2029)
      1F (NPRES.EQ.NRES) WRITE (6,2030)
      WRITE (6,2001) URUSE
      VOLCC = 2.0*VOL1NT*URUSE/R1NT
      WRITE (6,2027) VOLCC
      VDEN = VOLINT + VOLCC
      WRITE (6,2047)  VDEN
      VOLSTR=VOLCC/VDEN
      WRITE (6,2036)  VOLSTR
      WRITE (6,2048)
      VOLCB=VOLCC*((URUSE+2.0*R1NT)/(2.0*RINT))
      WRITE (6,2027)  VOLCB
      VDEN2=VOLINT+VOLCB
      WRITE (6,2047) VDEN2
      VOLST2=VOLCB/VDEN2
      WRITE (6,2036) VOLST2
      1F (VOLCC.GT.VCONT)  STOP=1.0
C     CALCULATE RADIAL STRAINS IN PERCENT
      WRITE (6,2023) NPRES
      WRITE (6,2025)
      WRITE (6,2026)
      1SR = 1BC(1)
      1SREND = 1SR + NUMPC
      IROW = 1SR+NUMCOL-1
 3000 LNNN=1SR
      DO 721 LN=LNNN,1SREND
      DO 720 KN=1SR,1ROW
      1NEX = KN+1
      OIFDIS = D1SP(1NFX,1) - DISP(KN,1)
      DENDIS = R(1NEX) - R(KN)
      PERSTR =-100.0*(DIFDIS/DENDIS)
      WRITE (6,1008) KN,1NEX,PERSTR
  720 CONTINUE
      WRITE (6,2028)
      ISR=1SR+1+NUMCOL
      1ROW = 1SR+NUMCOL-1
      1F(1SR.LT.1SREND) GO TO 3000
  721 CONTINUE
C     COMPUTE STRESSES
      CALL STRESS
      NPRES=NPRES+1
      1F (STOP) S99,600,S99
  S99 CALL EXIT
  600 CONTINUE
      GO TO 50
C*****************************************************************
 1000 FORMAT (20A4/8I10)
 1001 FORMAT (1I10,7F10.0)
 1002 FORMAT (2I10,6F10.0)
 1003 FORMAT (6I5,5F10.0)
 1006 FORMAT (I10,7F10.0)
 1007 FORMAT (8F10.3/8E10.3)
 1008 FORMAT (2I10,3F15.4)
 1009 FORMAT (3I10,5F10.0)
 1010 FORMAT (8F10.0)
 1997 FORMAT (1H1,' INITIAL STRESSES*)
 1998 FORMAT (7H0EL.NO.,11X,4HS1GR,11X,4HS1GZ,7X,8HS1GTHETA,10X,5HTAURZ)
 1999 FORMAT (17,4F15.2)
 2000 FORMAT (1H1 20A4//
     1 30H0 NUMMER OF NODAL POINTS------ 110 /
     2 30H0 NUMMER OF ELEMENTS---------- 110 /
     3 30H0 NUMMER OF DIFF. MATERIALS--- 110 /
     4 30H0 NUMMER OF DIFF. PRES. CARDS- 110 /
     5 30H0 NUMMER OF APPROXIMATIONS---- 110 /
     6 30H0 NUMMER OF PRESSURE CARDS---- 110 /
```

```
   7 30H0 NUMBER OF APPROXIMATIONS==== I10 //)
2001 FORMAT (48H0AVERAGE RADIUS CHANGE OF MEASURING CELL IN FT = E20.7)
2002 FORMAT (112,3F12,2,2E24,4)
2003 FORMAT (118,A16,118,4F12,2)
2004 FORMAT (1W1,'     NODAL POINT     TYPE     R-ORDINATE   Z-ORDINATE
  1R LOAD OR DISPLACEMENT   Z LOAD OR DISPLACEMENT')
2005 FORMAT (29H0PRESSURE BOUNDARY CONDITIONS/ 24H     I       J     PRESS
  1URE )
2006 FORMAT (111Z,2E20,7)
2007 FORMAT (216,F12,2)
2008 FORMAT (2112,3F12,2,2E24,4)
2009 FORMAT (26H0NODAL POINT CARD ERROR N= I5)
2010 FORMAT (1H0,2X,8HCONEST=,2X,8HFRICTION=,2X,
   110HFAIL=RATIO=,5X,1HK=6X,1HN=,3X,11HFAILED MOO=,2X,9HPOISSON G=,
   22X,9HPOISSON F=,2X,9HPOISSON D=,2X,8HTENS STR=,2X=,3HKUR)
2011 FORMAT (1H0,6HMTYPE=,I3=3X,8HDENSITY=,F9,2=3X,6HKZERO=,F6,2=3X,
   19HMAT CODE=,I3=3X,7HCONS P=,F8,2)
2012 FORMAT (1I13,4I6,1I13)
2013 FORMAT (1H0=5X,7HELEMENT=5X=1HI=5X=1HJ=5X=1HK=5X=1HL=5X8HMATERIAL)
2014 FORMAT (12H1STEP NUMBER  I3)
2015 FORMAT (1H =1P11E10,2=//)
2016 FORMAT (29H08OREHOLE BOUNDARY CONDITIONS/ 24H     I       J     PRESS
  1URE )
2017 FORMAT (29H08AND WIDTH EXCEEDS ALLOWABLE )
2018 FORMAT (1H0=22I6)
2019 FORMAT (1H0=1I9=2I16)
2020 FORMAT (1H1=25HNODAL POINTS AND ELEMENTS )
2022 FORMAT (12H0N,=P, NUMBER 18X 2HUR 18X 2HUZ )
2023 FORMAT (21H1PRESSURE STEP NUMBER  I3)
2024 FORMAT (2H=18OREHOLE UNLOADING STEP )
2025 FORMAT (1H0,'RADIAL STRAIN CALCULATIONS IN PERCENT')
2026 FORMAT (1H0,8X,1HR=6X,4HRNEX,10X=6HSTRAIN/)
2027 FORMAT (48H0AVERAGE VOLUME CHANGE OF MEASURING CELL IN CC = F10,3)
2028 FORMAT (1H )
2029 FORMAT (1H0,'UNLOADING OF PRESSUREMETER')
2030 FORMAT (1H0,'RELOADING OF PRESSUREMETER')
2031 FORMAT (//,=1H0,'UNLOADING INFORMATION'=/
   1 30H0 UNLOADING STEP NUMBER=======  I10 /
   2 30H0 RELOADING STEP NUMBER=======  I10 /
   3 30H0 UNLOADING PRESSURE IN PSI===  F10,1)
2032 FORMAT (1H0,'NO UNLOADING OF PRESSUREMETER')
2033 FORMAT (//,1H0,'VERTICAL MATERIAL PROPERTIES ARE LISTED FIRST')
2034 FORMAT (1H0,'OCTAHEDRAL STRESSES USED')
2035 FORMAT (1H0,'MINOR PRINCIPAL STRESS USED')
2036 FORMAT (20H0VOLUMETRIC STRAIN =   F15,8)
2037 FORMAT (///,12H0STEP NUMBER   I3)
2038 FORMAT (///,21H0PRESSURE STEP NUMBER   I3)
2039 FORMAT (1H0,'FULL KUR ON BOREHOLE UNLOADING ONLY')
2040 FORMAT (29H0KUR UP THRU STEP(S) NUMBER   F10,1)
2041 FORMAT (2H=0VOLUME CONTROL IN CC =   F10,2 )
2042 FORMAT (1H0,'FAILURE MODULUS USED IN FAILED ELEMENTS')
2043 FORMAT (1H0,'BULK MODULUS USED IN FAILED ELEMENTS')
2044 FORMAT (2H=0INITIAL VOLUME IN CC =   F10,2)
2045 FORMAT (2H=0INITIAL RADIUS IN FT =   F10,2)
2046 FORMAT (1H0,' * = BOREHOLE NOT UNLOADED * = ')
2047 FORMAT (39H0TOTAL VOLUME OF MEASURING CELL IN CC =  F10,3)
2048 FORMAT (1H0,'MORE PRECISE VOLUME MEASUREMENT * = * = * = * = * = ')
2049 FORMAT (1H0,'FULL UNLOAD=RELOAD MODULUS USED')
2050 FORMAT (25H0RELOAD MODULUS FACTOR =     F10,3)
C*************************************************************************
      END
C*************************************************************************
      SUBROUTINE STRESS
C*************************************************************************
      COMMON/INTGR/NUMNP,NUMEL,NUMAT,NUMPC,NP,IBC(40),JBC(40),NXPAN,
     1 IX(850,5),HED(20),NPP,MTYPE,NSTEP,NUMCOL,NUMROW,NPPP,NUMPCP,NPPN,
     2 NPRES,IBCP(50),JBCP(50),IBCE(50),JBCE(50),URU(51),URU1(51),VOL,
     3 URU2(51),NUNS,NRES,NUMPRES,OCT,REST,VCONT,BLK,YOLINT,RINT,BNO,DIST
      COMMON/BULK/ESBH(850),ESHB(850),POHB(850),POBH(850)
      COMMON/PROP/MATYP(50),E(11,10),RO(10),AKO(10),EE(7),ET(11),
     1 COAD(10),CP(10),EH(11,10),EEH(7),ETH(11)
      COMMON/LOAD/CODE(900),PR(40),ANGLE(4),PRP(50),PRE(50)
      COMMON/GEOM/R(900),Z(900),UR(900),UZ(900),DISP(900,2),
     1 RADIST(30),ELEV(50)
      COMMON/STRSS/SIGMA(4,850),SIG(11),SIGMAD(4,850),OSTRSS(850),SIGDEP
      COMMON /ABB/ RRR(5),ZZZ(5),S(10,10),P(10),TT(4),LM(4),DD(3,3),
     1 HH(6,10),RR(4),ZZ(4),C(4,4),H(6,10),D(6,6),F(6,10),TP(6),XI(10)
      COMMON /BANARG/ MBAND,NUMBLK,B(108),A(108,54)
C*************************************************************************
C     COMPUTE ELEMENT STRESSES
C*************************************************************************
      NPRINT=0
      DO 300 M=1,NUMEL
      N=M
      IX(N,5)=IABS(IX(N,5))
      MTYPE=IX(N,5)
      CALL QUAD(N,VOL)
      IX(N,5)=MTYPE
      DO 120 I=1,4
      II=2*I
      JJ=2*IX(N,I)
      P(II-1)=R(JJ-1)
  120 P(II)=R(JJ)
      DO 150 I=1,2
      RR(I)=P(I+8)
      DO 150 K=1,8
  150 RR(I)=RR(I)-S(I+8,K)*P(K)
      COMM=S(9,9)*S(10,10)-S(9,10)*S(10,9)
      IF (COMM) 155,160,155
  155 P(9)=(S(10,10)*RR(1)-S(9,10)*RR(2))/COMM
      P(10)=(-S(10,9)*RR(1)+S(9,9)*RR(2))/COMM
  160 DO 170 I=1,6
      TP(I)=0,0
      DO 170 K=1,10
  170 TP(I)=TP(I)+HH(I,K)*P(K)
  171 RR(1)=TP(2)
      RR(2)=TP(6)
      RR(3)=(TP(1)+TP(2)*RRR(5)+TP(3)*ZZZ(5))/RRR(5)
      RR(4)=TP(3)+TP(5)
C     CALCULATE STRESSES DUE TO STRAINS
   10 DO 5 K=1,3
    5 SIG(K)=0,0
      DO 6 I=1,3
      DO 6 K=1,3
      SIG(I)=SIG(I)+C(I,K)*RR(K)
    6 CONTINUE
      SIG(4)=C(4,4)*RR(4)
C     ADD STRESS INCREMENTS TO PREVIOUS STRESSES
```

```
C     NEGATIVE SIGN IS FOR SOIL MECHANICS POSITIVE COMPRESSION
    7 CONTINUE
      DO 9 I=1,4
      SIG(I)=SIGMA(I,N)-SIG(I)
    9 CONTINUE
      DO 8 I=1,4
      SIGMA(I,N)=SIG(I)
    8 CONTINUE
      NPR=0
C*****************************************************************
C     OUTPUT STRESSES
C*****************************************************************
C     CALCULATE PRINCIPAL STRESSES
C*****************************************************************
   88 CC=(SIG(1)+SIG(2))/2.0
      BB=(SIG(1)-SIG(2))/2.
      CR=SQRT(BB**2+SIG(4)**2)
      SIG(5)=CC+CR
      SIG(6)=CC-CR
      IF (SIG(3),LT,SIG(6))  CR=(SIG(5)-SIG(3))/2.0
      SIG(7)=28.648*ATAN2(SIG(4),BB)
      RATIO=SIG(5)/SIG(6)
      IF (SIG(3),LT,SIG(6))  RATIO = SIG(5)/SIG(3)
      SIG(8)=EE(1)
      SIG(9)=EE(2)
      SIG(10)=EEH(1)
      SIG(11)=EEH(2)
      ESVB(N)=SIG(8)
      POVB(N)=SIG(9)
      ESHB(N)=SIG(10)
      POHB(N)=SIG(11)
  104 IF (NPRINT) 110,105,110
  105 IF (NXPAN,EQ,1) GO TO 111
      IF (NPRES,EQ,0) GO TO 106
      WRITE (6,2005)  NPRES
      IF (NPRES,EQ,NUNS) WRITE (6,2007)
      IF (NPRES,EQ,NRES) WRITE (6,2008)
      GO TO 107
  111 WRITE (6,2006)
      GO TO 107
  106 WRITE (6,2004)  NSTEP
  107 WRITE (6,2001)
      NPRINT = 52
  110 NPRINT=NPRINT-1
      WRITE(6,2002)N,RRR(5),ZZZ(5),SIG(8),SIG(9),SIG(10),SIG(11),SIG(1),
     1SIG(2),SIG(4),SIG(5),SIG(6),CR,SIG(3),SIG(7),RATIO
      IF (NSTEP,EQ,1,AND,SIG(8),EQ,111,0)  STOP
      IF (NSTEP,EQ,1,AND,SIG(10),EQ,111,0)  STOP
  300 CONTINUE
  320 RETURN
C*****************************************************************
 2000 FORMAT (*  FIRST LINE WITH INITIAL STRESSES, SECOND LINE WITHOUT*)
 2001 FORMAT (5HOELEM,3X,1HR,5X,1HZ,4X,7HVER MOD,2X,4HVPOI,1X,7HMOR MOD,
     12X,4HMPOI,3X,4HSIGR,5X,4HSIGZ,4X,5HTAURZ,4X,6HSIGIRZ,3X,6HSIGRZ,
     23X,6HTAUMAX,3X,5HSIGTH,3X,5HANGLE,1X,5HRATIO/)
 2002 FORMAT (1H ,I3,2FT,2,1PE9,2,0PF5,2,1PE9,2,0PF5,2,1PTE9,2,0PF6,1,
     10PF6,2)
 2003 FORMAT (1H )
 2004 FORMAT (12H1STEP NUMBER  I3)
 2005 FORMAT (14H1PRESSURE STEP  I3)
 2006 FORMAT (24H1BOREHOLE UNLOADING STEP )
 200T FORMAT (1H0,*UNLOADING OF PRESSUREMETER*)
 2008 FORMAT (1H0,*RELOADING OF PRESSUREMETER*)
C*****************************************************************
      END
C*****************************************************************
      SUBROUTINE STIFF
C*****************************************************************
      COMMON/INTGR/NUMNP,NUMEL,NUMNPT,NUMPC,NP,IBC(40),JBC(40),NXPAN,
     1 IX(850,5),HED(20),NPP,MTYPE,NSTEP,NUMCOL,NUMROW,NPPP,NUMPCP,NPPN,
     2 NPRES,IBCP(50),JBCP(50),IBCE(50),JBCE(50),URU(51),URU1(51),VOL,
     3 URUZ(51),NUNS,NRES,UNPRES,DCT,REST,VCONT,BLK,VOLINT,RINT,8NO,DIST
      COMMON/BULK/ESVB(850),ESHB(850),POHB(850),POVB(850)
      COMMON/PROP/MATYP(50),E(11,10),RO(10),AKO(10),EE(7),ET(11),
     1 COAO(10),CP(10),EH(11,10),EEH(7),ETH(11)
      COMMON/LOAD/CODE(900),PR(40),ANGLE(4),PRP(50),PRE(50)
      COMMON/GEOM/R(900),Z(900),UR(900),UZ(900),DISP(900,2),
     1 RAOIST(30),ELEV(50)
      COMMON/STRSS/SIGMA(4,850),SIG(11),SIGMAD(4,850),GSTRSS(850),SIGDEP
      COMMON /ARB/ RRR(5),ZZZ(5),S(10,10),P(10),TT(4),LM(4),OD(3,3),
     1 HH(6,10),RR(4),ZZ(4),C(4,4),M(6,10),O(6,6),F(6,10),TP(6),XI(10)
      COMMON /BANARG/ MBAND,NUMBLK,B(108),A(108,54)
C*****************************************************************
C     INITIALIZATION
C*****************************************************************
      NB=27
      NO=2*NB
      ND2=2*NO
      STOP=0.0
      NUMBLK=0
      DO 50 N=1,NO2
      B(N)=0.0
   50 A(N,M)=0.0
C*****************************************************************
C     FORM STIFFNESS MATRIX IN BLOCKS
C*****************************************************************
   60 NUMBLK=NUMBLK+1
      NM=NB*(NUMBLK+1)
      NN=NM-NB
      NL=NM-NB+1
      KSHIFT=2*NL-2
      DO 210 N=1,NUMEL
      IF (IX(N,5)) 210,210,65
   65 DO 80 I=1,4
      IF (IX(N,I)-NL) 80,70,70
   70 IF (IX(N,I)-NM) 90,90,80
   80 CONTINUE
      GO TO 210
   90 CALL QUAD(N,VOL)
      IF(VOL) 142,142,144
  142 WRITE (6,2003) N
      STOP=1.0
  144 IF(IX(N,3)-IX(N,4)) 145,165,145
  145 DO 150 II=1,9
      CC=S(II,10)/5(10,10)
      P(II)=P(II)-CC*P(10)
      DO 150 JJ=1,9
```

```
  150 S(II+JJ)=S(II+JJ)-CC*S(10+JJ)
      DO 160 II=1,8
      CC=S(II,9)/S(9,9)
      P(II)=P(II)-CC*P(9)
      DO 160 JJ=1,8
  160 S(II+JJ)=S(II+JJ)-CC*S(9+JJ)
C     ADD ELEMENT STIFFNESS TO TOTAL STIFFNESS
  165 DO 166 I=1,4
  166 LM(I)=2*IX(N,I)-2
      DO 200 I=1,4
      DO 200 K=1,2
      I=LM(I)+K-KSHIFT
      KK=2*I-2+K
      B(II)=B(II)+P(KK)
      DO 200 JM=1,4
      DO 200 L=1,2
      JJ=LM(JJ)+L-II+1-KSHIFT
      LL=2*J-2+L
      IF(JJ) 200,200,175
  175 IF(NO-JJ) 180,195,195
  180 WRITE (6,2004) N
      STOP=1,0
      GO TO 210
  195 A(II,JJ)=A(II,JJ)+S(KK,LL)
  200 CONTINUE
  210 CONTINUE
C     ADD CONCENTRATED FORCES WITHIN BLOCK
      DO 250 NNNL=NN
      K=2*N-KSHIFT
      B(K)=B(K)+UZ(N)
  250 B(K-1)=B(K-1)+UR(N)
C*************************************************************************
C     BOUNDARY CONDITION5
C*************************************************************************
C     1. PRESSURE B.C.
C*************************************************************************
      IF (NXPAN.EQ.1) GO TO 251
      IF (NPRES.NE.0) GO TO 301
      IF (NUMPC) 260,310,260
  260 DO 300 L=1,NUMPC
      I=IBC(L)
      J=JBC(L)
      PP=PR(L)/6.
      DZ=(Z(I)-Z(J))*PP
      DR=(R(J)-R(I))*PP
      RX=2.0*R(I)+R(J)
      ZX=R(I)+2.0*R(J)
  264 II=2*I-KSHIFT
      JJ=2*J-KSHIFT
      IF (II) 280,280,265
  265 IF (II-ND) 270,270,280
  270 SINA=0.0
      COSA=1.0
  272 B(II-1)=B(II-1)+RX*(COSA*DZ+SINA*DR)
      B(II)=B(II)+RX*(SINA*DZ-COSA*DR)
  280 IF (JJ) 300,300,285
  285 IF (JJ-ND) 290,290,300
  290 SINA=0.0
      COSA=1.0
  292 B(JJ-1)=B(JJ-1)+ZX*(COSA*DZ+SINA*DR)
      B(JJ)=R(JJ)-ZX*(SINA*DZ-COSA*DR)
  300 CONTINUE
  251 DO 259 L=1,NUMROW
      I=IBC(L)
      J=JBC(L)
      PP=PRE(L)/6.0
      DZ=(Z(I)-Z(J))*PP
      DR=(R(J)-R(I))*PP
      RX=2.0*R(I)+R(J)
      ZX=R(I)+2.0*R(J)
      II=2*I-KSHIFT
      JJ=2*J-KSHIFT
      IF (II) 255,255,252
  252 IF (II-ND) 253,253,255
      COSA=1.0
  253 SINA=0.0
  254 B(II-1)=B(II-1)+RX*(COSA*DZ+SINA*DR)
      B(II)=B(II)-RX*(SINA*DZ-COSA*DR)
  255 IF (JJ) 259,259,256
  256 IF (JJ-ND) 257,257,259
  257 SINA=0.0
      COSA=1.0
  258 B(JJ-1)=B(JJ-1)+ZX*(COSA*DZ+SINA*DR)
      B(JJ)=B(JJ)-ZX*(SINA*DZ-COSA*DR)
  259 CONTINUE
      GO TO 310
  301 DO 309  L = 1,NUMPCP
      I=IBCP(L)
      J=JBCP(L)
      PP=PRP(L)/6.
      IF (NPRES.EQ.NUN5)  PP=-UNPRES/6.0
      IF (NPRES.EQ.NPRES)  PP=UNPRES/6.0
      DZ=(Z(I)-Z(J))*PP
      DR=(R(J)-R(I))*PP
      RX=2.0*R(I)+R(J)
      ZX=R(I)+2.0*R(J)
      II=2*I-KSHIFT
      JJ=2*J-KSHIFT
      IF (II) 305,305,302
  302 IF (II-ND) 303,303,305
  303 SINA=0.0
      COSA=1.0
  304 B(II-1)=B(II-1)+RX*(COSA*DZ+SINA*DR)
      B(II)=B(II)-RX*(SINA*DZ-COSA*DR)
  305 IF (JJ) 309,309,306
  306 IF (JJ-ND) 307,307,309
  307 SINA=0.0
      COSA=1.0
  308 B(JJ-1)=B(JJ-1)+ZX*(COSA*DZ+SINA*DR)
      B(JJ)=R(JJ)-ZX*(SINA*DZ-COSA*DR)
  309 CONTINUE
C*************************************************************************
C     2. DISPLACEMENT B.C.
C*************************************************************************
  310 DO 400 NNNL=NN
      IF (N-NUMNP) 315,315,400
  315 U=UR(N)
```

```
      N=2*M-1-KSHIFT
      IF (CDDE(M)) 390,400,316
  316 IF (CDDE(M)-1.) 317,370,317
  317 IF (CDDE(M)-2.) 318,390,318
  318 IF (CDDE(M)-3.) 390,380,390
  370 CALL MODIFY(A,B,ND2,MBAND,N,U)
      GO TO 400
  380 CALL MODIFY(A,B,ND2,MBAND,N,U)
  390 U=UZ(M)
      N=N-1
      CALL MODIFY(A,B,NO2,MBAND,N,U)
  400 CONTINUE
C     WRITE BLOCK OF EQUATIONS ON TAPE AND SHIFT UP LOWER BLOCK
      WRITE (2) (B(N),(A(N,M),M=1,MBAND),N=1,ND)
      DO 420 N=1,ND
      K=N+NO
      B(N)=B(K)
      B(K)=0.0
      DO 420 M=1,NO
      A(N,M)=A(K,M)
  420 A(K,M)=0.0
C     CHECK FOR LAST BLOCK
      IF (NM-NUMNP) 60,480,480
  480 CONTINUE
      IF(STOP) 490,500,490
  490 CALL EXIT
  500 REWIND 2
      RETURN
C*****************************************************************
 2003 FORMAT (26H0NEGATIVE AREA ELEMENT NO. 14)
 2004 FORMAT (29H0BAND WIDTH EXCEEDS ALLOWABLE 14)
C*****************************************************************
      END
C*****************************************************************
      SUBROUTINE TRISTF(11,JJ,KK)
C*****************************************************************
      COMMON/INT0R/NUMNP,NUMEL,NUMMAT,NUMPC,NP,IBC(40),JBC(40),NXPAN,
     1 IX(850,5),HED(20),NPP,MTYPE,NSTEP,NUMCDL,NUMRDR,NPPP,NUMPCP,NPPN,
     2 NPRES,IBCP(50),JBCP(50),IBCE(50),JBCE(50),URU(51),URU1(51),VDL,
     3 URU2(51),NUNS,NRES,UNPRES,OCT,REST,VCONT,BLK,VDLINT,R1NT,BNO,DIST
      COMMON/BLK/ESV8(850),ESH8(850),POW8(850),POV8(850)
      COMMON/PROP/MATYP(50),E(11,10),RO(10),AKO(10),EE(7),ET(11),
     1 CDA0(10),CP(10),EM(11,10),EEM(7),ETH(11)
      COMMON/LOAD/CODE(900),PR(40),ANGLE(4),PRP(50),PRE(50)
      COMMON/BEOM/R(900),Z(900),UR(900),UZ(900),01SP(900,2),
     1 RAOIST(30),ELEV(50)
      COMMON/STRSS/SIGMA(4,850),SIG(11),SIGMA0(4,850),BSTRSS(850),SIGOEP
      COMMON /ARB/ ARR(5),ZZZ(5),S(10,10),P(10),TT(4),LM(4),OO(3,3),
     1 HM(6,10),RR(4),ZZ(4),C(4,4),M(6,10),D(6,6),F(6,10),TP(6),X1(10)
      COMMON /BANARR/ MBAND,NUMBLK,B(108),A(108,54)
C*****************************************************************
C     1. INITIALIZATION
      LM(1)=11
      LM(2)=JJ
      LM(3)=KK
      RR(1)=RRR(11)
      RR(2)=RRR(JJ)
      RR(3)=RRR(KK)
      RR(4)=RRR(I1)
      ZZ(1)=ZZZ(11)
      ZZ(2)=ZZZ(JJ)
      ZZ(3)=ZZZ(KK)
      ZZ(4)=ZZZ(I1)
   85 DO 100 I=1,6
      DO 90 J=1,10
      F(I,J)=0.0
   90 M(I,J)=0.0
      DO 100 J=1,6
  100 D(I,J)=0.0
C     2. FORM INTEGRAL(8)T*(C)*(G)
      CALL INTER(X1,RR,ZZ)
      O(2,6)=X1(1)*(C(1,2)+C(2,3))
      O(3,5)=X1(1)*C(4,4)
      O(5,5)=X1(1)*C(4,4)
      O(6,6)=X1(1)*C(2,2)
  106 O(1,1)=XI(3)*C(3,3)
      O(1,2)=XI(2)*(C(1,3)+C(3,3))
      D(1,3)=X1(5)*C(3,3)
      D(1,6)=X1(2)*C(2,3)
      D(2,2)=X1(1)*(C(1,1)+2.0*C(1,3)+C(3,3))
      O(2,3)=X1(4)*(C(1,3)+C(3,3))
      O(3,3)=X1(6)*C(3,3)+XI(1)*C(4,4)
      O(3,6)=X1(4)*C(2,3)
  108 DO 110 I=1,6
      DO 110 J=I,6
  110 D(J,I)=D(I,J)
C     3. FORM  COEFFICIENT=DISPLACEMENT TRANSFORMATION 4AT91X
      COMM=RR(2)*(ZZ(3)-ZZ(1))+RR(1)*(ZZ(2)-ZZ(3))+RR(3)*(ZZ(1)-ZZ(2))
      OO(1,1)=(RR(2)*ZZ(3)-RR(3)*ZZ(2))/COMM
      OO(1,2)=(RR(3)*ZZ(1)-RR(1)*ZZ(3))/COMM
      OO(1,3)=(RR(1)*ZZ(2)-RR(2)*ZZ(1))/COMM
      DO(2,1)=(ZZ(2)-ZZ(3))/COMM
      DO(2,2)=(ZZ(3)-ZZ(1))/COMM
      DO(2,3)=(ZZ(1)-ZZ(2))/COMM
      DO(3,1)=(RR(3)-RR(2))/COMM
      DO(3,2)=(RR(1)-RR(3))/COMM
      DO(3,3)=(PR(2)-RR(1))/COMM
      DO 120 I=1,3
      J=2*LM(I)-1
      M(1,J)=OO(1,1)
      M(2,J)=DO(2,1)
      M(3,J)=DD(3,1)
      M(4,J)=DO(1,2)
      M(5,J+1)=DO(2,2)
  120 M(6,J+1)=DO(3,2)
C     4. ROTATE UNKNOWNS IF REQUIRED
      DO 125 J=1,2
      I=LM(J)
      IF (ANGLE(I)) 122,125,125
  122 SINA=SIN(ANGLE(I))
      COSA=COS(ANGLE(I))
      I=2*I
      DO 124 K=1,6
      TEM=H(K,I-1)
      H(K,I-1)=TEM*COSA+H(K,I)*SINA
  124 H(K,I)= -TEM*SINA+H(K,I)*COSA
  125 CONTINUE
C     5. FORM ELEMENT STIFFNESS MATRIX (H)T*(D)*(H)
```

```
      DO 130 J=1,10
      DO 130 K=1,6
      IF (H(K,J)) 128,130,128
  128 DO 129 I=1,6
  129 F(I,J)=F(I,J)+O(I,K)*H(K,J)
  130 CONTINUE
      DO 140 I=1,10
      DO 140 K=1,6
      IF (H(K,I)) 138,140,138
  138 DO 139 J=1,10
  139 S(I,J)=S(I,J)+H(K,I)*F(K,J)
  140 CONTINUE
C     6.  FORM STRAIN TRANSFORMATION MATRIX
  400 DO 410 I=1,6
      DO 410 J=1,10
  410 HH(I,J)=HH(I,J)+H(I,J)
      RETURN
      END
C*************************************************************************
      SUBROUTINE QUAD(N,VOL)
C*************************************************************************
      COMMON/INTGR/NUMNP,NUMEL,NUMMAT,NUMPC,NP,IBC(40),JBC(40),NXPAN,
     1 IX(850,5),HED(20),NPP,MTYPE,NSTEP,NUMCOL,NUMROW,NPPP,NUMPCP,NPPN,
     2 NPRES,IBCP(50),JBCP(50),IBCE(50),JBCE(50),URU(51),URU1(51),DVOL,
     3 URU2(51),NUNS,NRES,UNPRES,OCT,REST,VCONT,BLK,VOLINT,RINT,BNO,DIST
      COMMON/BULK/ESV8(850),ESH8(850),POHB(850),POVB(850)
      COMMON/PROP/MATYP(50),E(11,10),RO(10),AKO(10),EE(7),ET(11),
     1 CDAO(10),CP(10),EH(11,10),EEH(7),ETH(11)
      COMMON/LOAD/CODE(900),PR(40),ANGLE(4),PRP(50),PRE(50)
      COMMON/BEOM/R(900),Z(900),UR(900),UZ(900),DISP(900,2),
     1 RAO(ST(30),ELEV(50)
      COMMON/STRSS/SIGMA(4,850),SIG(11),SIGMAO(4,850),GSTRSS(850),SIGOEP
      COMMON /ARG/ RPR(5),ZZZ(5),S(10,10),P(10),TT(4),LM(4),DO(3,3),
     1 HH(6,10),RM(4),ZZ(4),C(4,4),H(6,10),D(6,6),F(6,10),TP(6),XI(10)
      COMMON /BANAR8/ MBANO,NUMBLK,R(108),A(108,54)
C*************************************************************************
   90 I=IX(N,1)
      J=IX(N,2)
      K=IX(N,3)
      L=IX(N,4)
      MTYPE=IX(N,5)
      IX(N,5)=-IX(N,5)
C     FORM STRESS-STRAIN RELATIONSHIP
      CC=(SIGMA(1,N)+SIGMA(2,N))/2.0
      BB=(SIGMA(1,N)-SIGMA(2,N))/2.0
      CR=SQRT(SIGMA(4,N)*SIGMA(4,N)+BB*BB)
      SIG3=CC-CR
      SIG1=CC+CR
      SIG2=SIGMA(3,N)
      SIGDCT=(SIG1+SIG2+SIG3)/3.0
      IF(SIGMA(3,N).LT.SIG3)SIG3 = SIGMA(3,N)
      IF(SIGMA(3,N).GT.SIG1)SIG1 = SIGMA(3,N)
      CR=(SIG1 - SIG3)/2.0
      DO 20 MM=1,11
      ET(MM) = F(MM,MTYPE)
      ETH(MM) = EH(MM,MTYPE)
   20 CONTINUE
C     COMPUTE MODULI AND POISSONS RATIOS
      ET(2)=ET(2)/57.28
      ETH(2) = ETH(2)/57.28
      RCS=2.0*(ET(1)*COS(ET(2))+SIG3*SIN(ET(2)))/(1.0-SIN(ET(2)))
      RCSH=2.0*(ETH(1)*COS(ETH(2))+SIG3*SIN(ETH(2)))/(1.0-SIN(ETH(2)))
      HCS=RCS/ET(3)
      HCSH = RCSH/ETH(3)
      SHBFOR=(GSTRSS(N)-AKO(MTYPE)*GSTRSS(N))/2.0
      IF(COAD(MTYPE),EQ.0.0)F(11)=SIG3
      IF(COAD(MTYPE),EQ.0.0.AND.OCT,NE.0.0)F(11)=SIGOCT
      IF(COAD(MTYPE),EQ.1.0)F(11)=CP(MTYPE)
      IF(CDAD(MTYPE),EQ.2.0)F(11)=ET(1)
      IF (F(11).LE.0.0) F(11) = 1.0
      EI=ET(4)*(F(11)**ET(5))
      EE(1)=EI*(1.0-(2.0*CR/HCS))*(1.0-(2.0*CR/HCS))
      IF(CDAD(MTYPE)) 24,25,24
   25 IF(NXPAN,EQ,1)   EE(1)=ET(11)*(F(11)**ET(5))
      IF(NSTEP,EQ,1.AND.DIST,NE,0.0) EE(1)=ET(11)*(F(11)**ET(5))*DIST
      INREST=REST
      IF((NSTEP,GE,1),AND.(NSTEP,LE,INREST)) GO TO 669
      GO TO 778
  669 IF (DIST,EQ,0.0) EE(1)=ET(11)*(F(11)**ET(5))
      IF (DIST,NE,0.0) EE(1)=ET(11)*(F(11)**ET(5))*DIST
  778 IF(NPRES) 23,24,23
   23 IF(NPRES,EQ,NUNS)EE(1)=ET(11)*(F(11)**ET(5))
      IF(NPRES,EQ,NRES)EE(1)=ET(11)*(F(11)**ET(5))
   24 EIH = ETH(11)*(F(11)**ETH(5))
      EEH(1)=EIH*(1.0-(2.0*CR/HCSH))*(1.0-(2.0*CR/HCSH))
      IF(COAD(MTYPE)) 26,27,26
   27 IF(NXPAN,EQ,1)   EEH(1)=ETH(11)*(F(11)**ETH(5))
      IF(NSTEP,FQ,1,AND,DIST,NE,0.0)EEH(1)=ETH(11)*(F(11)**ETH(5))*DIST
      INREST=REST
      IF((NSTEP,GE,1),AND.(NSTEP,LE,INREST)) GO TO 666
      GO TO 779
  666 IF (DIST,FQ,0.0) EEH(1)=ETH(11)*(F(11)**ETH(5))
      IF (DIST,NE,0.0) FEH(1)=ETH(11)*(F(11)**ETH(5))*DIST
  779 IF(NPRES) 28,26,28
   28 IF(NPRES,EQ,NUNS)EEH(1)=ETH(11)*(F(11)**ETH(5))
      IF(NPRES,EQ,NRES)EEH(1)=ETH(11)*(F(11)**ETH(5))
   26 SIGT = SIG3
      IF(SIGT.LE.1.0)SIGT=1.0
      STRAIN=2.0*CR/(EI*(1.0-(2.0*CR/HCS)))
      PRAT=ET(7)-ET(8)*ALOG10(SIGT)
      EF(2)=PRAT/(1.0-ET(9)*STRAIN)*(1.0-ET(9)*STRAIN))
      HORST  =2.0*CR/(EIH*(1.0-(2.0*CR/HCSH)))
      PRATH=ETH(7) - ETH(8)*ALOG10(SIGT)
      EEH(2)=PRATH/(1.0-ETH(9)*HORST)*(1.0-ETH(9)*HORST))
      IF(NPRES) 11,12,11
   11 IF(NPRES,FQ,NUNS) GO TO 50
      IF(NPRES,EQ,NRES) GO TO 50
   12 IF(BB,GE,0.0) GO TO 37
      IF(2.0*CR,GE,RCS,AND,BLK,GT,0.0) GO TO 498
      IF(2.0*CR,GE,RCS,AND,BLK,EQ,0.0) GO TO 35
      IF(SIG3,LF,0.0,AND,ABS(SIG3),GE,ABS(ET(10)))GO TO 30
      IF (F(1+1),LE,1.0)  GO TO 30
      GO TO 50
   30 EE(1)=FT(6)
      EF(2)=ET(7)
      GO TO 50
   35 WRITE (6,2002) N
      EE(1) = 1.11*ET(6)
```

```
      EE(2) = ET(7)-0.01
      GO TO 50
   37 IF (2.0*CR.GE.RC5H.AND.BLK.GT.0.0) GO TO 498
      IF (2.0*CR.GE.RC5H.AND.BLK.EQ.0.0) GO TO 39
      IF(5IG3.LE.0.0.AND.ABS(5IG3).GE.ABS(ETH(10))) GO TO 38
      IF (F(1+1).LE.1.0) GO TO 38
      GO TO 50
   38 EEH(1) = ETH(6)
      EEH(2) = ETH(7)
      GO TO 50
   39 WRITE (6,2003) N
      EEH(1) = 1.1*ETH(6)
      EEH(2) = ETH(7)-0.01
      GO TO 50
   50 IF(EE(2).GT.0.48)EE(2)=0.48
      IF (EEH(2).GT.0.48)  EEH(2) = 0.48
  400 EE(3)=EE(1)
      EE(4)=EE(2)
      EEH(3) = EEH(1)
      EEH(4) = EEH(2)
   86 C(1+1)=1.0/EEH(1)
      C(1,2)=-EE(2)/EE(1)
      C(1+3)=-EEH(4)/EEH(3)
      C(2+1)=C(1+2)
      C(2,2)=1.0/EE(1)
      C(2+3)=-EE(2)/EE(1)
      C(3+1)=C(1+3)
      C(3+2)=C(2+3)
      C(3+3)=1.0/EEH(3)
      CALL SYMINV(C+3)
      C(4+4)=EE(1)/(1.0 + EE(1)/EEH(1) + 2.0*EE(2))
      GO TO 500
C     FORM BULK MATRIX FOR FAILURE CONDITION
  498 IF(EE(2).GT.0.48)EE(2)=0.48
      IF (EEH(2).GT.0.48)  EEH(2) = 0.48
      WRITE (6+2001) N
      ENRAT = ESVB(N)/ESHB(N)
      DENKB=1.0+2.0*ENRAT-4.0*POVB(N)-2.0*PDHB(N)*ENRAT
      KB=ESVB(N)/DENKB
      DO 77  III=1+3
      DO 78   JJJ=1+3
      C(III+JJJ)=KB
   78 CONTINUE
   77 CONTINUE
      C(4+4)=0.0
C     FORM QUADRILATERAL STIFFNESS MATRIX
  500 RRR(5)=(R(I)+R(J)+R(K)+R(L))/4.0
      ZZZ(5)=(Z(I)+Z(J)+Z(K)+Z(L))/4.0
      DO 94 MM=1+4
      MM=IX(N+M)
      IF(R(MM)) 93+91+93
   91 R(MM)=0.01*RRR(5)
      IF(CODE(MM)) 93,92+93
   92 CODE(MM)=1.0
   93 RRR(M)=R(MM)
   94 ZZZ(M)=Z(MM)
      DO 96  II=1+10
      P(II)=0.0
      DO 95 JJ=1+6
   95 HH(JJ+II)=0.0
      DO 96   JJ=1+10
   96 S(II+JJ)=0.0
      DO 119 II=1+4
      JJ=IX(N+II)
  119 ANGLE(II)=CODE(JJ)/57.3
      IF (K-L) 125+120+125
  120 CALL TRISTF(1+2+3)
      RRR(5)=(RRR(1)+RRR(2)+RRR(3))/3.0
      ZZZ(5)=(ZZZ(1)+ZZZ(2)+ZZZ(3))/3.0
      VOL=XI(1)
      GO TO 130
  125 VOL=0.0
      CALL TRISTF(4+1+5)
      VOL=VOL+XI(1)
      CALL TRISTF(1+2+5)
      VOL=VOL+XI(1)
      CALL TRISTF(2+3+5)
      VOL=VOL+XI(1)
      CALL TRISTF(3+4+5)
      VOL=VOL+XI(1)
      DO 140 II=1+6
      DO 140 JJ=1+10
  140 HH(II+JJ)=HH(II+JJ)/4.0
  130 RETURN
C*****************************************************************
 2001 FORMAT (34H0BULK MODULUS USED IN ELEMENT NO.   I4)
 2002 FORMAT (40H0FAILED VERTICAL MODULUS IN ELEMENT NO.   I4)
 2003 FORMAT (42H0FAILED HORIZONTAL MODULUS IN ELEMENT NO.   I4)
C*****************************************************************
      END
C*****************************************************************
      SUBROUTINE MODIFY(A+B+NEQ+MBAND+N+U)
C*****************************************************************
      DIMENSION A(108+54)+B(108)
      DO 250 M=2+MBAND
      K=N-M+1
      IF(K) 235+235+230
  230 B(K)=B(K)-A(K+M)*U
      A(K+M)=0.0
  235 K=N+M-1
      IF(NEQ-K) 250+240+240
  240 B(K)=B(K)-A(N+M)*U
      A(N+M)=0.0
  250 CONTINUE
      A(N+1)=1.0
      B(N)=U
      RETURN
      END
C*****************************************************************
      SUBROUTINE INTFR(XI+RR+ZZ)
C*****************************************************************
      DIMENSION RR(4)+ZZ(4)+XI(10)+XM(6)+R(6)+Z(6)+XX(6)
      DATA XX/1.0+1.0+1.0+3.0+3.0+3.0/
      COMM=RR(2)*(ZZ(3)-ZZ(1))+RR(1)*(ZZ(2)-ZZ(3))+RR(3)*(ZZ(1)-ZZ(2))
      COMM=COMM/24.0
      R(1)=RR(1)
      R(2)=RR(2)
      R(3)=RR(3)
```

```
      R(4)=(R(1)+R(2))/2.
      R(5)=(R(2)+R(3))/2.
      R(6)=(R(3)+R(1))/2.
      Z(1)=ZZ(1)
      Z(2)=ZZ(2)
      Z(3)=ZZ(3)
      Z(4)=(Z(1)+Z(2))/2.
      Z(5)=(Z(2)+Z(3))/2.
      Z(6)=(Z(3)+Z(1))/2.
   30 DO 35 I=1,6
   35 XM(I)=XX(I)*R(I)
   40 DO  50 I=1,10
   50 XI(I)=0.0
      DO 100 I=1,6
      XI(1)=XI(1)+XM(I)
      XI(2)=XI(2)+XM(I)/R(I)
      XI(3)=XI(3)+XM(I)/(R(I)**2)
      XI(4)=XI(4)+XM(I)*Z(I)/R(I)
      XI(5)=XI(5)+XM(I)*Z(I)/(R(I)**2)
      XI(6)=XI(6)+XM(I)*Z(I)**2/(R(I)**2)
      XI(7)=XI(7)+XM(I)*R(I)
      XI(8)=XI(8)+XM(I)*Z(I)
      XI(9)=XI(9)+XM(I)*R(I)**2
      XI(10)=XI(10)+XM(I)*R(I)*Z(I)
  100 CONTINUE
      DO 150 I=1,10
  150 XI(I)=XI(I)*COMM
      RETURN
      END
C*******************************************************************************
      SUBROUTINE SYMINV(A,NMAX)
C*******************************************************************************
      DIMENSION A(4,4)
      DO 200 N=1,NMAX
      D=A(N,N)
      DO 100 J=1,NMAX
  100 A(N,J)=-A(N,J)/D
      DO 150 I=1,NMAX
      IF(N-I) 110,150,110
  110 DO 140 J=1,NMAX
      IF(N-J) 120,140,120
  120 A(I,J)=A(I,J)+A(I,N)*A(N,J)
  140 CONTINUE
  150 A(I,N)=A(I,N)/D
      A(N,N)=1.0/D
  200 CONTINUE
      RETURN
      END
C*******************************************************************************
      SUBROUTINE BANSOL
C*******************************************************************************
      COMMON /BANARG/ MM,NUMBLK,B(108),A(108,54)
      NN=54
      NL=NN+1
      NH=NN+NN
      NB=0
      GO TO 150
C     REDUCE EQUATIONS BY BLOCKS
C     1. SHIFT BLOCK OF EQUATIONS
  100 NB=NB+1
      DO 125 N=1,NN
      NM=NN+N
      B(N)=B(NM)
      B(NM)=0.0
      DO 125 M=1,MM
      A(N,M)=A(NM,M)
  125 A(NM,M)=0.0
C     2. READ NEXT BLOCK OF EQUATIONS INTO CORE
      IF (NUMBLK-NB) 150,200,150
  150 READ (2) (B(N),(A(N,M),M=1,MM),N=NL,NH)
      IF (NB) 200,100,200
C     3. REDUCE BLOCK OF EQUATIONS
  200 DO 300 N=1,NN
      IF (A(N,1)) 225,300,225
  225 B(N)=B(N)/A(N,1)
      DO 275 L=2,MM
      IF (A(N,L)) 230,275,230
  230 C=A(N,L)/A(N,1)
      I=N-L-1
      J=0
      DO 250 K=L,MM
      J=J+1
  250 A(I+J)=A(I+J)-C*A(N,K)
      B(I)=B(I)-A(N,L)*B(N)
      A(N,L)=C
  275 CONTINUE
  300 CONTINUE
C     4. WRITE BLOCK OF REDUCED EQUATIONS ON TAPE
      IF (NUMBLK-NB) 375,400,375
  375 WRITE (1) (B(N),(A(N,M),M=2,MM),N=1,NN)
      GO TO 100
C     BACK-SUBSTITUTION
  400 DO 450 N=1,NN
      N=NN+1-N
      DO 425 K=2,MM
      L=N-1
  425 B(N)=B(N)-A(N,K)*B(L)
      NM=N+NN
      B(NM)=B(N)
  450 A(NM,NB)=B(N)
      NB=NB-1
      IF (NB) 475,500,475
  475 BACKSPACE 1
      READ (1) (B(N),(A(N,M),M=2,MM),N=1,NN)
      BACKSPACE 1
      GO TO 400
C     ORDER UNKNOWNS IN B ARRAY
  500 K=0
      DO 600 NB=1,NUMBLK
      DO 600 N=1,NN
      NM=N+NN
      K=K+1
  600 B(K)=A(NM,NB)
      REWIND 1
      REWIND 2
      RETURN
      END
```

APPENDIX IV

LABORATORY TRIAXIAL TESTS ON EDGAR SAND

EDGAR SAND TRIAXIAL TEST DATA - 0.5 KG/SQ CM CONFINING PRESSURE

INITIAL SAMPLE HEIGHT IN CM ----------	7.82
HEIGHT CHANGE DUE TO CONSOL IN CM ------	0.0
INITIAL SAMPLE DIAMETER IN CM ----------	3.56
VOLUME CHANGE DUE TO CONSOL IN CC ------	0.95

COMPRESSION DIAL FACTOR IN CM/DIV ------	0.000254
LMD DIAL FACTOR IN KG/DIV -------------	0.022900
INITIAL COMPRESSION DIAL READING -------	580.0
INITIAL LMD DIAL READING ----------	30225.0
INITIAL VOLUME READING IN CC ----------	13.98

INITIAL AREA IN SQ CM ------------------	9.95
INITIAL VOLUME IN CC -------------------	76.89
CONFINING PRESSURE IN KG/SQ CM ---------	0.50

INITIAL DENSITY IN GM/CC ---------------	1.630
INITIAL DENSITY IN LB/CU FT ------------	101.79
INITIAL VOID RATIO ---------------------	0.626
INITIAL RELATIVE DENSITY IN PERCENT ----	76.18

LMD READING	LOAD (KG)	COMP DIAL READING	AXIAL STRAIN	VOL CHG	VOLUME STRAIN	AREA (SQ CM)	SIG1-SIG3 (KG/SQ CM)	EPS/SIG RATIO	RADIAL STRAIN	RAD/AX RATIO	SIGOCT (KG/SQ CM)
30502.0	6.3	630.0	0.00162	-0.060	-0.00078	9.96	0.64	0.00255	0.00042	0.25975	0.71224
30675.0	10.3	720.0	0.00455	-0.080	-0.00104	9.99	1.03	0.00441	0.00175	0.38560	0.84388
30725.0	11.4	780.0	0.00650	0.020	0.00026	10.02	1.14	0.00569	0.00338	0.52002	0.88085
30750.0	12.0	880.0	0.00974	0.020	0.00026	10.05	1.20	0.00815	0.00500	0.51335	0.89858
30782.0	12.8	980.0	0.01299	0.050	0.00065	10.09	1.26	0.01028	0.00682	0.52503	0.92133
30812.0	13.4	1080.0	0.01624	0.140	0.00182	10.14	1.33	0.01225	0.00903	0.55606	0.94204
30830.0	13.9	1180.0	0.01949	0.240	0.00312	10.18	1.36	0.01432	0.01130	0.58008	0.95350
30860.0	14.5	1380.0	0.02598	0.420	0.00546	10.28	1.42	0.01836	0.01572	0.60511	0.97174
30870.0	14.8	1580.0	0.03248	0.600	0.00780	10.37	1.42	0.02280	0.02014	0.62012	0.97486
30880.0	15.0	1700.0	0.03638	0.700	0.00910	10.42	1.44	0.02528	0.02274	0.62513	0.97966

EDGAR SAND TRIAXIAL TEST DATA - 1.0 KG/SQ CM CONFINING PRESSURE

INITIAL SAMPLE HEIGHT IN CM ----------	7.88
HEIGHT CHANGE DUE TO CONSOL IN CM ------	0.0
INITIAL SAMPLE DIAMETER IN CM ----------	3.57
VOLUME CHANGE DUE TO CONSOL IN CC ------	1.62

COMPRESSION DIAL FACTOR IN CM/DIV ------	0.000254
LMD DIAL FACTOR IN KG/DIV --------------	0.022900
INITIAL COMPRESSION DIAL READING -------	738.0
INITIAL LMD DIAL READING ---------------	30255.0
INITIAL VOLUME READING IN CC -----------	16.05

INITIAL AREA IN SQ CM -------------------	10.01
INITIAL VOLUME IN CC --------------------	77.26
CONFINING PRESSURE IN KG/SQ CM ---------	1.00

INITIAL DENSITY IN GM/CC ---------------	1.633
INITIAL DENSITY IN LB/CU FT ------------	101.97
INITIAL VOID RATIO ----------------------	0.623
INITIAL RELATIVE DENSITY IN PERCENT ----	76.92

LMD READING	LOAD (KG)	COMP DIAL READING	AXIAL STRAIN	VOL CHG	VOLUME STRAIN	AREA (SQ CM)	SIG1-SIG3 (KG/SQ CM)	EPS/SIG RATIO	RADIAL STRAIN	RAD/AX RATIO	SIGOCT (KG/SQ CM)
30575.0	7.3	780.0	0.00135	-0.050	-0.00065	10.02	0.73	0.00185	0.00035	0.26103	1.24385
30995.0	16.9	880.0	0.00458	-0.070	-0.00091	10.05	1.69	0.00271	0.00184	0.40104	1.56224
31135.0	20.2	940.0	0.00651	-0.060	-0.00078	10.07	2.00	0.00325	0.00287	0.44037	1.66722
31294.0	23.8	1050.0	0.01006	0.0	0.0	10.11	2.35	0.00427	0.00503	0.50000	1.78436
31340.0	24.8	1100.0	0.01167	0.050	0.00065	10.13	2.45	0.00476	0.00616	0.52773	1.81722
31390.0	26.0	1200.0	0.01489	0.130	0.00168	10.18	2.55	0.00583	0.00829	0.55650	1.85121
31430.0	26.9	1310.0	0.01844	0.250	0.00324	10.23	2.63	0.00701	0.01084	0.58775	1.87668
31460.0	27.6	1400.0	0.02134	0.330	0.00427	10.27	2.69	0.00794	0.01281	0.60009	1.89548
31488.0	28.2	1500.0	0.02456	0.420	0.00544	10.32	2.74	0.00898	0.01500	0.61067	1.91221
31505.0	28.6	1600.0	0.02779	0.500	0.00647	10.36	2.76	0.01006	0.01713	0.61646	1.92078
31525.0	29.1	1800.0	0.03423	0.700	0.00906	10.46	2.78	0.01231	0.02165	0.63234	1.92693
31540.0	29.4	2000.0	0.04068	0.850	0.01100	10.55	2.79	0.01458	0.02584	0.63523	1.92983
31560.0	29.9	2200.0	0.04713	1.050	0.01359	10.65	2.81	0.01679	0.03036	0.64420	1.93556
31575.0	30.2	2600.0	0.06002	1.370	0.01773	10.84	2.79	0.02152	0.03888	0.64773	1.92971
31585.0	30.5	2900.0	0.06969	1.630	0.02110	10.99	2.77	0.02514	0.04539	0.65138	1.92406
31590.0	30.6	3200.0	0.07936	1.850	0.02395	11.13	2.75	0.02890	0.05165	0.65087	1.91534

EDGAR SAND TRIAXIAL TEST DATA - 2.0 KG/SQ CM CONFINING PRESSURE

INITIAL SAMPLE HEIGHT IN CM ----------	8.00
HEIGHT CHANGE DUE TO CONSOL IN CM ------	0.0
INITIAL SAMPLE DIAMETER IN CM ----------	3.57
VOLUME CHANGE DUE TO CONSOL IN CC ------	1.27

COMPRESSION DIAL FACTOR IN CM/DIV ------	0.000254
LMD DIAL FACTOR IN KG/DIV ----------	0.022900
INITIAL COMPRESSION DIAL READING -------	115.0
INITIAL LMD DIAL READING ----------	30300.0
INITIAL VOLUME READING IN CC ----------	16.73

INITIAL AREA IN SQ CM ----------	10.01
INITIAL VOLUME IN CC ----------	78.81
CONFINING PRESSURE IN KG/SQ CM ---------	2.00

INITIAL DENSITY IN GM/CC ----------	1.611
INITIAL DENSITY IN LB/CU FT ----------	100.60
INITIAL VOID RATIO ----------	0.645
INITIAL RELATIVE DENSITY IN PERCENT ----	71.10

LMD READING	LOAD (KG)	COMP DIAL READING	AXIAL STRAIN	VOL CHG	VOLUME STRAIN	AREA (SQ CM)	SIG1-SIG3 (KG/SQ CM)	EPS/SIG RATIO	RADIAL STRAIN	RAD/AX RATIO	SIGOCT (KG/SQ CM)
30930.0	14.4	140.0	0.00079	-0.030	-0.00038	10.01	1.44	0.00055	0.00021	0.26022	2.48023
31400.0	25.2	200.0	0.00270	-0.110	-0.00140	10.02	2.51	0.00107	0.00065	0.24140	2.83775
31715.0	32.4	250.0	0.00429	-0.130	-0.00165	10.04	3.23	0.00133	0.00132	0.30757	3.07621
32130.0	41.9	350.0	0.00746	-0.130	-0.00165	10.07	4.16	0.00179	0.00291	0.38945	3.38741
32410.0	48.3	480.0	0.01159	-0.030	-0.00038	10.12	4.77	0.00243	0.00560	0.48358	3.59101
32495.0	50.3	550.0	0.01381	0.020	0.00025	10.15	4.95	0.00279	0.00703	0.50919	3.65034
32600.0	52.7	650.0	0.01699	0.080	0.00102	10.19	5.17	0.00329	0.00900	0.52988	3.72240
32630.0	53.4	750.0	0.02016	0.170	0.00216	10.24	5.21	0.00387	0.01116	0.55350	3.73725
32725.0	55.5	950.0	0.02651	0.350	0.00444	10.33	5.38	0.00493	0.01548	0.58376	3.79228
32765.0	56.4	1150.0	0.03286	0.490	0.00622	10.41	5.42	0.00606	0.01954	0.59460	3.80677
32765.0	56.4	1250.0	0.03604	0.570	0.00723	10.46	5.40	0.00668	0.02163	0.60035	3.79902
32770.0	56.6	1350.0	0.03921	0.660	0.00837	10.51	5.38	0.00728	0.02379	0.60679	3.79470
32770.0	56.6	1450.0	0.04239	0.740	0.00939	10.55	5.36	0.00791	0.02589	0.61076	3.78697

EDGAR SAND TRIAXIAL TEST DATA - 0.5 KG/SQ CM CONFINING PRESSURE

INITIAL SAMPLE HEIGHT IN CM ----------	7.93
HEIGHT CHANGE DUE TO CONSOL IN CM ------	0.0
INITIAL SAMPLE DIAMETER IN CM ----------	3.56
VOLUME CHANGE DUE TO CONSOL IN CC ------	0.0

COMPRESSION DIAL FACTOR IN CM/DIV ------	0.000254
LMD DIAL FACTOR IN KG/DIV -------------	0.022900
INITIAL COMPRESSION DIAL READING -------	496.0
INITIAL LMD DIAL READING ---------------	34450.0
INITIAL VOLUME READING IN CC -----------	17.20

INITIAL AREA IN SQ CM -------------------	9.95
INITIAL VOLUME IN CC --------------------	78.93
CONFINING PRESSURE IN KG/SQ CM ---------	0.50

INITIAL DENSITY IN GM/CC ---------------	1.755
INITIAL DENSITY IN LB/CU FT ------------	109.61
INITIAL VOID RATIO ----------------------	0.510
INITIAL RELATIVE DENSITY IN PERCENT ----	106.66

LMD READING	LOAD (KG)	COMP DIAL READING	AXIAL STRAIN	VOL CHG	VOLUME STRAIN	AREA (SQ CM)	SIG1-SIG3 (KG/SQ CM)	EPS/SIG RATIO	RADIAL STRAIN	RAD/AX RATIO	SIGOCT (KG/SQ CM)
34749.0	6.8	520.0	0.00077	-0.080	-0.00101	9.95	0.69	0.00112	-0.00012	-0.15923	0.72935
35004.0	12.7	580.0	0.00269	-0.100	-0.00127	9.97	1.27	0.00211	0.00071	0.26455	0.92424
35150.0	16.0	640.0	0.00461	-0.020	-0.00025	10.00	1.60	0.00288	0.00218	0.47253	1.03447
35234.0	18.0	700.0	0.00653	0.080	0.00101	10.03	1.79	0.00365	0.00377	0.57756	1.09670
35338.0	20.3	800.0	0.00974	0.220	0.00279	10.08	2.02	0.00483	0.00626	0.64312	1.17248
35391.0	21.5	900.0	0.01294	0.450	0.00570	10.14	2.12	0.00609	0.00932	0.72028	1.20825
35434.0	22.5	1000.0	0.01614	0.700	0.00887	10.21	2.21	0.00731	0.01251	0.77467	1.23590
35480.0	23.6	1100.0	0.01935	0.920	0.01166	10.27	2.30	0.00842	0.01550	0.80123	1.26568
35472.0	23.4	1200.0	0.02255	1.150	0.01457	10.33	2.27	0.00995	0.01856	0.82305	1.25507
35480.0	23.6	1300.0	0.02575	1.430	0.01812	10.40	2.27	0.01136	0.02193	0.85174	1.25585
35490.0	23.8	1400.0	0.02896	1.700	0.02154	10.47	2.27	0.01273	0.02525	0.87190	1.25813
35500.0	24.0	1600.0	0.03536	2.200	0.02787	10.61	2.27	0.01560	0.03162	0.89409	1.25568

EDGAR SAND TRIAXIAL TEST DATA - 1.0 KG/SQ CM CONFINING PRESSURE

INITIAL SAMPLE HEIGHT IN CM ----------	8.00
HEIGHT CHANGE DUE TO CONSOL IN CM ------	0.0
INITIAL SAMPLE DIAMETER IN CM ----------	3.55
VOLUME CHANGE DUE TO CONSOL IN CC ------	0.85

COMPRESSION DIAL FACTOR IN CM/DIV ------	0.000254
LMD DIAL FACTOR IN KG/DIV -------------	0.002900
INITIAL COMPRESSION DIAL READING -------	608.0
INITIAL LMD DIAL READING ----------	34532.0
INITIAL VOLUME READING IN CC ----------	14.75

INITIAL AREA IN SQ CM -------------------	9.90
INITIAL VOLUME IN CC -------------------	78.33
CONFINING PRESSURE IN KG/SQ CM ---------	1.00

INITIAL DENSITY IN GM/CC ----------	1.744
INITIAL DENSITY IN LB/CU FT ----------	108.89
INITIAL VOID RATIO ----------	0.520
INITIAL RELATIVE DENSITY IN PERCENT ----	104.03

LMD READING	LOAD (KG)	COMP DIAL READING	AXIAL STRAIN	VOL CHG	VOLUME STRAIN	AREA (SQ CM)	SIG1-SIG3 (KG/SQ CM)	EPS/SIG RATIO	RADIAL STRAIN	RAD/AX RATIO	SIGOCT (KG/SQ CM)
35055.0	12.0	630.0	0.00070	-0.050	-0.00064	9.90	1.21	0.00058	0.00003	0.04309	1.40331
35345.0	18.6	700.0	0.00292	-0.070	-0.00089	9.92	1.88	0.00156	0.00101	0.34704	1.62571
35706.0	26.9	800.0	0.00610	0.0	0.0	9.96	2.70	0.00226	0.00305	0.50000	1.89987
35933.0	32.1	900.0	0.00927	0.150	0.00191	10.01	3.21	0.00289	0.00559	0.60327	2.06839
36038.0	34.5	1000.0	0.01245	0.280	0.00357	10.06	3.43	0.00363	0.00801	0.64360	2.14289
36150.0	37.1	1100.0	0.01562	0.480	0.00613	10.12	3.66	0.00427	0.01087	0.69513	2.22083
36215.0	38.5	1200.0	0.01880	0.680	0.00868	10.18	3.79	0.00496	0.01374	0.73092	2.26258
36260.0	39.6	1300.0	0.02197	0.870	0.01111	10.23	3.87	0.00568	0.01654	0.75275	2.28904
36295.0	40.4	1400.0	0.02515	1.130	0.01443	10.30	3.92	0.00642	0.01979	0.78683	2.30659
36310.0	40.7	1500.0	0.02832	1.350	0.01723	10.36	3.93	0.00721	0.02278	0.80426	2.30979
36345.0	41.5	1600.0	0.03150	1.550	0.01979	10.42	3.98	0.00791	0.02564	0.81412	2.32788
36345.0	41.5	1700.0	0.03467	1.750	0.02234	10.48	3.96	0.00875	0.02851	0.82218	2.32022
36345.0	41.5	1800.0	0.03785	1.960	0.02502	10.54	3.94	0.00961	0.03143	0.83056	2.31243
36335.0	41.3	2000.0	0.04420	2.370	0.03026	10.67	3.87	0.01142	0.03723	0.84228	2.28999

EDGAR SAND TRIAXIAL TEST DATA - 2.0 KG/SQ CM CONFINING PRESSURE

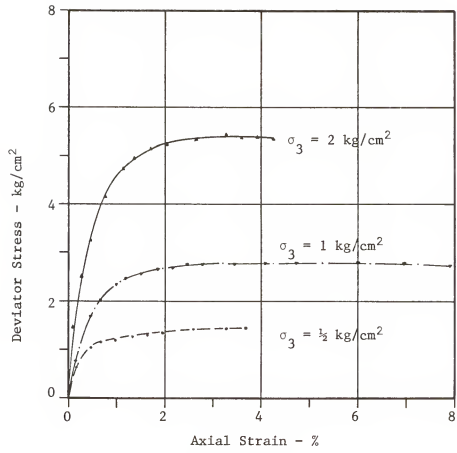
INITIAL SAMPLE HEIGHT IN CM ----------	7.91
HEIGHT CHANGE DUE TO CONSOL IN CM ------	0.0
INITIAL SAMPLE DIAMETER IN CM ----------	3.55
VOLUME CHANGE DUE TO CONSOL IN CC ------	2.45

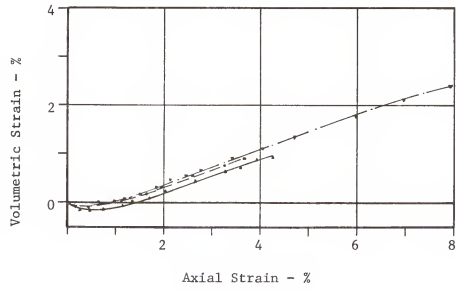
COMPRESSION DIAL FACTOR IN CM/DIV ------	0.000200
LMD DIAL FACTOR IN KG/DIV --------------	0.022900
INITIAL COMPRESSION DIAL READING -------	1564.0
INITIAL LMD DIAL READING ---------------	34544.0
INITIAL VOLUME READING IN CC -----------	16.75

INITIAL AREA IN SQ CM -------------------	9.90
INITIAL VOLUME IN CC --------------------	75.84
CONFINING PRESSURE IN KG/SQ CM ---------	2.00

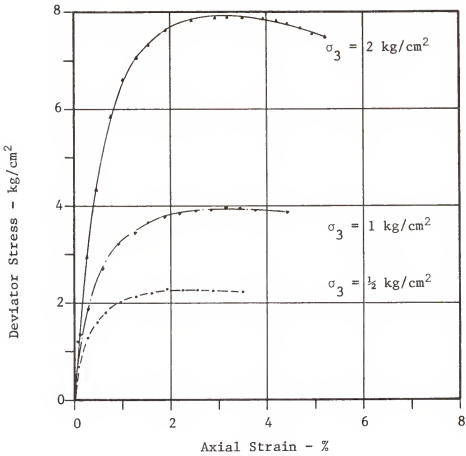
INITIAL DENSITY IN GM/CC ----------------	1.790
INITIAL DENSITY IN LB/CU FT ------------	111.76
INITIAL VOID RATIO ----------------------	0.481
INITIAL RELATIVE DENSITY IN PERCENT ----	114.31

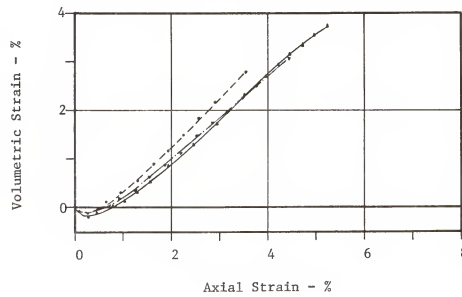
LMD READING	LOAD (KG)	COMP DIAL READING	AXIAL STRAIN	VOL CHG	VOLUME STRAIN	AREA (SQ CM)	SIG1=SIG3 (KG/SQ CM)	EPS/SIG RATIO	RADIAL STRAIN	RAD/AX RATIO	SIGOCT (KG/SQ CM)
35127.0	13.4	1618.0	0.00137	-0.050	-0.00066	9.90	1.35	0.00101	0.00035	0.25856	2.44929
35828.0	29.4	1668.0	0.00263	-0.150	-0.00198	9.90	2.97	0.00089	0.00033	0.12392	2.98958
36430.0	43.2	1748.0	0.00465	-0.060	-0.00079	9.94	4.35	0.00107	0.00193	0.41496	3.44887
37088.0	58.3	1868.0	0.00769	0.030	0.00040	9.98	5.84	0.00132	0.00404	0.52573	3.94609
37428.0	66.0	1968.0	0.01021	0.100	0.00132	10.01	6.60	0.00155	0.00577	0.56453	4.19853
37644.0	71.0	2078.0	0.01300	0.250	0.00330	10.06	7.06	0.00184	0.00815	0.62682	4.35190
37787.0	74.3	2178.0	0.01552	0.420	0.00554	10.11	7.35	0.00211	0.01053	0.67835	4.44862
37930.0	77.5	2328.0	0.01932	0.650	0.00857	10.18	7.62	0.00254	0.01394	0.72183	4.53909
38055.0	80.4	2528.0	0.02437	0.980	0.01292	10.28	7.82	0.00312	0.01865	0.76506	4.60799
38127.0	82.1	2728.0	0.02943	1.350	0.01780	10.38	7.90	0.00372	0.02362	0.80240	4.63499
38150.0	82.6	2828.0	0.03196	1.520	0.02004	10.43	7.92	0.00404	0.02600	0.81354	4.63918
38162.0	82.9	2958.0	0.03525	1.750	0.02307	10.50	7.89	0.00447	0.02916	0.82732	4.63115
38168.0	83.0	3128.0	0.03954	2.030	0.02677	10.58	7.84	0.00504	0.03316	0.83842	4.61434
38172.0	83.1	3228.0	0.04207	2.230	0.02940	10.64	7.81	0.00539	0.03574	0.84942	4.60365
38160.0	82.8	3328.0	0.04460	2.370	0.03125	10.68	7.75	0.00575	0.03793	0.85031	4.58355
38144.0	82.4	3428.0	0.04713	2.550	0.03362	10.74	7.68	0.00614	0.04038	0.85669	4.55942
38118.0	81.8	3528.0	0.04966	2.680	0.03534	10.78	7.59	0.00654	0.04250	0.85579	4.53000
38110.0	81.7	3628.0	0.05219	2.830	0.03731	10.83	7.54	0.00692	0.04475	0.85750	4.51282



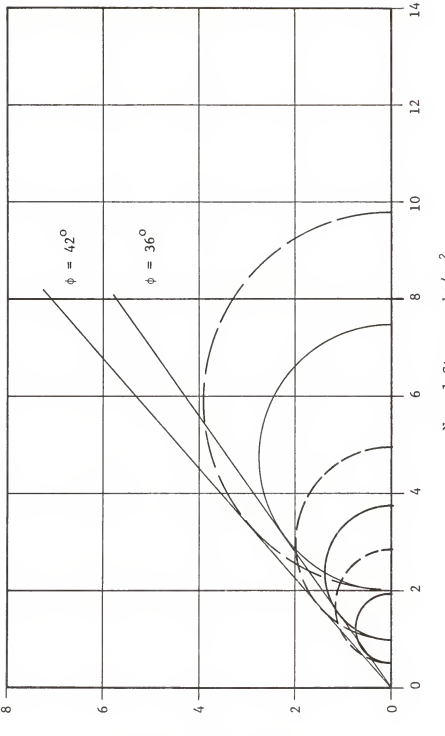


Triaxial Tests on Loose Edgar Sand

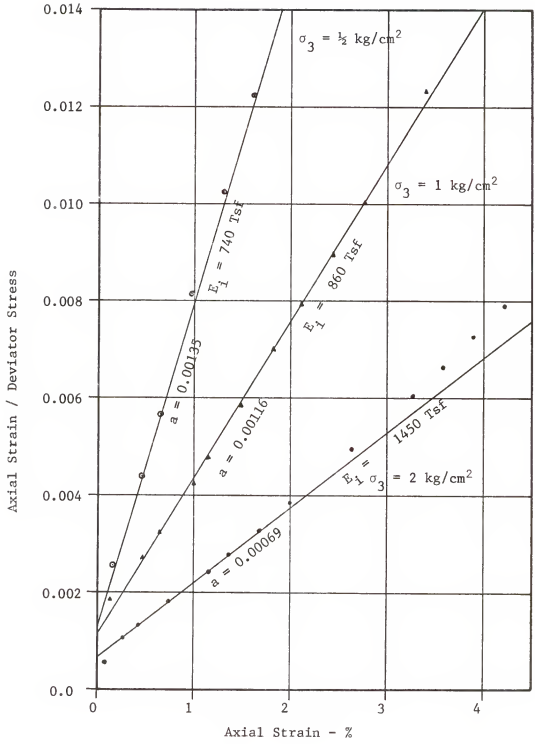




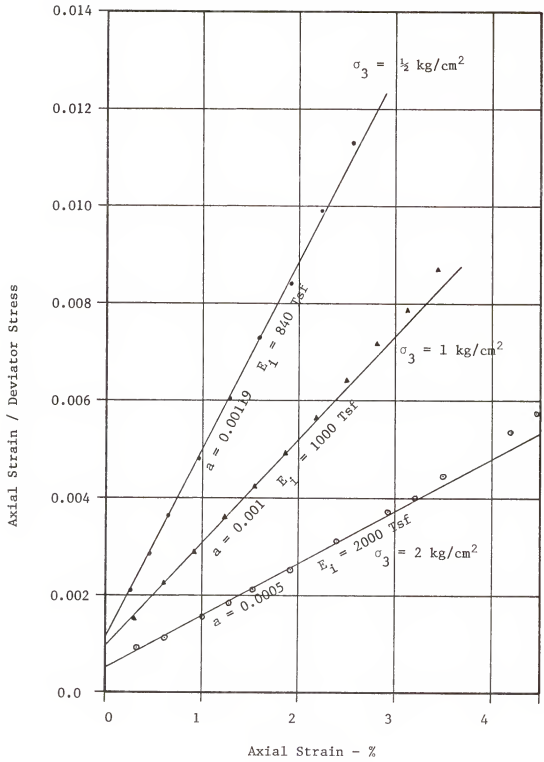
Triaxial Tests on Dense Edgar Sand



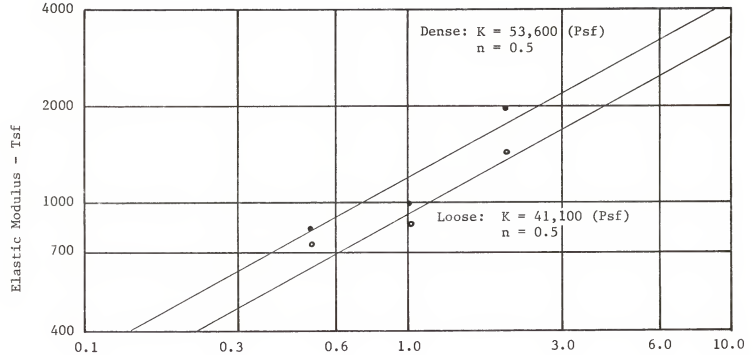
Mohr Circles for Loose and Dense Edgar Sand Tests



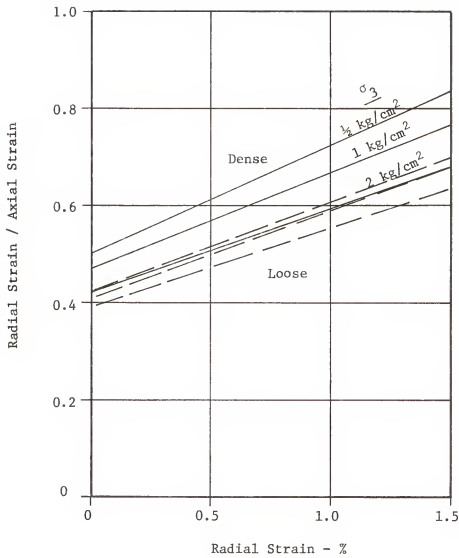
Loose Edgar Sand Triaxial Tests



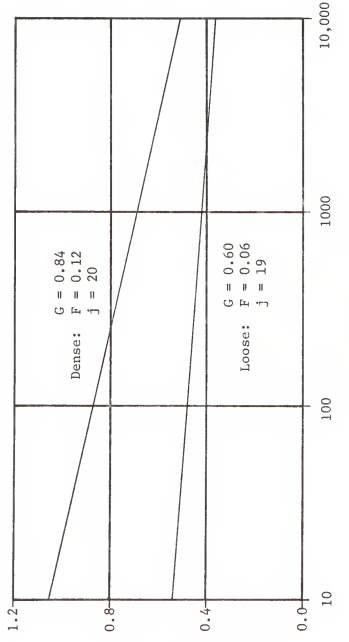
Dense Edgar Sand Triaxial Tests



Edgar Sand Triaxial Tests



Edgar Sand Triaxial Tests



Edgar Sand Triaxial Tests

APPENDIX V

LABORATORY PLATE BEARING TESTS ON EDGAR SAND

University of Florida
Soil Mechanics Research

Plate Bearing Test
Data and Calculations

Date: 3-13-72 Plate Area: 1 ft² Test Number: PBT-1

Party: Hartman, Laier Location: Test Chamber Soil: Edgar Sand

Remarks: $\sigma_v = 6.00$ psi $\sigma_h = 2.84$ psi $K_o = 0.444$ $D_r = 92.8\%$

Deflection corrected for elastic compression of rod.

Load Tons	Time Min.	Left Dial	Right Dial	Defl. Left	Defl. Right	Defl. Avg.	Notes
Piston		1.747	1.697				$\sigma_v = 2.95$ psi
Valve		1.790	1.724	+0.043	+0.027	+0.035 in.	$\sigma_v = 4.00$ psi
Opened		1.801	1.733	+0.054	+0.036	+0.045 in.	$\sigma_v = 5.00$ psi
		1.808	1.739	+0.061	+0.042	+0.0515 in.	$\sigma_v = 6.00$ psi
		Dials reset and loads applied.					
0		1.815	1.796				
0.25		1.8022	1.784	-0.0128	-0.012	-0.0119	
0.5		1.7861	1.7752	-0.0289	-0.0208	-0.0248	
0.75		1.7731	1.7643	-0.0419	-0.0317	-0.0353	
1.0		1.7575	1.7520	-0.0575	-0.0440	-0.0488	
1.5	¼ min.	1.7190	1.7235	-0.0960	-0.0725	-0.0813	
2.0		1.6732	1.6888	-0.1418	-0.1072	-0.1205	
2.5	a minimum of 0.001	1.6072	1.6358	-0.2078	-0.1602	-0.1790	Piston moved slightly
3.0		1.465	1.5042	-0.350	-0.2918	-0.3149	Pronounced Piston movement
3.5		1.3695	1.415	-0.4455	-0.381	-0.4068	$\sigma_v = 6.8$ psi $\sigma_h = 1.15$ psi
3.75		1.286	1.337	-0.529	-0.459	-0.4815	Pronounced lateral flow
4.0		1.202	1.239	-0.613	-0.557	-0.577	$\sigma_v = 7$ psi
		Unloading Data					
2.5	Loads left on a minutes or until rate <	1.251	1.274	-0.564	-0.522	-0.5385	
1.5		1.326	1.330	-0.489	-0.466	-0.4745	
0.5		1.395	1.380	-0.420	-0.416	-0.4175	
0		1.462	1.405	-0.353	-0.391	-0.372	
	3						

University of Florida
Soil Mechanics Research

Plate Bearing Test
Data and Calculations

Date: 5-11-72 Plate Area: 1 ft² Test Number: PBT-2

Party: Hartman, Laier Location: Test Chamber Soil: Edgar Sand

Remarks: σ_v = 6.00 psi σ_h = 2.84 psi k_o = 0.467 D_r = 57.4%

Deflection corrected for elastic compression of rod.

Load Tons	Time Min.	Left Dial	Right Dial	Defl. Left	Defl. Right	Defl. Avg.	Notes
Piston		0.756	0.596				
Valve		0.830	0.670				σ_v = 4.00 psi
Opened		0.844	0.684				σ_v = 5.00 psi
		0.849	0.689				σ_v = 6.00 psi
		Dials	reset	and loads	applied		
0		2.016	1.936				
0.25	2 min.	1.972	1.895	-0.044	-0.041	-0.039	
0.50	2	1.953	1.858	-0.063	-0.078	-0.065	
0.75	2	1.936	1.841	-0.080	-0.095	-0.081	
1.00	2	1.917	1.818	-0.099	-0.118	-0.102	
1.25	3	1.881	1.790	-0.135	-0.146	-0.133	
1.50	2	1.829	1.744	-0.187	-0.192	-0.180	σ_v (bot) = 6.2 psi; σ_h (top) = 1.6 psi
1.75	2	1.778	1.698	-0.238	-0.238	-0.228	
2.00	4	1.717	1.643	-0.294	-0.295	-0.287	
2.25	4	1.651	1.583	-0.365	-0.353	-0.348	σ_v (bot) = 6.9 psi; σ_h (top) = 1.6 psi
2.50	8	1.526	1.465	-0.490	-0.471	-0.469	
2.75	7	1.326	1.271	-0.690	-0.665	-0.666	σ_v (bot) = 6.5 psi; σ_h (top) = 1.5 psi
3.00	4	1.197	1.149	-0.819	-0.787	-0.791	σ_v (bot) = 6.7 psi; slight lateral flow
		Un	loading	Data			
2.25	1	1.201	1.147				
1.50	1	1.208	1.145				
0.75	1	1.225	1.151				
0	1	1.274	1.152				

APPENDIX VI

LABORATORY MODEL FOOTING TESTS ON OTTAWA SAND

Model Footing Settlement Tests

Ottawa Sand Dry Density = 104 pcf Relative Density = 80%

I. Square Footing: 7.6 cm x 7.6 cm

Δ Load (gms)	Load (gms)	Pressure (gm/cm^2)	Dial Rdg. (inches)	Deflection (inches)
Seating	(472.0)	(8.2)	0.04000	0.00000
1001.8	1001.8	17.3	0.03930	0.00070
1003.4	2005.2	34.7	0.03821	0.00179
1013.2	3018.4	52.2	0.03732	0.00268
1010.2	4028.6	69.7	0.03542	0.00458
278.2	4306.8	74.5	0.03498	0.00502
1005.8	5312.6	91.9	0.03270	0.00730
1004.4	6317.0	109.2	0.03000	0.01000
1006.0	7323.0	126.8	0.02692	0.01308
1005.5	8328.5	144.1	0.02265	0.01735
1003.3	9331.8	161.4	0.01875	0.02125
1003.3	10335.1	178.7	0.01120	0.02880

II. Small Rectangular Footing: 7.6 cm x 26.8 cm (1:3.5 Ratio)

Δ Load (gms)	Load (gms)	Pressure (gm/cm^2)	Dial Rdg. (inches)	Deflection (inches)
Seating	(1772.4)	(8.7)	0.09000	0.00000
2005.1	2005.1	9.8	0.08968	0.00032
2006.7	4011.8	19.7	0.08838	0.00162
2011.3	6023.1	29.6	0.08751	0.00249
2023.4	8046.5	39.5	0.08605	0.00395
2010.4	10056.9	49.4	0.08469	0.00531
2006.3	12063.2	59.3	0.08300	0.00700
2020.1	14083.3	69.2	0.08150	0.00850
2009.0	16092.3	79.0	0.07840	0.01160
1997.8	18090.1	88.8	0.07570	0.01430
2006.8	20096.9	98.7	0.07370	0.01630

III. Large Rectangular Footing: 7.6 cm x 45.9 cm (1:6 Ratio)

Δ Load (gms)	Load (gms)	Pressure (gm/cm^2)	Dial 1 (inches)	Dial 2 (inches)	Deflection (inches)
Seating	(3297)	(9.5)	0.10000	0.09305	0.00000
8033	8033	23.0	0.09528	0.09080	0.00349
7988	16021	46.0	0.08730	0.08312	0.01132
8010	24031	69.0	0.08230	0.07825	0.01626
8050	32081	92.0	0.07430	0.07315	0.02281
7995	40076	114.8	0.06861	0.06701	0.02873
16074	56150	161.0	0.05460	0.05610	0.04118

LIST OF REFERENCES

Baguelin, F., Jezequel, J.F., LeMee, E., and LeMehaute, A., 1972, "Expansion of Cylindrical Probes in Cohesive Soils," Journal of the Soil Mechanics and Foundations Division, ASCE, Vol. 98, No. SM 11, November.

Barden, L., 1967, "Stresses and Displacements in a Cross-Anisotropic Soil," Geotechnique, Vol. XIII, No. 3, September.

Boresi, A.P., 1965, Elasticity in Engineering Mechanics, Englewood Cliffs, New Jersey: Prentice-Hall, Inc.

Boussinesq, J., 1885, "Applications des potentiels á l'étude de l'équilibre et du mouvement des solides élastiques," Paris.

Bowles, J.E., 1968, Foundation Analysis and Design, New York: McGraw-Hill Book Co.

Calhoon, M.L., 1969, "Pressuremeter Field Testing of Soils," Civil Engineering, Vol. 39, No. 7, July.

Chaplin, T.K., 1961, "Compressibility of Sands and Settlements of Model Footings and Piles," Proceedings, 5th International Conference on Soil Mechanics and Foundation Engineering, Paris, Vol. III.

Chen, L.S., 1948, "An Investigation of the Stress-Strain and Strength Characteristics of Cohesionless Soils by Triaxial Compression Tests," Proceedings, 2nd International Conference on Soil Mechanics and Foundation Engineering, Rotterdam, Vol. V.

Clough, R.W., 1960, "The Finite Element Method in Plane Stress Analysis," Proceedings, 2nd ASCE Conference on Electronic Computation, Pittsburgh, September.

Clough, R.W., and Woodward, R.J., III, 1967, "An Analysis of Embankment Stresses and Deformations," Journal of the Soil Mechanics and Foundations Division, ASCE, Vol. 93, No. SM 4, July.

Cornforth, D.H., 1964, "Some Experiments on the Influence of Strain Conditions on the Strength of Sand," Geotechnique, Vol. XIV, No. 2, June.

Courant, R., 1943, "Variational Methods for the Solution of Problems of Equilibrium and Vibrations," Bulletin of the American Mathematical Society, Vol. 49.

Dauvisis, J.P., and Menard, L., 1964, "Etude expérimentale du tassement et de la force portante de fondations superficielles," Sols-Soils, No. 10, September.

De Mello, V.F.B., 1971, "The Standard Penetration Test," Proceedings, Fourth Panamerican Conference on Soil Mechanics and Foundation Engineering, Vol. I, June.

De Ruiter, J., 1971, "Electric Penetrometer for Site Investigations," Journal of the Soil Mechanics and Foundations Division, ASCE, Vol. 97, No. SM 2, February.

Department of the Navy, 1971, Design Manual: Soil Mechanics, Foundations, and Earth Structures, NAVFAC DM-7, Washington, D.C.: U.S. Government Printing Office.

Desai, C.S., 1972, Editor, Applications of the Finite Element Method in Geotechnical Engineering, U.S. Army Waterways Experiment Station, Vicksburg, Mississippi, September.

Desai, C.S., and Abel, J.F., 1972, Introduction to the Finite Element Method, New York: Reinhold Co.

Duncan, J.M., and Chang, C-Y, 1970, "Nonlinear Analysis of Stress and Strain in Soils," Journal of the Soil Mechanics and Foundations Division, ASCE, Vol. 96, No. SM 5, September.

Fletcher, G.F.A., 1965, "Standard Penetration Test: Its Uses and Abuses," Journal of the Soil Mechanics and Foundations Division, ASCE, Vol. 91, No. SM 4, July.

Gambin, M., 1963, "Calcul du tassement d'une fondation profonde en fonction des résultats pressiométriques," Sols-Soils, No. 7, December.

Gibson, R.E., and Anderson, W.F., 1961, "In-Situ Measurement of Soil Properties with the Pressuremeter," Civil Engineering and Public Works Review, Vol. 56, London, May.

Goulet, G., Hulo, Y., and Jezequel, J., 1964, "Comparison entre les résultats de chargement statique d'un pieu et les prévisions déduites des essais géotechniques," Sols-Soils, No. 11, December.

Harding, J.W., and Sneddon, I.N., 1945, "The Elastic Stresses Produced by the Indentation of the Plane Surface of a Semi-Infinite Elastic Solid by a Rigid Punch," Proceedings, Cambridge Philosophical Society, Vol. 41, Part I.

Harr, M.E., 1966, Foundations of Theoretical Soil Mechanics, New York: McGraw-Hill Book Co.

Herrmann, L.R., 1965, "Elasticity Equations for Incompressible and Nearly Incompressible Materials by a Variational Theorem, AIAA Journal, Vol. 3, No. 10, October.

Higgins, C.M., 1969, "Pressuremeter Correlation Study," Highway Research Record, No. 284.

Holden, J.C., 1971, "Laboratory Research on Static Cone Penetrometers," University of Florida Internal Report CE-SM-71-1, August.

Janbu, N., 1963, "Soil Compressibility as Determined by Oedometer and Triaxial Tests," Proceedings, European Conference on Soil Mechanics and Foundation Engineering, Wiesbaden, Vol. I.

Jordan, J.C., and Schiffman, R.L., 1967, ICES-SEPOL-I: A Settlement Problem Oriented Language - USERS' MANUAL, Soil Publication No. 204, Massachusetts Institute of Technology, December.

Kondner, R.L., and Zelasko, J.S., 1963, "A Hyperbolic Stress-Strain Formulation for Sands," Proceedings, Second Panamerican Conference on Soil Mechanics and Foundation Engineering, Brazil, Vol. I.

Kulhawy, F.H., Duncan, J.M., and Seed, H.B., 1969, "Finite Element Analyses of Stresses and Movements in Embankments During Construction," University of California Report No. TE-69-4, November.

Ladanyi, B., 1963a, "Evaluation of Pressuremeter Tests in Granular Soils," Proceedings, Second Panamerican Conference on Soil Mechanics and Foundation Engineering, Brazil, Vol. I.

Ladanyi, B., 1963b, "Expansion of a Cavity in a Saturated Clay Medium," Journal of the Soil Mechanics and Foundations Division, ASCE, Vol. 89, No. SM 4, July.

Ladanyi, B., 1967, "Expansion of Cavities in Brittle Media," International Journal of Rock Mechanics and Mining Sciences, Vol. 4.

Ladanyi, B., 1972, "In-Situ Determination of Undrained Stress-Strain Behavior of Sensitive Clays with the Pressuremeter," Canadian Geotechnical Journal, Vol. 9, No. 3, August.

Laier, J.E., 1973, Effects of Pressuremeter Probe Length/Diameter Ratio and Borehole Disturbance on Pressuremeter Test Results in Dry Sand, PhD Dissertation, University of Florida.

Lambe, T.W., 1970, "Braced Excavations," Proceedings, ASCE Specialty Conference on Lateral Stresses in the Ground and Design of Earth Retaining Structures, Ithaca, New York, June.

Lee, K.L., 1970, "Comparison of Plane Strain and Triaxial Tests on Sand,"Journal of the Soil Mechanics and Foundations Division, ASCE, Vol. 96, No. SM 3, May

Lee, K.L., and Seed, H.B., 1967, "Drained Strength Characteristics of Sands," Journal of the Soil Mechanics and Foundations Division, ASCE, Vol. 93, No. SM 6, November.

Little, A.L., and Price, V.E., 1958, "The Use of an Electronic Computer for Slope Stability Analysis," Geotechnique, Vol. VIII, No. 3, September.

Livneh, M., Gellert, M., and Uzan, J., 1971, "Determination of the Elastic Modulus of Soil by the Pressuremeter Test - Theoretical Background," Journal of Materials, JMLSA, Vol. 6, No. 2, June.

Martin, H.C., and Carey, G.F., 1973, Introduction to Finite Element Analysis, New York: McGraw-Hill Book Co.

Ménard, L.F., 1956, "An Apparatus for Measuring the Strength of Soils in Place," Master of Science in Civil Engineering Thesis, University of Illinois.

Ménard, L.F., 1963a, "Calcul de la force portante des fondations sur la base des résultats des essais pressiométriques," Sols-Soils, No. 5, June.

Ménard, L.F., 1963b, "Calcul de la force portante des fondations sur la base des résultats des essais pressiométriques - Seconde partie: resultats experimentaux et conclusion," Sols-Soils, No. 6.

Ménard, L.F., 1965, "Règles pour le calcul de la force portante et du tassement des fondations en fonction des résultats pressiométriques," Proceedings, Sixth International Conference on Soil Mechanics and Foundation Engineering, Montreal, Vol. II.

Ménard, L.F., 1971,"Le tassement des fondations et les techniques pressiométriques bilan après dix ans de resultats expérimentaux," Proceedings, I.T.B.T.P. Conference, March.

Ménard, L.F., Bourdon, G., and Houy, A., 1964, "Etude expérimentale de l'encasterement d'un rideau en fonctions des caractéristiques pressiométriques du sol de fondation," Sols-Soils, No. 9, June.

Ménard, L.F., and Rousseau, J., 1962, "L'évaluation des tassements, tendances nouvelles," Sols-Soils, No. 1.

Newmark, N.M., 1960, "Failure Hypotheses for Soils," Proceedings, Research Conference on Shear Strength of Cohesive Soils, Boulder, Colorado, June.

Oden, J.T., 1972, Finite Elements of Nonlinear Continua, New York: McGraw-Hill Book Co.

Palmer, A.C., 1972, "Undrained Plane-Strain Expansion of a Cylindrical Cavity in Clay: A Simple Interpretation of the Pressuremeter Test," Geotechnique, Vol. XXII, No. 3, September.

Parsons, Brinkerhoff, Quade, and Douglas, 1961, The Menard Pressuremeter Technical Digest, Philadelphia: The American Soil Testing Co.

Schleicher, F., 1926, "Zur Theorie des Baugrundes,"Der Bauingenieur, Vol. 7.

Schmertmann, J.H., 1967, "Static Cone Penetrometers for Soil Exploration," Civil Engineering, Vol. 37, No. 6, June.

Schmertmann, J.H., 1970, "Static Cone to Compute Static Settlement over Sand," Journal of the Soil Mechanics and Foundations Division, ASCE, Vol. 96, No. SM 3, May.

Schofield, A., and Wroth, P., 1968, Critical State Soil Mechanics, London: McGraw-Hill Book Co.

Smith, I.M., and Kay, S., 1971, "Stress Analysis of Contractive or Dilative Soil," Journal of the Soil Mechanics and Foundations Division, ASCE, Vol. 97, No. SM 7, July.

Steinbrenner, W., 1934,"Tafeln zur Setzungsberechnung," Die Strasse, Vol. 1.

Terzaghi, K.T., 1943, Theoretical Soil Mechanics, New York: John Wiley and Sons, Inc.

Thorley, A., Broise, Y., Calhoon, M.L., Zeman, Z.P., and Watt, W.G., 1969, "Borehole Instruments for Economical Strength and Deformation In-Situ Testing," Proceedings of the Conference on In-Situ Investigations in Soils and Rocks, British Geotechnical Society, London.

Tranter, C.J., 1946, "On the Elastic Distortion of a Cylindrical Hole by a Localised Hydrostatic Pressure," Quarterly of Applied Mathematics, Vol. 4, No. 3.

Turner, M.J., Clough, R.W., Martin, H.C., and Topp, L.J., 1956, "Stiffness and Deflection Analysis of Complex Structures," Journal of the Aeronautical Sciences, Vol. 25, No. 9, September.

Ural, O., 1973, Finite Element Method, New York: Intext Educational Publishers.

Venkatraman, B., and Patel, S.A., 1970, Structural Mechanics with Introductions to Elasticity and Plasticity, New York: McGraw-Hill Book Co.

Vesić, A.S., 1972, "Expansion of Cavities in Infinite Soil Mass," Journal of the Soil Mechanics and Foundations Division, ASCE, Vol. 98, No. SM 3, March.

Westergaard, H.M., 1941, "On the Elastic Distortion of a Cylindrical Hole by a Localized Hydrostatic Pressure," Karman Anniversary Volume, California Institute of Technology.

Whitman, R.V., 1960, "Discussion on Shear Strength of Undisturbed Cohesive Soils," Proceedings, Research Conference on Shear Strength of Cohesive Soils, Boulder, Colorado, June.

Wilson, E.L., 1963, "Finite Element Analysis of Two-Dimensional Structures," Structural Engineering Laboratory Report No. 63-2, University of California, June.

Wilson, E.L., 1965, " Structural Analysis of Axisymmetric Solids," AIAA Journal, Vol. 3, No. 12, December.

Zienkiewicz, O.C., 1971, The Finite Element Method in Engineering Science, New York: McGraw-Hill Book Co.

BIOGRAPHICAL SKETCH

John Paul Hartman was born on August 15, 1936 in Glasgow, Montana. He was raised in St. Louis, Missouri and graduated from Principia Upper School in 1954. After obtaining a Bachelor of Science degree from Principia College in 1957, he earned a Bachelor of Science in Civil Engineering from Washington University (St. Louis) in 1959, followed by a Master of Science from Harvard University in 1960.

After commissioning in the United States Naval Reserve, Mr. Hartman was on the Staff of the U.S. Naval Nuclear Power School at Mare Island, California from 1960 to 1965. After release from active duty he worked briefly for Ardaman and Associates, consulting engineers in Orlando, Florida, and then joined the Martin-Marietta Corporation in Orlando where he worked as a Senior Engineer in Nuclear Effects from 1966 to 1968.

In 1968 Mr. Hartman joined the charter faculty in the College of Engineering at Florida Technological University where he is currently employed as an Associate Professor of Engineering. In 1970-71 he held a National Science Foundation Science Faculty Fellowship while completing his formal coursework for the Ph.D.

Mr. Hartman is married to the former Mary Alice Creekmore of Miami, Florida and they have two children, Jeffrey (11) and David (9½).

I certify that I have read this study and that in my opinion it conforms to acceptable standards of scholarly presentation and is fully adequate, in scope and quality, as a dissertation for the degree of Doctor of Philosophy.

John H. Schmertmann, Chairman
Professor of Civil Engineering

I certify that I have read this study and that in my opinion it conforms to acceptable standards of scholarly presentation and is fully adequate, in scope and quality, as a dissertation for the degree of Doctor of Philosophy.

James H. Schaub
Professor of Civil Engineering

I certify that I have read this study and that in my opinion it conforms to acceptable standards of scholarly presentation and is fully adequate, in scope and quality, as a dissertation for the degree of Doctor of Philosophy.

H. Kelly Brooks
Professor of Geology

This dissertation was submitted to the Graduate Faculty of the College of Engineering and to the Graduate Council, and was accepted as partial fulfillment of the requirements for the degree of Doctor of Philosophy.

March, 1974

Dean, College of Engineering

Dean, Graduate School